2012

Use of UHPC piles in integral abutment bridges

Jessica Ann Garder
Iowa State University

Use of UHPC piles in integral abutment bridges

by

Jessica A. Garder

A thesis submitted to the graduate faculty
in partial fulfillment of the requirements for the degree of
MASTER OF SCIENCE

Major: Civil Engineering (Structural Engineering)

Program of Study Committee:
Sri Sritharan, Major Professor
Jeramy Ashlock
Lester Schmerr

Iowa State University
Ames, Iowa
2012

TABLE OF CONTENTS

LIST OF FIGURES

LIST OF TABLES

ACKNOWLEGMENTS

The research presented in this thesis is part of a project that was sponsored by the Iowa Highway Research Board. Lafarge North America donated the UHPC material needed for the project and Coreslab Structures, Inc. of Omaha prefabricated all the UHPC test units, test piles, and production piles at no cost. The author would like to specifically like to thank Todd Culp and John Heimann for their time and efforts. Graves Construction Co, Inc. of Spencer, Iowa performed the installation setup for the load frame for the field work. The Technical Advisory Committee of this research project included: Ahmad Abu-Hawash, Dean Bierwagen, Kenneth Dunker, Chris Chromwell, Robert Stanley, Kyle Frame, Stephen Megivern, Wayne Sunday, John Rasmussen, Terry Wipf, and Mark Dunn. Their guidance and feedback during the course of the project are also greatly appreciated.

The author would like to thank Dr. Sritharan for the opportunity to work on this project and gain experience in the laboratory and field. The author would also like to thank Dr. Rouse for approving the fielding testing and UHPC production pile instrumentation plans. In addition the author would like to recognize Dr. Ashlock and Dr. Schmerr for serving as her committee members.

The author would like to recognize Sriram Aaleti for his help with laboratory testing, Kam Ng for his help with the geotechnical aspects of the field testing and GRLWEAP and Aaron Schelman for his help with LPILE. Kyle Frame from the Iowa DOT provided assistance with the Pile Driving Analyzer (PDA) tests during pile driving and his contribution is greatly appreciated. Doug Wood and Owen Steffens were essential during instrumentation, setup and testing of the UHPC piles, and their contributions are also greatly appreciated. The author would like to thank Danielle Deboer, Grant Schmitz, William Cord, Karly Rager, and Sasha Weir for helping with instrumentation and field work phases of the project. The author would like to thank Jennifer Mitts and, Jason Garder for editing her thesis.

The author would like to thank her parents, husband and friends for their prayers and support during the project duration. She is blessed to be surrounded by such a great group of people.

ABSTRACT

In order to make the Ultra High Performance Concrete (UHPC) pile, developed in Phase I of the UHPC Pile Project at Iowa State University (ISU), a viable option in practice, laboratory testing, field testing and installation of a production pile in the field were undertaken during Phase II of this project. A detailed understanding of the section behavior and lateral loading behavior was determined and compared to that of a steal HP 10 x 57 pile through lateral load analyses of a UHPC pile section. The analysis found that UHPC piles were suitable for integral abutments of bridges.

To make the field installation of UHPC piles possible, the overall performance of a common pile-to-abutment connection was verified in the laboratory by defining the UHPC pile-to-abutment connection, which is similar to the currently used connection for steel HP 10 x 57 piles. Both piles performances were verified by testing their connection when subjected to weak-axis bending. The test piles met performance criteria during the laboratory displacements of 0.28 and 0.42 inches which correspond to 1.0 and 1.55 inches in the field.

Next, the field testing began to ensure that the production pile would achieve the desired behavior and capacities required by integral abutment bridges. A vertical load test on a 46-ft UHPC test pile was completed one week after being driven into the ground at the same site where the UHPC production pile was implemented into a 223-ft long integral bridge with a 24˚ skew. Before failure, the test pile resisted 1.5 times the predicted capacity based on the Iowa Bluebook method of design for concrete piles, verifying appropriateness of reducing the UHPC production pile by 16% in length compared to the specified length of 65-ft for the HP 10 x 57 piles on the integral bridge.

Additionally, a lateral load test was conducted between the second test pile with a newly designed splice detail and the vertical load test pile, which confirmed the adequacy of the splice detail and the lateral load resistance of the pile. The 46-ft test pile was also tested during the lateral load test. The results of the laboratory and field studies indicated that the UHPC pile in the field is a viable option.

CHAPTER 1: INTRODUCTION

1.1. INTRODUCTION

In 2005, the American Association of State Highway Transportation Officials (AASHTO) identified grand challenges that should be addressed through more research advancement. Two of these challenges focus on extending service life of bridges and optimizing structural systems. Currently, AASHTO calls for a 75-year service life for bridges and highway structures. In recent years, some bridges in the United States have been designed with a 100 to 150-year service life (Freyermuth 2009). The service life of new bridge foundations may be increased due to the desirable qualities of the UHPC materials.

In 2008, a report entitled "Iowa's Deficient Bridges" identified Iowa as having 21 percent of its bridges (i.e., 5,153) in the structurally deficient category, which is the fourth-highest percentage in the nation. A bridge is considered structurally deficient when there is a significant amount of deterioration to any of the bridge's major components, such as the deck or supports. An additional 6 percent of Iowa's bridges (i.e., 1,455) were classified as functionally obsolete (Iowa's Deficient Bridges 2008), which includes any bridge that was built to standards that are not used in today's design. For example, a bridge having a vertical clearance that does not adequately serve the current traffic demand would be considered functionally obsolete.

To keep up with the rate of bridges becoming structurally deficient or functionally obsolete and to start reversing the percentage of structurally deficient bridges, Iowa Department of Transportation (DOT) and other local agencies are looking for solutions to extend the service life of new and existing bridges as well as reduce or eliminate maintenance costs. As the service life of a bridge is improved, its foundation performance should also be enhanced because a major portion of bridge construction costs lies in the foundation. The average cost of a bridge substructure is 30% of the total bridge cost (Menn 1990). Due to the cost and difficulty of maintaining bridge substructures, creative solutions are needed to extend the service life of structural systems by utilizing existing and new materials more efficiently. The high strength available when using Ultra High Performance

Concrete (UHPC) allows for reduced cross-section design and more efficient use of the material. In addition, the durability of UHPC also indicates the possibility of dramatically reducing or eliminating the deterioration associated with commonly used piles for bridge foundations.

1.2. CURRENT DEEP FOUNDATION PRACTICE AND LIMITATIONS

There are many different types of piles used to support structural loads in the United States. The four main categories are concrete, steel, timber, and composite piles, which are then broken up into many subgroups as shown in Figure 1-1. The most common deep foundation chosen for bridge foundations are steel H-piles and precast, prestressed concrete piles, which will be the focus of this chapter as a comparison to UHPC piles. Both of these piles have certain limitations when it comes to durability and driveability, which are outlined in the following sections.

1.2.1. Precast, Prestressed Concrete Piles

Commonly, precast concrete piles are used in marine environments on the cost. One disadvantage associated with precast, prestressed concrete piles is the fact that the ends of the piles are not effectively prestressed due to the development length of the prestressing strands to make them fully effective, thus causing a reduced tensile capacity in these regions. Tensile stresses can be developed in concrete piles during diving in certain soil conditions. For example, driving of a concrete pile in a hard soil layer that is overlying a soft layer can induce tensile stresses in the pile. Once the pile breaks through the hard layer, a tension stress develops at the pile toe. Another example is when driving a concrete pile in soft clay conditions. At the beginning of drive, the pile is susceptible to a tensile stress at the pile head as a result from the reflected wave of the hammer blow.

Concrete piles can fail as a result of large compressive stresses developed during driving. This can be attributed to an excessively large driving hammer used during installation or when driving through hard soil conditions. Figure 1-2 illustrates the crushing of concrete due to hard driving conditions for normal concrete piles. It is important to

perform an accurate drivability analysis to ensure that damage does not occur during driving of concrete piles.

In addition to the disadvantages during installation, precast concrete piles must be handled carefully in order to avoid cracking when picking up the pile during loading and unloading as well as picking up for field installation. Improper lifting procedures can crack or even break precast concrete piles.

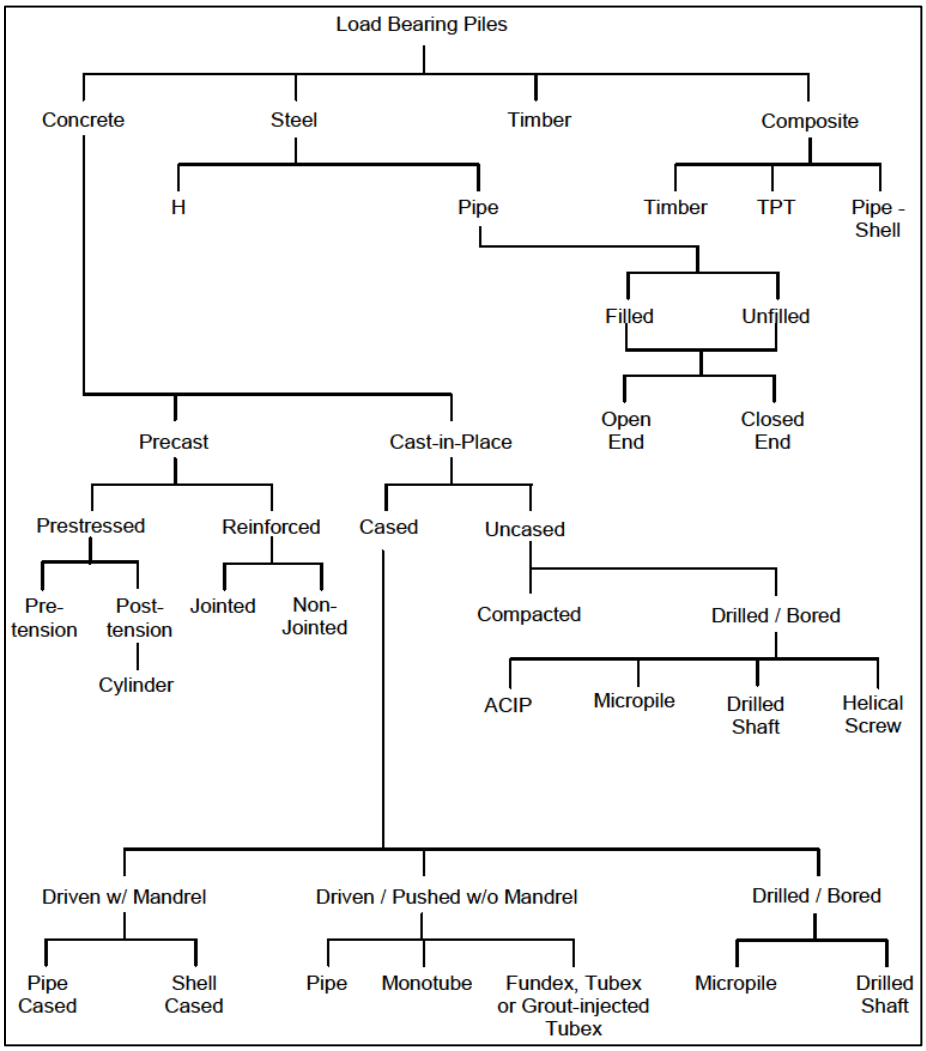

Figure 1-1: Deep Foundation Type Options (Hannigan et al. 2006)

Figure 1-2: Concrete Piles Damaged by Difficult Driving Conditions (DiMillio 1998)

Precast concrete piles that are subjected to sulfate ions undergo an expansive chemical reaction, which leads to cracking and spalling of the concrete and ultimately a reduction in available structural capacity (Moser et al. 2011). When concrete piles are subjected to chlorides, it is the steel reinforcement that will corrode instead of the concrete itself. As the reinforcement steel expands from corrosion, the concrete bursts. This type of corrosion leads to loss of bond between steel and concrete as well as a reduction in pile capacity (Moser et al. 2011). Figure 1-3 depicts the bursting of the concrete due to corrosion of the reinforcement steel as well as the abrasion of the water.

Figure 1-3: Damage to Prestressed Concrete Pile Due to Corrosion (Moser et al. 2011)

1.2.2. Steel H-Piles

Steel H-piles are commonly used in Iowa for integral abutment bridge. During driving, the disadvantages of steel H-piles include buckling under harsh driving conditions,

as well as the tendency to deviate from the designed location when obstructions are encountered, such as boulders. When driving steel H-piles through very dense gravels or soils containing boulders, the toe of the pile may severely deform and separation of the flanges and web may occur as shown in Figure 1-4. Additionally, the Iowa Department of Transportation (DOT) requires the top 12 inches of all steel piles to be trimmed due to the expected deformation of the pile head during driving (IA DOT 2011), which is depicted in Figure 1-5.

Not only can the driving conditions influence the performance of steel H-piles, but also the corrosion as the bridge service life is dramatically influenced when the corrosion of steel piles occurs. Corrosion is also a major problem for steel piles embedded in fill materials or above the water table. The water table fluctuation zone (Decker et al. 2008) is the zone in which the most corrosion occurs on steel H-piles. A summary of the maximum corrosion rate observed for various conditions was completed by Decker et al. (2008) and corrosion rate corresponding to number of years exposed, pH, Resistivity, and chloride content is summarized in Table 1-1 along with the references. Corrosion of steel piles does not only happen beneath the soil; Figure 1-6 indicates severe corrosion to the steel H-piles used in a bridge in St. Louis, Missouri located above the soil.

Figure 1-4: Damaged H-Pile Toe (Hannigan et al. 2006)

Figure 1-5 Damage to Pile Head at End of Driving (Ng et al. 2011)

Table 1-1: Corrosion Rate of Steel Piles with Various Soil Conditions

Corrosion Rate, in./year	Years Exposed	pH	Resistivity, Ω in.	Chloride, ppm	Reference
0.0007	22	5.1-6.0	19685-27559	16-59	Wong and Law 1999
0.0019	7	7.4-8.2	335-2756	0.3	Ramanoff 1962
0.0032	11	6.9	1693-4331	0.6	Ramanoff 1962
0.0019	11	8.1	315-508	0.5	Ramanoff 1962
0.0006	12	7.7-8.4	136-512	0.5	Ramanoff 1962
0.0007	34	8.2	118110	17.8	Decker et al. 2008
0.0005	35	7.7	59055	256	Decker et al. 2008
0.0006	38	7.5	59055	444	Decker et al. 2008

Figure 1-6: Corroded Steel H-Pile (Ehsani et al. 2012)

1.3. BENEFITS OF UHPC RELATED TO PILING

Ultra High Performance Concrete (UHPC) is a cement matrix often used with steel fibers with a compressive strength ranging from 22 ksi to 36 ksi (Resplendino 2012). UHPC has several advantages including strength, ductility, durability, and aesthetic design flexibility, which were achieved by eliminating the characteristic weaknesses of normal concrete.

The material and durability properties of UHPC and a UHPC pile section completed in Phase I of this project attribute many benefits of UHPC materials which can be found in the final report written by Vande Voort et al. (2008). A comparison between the UHPC pile section, comparable steel HP 10 x 57 and concrete pile sections is presented in Figure 1-7. Notice that the UHPC pile has similar outer dimensions as the HP 10 x 57 pile to allow for the same driving equipment to be used during installation. Additionally, the reduced cross-section when compared to the normal concrete pile allows for easier driving.

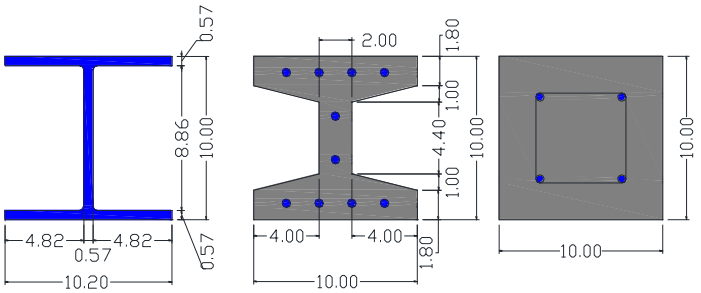

Figure 1-7: Cross-section of (a) Steel HP 10 x 57 Pile; (b) UHPC Pile; and (c) 10 x 10-in. Normal Concrete Pile (all dimensions in inches)

1.3.1. Durability

The tightly packed nature of the mix design gives UHPC its excellent durability characteristics. As a result of the low water-binder-ratio, the capillary porosity of an uncracked UHPC specimen is much less than that of normal concrete (NC) or high performance concrete (HPC), and also has the benefit of a greatly reduced chloride permeability (Scheydt et al. 2012).

Because UHPC is very durable material, the required concrete cover thickness for steel reinforcement is typically reduced, allowing for a further reduction in section size, thus resulting in an efficient use of the material. An additional benefit resulting from the

durability of the material is its potential to extend the lifespan of bridges and lower the maintenance costs.

1.3.2. Strength

UHPC exhibits very high strength characteristics when compared to HPC or NC, which are given in Table 1-2. Due to the high strength of UHPC, the cross-section could be designed efficiently to reduce the amount of material needed for fabrication and to withstand both the compressive and tensile stresses developed during driving. From the casting of the ¾ scale test units and the full-scale test piles, the proposed UHPC piles with the tapered H section can be cast successfully in a precasting plant and can achieve the required high strength of 26 to 29 ksi, as long as the recommended heat treatment procedures are employed (Vande Voort et al. 2008).

Table 1-2: Strength Characteristics of UHPC vs. HPC and NC

Property	UHPC	HPC	Normal Concrete
Compressive Strength, ksi	26-30	12-18	4-8
Tensile Strength, ksi	1.7	0.8-0.9	0.3-0.7
Elastic Modulus, ksi	8000	4800-6400	3600-5100

1.4. UHPC PILE

The UHPC pile was designed as described by Vande Voort et al. in 2008 as Phase I of the project. A brief summary of the research is given in this section.

During Phase I of the project, the design of the UHPC pile cross-section was optimized and is reproduced in Figure 1-8a. There were some concerns regarding the effectiveness of the prestressing in the head and toe of the pile and the performance of the pile due to driving stresses. It was decided that the top 9 inches would be cast as a solid 10-in. by 10-in. block as shown in Figure 1-8b that was tapered into the designed cross-section. The moment-curvature response of the UHPC pile was predicted and confirmed in the laboratory flexural test. A vertical load test was performed on two test piles driven in the field after the laboratory testing and results were then compared to the performance of a steel HP 10 x 57. Additionally, a lateral load test was completed between the two UHPC test piles.

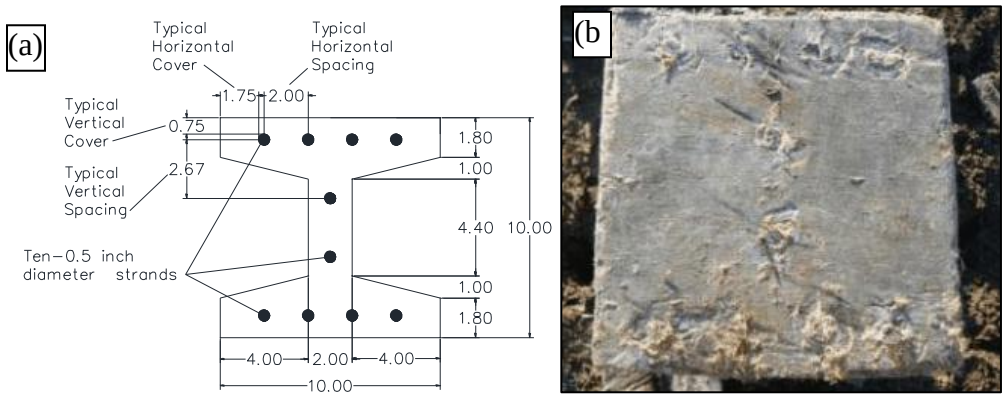

Figure 1-8: a) Cross-Section of UHPC Pile; and b) Top 18-in. of Test Pile

1.5. SCOPE OF RESEARCH

The successful completion of Phase I of the UHPC project was a stepping stone towards Phase II of the project, in which the options to improve the driveability, installation, connection details, and performance verification in the field were planned. The objectives of this thesis include the following:

- Predict the performance of a UHPC pile in an integral bridge abutment;
- Perform a laboratory test on typical pile-to-abutment connection by subjecting it to axial and cyclic lateral loading;
- Perform a lateral load test in the field on the splice connection designed to extend the length of UHPC piles;
- Perform a vertical load test to failure in the field; and
- Instrument and install a UHPC pile as part of a bridge foundation and compare its driving behavior to that of a steel H-pile.

1.6. REPORT LAYOUT

This report has seven chapters describing the development of various connection details and both laboratory and field testing of UHPC piles. A summary of each chapter's content is presented below.

- Chapter 1 – Introduction: A brief introduction to the limitations of traditional concrete and steel piles and details of the UHPC pile.
- Chapter 2 – Literature Review: A review of published studies describing the composition, microstructure, durability, material properties, applications, practice for splicing details and pile-to-abutment connections, integral abutments, and analysis procedures for driveability and lateral loading.
- Chapter 3 – Analysis of UHPC Piles in Integral Abutments: Description of the results from the analysis of the pile section in weak-axis bending comparing it to strong-axis bending for moment-curvature response analysis and lateral load parametric study.
- Chapter 4 – Pile-to-Abutment Connection Test: Description of the fabrication and casting of the UHPC test units and abutment cap; weak-axis bending on a short HP 10 x 57 pile and a short UHPC pile anchored to the abutment cap.
- Chapter 5 – Field testing of UHPC Test Piles: Description of the fabrication and casting of the UHPC test piles; driving of the UHPC test piles; vertical load test; lateral load test; and analysis of the weak-axis bending performance of the UHPC pile during the lateral load test.
- Chapter 6 – Field Implementation of a UHPC Production Pile: Description of the fabrication and casting process of the UHPC Production pile; instrumentation plan; the driving of the three instrumented HP 10 x 57 piles and the UHPC production pile; and an analysis predicting the performance of the UHPC and HP 10 x 57 piles.
- Chapter 7 – Summary and Conclusions: A summary of the results on UHPC piles found from casting, field testing, and long-term monitoring; and a description of future research potential.

CHAPTER 2: LITERATURE REVIEW

2.1. INTRODUCTION

This chapter introduces the history, background, material properties, and applications of UHPC in order to characterize the material being used in the pile project as well as the deep foundation design methods used to design the UHPC test piles and UHPC production piles. Because the UHPC production pile will be installed in an integral abutment for long-term monitoring, current design guidelines are identified, along with a summary of previous research on long-term monitoring of integral abutments. Finally, to predict the behavior of the test and production piles during driving, testing and monitoring, the two computer software packages LPILE and GRLWEAP were used and they are described in detail in Section 2.7.

2.2. HISTORY AND BACKGROUND

Relatively recent advances in concrete technology have introduced UHPC although the idea to create new concrete mixes with higher strength has been around for over 150 years, but structural applications using the improved concrete have often lagged behind due to high cost of material and lack of design guidelines for the new material (Tang 2004). Four milestones have been key to the development of UHPC, which includes the development of the cement matrix, the fiber, the bond at the interface between fiber and matrix, and the resulting composite (Naaman and Wille, 2012). Naaman and Wille (2012) have identified the achievements of each milestone in chronological order as well as giving consideration to different geographical region.

Richard and Cheyrezy (1995) outlined the basic design principles that should be followed when designing UHPC materials, which are: (1) ensuring homogeneity of the material by eliminating coarse aggregates; (2) providing a compacted density by optimizing particle sizes; (3) achieving a good microstructure by subjecting the material to heat-treatment; and (4) providing ductility of the material by adding steel fibers.

Normal concrete is a heterogeneous material. In order to reduce the effects of the problems related with the non-uniformity in concrete, coarse aggregates are replaced by fine sands, the paste is mechanically improved by forming a more tightly packed mix design, and the aggregate ratio is decreased (Richard and Cheyrezy 1995). The small diameter of the aggregates used in UHPC causes the aggregate to behave as an inclusion in a continuous matrix instead of a rigid skeleton of normal concrete. This quality allows UHPC to accommodate a much larger compressive force that is transmitted by the matrix of material (Vande Voort et al. 2008). Figure 2-1 compares the representation of the force transfer between normal concrete and UHPC.

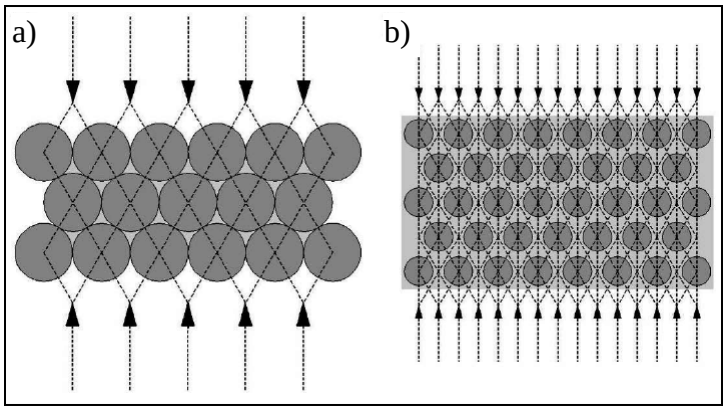

Figure 2-1: Depiction of Force Transfer through a) Normal Concrete and b) UHPC (after Walraven 2002)

There are several types of UHPC used around the world. The main difference between each is the type and quantity of fibers used in the mix design. A summary including the advantages, as well as the disadvantages of UHPC is given in Table 2-1. The four main types of UHPC are BSI®/CERACEM, compact reinforced composites (CRC), multi-scale cement composite (MSCC), and reactive powder concrete (RPC) (Vande Voort et al. 2008).

BSI®/CERACEM was developed by SIKA and EIFFAGE and includes coarse aggregates unlike the other three types of UHPC (Jungwirth and Muttoni 2004). Both CRC and MSCC use larger amounts and different sizes of fiber when compared to RPC (Vande Voorte et al. 2008). RPC's typically contain steel fibers that occupy 2% of the volume to gain ductility (Richard and Cheyrezy 1995). A form of RPC is Ductal,® which is produced by the French companies Lafarge and Bouygues. A composition of UHPC is provided in Table 2-2.

Because of its availability and use in several bridge research and implementation projects in the United States (e.g., Perry and Seibert 2011, Behloul 2006 and FHWA 2011), the UHPC used in the current and previous phase of the pile project is Ductal®. Unless otherwise noted, the UHPC in the remainder of the report refers specifically to Ductal®, while the research outcomes are applicable to any form of UHPC with engineering properties comparable to those of Ductal®.

Table 2-1: Advantages and Disadvantages of UHPC (Wipf et al., 2009)

Advantages	Disadvantages
High Compressive Strength	Short-Term Costs
High Tensile Strength	Material Cost
High Shear Strength	Mixing Time
High Impermeability	Casting Bed Time
High Durability	Heat Treatment
Self Leveling	Cast-In-Place Construction May Not Be Feasible
Self Healing of Unhydrated Cement	
Long-Term Costs	
Eliminate Labor Installing Stirrups	
Fewer Deck Replacements	
Reduced Weight for Shipping	

Table 2-2: Common UHPC Mix Components (Cheyrezy and Behloul, 2001)

Component	Weight per Cubic Foot, lb	Mass Ratio /Cement	Volume Fraction, %
Sand	61.9	1.430	38.8
Cement	42.3	1.000	22.7
Silica Fume	14.0	0.325	10.6
Crushed Quartz/Fly Ash	13.0	0.300	8.1
Fibers	9.4	0.218	2.0
Superplasticizer*	0.9	0.021	1.4
Water	9.9	0.229	16.5

*Superplasticizer is expressed as the weight of the solid fraction; the liquid fraction is included in the water weight.

2.3. MATERIAL PROPERTIES

An extensive literature review was completed by Vande Voort et al. (2008) on the material properties of UHPC. This section includes a brief summary of Vande Voort's literature review with appropriate updates for the material properties of UHPC used for Phase

II of the UHPC pile project, which include compressive strength, tensile strength, shrinkage and creep, elastic modulus, strain limits, and allowable driving limits. Additional information provided below was found with regards to standard and calculation method manuals and tolerances for prefabrication of structural elements using UHPC.

2.3.1. Compressive Strength

UHPC does not have any compressive strength for almost one day after pouring and a set time of 17 hours is recommended (Graybeal 2006). After the set time, UHPC develops its compressive strength very rapidly. Thus, the majority of the strength is gained in the first seven days of curing when heat treatment is not applied. The influence of heat treatment applied during the curing process of UHPC structural elements plays a large role in developing the compressive strength. The rate of strength gain for heat treated UHPC, from 7 to 56 days, is only five percent of the compressive strength (Vande Voort et al. 2008). Heat treatment allows the structural elements to reach their final maturity before the typical 28 day strength that is required for normal concrete (AFGC 2002). In addition, the final compressive strength of UHPC is typically ten percent higher for heat treated UHPC elements than non-heat treated UHPC elements (Graybeal 2006). The effect of delaying the heat treatment only slightly decreases the compressive strength than if applied right after stripping the forms (Graybeal 2006).

In comparison, normal concrete has a compressive strength within the range of 4 to 8 ksi and high performance concrete (HPC) has a compressive strength between 12 and 18 ksi. Heat treated UHPC has a compressive strength approximately two times that of HPC and five times that of normal concrete (Vande Voort et al. 2008).

2.3.2. Tensile Strength

Normal concrete has a tensile strength in the range of 300 and 700 psi and HPC has a tensile strength in the range of 800 to 900 psi. In comparison, UHPC develops more tensile strength than normal concrete and HPC, even beyond the development of micro-cracking which is due to the steel fibers effectively spanning the cracks. Additionally, UHPC can also experience strain-hardening between the first tensile crack strength and the ultimate tensile

strength (Vande Voort et al. 2008). Heat treatment decreases the amount of time it takes to reach the tensile strength and typically increases the tensile capacity by about ten percent (AFGC 2002). After exposing cracked UHPC cylinders to harsh environments, no noticeable decrease in peak tensile load-carrying capacity was observed (Graybeal 2006).

The behavior of UHPC can be described based on the crack width. UHPC can be characterized as elastoplastic up to a crack width of around 0.012 inches (Chanvillard and Rigaud 2003). The same crack width of 0.012 inches corresponds to the stress associated with the basis for fiber tensile strength (AFGC 2002).

2.3.3. Shrinkage and Creep

Shrinkage is the loss of free water through evaporation, which leads to the gradual shortening of the element with time. Heat treatment substantially reduces the effects of delayed shrinkage and creep (AFGC 2002), which allows for the valid assumption that there will not be any shrinkage of the concrete after heat treatment. If no heat treatment is performed on the material, the shrinkage can be assumed to be 550 μm (AFGC 2002).

Creep is an additional time dependent strain added to the concrete due to sustained load on the concrete matrix. The ultimate creep coefficient for untreated UHPC is 0.8 and drops to 0.2 for heat treated UHPC (AFGC 2002).

2.3.4. Elastic Modulus

Normal concrete has an elastic modulus within a range of 3500 to 5100 ksi and HPC has an elastic modulus of approximately 4800 to 6400 ksi (Vande Voort et al. 2008). AFGC recommends using a modulus of elasticity of 8000 ksi during the design stage when experimental information is not available on the UHPC material, as well as an initial modulus of 5700 ksi. The modulus of elasticity of UHPC is linear elastic for both compression and tension until specific strain limits are reached. For compression, the elastic portion limit is approximately 80 to 90 percent of the compressive strength of heat treated UHPC with only a 5 percent deviation from the stress-strain linearity (Graybeal 2007). A delay in the heat treatment of the UHPC material is a factor that will affect the modulus of

elasticity, which causes the modulus of elasticity to be slightly reduced, rather than for full steam treatment (Graybeal 2006).

Many equations have been developed to estimate the modulus of elasticity of concrete. Four equations were specifically developed for UHPC and are given below as Equations 2-1 through 2-4; all based on the compressive strength, where E is the elastic modulus in psi and f_c' is the compressive strength in psi. Vande Voort et al. (2008) recommended the use of Equation 2-2 to estimate the elastic modulus of UHPC based on laboratory tests completed in Phase I of the pile project.

$$E = 50{,}000\sqrt{f_c'} \quad \text{(Sritharan et al. 2003)} \quad (2\text{-}1)$$

$$E = 46{,}000\sqrt{f_c'} \quad \text{(Graybeal 2007)} \quad (2\text{-}2)$$

$$E = 2{,}373{,}400\ln(f_c') - 468{,}010 \quad \text{(Ma et al. 2002)} \quad (2\text{-}3)$$

$$E = 525{,}000\sqrt[3]{f_c'} \quad \text{(Ma et al. 2004)} \quad (2\text{-}4)$$

2.3.5. Strain Limits

2.3.5.1 Compression

Vande Voort et al. (2008) found several variations for the compression strain limit of UHPC in various studies. The compression limits range from 3200 to 4400 microstrain. The compression strain limit recommended by Sritharan et al. (2003) and Dugat et al. (1996) for elastic behavior of 3200 microstrain is used to characterize the limits in compression of heat treated UHPC in this study.

2.3.5.2 Flexural Tension

There is a close agreement for the cracking tensile strain, which ranges from 300 to 330 microstrain (Vande Voort et al. 2008). However, the ultimate tensile strain has some noticeable variation between various reported results. An ultimate tensile strain ranging from 5000 to 7000 microstrain was reported by Richard and Cheyrezy (1995), while an ultimate tensile strain of 7500 microstrain was reported by Dugat et al. (1996).

AFGC (2002) proposed the relationship given in Figure 2-2 for crack width versus stress. Vande Voort et al. (2008) reported the corresponding strains with cracking width for

various locations on the relationship for Ductal®. Micro-cracking begins at 160 microstrain, cracking starts at 1350 microstrain and the limit where cracks start exceeding the 0.012-in. limit is at 2400 microstrain.

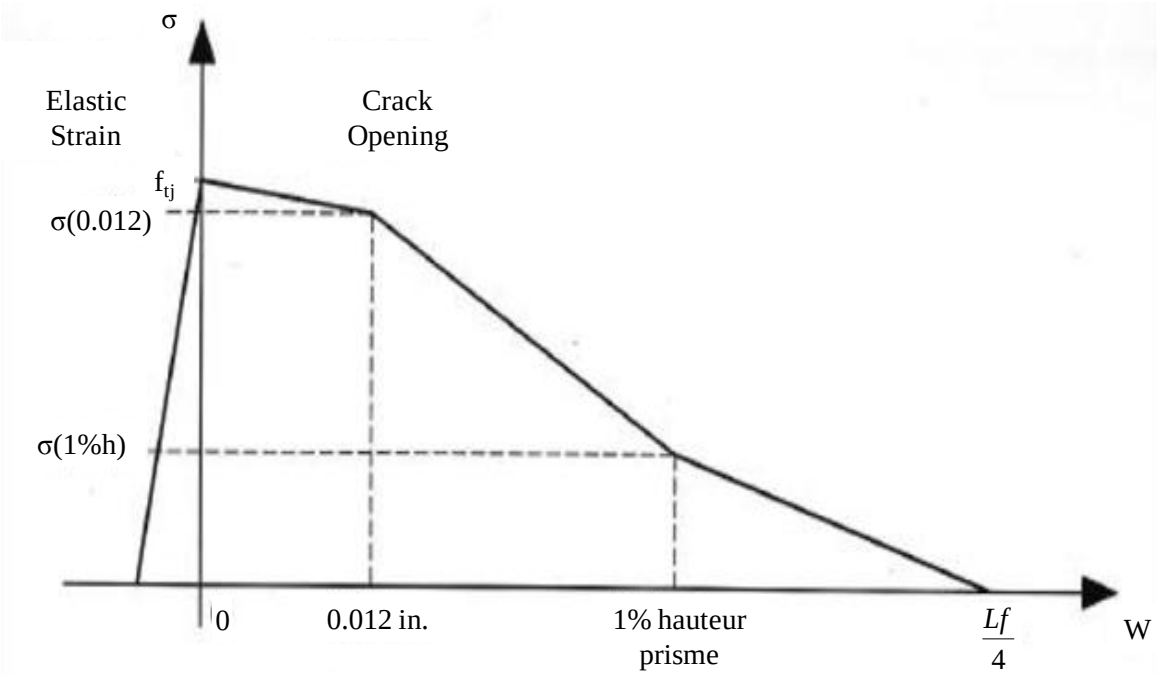

Figure 2-2: Simplified Tensile-Strength Law (after AFGC 2002)

2.3.6. Allowable Driving Stresses

In many cases, a pile may experience the highest tensile stress during driving. AASHTO (2007) limits the compression and tension driving stresses to $0.9f_y$ for H-piles, where f_y is the yield strength of the steel. For concrete piles, Equation 2-5 gives the limit on compression stresses, and Equation 2-6 limits the tension driving stresses.

$$\sigma_c = 0.85f_c' - f_{pe} \quad \text{(psi)} \quad (2\text{-}5)$$

$$\sigma_t = 3\sqrt{f_c'} + f_{pe} \quad \text{(psi)} \quad (2\text{-}6)$$

where: f_c' = concrete compressive strength; and

f_{pe} = effective prestressing after losses.

It is important to control the driving stresses when driving the pile though a hard layer above a weaker soil for concrete piles. As the pile punches through the hard layer during driving, the pile toe experiences less resistance, resulting in large tension stresses in this region. Also, concrete piles are at risk from tensile stresses at the beginning of drive in soft clays due to the compressive stress wave that is reflected up the length of pile as a tension wave.

2.3.7. Standards and Calculation Methods

Because UHPC is a fairly new material, there is no united standard design procedure or recommendations available. Many countries have developed their own recommendations and guides for the design of UHPC structural elements. A brief description of the recommendations from Australia, France, Japan, and the United States are made for each of these countries in this section.

Australia developed design guidelines for using Ductal® in prestressed concrete beams in 1999 based on research completed at the University of New South Wales (Gowripalan and Gilber, 2000). The intentions of these guidelines were made to relate design of members with Ductal® to prestressed structural members. The design limits of Ductal® for preventing tension and compression failure, as well as defining the strength in flexure, shear and torsion, crack control, deflections, fire resistance, fatigue, prestressing losses, and anchorage zones were provided.

France first developed interim recommendations in 2002 and the guide is broken into three main parts: (1) characterize the material performance; (2) structural element design; and (3) durability of the material (BFUP-AFGC 2002). Recommendations for how to perform checks and inspections on finished products are also included. The recommendations allow for designers to predict the behavior of UHPC members that are reinforced, prestressed or not reinforcement.

New AFGC recommendations have been proposed based on major research and feedback to better characterize the characteristics of Ultra High Performance Fiber Reinforced Concrete (UHPFRC) or UHPC (Resplendino 2012). Some of the

recommendations that have been improved are regarding the characterization of fire behavior of UHPC, punching resistance, abrasion, shear resistance, and tensile strength.

Recommendations for High Performance Fiber Reinforced Cement Composites (HPFRCC), which are essentially UHPC, were developed in Japan by the Concrete Committee in the Japan Society of Civil Engineers in 2004 (JSCE 2008). The recommendations satisfy the safety, serviceability, recoverability, and compatibility to the environment performance requirements by proposing methods for uniaxial tensile tests and crack width measurements. Additionally, recommendations were made for the design tensile strength, design tensile strain and design crack width.

The FHWA developed guidelines for the material property characterization of UHPC materials in 2006 (Graybeal 2006). Both experimental phases as well as an analytical phase were completed during the research. Through this research, recommendations were made to define the behaviors of UHPC compared to those of normal concrete.

2.3.8. Tolerances

In order to ensure the quality of UHPC when mixing and pouring, certain tolerances are required. When mixing UHPC at a batch plant, a tolerance of ±2 percent for each weighed ingredient should be used and reduced to ±1 percent for powders (AFGC 2002). The drop height when placing the UHPC should not exceed more than about 1.5-ft to ensure that no segregation or clustering of fibers occurs (AFGC 2002). It is recommended that no delay in-between batches be allowed because a skin can form on the surface of the last concrete layer. If a delay does occur, the two layers must be joined together by raking the interface surface (AFGC 2002).

UHPC is sensitive to ambient temperatures during mixing and thus recommended minimum and maximum temperatures are given for which no additional steps are required. The minimum temperature recommended is 41ºF. If the temperature is below this minimum, additional steps, such as heating the aggregate or mix water, using insulated forms, or using setting or hardening accelerators should be used (AFGC 2002). If the temperature is above 95ºF, precautions similar to those used for normal concrete should be taken (AFGC 2002).

2.4. APPLICATIONS

Since UHPC was developed in the 1990's, it has been used for various applications ranging from designing architectural elements to structural elements. Vande Voort et al. (2008) provides a detailed list of applications for UHPC up until 2008. This section summarizes a few of the applications listed by Vande Voort relative to the control study, and newly completed projects to that list of applications.

2.4.1. Structural Members

2.4.1.1 Bridge Components

Research related to completed or ongoing project on UHPC bridge applications are:

- UHPC joint fill for precast concrete accelerated bridge construction – UHPC was used to fill the voids between the precast abutments and steel H-pile foundations, joints between the precast deck panels, and joints between the precast approach slab panels (Young 2012).
- UHPC waffle deck panel – The benefits of UHPC and precasting were combined to create durable deck and optimize design (Aaleti et al. 2011).
- UHPC to normal concrete deck interface – Developing shear friction interfaces that are appropriate for overlying UHPC on new and existing normal concrete bridge decks (Sritharan et al. 2012).
- UHPC bridge bearings – UHPC was used to create a new generation of sliding bearing joint for bridge applications to replace single steel slide bearings (Hoffman and Weiher 2012)
- Second Generation of JI-shaped girder – The girder was developed for short and medium span highway bridges similar to the prototype UHPC Pi-Girder, but with an increased deck thickness and width, increased web thickness, decreased web spacing and rounded reentrant corners to improve what one to improve on the first generation of girders (Graybeal 2009).
- Super Bridge 200 – The bridge is a cable stayed bridge with the purpose of developing technologies to improve UHPC behavior, construct girders and

plates, construct a UHPC deck, and develop a UHPC cable stayed bridge system (Kim et al. 2012).

2.4.2. Field Implementation

2.4.2.1 Bridges

Several traffic and foot bridges have been constructed around the world using UHPC for design and construction of the structural components. The first of these bridges was the Sherbrooke pedestrian bridge shown in Figure 2-3, which was constructed in Quebec, Canada in July of 1997. It is the world's first pedestrian bridge to have RPC components. The deck and the top and bottom chord of the open-web space trusses were made with RPC that had a 29 ksi compressive strength. The web of the truss contained RPC, but was confined by stainless steel tubes (Blais et al. 1999). To date, two other pedestrian bridges with UHPC structural members have been constructed in Canada (Perry and Seibert 2011).

Figure 2-3: Sherbrooke Pedestrian Bridge, Quebec, Canada (Ductal 2012)

The first UHPC bridge in the United States was a 110-ft single span bridge built in Wapello County, Iowa in 2006 using UHPC bridge beams as shown in Figure 2-4. The bridge project allowed researchers to develop a shear design procedure, evaluate the performance of the UHPC girder, and evaluate the structural performance of the bridge (Wipf et al. 2009).

In Mayenne, France, the Saint Pierre La Cour Bridge was built in 2005 with two lanes for traffic and one lane for pedestrians and is pictured in Figure 2-5. Ductal® was used for the pretensioned beams and thin precast deck. The bridge was designed by VSL & Bouygues

Travaux Publics using the new recommendations for the use of ultra-high strength concretes reinforced with fibres (Behloul 2006).

Figure 2-4: The UHPC Girder Bridge in Wapello County, Iowa (Wipf 2009)

Figure 2-5: Saint Pierre La Cour Bridge in France after Completion (Behloul 2006)

Cat Point Creek Bridge was constructed in 2008, and was the first bridge involving UHPC structural components to be constructed in Richmond County, Virginia. One of the ten spans of the bridge contains UHPC girders, as shown in Figure 2-6, that were monitored over a period for performance compared to the HPC girders for the other nine spans (Ozyildirim 2011).

Jakway Park Bridge was built using UHPC PI-girders in Buchanan County, Iowa. This was the first highway bridge using UHPC batched in a ready-mix truck. The bridge was open to traffic in November of 2008 (PCA 2012). A picture of the Jakway Park Bridge is shown in Figure 2-7.

Figure 2-6: Cat Point Creek Bridge with UHPC Girders on one Span in Virginia (Ductal 2012)

Figure 2-7: Jakway Park Bridge in Iowa using PI-Girders (FHWA 2011)

2.4.2.2 Columns

The Queen Sofia Museum in Madrid, Spain underwent an expansion by adding three new buildings on a support structure consisting of 24 slender steel columns in 2005. To support the new structures Ductal® was poured directly inside of the steel columns (Ductal 2012). Figure 2-8 shows how the UHPC was handled for the onsite mix and pour of the tall thin columns.

Figure 2-8: Onsite Pour for UHPC Columns during Queen Sofia Museum Expansion (Ductal 2012)

2.4.2.3 Other Structures

Due to the superior qualities of UHPC compared to normal concrete, many other structures have been designed and constructed using this material. One example of the innovative uses for UHPC is stairs, which are used at Roissy Airport in Paris and at the Lafarge office in Birmingham. Additionally, the durability of the material makes UHPC a good option for corrosive environments such as the Cattenom Power Plant cooling tower in France, which used UHPC beams and girders to support the structure. Two other structures that have used UHPC are a retained earth anchorage system used in Reunion Island in France and the gold bar troughs at the Gold Bar Wastewater Treatment Plant in Edmonton, Alberta, Canada (Behloul 2008).

2.4.3. Deep Foundations

2.4.3.1 Prefabricated Concrete Sheet Piles

Grünewald (2004) designed prefabricated concrete sheet piles with steel fibers after d developing a self-compacting, fiber-reinforced concrete mix for precast sheet piles. Similar to UHPC, Grünewald limited the length of the steel fibers as well as the maximum aggregate size. Each sheet pile segment was prestressed with eighteen ½-in prestressing strands, with a flange thickness of 2.0 inches and a web thickness of 1.8 inches. Three of the six SCFRC sheet piles that were cast were driven into the ground with a vibratory hammer and it was reported that they performed as expected (Grünewald 2004).

2.4.3.2 UHPC Pile Project - Phase I

As introduced in Section 1.4, a UHPC pile was designed and tested in Phase I of the UHPC pile project at Iowa State University. The cross-section was designed, a prediction of the moment-curvature response was calculated and then verified in the laboratory. After laboratory testing, the pile was field tested as part of Phase I (Vande Voort et al. 2008).

The cross-section of this pile was designed keeping in mind that solid sections would use too much of the expensive UHPC material and hollow sections are difficult to construct. Therefore an H-shaped pile section was explored for designing the UHPC piles. Finally, a

tapered H-shaped section was decided upon taking advantage of the several inherent benefits, as shown in Figure 1-8.

Due to the high compressive strength of UHPC, ten ½-in. diameter 270 ksi low relaxation prestressing strands were used to increase the tensile capacity of the pile. A ¾-in. cover thickness for the ½-in. prestressing strands was used in design based on research at minimum spacing and cover requirements for UHPC. The minimum strand spacing used in the design of the UHPC pile was 2.0-in. center-to-center.

To predict the moment-curvature response for strong-axis bending of the UHPC pile, a section analysis spreadsheet was developed for various axial loads using Microsoft Excel. The results from the analysis were used in LPILE to estimate the behavior of the UHPC pile for the soil conditions at the location of the field test. Seven assumptions were used for the section analysis calculations, which are: (1) plane sections remain plane; (2) prestress losses occur due to only elastic shortening and shrinkage of UHPC; (3) strands have perfect bonding to UHPC outside the transfer regions resulting in the change in strain in the prestressing strands and concrete being equal at a given location; (4) effective prestressing is applied at the centroid of the section; (5) bending only occurs about the major flexural axis; (6) initial prestressing does not induce any inelastic strains on the strands; and (7) axial loads on the pile are applied through the centroidal axes with no eccentricity. The effect of creep was not considered in the section analysis due to the loads during testing having a relatively short duration.

A driveability analysis was conducted using GRLWEAP on the proposed cross-section. The analysis was completed to ensure the driving stresses under various parameters were well below the allowable limits for UHPC. The results for the UHPC pile were compared to the performance of normal concrete (NC), high performance concrete (HPC) and HP 10 x 57 piles.

To characterize moment-curvature response of the UHPC pile section and verify the analysis procedures, two tests on a ¾ scale UHPC test specimen were completed. The first test unit was tested with an axial load of 80 kips and a cyclic lateral load in a push-pull manner. Cracking in the welds of the test setup occurred during testing and resulted in a

slight modification of the test setup for the second test specimen. The second specimen was tested in a similar push-pull protocol but had an increased axial load of 200 kips.

The results from the first laboratory test provided a good correlation between the test results and the predicted moment-curvature response. No reliable curvature data was obtained from the instrumentation of the second specimen due to premature diagonal cracking occurring during the test, which is believed to be caused by the small scale used for the test specimen and lack of steel fibers bridging the cracks. For the design of the ¾ scale test specimen, the fibers were not scaled in size accordingly, which presumably did not allow the fibers to flow freely. The full-scale UHPC pile should allow the fibers to pass more freely to avoid this problem.

Driving stresses calculated using GRLWEAP for a variety of cushions, soils, and driving hammers were found to be well below the allowable stress limits for UHPC piles, resulting in the possible elimination of a pile cushion. UHPC piles exhibited an increased driveability over normal concrete piles due to the reduced cross-sectional area and increased strength characteristics of the material. Through the field testing, it was confirmed that the same driving equipment can be used for UHPC piles as used for steel H-piles of the same size and weight, except for the helmet used to drive the pile.

To verify the potential benefits of UHPC piles for bridge substructure applications, two full-scale 35-ft long UHPC test piles were driven next to a bridge being constructed in Oskaloosa, Iowa. Additionally, a steel HP 10 x 57 test pile was installed and tested to provide a performance comparison. The soil at the site consisted of 15-ft of a loess soil, 20-ft of Pre-Illinoian glacial till, and bedrock with a water table located at approximately 10-ft from the ground surface.

The test piles and reaction frame anchor piles were driven using a DELMAC D19-42 hammer. A lifting hook was cast into the UHPC piles 7-ft from the pile head, but could not be utilized due to the risk of the pile head colliding with the hammer leads. To remedy this problem, a lifting strap was connected to the pile head and to the hammer and helmet. The contractor suggested improving the lifting procedure of the UHPC pile by moving the lifting

hook closer to the pile head. No visible damage to the UHPC pile heads were observed after driving of the test piles.

Once the test piles were installed, a vertical load tests was performed on one of the UHPC test piles. The predicted failure load of both test pile was between 150 kips and 179 kips depending on which method was used to calculate the estimated axial load capacity. A vertical load of 200 kips was applied to the test pile but was not able to fail the pile based on Davisson's Criteria (1972). A second vertical load test was performed on the UHPC test pile which was loaded until 300 kips which was the limit for the test setup. Again, this magnitude of load was unable to fail the UHPC pile. Using an extrapolation of the load test results, the theoretical ultimate load was found to be 368 kips for the second UHPC test pile.

The axial load capacity of the UHPC pile was 86 percent greater than that of the steel HP 10 x 57 pile, as measured from the vertical load test of the steel pile performed in the field. The increase in capacity of the UHPC pile was attributed to the increased cross-sectional area of the UHPC pile and possible increase in perimeter when compared to the steel test pile, resulting in an increased toe resistance and skin friction. It was determined that it may be possible to reduce the length or number of UHPC piles in comparison to HP 10 x 57 piles in bridges due to the increased capacity.

Following the vertical load tests, the two UHPC test piles were then used for a lateral load test. A horizontal actuator was positioned between the two UHPC test piles so that both could be tested simultaneously. Each test pile was subjected to a lateral load so that the pile sections were subjected to bending about the strong-axis direction. LPILE was used to predict the maximum lateral load that the test piles would develop in the soil before experiencing structural failure or exceed the limitations set by the equipment used.

Shear failure occurred in one of the tests piles at 22.8 kips which was much less than the predicted ultimate lateral load for the UHPC test piles. The reason given for the failure of the first test pile was thought to be that the critical section for shear was weakened by a significant portion of the web rendered ineffective due to the instrumentation bundle passing through the location. As a result of the first test pile failure, the second test pile was not pushed to failure because the displacement could not be increased past 2.54 inches.

2.5. PILE DESIGN METHOD

Typically for integral bridges, a single row of piles are used to support the abutments (Iowa DOT 2011). Thus, the pile is designed based on the capacity of a single pile and not a group because there is sufficient distance between piles.

2.5.1. Geotechnical Resistance

There are many different static methods used to design the ultimate capacity of single piles. Commonly, all of the methods use the same basic equations to calculate the ultimate bearing capacity of a single pile which are given in Equations 2-7 through 2-9.

$$Q_u = R_s + R_t \quad \text{(Hannigan et al. 2006)} \quad (2\text{-}7)$$

$$R_s = f_s A_s \quad (2\text{-}8)$$

$$R_t = q_t A_t \quad (2\text{-}9)$$

where: Q_u = ultimate bearing capacity;
R_s = shaft resistance;
R_t = toe bearing resistance;
f_s = unit shaft resistance;
A_s = pile shaft surface area;
q_t = unit toe resistance; and
A_t = pile toe area.

The methods have developed different approaches to calculate f_s and q_t. Fequently used Methods that have been developed for cohesionless soils are the Meyerhof Method (Meyerhof 1976), Brown Method (Brown et al. 2001), Nordlund Method (Nordlund 1963), Effective Stress Method (Fellenius 1991), L.P.C. Method (Bustamante and Gianeselli 1983), and Nottingham and Schmertmann Method (Nottingham and Shmertmann 1975). Additionally, methods that have been developed for cohesive soils are the Total Stress – α-Method (Tomlinson 1994), Effective Stress Method (Fellenius 1991), and λ-Method (API 1993). A detailed description of the methods and how to calculate f_s and q_t are given by Hannigan et al. (2006). The Iowa Blue Book Method (Iowa DOT 2011) was used for design

of the test and production piles during this portion of the research project and is outlined here.

Table 2-3 shows the recommended nominal resistance values for end bearing of steel H-piles, prestressed concrete piles, and steel pipe piles. Based on Standard Penetration Test (SPT) data from the site and type of pile used, the R_t value can be found using Equation 2-9. When Table 2-3 has square brackets around the number, the value given is q_t and should be used in conjunction with Equation 2-9. To calculate R_s, Table 2-4 and Table 2-5 are used along with Equation 2-10.

$$R_s = f_s^* l \tag{2-10}$$

where: f_s^* = unit shaft resistance, kips/ft; and

l = length of soil layer.

The Iowa DOT (2011) uses Equation 2-11 to design the pile to satisfy the design requirements for a downward load. The Iowa Highway Research Board recently sponsored a project to calibrate resistance factors for the state of Iowa. The interim soil resistance factor is taken as 0.725. AbdelSalam et al. (2012) made recommendations for improved resistance factors for the Iowa Blue Book Method that accounted for construction control and setup. Table 2-6 includes the recommended resistance factors based on soil type, construction control and setup.

Table 2-7 provides guidelines to assist in classifying the soil type.

$$\sum \eta_i \gamma_i P_i \leq \varphi_c Q_u \tag{2-11}$$

where: $\sum \eta_i \gamma_i P_i$ = total factored load per pile;

γ_i = average load factor, γ_i = 1.45;

η = number of piles; and

φ_c = soil resistance factor.

Table 2-3: LRFD Driven Pile Foundation End Bearing Geotechnical Resistance Chart (after Iowa DOT 2011)

Soil Description	Blow Count		Estimated Nominal Resistance Values for End Bearing Pile in Kips [ksi]										
	N-Value		Wood Pile[1],[3]	Steel "H" Grade 50			Prestressed Concrete[2]			Steel Pipe[4]			
	Mean	Range		10	12	14	12	14	16	10	12	14	18
Granular Material													
	<15	---	[5]	[5]	[5]	[5]	[5]	[5]	[5]	[5]	[5]	[5]	[5]
Fine or medium sand	15	---	32	[5]	[5]	[5]	60	84	108	32	48	64	108
Coarse sand	20	---	44	[5]	[5]	[5]	84	116	148	44	64	88	144
Gravelly sand	21	---	44	[5]	[5]	[5]	84	116	148	44	64	88	144
	25	---	56	[5]	[5]	[5]	[6],[7]	[6],[7]	[6],[7]	[7]	[7]	[7]	[7]
	---	25-50	[6]	[2-4]	[2-4]	[2-4]	[7]	[7]	[7]	[7]	[7]	[7]	[7]
	---	50-100	[6]	[4-8]	[4-8]	[4-8]	[6]	[6]	[6]	[7]	[7]	[7]	[7]
	---	100-300	[6]	[8-16]	[8-16]	[8-16]	[6]	[6]	[6]	[7]	[7]	[7]	[7]
	---	>300	[6]	[18]	[18]	[18]	[6]	[6]	[6]	[7]	[7]	[7]	[7]
Bedrock													
	---	100-200	[6]	[12]	[12]	[12]	[7]	[7]	[7]	[7]	[7]	[7]	[7]
	---	>200	[6]	[18]	[18]	[18]	[7]	[7]	[7]	[7]	[7]	[7]	[7]
Cohesive material													
	12	10-50	16	[5]	[5]	[5]	28	40	52	16	24	62	52
	20	---	24	[1]	[1]	[1]	44	64	84	28	36	52	84
	25	---	32	[2]	[2]	[2]	60	84	108	32	48	64	108
	50	---	[6]	[4]	[4]	[4]	116[6]	164[6]	212[6]	56	96	128	212
	100	---	[6]	[7]	[7]	[7]	[6]	[6]	[6]	[6]	[6]	[6]	[6]

Table notes: (1) Wood piles shall not be driven through soils with N > 25; (2) With prestressed concrete piles the preffered N for soil at the tip ranges from 25 to 35. Prestressed concrete piles have been proven to be difficult to drive in very firm glacial clay and very firm sandy glacial clay. Prestressed concrete piles should not be adjusted for a different tip area; (3) End bearing resistance values for wood piles are based on a tip area of 72 in^2. Values shall be adjusted for a different tip area; (4) Steel pipe piles should not be driven in soils with consistent N > 40. See the 1994 soils information chart [BDM 6.2.1.5] for end bearing when a conical driving point is used; (5) Do not consider end bearing; (6) Use of end bearing is not recommended for timber piles when N > 25 or for prestressed concrete piles when N > 35 or for any condition identified with this note; and (7) End bearing resistance shall be 0.0389 x N value [ksi].

Table 2-4: LRFD Driven Pile Foundation Friction Geotechnical Resistance Chart for Alluvium (after Iowa DOT 2011)

Soil Description	Blow Count		Estimated Nominal Resistance Values for Friction Pile in kips/foot										
	N-Value		Wood Pile[(1),(3)]	Steel "H" Grade 50			Prestressed Concrete			Steel Pipe			
	Mean	Range		10	12	14	12	14	16	10	12	14	18
Alluvium													
Very soft silty clay	1	0-1	0.8	0.4	0.8	0.8	0.8	0.8	0.8	0.4	0.4	0.4	0.8
Soft silty clay	3	2-4	1.2	0.8	1.2	1.2	0.8	0.8	0.8	0.8	0.8	0.8	1.2
Stiff silty clay	6	4-8	1.6	1.2	1.6	2.0	1.2	1.6	2.0	1.2	1.2	1.6	2.0
Firm silty clay	11	7-15	2.4	2.0	2.4	2.8	2.4	2.8	3.2	1.6	2.0	2.4	2.8
Stiff silt	6	3-7	1.6	1.2	1.6	1.6	1.6	1.6	1.6	1.2	1.2	1.6	1.6
Stiff sandy silt	6	4-8	1.6	1.2	1.6	1.6	1.6	1.6	1.6	1.2	1.2	1.6	1.6
Stiff sandy clay	6	4-8	1.6	1.2	1.6	2.0	2.0	2.0	2.4	1.2	1.6	1.6	2.0
Silty sand	78	3-13	1.2	1.2	1.2	1.6	1.6	1.6	1.6	0.8	0.8	1.2	1.6
Clayey sand	13	6-20	2.0	1.6	2.0	2.8	2.4	2.4	2.8	1.6	2.0	2.4	2.8
Fine sand	15	8-22	2.4	2.0	2.4	2.8	2.4	2.8	3.2	1.6	2.0	2.4	2.8
Coarse Sand	20	12-28	3.2	2.8	3.2	3.6	3.2	3.6	4.0	2.0	2.4	2.8	3.6
Gravely sand	21	11-31	3.2	2.8	3.2	3.6	3.6	3.6	4.0	2.0	2.4	2.8	3.6
Granular material	> 40	---	[(2)]	4.0	4.8	5.6	[(2)]	[(2)]	[(2)]	[(2)]	[(2)]	[(2)]	[(2)]

Table notes: (1) For double entries the upper value is for an embedded pile within 30 feet of the natural ground elevation, and the lower value [ ] is for depths more than 30 feet below the natural ground elevation; (2) Do not consider the use of this pile type for this soil condition, wood with N > 25, prestressed concrete with N > 35, or steel pipe with N > 40; and (3) Prestressed concrete piles have proven difficult to drive in these soils. Prestressed piles should not be driven in glacial clay with consistent N > 30 to 35.

Table 2-5: LRFD Driven Pile Foundation Friction Geotechnical Resistance Chart for Glacial Clay (after Iowa DOT 2011)

Soil Description	Blow Count		Estimated Nominal Resistance Values for Friction Pile in kips/foot										
	N-Value		Wood Pile[1],[3]	Steel "H" Grade 50			Prestressed Concrete			Steel Pipe			
	Mean	Range		10	12	14	12	14	16	10	12	14	18
Glacial Clay													
Firm silty glacial clay	11	7-15	2.8	2.4	2.8	3.2	2.8	3.2	3.6	2.0	2.4	2.4	3.2
Firm clay (gumbotil)	12	9-15	2.8	2.4	2.8	3.2	2.8	3.2	3.6	2.0	2.4	2.4	3.2
Firm glacial clay[1]	11	7-15	2.4 [3.2]	2.8 [3.2]	3.2 [4.0]	3.6 [4.4]	3.2 [4.0]	3.6 [4.4]	4.0 [4.8]	2.0 [2.4]	2.4 [2.8]	2.8 [3.2]	3.6 [4.4]
Firm sandy glacial clay[1]	13	9-15	2.4 [3.2]	2.8 [3.2]	3.2 [4.0]	3.6 [4.4]	3.2 [4.0]	3.6 [4.4]	4.0 [4.8]	2.0 [2.4]	2.4 [2.8]	2.8 [3.2]	3.6 [4.4]
Firm –very firm glacial clay[1]	14	11-17	2.8 [3.6]	2.8 [4.0]	3.2 [4.8]	3.6 [5.6]	4.0 [4.8]	4.4 [5.2]	4.8 [5.6]	2.4 [3.2]	2.8 [3.6]	3.2 [4.0]	4.0 [5.2]
Very firm glacial clay[1]	24	17-30	2.8 [3.6]	2.8 [4.0]	3.2 [4.8]	3.6 [5.6]	3.2[3] [4.8]	3.6[3] [5.6]	4.4[3] [6.4]	2.4 [3.2]	2.8 [3.6]	3.2 [4.0]	4.0 [5.2]
Very firm sandy glacial clay[1]	25	15-30	3.2 [4.0]	2.8 [4.0]	3.2 [4.8]	3.6 [5.6]	3.2[3] [4.8]	3.6[3] [5.6]	4.4[3] [6.4]	2.4 [3.2]	2.8 [3.6]	3.2 [4.0]	4.0 [5.2]
Cohesive or glacial material[1]	> 35	---	[2]	2.8 [4.0]	3.2 [4.8]	3.6 [5.6]	[2]	[2]	[2]	2.0[4] [3.2]	2.4[4] [4.0]	2.8[4] [4.4]	3.6[4] [5.6]

Table notes: (1) For double entries the upper value is for an embedded pile within 30 feet of the natural ground elevations, and the lower value [ ] is for depths more than 30 feet below the natural ground elevation; (2) Do not consider the use of this pile type for this soil condition, wood with N > 25, prestressed concrete with N > 35, or steel pipe with N > 40; (3) Prestressed concrete piles have proven difficult to drive in these soils. Prestressed piles should not be driven in glacial clay with consistent N > 30 to 35; and (4) Steel pipe piles should not be driven in soils with consistent N > 40.

Table 2-6: Resistance Factors for Single Pile in Axial Compression (Green et al. 2012)

Theoretical Analysis[c]	Construction Control [a]					Resistance Factor [b]				
	Driving Criteria Basis		PDA/CAPWAP	Retap Test 3-Days After EOD	Static Pile Load Test	Cohesive			Mixed	Non-Cohesive
	Iowa DOT ENR Formula	WEAP				ϕ	ϕ_{EOD}	ϕ_{setup}	ϕ	ϕ
Iowa Blue Book	Yes	-	-	-	-	0.60	-	-	0.60	0.50
	-	Yes[d]	-	-	-	0.65	-	-	0.65	0.55
			Yes	-	-	0.70[e]	-	-	0.70	0.60
				Yes	-	0.80	-	-	0.70	0.60
			-	-	Yes	0.80	-	-	0.80	0.80

Table notes: (a) Determine the construction control that will be specified on the plans to achieve the target nominal driving resistance; (b) Resistance factors presented in Table E1 are for redundant pile groups (minimum of 5 piles); (c) Use BDM Article 6.2.7 to estimate the theoretical nominal pile resistance, based on the Iowa Blue Book; (d) Use the Iowa Blue Book Soil input procedure to complete WEAP analysis; and (e) Setup effect has been included when WEAP is used to establish driving criteria and CAPWAP is used as a construction control.

Table 2-7: Soil Classification Method (Green et al. 2012)

Generalized Soil Category	AASHTO	USDA Textural	BDM 6.2.7 Geotechnical Resistance Chart	
Cohesive	A-4, A-5, A-6, and A-7	Clay Silty clay Silty clay loam Silt Clay loam Silt loam Loam Sandy clay	Loess	Very soft silty clay
				Soft silty clay
				Stiff silty clay
				Firm silty clay
				Stiff silt
				Stiff sandy clay
			Glacial Clay	Firm silty glacial clay
				Firm clay (gumbotil)
				Firm glacial clay
				Firm sandy glacial clay
				Firm-very firm glacial clay
				Very firm glacial clay
				Very firm sandy glacial clay
				Cohesive or glacial material
Non-Cohesive	A-1, A-2, and A-3	Sandy clay Loam Sandy loam Loamy sand Sand	Alluvium or Loess	Stiff sandy silt
				Silty sand
				Clayey sand
				Fine sand
				Coarse sand
				Gravelly sand
				Granular material (n > 40)

2.5.2. Structural Resistance

Vande Voort et al. (2008) summarize the compressive stress limits used between 1983 to 2008 by the state DOT's, AASHTO, and American Society of Civil Engineers (ASCE) for steel H-piles and precast, prestressed concrete piles. Specifically, Table 2-8 outlines the current compressive stress limits for steel H-piles and precast, prestressed concrete piles used by the Iowa DOT which still follow AASHTO ASD.

Table 2-8: Compressive Stress Limits for Steel H-Piles in Precast, Prestressed Concrete Piles in Iowa (Iowa DOT 2011)

Steel H-Pile	Precast, Prestressed Concrete Piles
6.0 ksi – typical design	$0.33f_c' - 0.27f_{pe}$ (For 12-in. square pile only)
9.0 ksi – design stress allowed for end bearing piles on rock with SPT N-values of 100-200 or combinded end bearing and friction piles on rock with N-values ≥ 200	
12.0 ksi – design stress is permitted for the same cases as above, except it may only be used for piers and with approval from the soil Soil Design Section and Assistant Bridge Engineer.	

2.6. INTEGRAL ABUTMENTS

Integral bridges are bridges that have no movement joints and have foundations that accommodate the superstructure deformation due to temperature, creep, and shrinkage effects causing the bridge to expand or contract with time (Kamel et al. 1996). The changes in length cause the bridge to increase and decrease which results in a push-pull effect on abutments and pile heads. To minimize the cost of construction and maintenance, the Iowa DOT prefers to use integral abutments whenever possible in design (Iowa DOT 2011).

2.6.1. Current Integral Abutment Design Guidelines

Many research projects were conducted to provide maximum bridge lengths for integral abutment bridges. One such study was completed by Dicleli and Albhaisi (2003) and gives the recommendations based on climate as shown in Table 2-9. Abendroth and Greimann (2005) recommended including a prebore hole filled with a material that has low stiffness and orienting the piles such that they are subjected to weak-axis bending during bridge movement on how to achieve this such as having to improve the performance of the foundations in integral abutments.

Typically, each state DOT has developed its own design guidelines, including for integral abutments. Table 2-10 briefly summarizes the integral abutment guidelines for eight state DOTs. When comparing the recommendations by Dicleli and Albaisi (2003) to the maximum bridge length limits for HP 10 x 57 steel piles in Iowa, the maximum bridge length for steel bridges in Iowa is about 13 percent less in the study and 10 percent less for concrete bridges than recommended by Dicleli and Albaisi (2003). The Minnesota DOT uses a maximum bridge length for integral abutments 35 percent lower than the value given in the study by Dicleli and Alnaisi (2003) for steel bridges and 53 percent lower for concrete bridges.

Table 2-9: Recommendations for Maximum Bridge Length (after Dicleli and Albaisi 2003)

Pile Size	Steel Bridges		Concrete Bridges	
	Moderate Climate Length (ft)	Cold Climate Length (ft)	Moderate Climate Length (ft)	Cold Climate Length (ft)
HP 12 x 84	722	476	1050	869
HP 12 x 74	673	443	984	820
HP 10 x 57	525	461	787	640

Minnesota does not differentiate between types of bridges and none of the DOTs appear to differentiate between size and type of pile used for the guidelines given in Table 2-10. Additionally, not all DOTs specify the maximum skew, prebore holes, or orientation of the pile in integral bridges. Consequently, it may be stated that the design guidelines for many DOTs, with regards to integral abutments, can be improved to help reduce construction and maintenance costs.

2.6.2. Long-Term Field Monitoring

When monitoring an integral bridge, it should be realized that many factors influence the continuous movement of the bridge superstructure and substructure. A parametric study was completed by Huang et al. (2004) that looked at many variables and validated their effects on integral abutments through long-term monitoring of an integral abutment. Some of the key variables noted in this study were pile orientation, soil conditions, predrilled holes, pile head condition, and bridge length. Findings from this parametric study are:

- H-piles in strong-axis bending improve the piles performance, but increase the concrete tensile stresses in the superstructure;

- Stiffer soils cause larger stresses in the superstructure and piles.
- Prebored holes are effective at reducing the stresses in the superstructure and piles;
- A hinged connection at the pile head may cause the stresses in the superstructure to decrease, but rotation of the pile cap may cause large pile curvatures during expansion and contraction of the bridge; and
- Increases in bridge length increase the stresses the superstructure develops correspondingly.

Abendroth and Greimenn (2005) also recommended that the abutment piles have a weak-axis orientation to provide the least resistance to the longitudinal expansion and contraction of the bridge superstructure.

Table 2-10: Summary of Eight DOT Design Guidelines for Integral Abutments

State	Girder Type	Max Bridge Length limit, ft	Max. Skew, °	Prebore Hole Length, ft	Pile Orientation	Reference
IA	Concrete Steel	575 400	45	10	0 to 30° skew: Parallel to abutment 31 to 45° skew: weak-axis bending	Iowa DOT 2011
NY	Concrete Steel	330	45	8	Weak axis bending	NYSDOT 2011
ME	Concrete Steel	330 200	25	-	Weak axis bending	MaineDOT 2003
MA	Concrete Steel	590 330	30	10	Web parallel to centerline of the abutment	MassDOT 2009
RI	Concrete Steel	600 350	30	10	Weak axis bending	Rhode Island DOT 2007
VT	Concrete Steel	695 395	20	-	Weak axis bending	VTrans 2008
CO	Concrete Steel	790 640	-	-	-	CDOT 2009
MN	Concrete Steel	300	45	-	-	Minnesota DOT 2011

In a few studies as listed in Table 2-11, integral bridges were continuously monitored in the field for long periods of time to determine the performance of integral abutments. In these investigations, long-term monitoring programs measured bridge temperatures, longitudinal displacement, soil pressures behind the abutments, strains in the bridge girders, vertical rotation of the abutments, and vertical-temperature gradients through the depth of the bridge girders (Abendroth and Greimann 2005). In most of these studies, an analytical model was validated by the performance of the monitored bridge.

In many instances, the movement of one integral abutment in a bridge does not equal the movement of the integral abutment on the other side (Abendroth and Greimann 2005 and Jorgenson 1983). Abendroth et al. (2007) found the reasons for these phenomena to be due to the difference in soil type, compaction of backfill, moisture content of backfill, vertical alignment of the roadway, geometric configuration of the bridge, and the bridge pitch at the two abutments. Another common finding from this study is that the contraction mode of displacement for the bridge induces slightly higher stresses than for the expansion displacements (Duncan and Arsoy 2003).

The seasonal expansion and contraction of integral abutment bridges are controlled by the ambient temperature, solar radiation, and relative humidity (Huang et al. 2004). Expansion is when the bridge elongates and is generally assigned the sign convention of positive displacement, while contraction is when the bridge shortens and is assigned a negative displacement.

Through long-term monitoring, it was discovered that longitudinal displacement due to thermal effects are present in a dominant cycle as a result of the seasons, but also a much smaller daily or weekly fluctuation can be visible (Girton et al. 1991). Typically the abutment tends to rotate away from the river or road the bridge is spanning during the warmer months due to the expansion of the bridge superstructure (Huang et al. 2004). These movements of the bridge cause the bridge to rotate in the vertical direction. The vertical rotations found in integral abutments are responsible for shifting the moments lower into the pile, which was confirmed by Hassiotis (2007) by monitoring the Scotch Road Bridge.

Table 2-11: Summary of Long-Term Monitoring of Integral Abutment Bridges

Name	Length, ft	Skew, °	Girder Type	Prebore Hole Length, ft	Longitudinal Displacement, in		Rotation, °	Pile Orientation	Reference
					Contraction	Expansion			
Boone River Bridge	324.5	45	Concrete	9	1.2	0.8	-	Weak-axis	Girton et al. 1991
Maple River Bridge	320	30	Steel	12	1.6	0.9		Weak-axis	
Bridge #55555 (North)	216.5	0	Concrete	None	1.41	0.3	0.11	Weak-axis	Huang et al. 2004
Bridge #55555 (South)	216.5	0	Concrete	None	1.98	0.3	0.095	Weak-axis	
Tama County Bridge, West	110	20	Concrete	None	negligible		-	Weak-axis	Abendroth et al. 2007
Tama County Bridge, East	110	20	Concrete	None	0.11	0.043	-	Weak-axis	
Guthrie County Bridge	318	30	Concrete	10	1.25	0.5	-0.056 to 0.032	Weak-axis	Abendroth and Griemann 2005
Story County Bridge	201.3	15	Concrete	8	1.3	0.46	-0.014 to 0.061	Weak-axis	
Mississinewa River Bridge	367	8	Concrete	None	0.59	0	1.5	Weak-axis	Frosch et al. 2005
Orange-Wendell Bridge, North	270		Steel	10	0.5	0.18	-0.15 to 0.13	Weak-axis	Bonczar et al. 2005
Orange-Wendell Bridge, South	270		Steel	10	0.28	0.34	-0.15 to 0.1	Weak-axis	
Scotch Road Bridge	298	15	Steel	0	0.5	0.55	-0.07 to 0.1	Weak-axis	Hassiotis 2007
Knox County Bridge	415.92	59.09	Steel	0	0.781		0.013	Strong-axis	Oesterle and Lotfi 2005

Typically when modeling the integral connection between abutment and pile head, the piles are assumed to behave in a fully fixed manner. Arsoy et al. (2002) found that the measured stresses in steel H-piles and pipe piles were about half of the theoretical stresses of fully fixed head piles, implying that the piles might not be fully fixed at the pile-to-abutment interface.

The skew of the bridge is also another factor that influences the behavior of the integral abutment. Many DOTs have maximum limits on the allowed skew for an integral abutment. Through long-term monitoring it was found that if a large skew is present in a bridge, the designer can expect the bridge to rotate in plane about the vertical axis as the bridge expands and contracts with temperature (Abendroth et al. 2007).

Duncan and Arsoy (2003) found by modeling the performance of the piles for integral abutments, the approach fill significantly reduces the loads on the pile. As the abutment expands and contracts due to the bridge movements, the approach fill is dragged across the top of the soil foundation, thus inducing a displacement in the foundation soil and reducing the relative displacement between the pile and the foundation soil. When not considering the effect of approach fill for modeling, it is considered conservative.

In many of the long-term field monitoring studies, strains were measured along the length of the piles in the integral abutments. Abendroth and Greimann (2005) found that the strains in the H-piles for the Guthrie County Bridge exceeded the yield strain of steel. Additionally, the Story County Bridge had pile strains that were smaller, but adding the combination of dead, live and impact loads on the superstructure of the bridge, a portion of the pile flange would exceed the yield strain of steel.

2.7. PILE ANALYSIS

To predict the performance of UHPC piles in the field, computer software was used to measure the response of the pile when subjected to lateral loading and the response during driving. This section summarizes the basic principles used in LPILE and GRLWEAP, which were used in this study.

2.7.1. LPILE

LPILE is a computer program created by Ensoft, Inc. to analyze a pile under lateral loading (Ensoft, 2004). Common types of piles subjected to lateral load are transmission towers, offshore structures, bridge foundations, overhead sign foundations, retaining walls, wind generators, poles, anchorages and marine piers. Specifically for this research, the lateral loads influence on pilesdue to the expansion and contraction of integral bridges are considered. Many parametric studies using LPILE have been completed in the past. One such study completed by Huang (2004) was mentioned above in Section 2.6.2.

The way LPILE analyzes a pile under a lateral load is by using the concept of Winkler analysis. Figure 2-9 illustrates the model used within LPILE. The pile and soil are broken up into a specified number of layers. The soil within each layer is modeled using springs controlled by p-y curves allowing for the simulation of nonlinear materials. To solve for the nonlinear response of a laterally loaded pile, a fourth-order differential equation was developed by Hetenyi (1946) and is given in Equation 2-12. Figure 2-10 illustrates the element form of a beam-column that LPILE uses to solve the differential equation by using the finite difference method where the moments can be positive or negative.

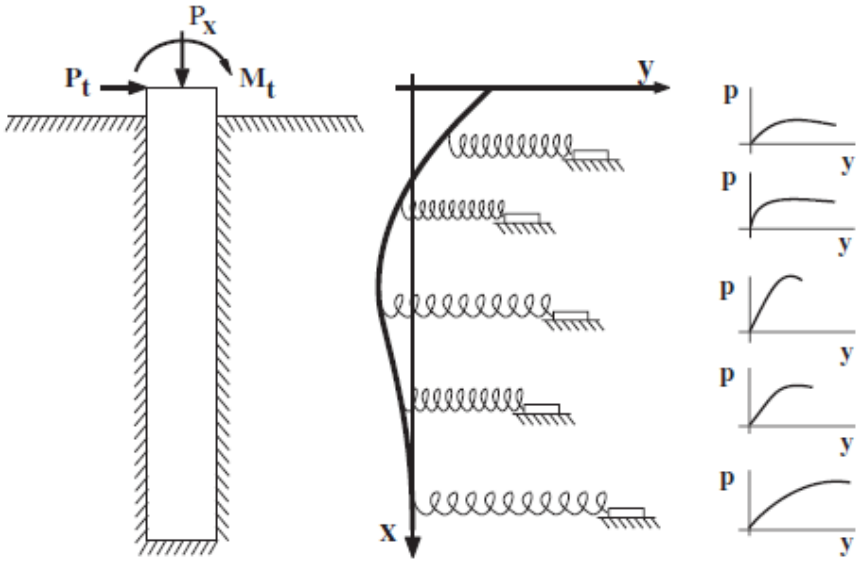

Figure 2-9: Model of a Pile Subjected to Loading (Ensoft, Inc. 2004)

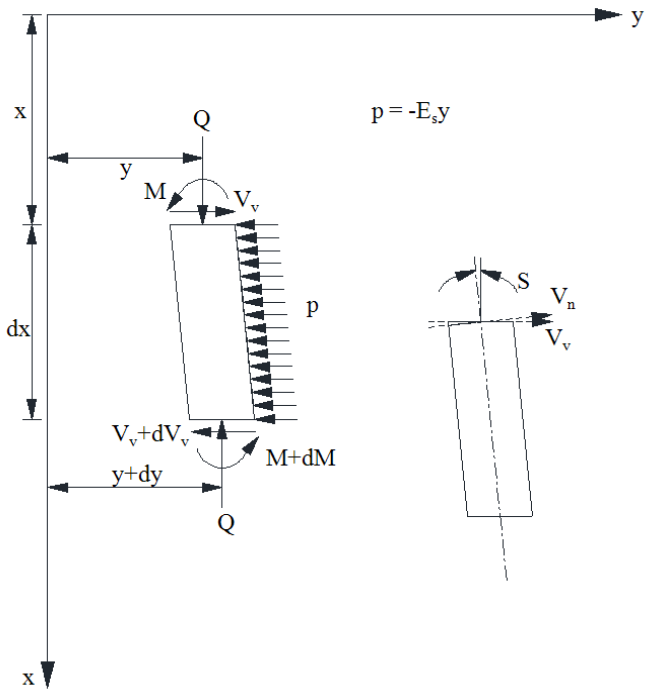

Figure 2-10: Element Form Beam-Column (after Hetenyi 1946)

$$EI\frac{d^4y}{dx^4} + Q\frac{d^2y}{dx^2} - p + W = 0 \qquad (2\text{-}12)$$

where: EI = flexural rigidity;

y = lateral deflection of the pile at a point X along the length of the pile;

Q = axial load on the pile;

p = soil reaction per unit length; and

W = distributed load along the length of the pile.

Assumptions made within LPILE by Reese et al. (2004) for a lateral load analysis are:

- The pile is straight and has a uniform cross section;
- The pile has a longitudinal plane of symmetry with the load and reactions lying in that plane;
- The pile material is homogeneous;

- The proportional limit of the pile material is not exceeded;
- The modulus of elasticity of the pile material is the same in tension and compression;
- Transverse deflections of the pile are small;
- The pile is not subjected to dynamic loading;
- Deflections due to shearing stresses are small; and
- The magnitude of the axial load is constant with depth.

The last assumption listed above is not strictly true. However, typically the maximum bending moment occurs close to the ground surface where the axial load is relatively unchanged. If there is concern about allowing this last assumption, the axial load can be varied along the length of the pile by including additional input values though a very lengthy iterative procedure.

Along the length of the pile, LPILE uses Equation 2-13 to calculate shear, Equation 2-14 to calculate moment and Equation 2-15 to calculate slope for each beam-column element.

$$V = EI\frac{d^3y}{dx^3} + Q\frac{dy}{dx} \tag{2-13}$$

$$M = EI\frac{d^2y}{dx^2} \tag{2-14}$$

$$S = \frac{dy}{dx} \tag{2-15}$$

where V = shear in the pile;
M = bending moment in the pile; and
S = slope of the elastic curve defined by the axis of the pile.

To perform a typical lateral load analysis within LPILE, the user would need to input the analysis type, pile properties, loading type, pile head boundary conditions and soil conditions. After the analysis is run, the user can obtain the shear, bending moment, and displacement along the length of the pile in a text or graphical file as output.

2.7.2. GRLWEAP

One of the most common computer programs used by the DOTS to perform a wave equation and driveability analysis is GRLWEAP. The current GRLWEAP program was developed from the WEAP program that was created in 1976 by Goble, Rausche, and Likins (PDI 2005). The program simulates the motions and forces attributed with driving of a foundation pile by various types of hammers using a numerical solution. To complete these calculations time is divided into small intervals. It is assumed that all velocities, forces and displacement will have constant values during each interval, and the velocities, forces and displacements at each interval will differ from the previous interval by just enough to represent the change occurring between intervals (Smith 1960).

Figure 2-11 illustrates the model of the hammer, pile and soil system during driving within GRLWEAP. W_1 and W_2 represent the weight of the hammer and the weight of the helmet, respectively. The hammer cushion is represented as k_1 and is assumed to have no weight. The pile is modeled by using a series of weights and springs representing the weight and stiffness of the pile, respectively.

The soil resistance is modeled by upward forces on each segment of the pile shown in Figure 2-11 by the symbol, R_i. Dashpots labeled J_i represent the damping within the soil. J_i takes into account the increase in soil resistance as the soil experiences a rapidly applied displacement compared to a slower displacement. Figure 2-12 represents the resistance-displacement diagram for the modeled soil.

The process of developing the driving forces are represented by the hammer striking the hammer cushion that develops a displacement corresponding to the stiffness of the spring used to model it. This displacement causes a force in the spring that accelerates the weight of the helmet, causing a displacement of the helmet, which then displaces the spring. The process continues along the length of the pile. To accurately calculate the stresses in each increment of pile, a sufficiently small time interval must be used. Smith (1960) recommends using 0.00025 second time interval for steel and timber piles and increases the time interval to 0.00033 seconds for concrete piles.

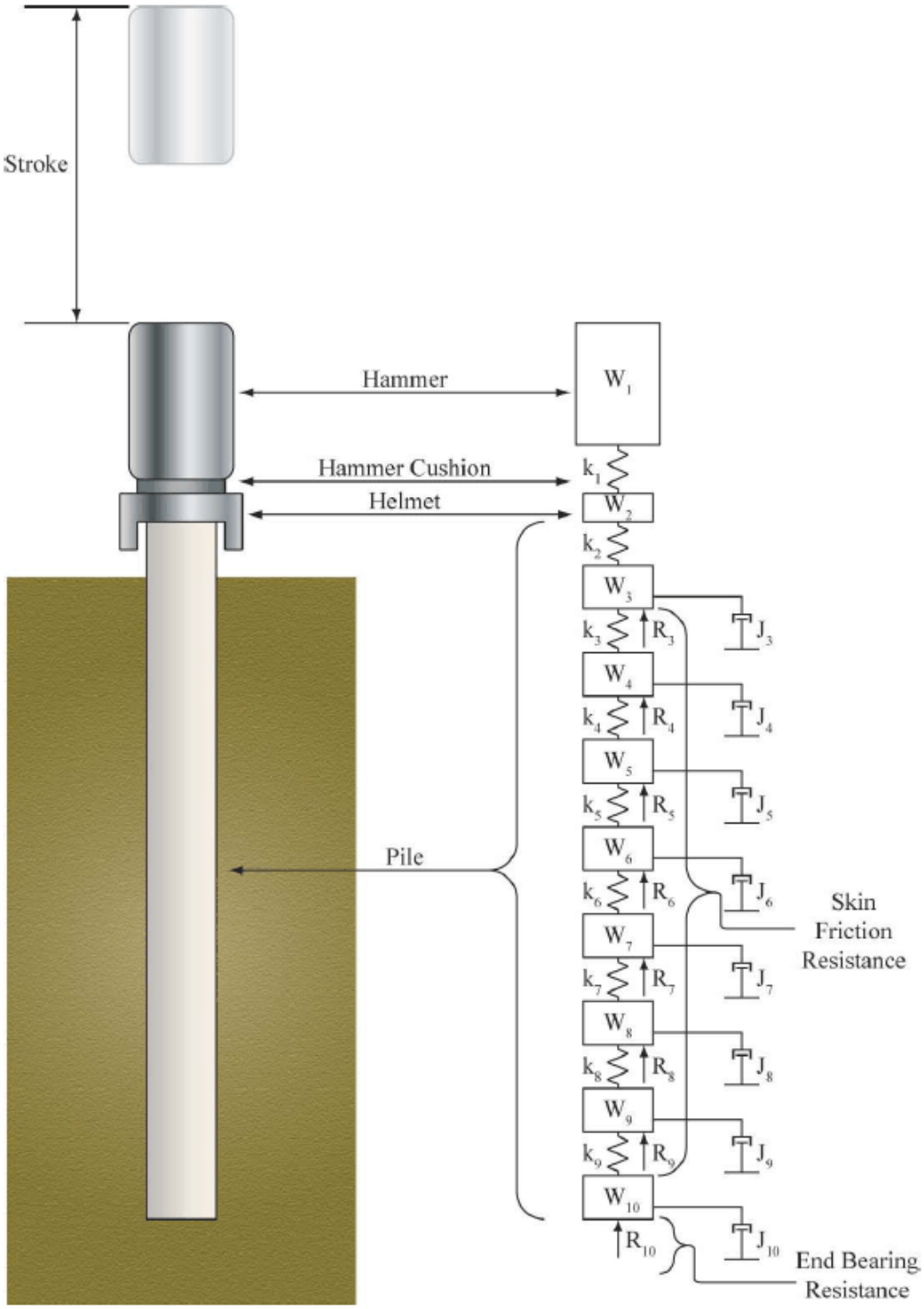

Figure 2-11: Model of Hammer, Pile and Soil used in the Wave Equation Analysis (Vande Voort et al. 2008)

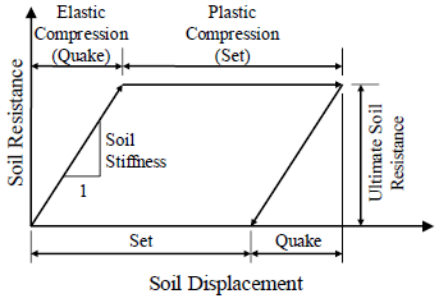

Figure 2-12: Soil Resistance-Displacement Relationship for Wave Equation Analysis (Vande Voort et al. 2008)

Input information that is required to run a wave equation analysis is hammer data, driving system data, pile data, and soil information. A library of hammer information is available for use within the program based on manufacturer specifications. If a special hammer is used, a new hammer can be added to the program. The driving system data includes information about the hammer cushion, helmet and pile cushion. The pile data required to run the analysis is total length, cross sectional area, elastic modulus, and specific weight as a function of depth. Information about the soil that is needed is input information about each soil layer which can include SPT N-values, water level, damping factors, and quake factors. Recommended input values for quake and damping factors are given by Smith (1960), GRL Engineers (2001) and Dirks and Kam (2003).

The solution for the wave equation goes through a calculation process by computing the forces, displacements, and velocities of each segment of the driving system at each time interval. The force, displacement, and velocities are assumed constant for each time interval and are used to calculate the new values for the next time interval. The calculation process goes through Equations 2-16 through 2-23 for each segment, m, at each time interval, n (Smith 1960).

$$V_{Impact} = \sqrt{\frac{2E_h \emptyset g}{W_1}} \tag{2-16}$$

$$D_m = d_m + v_m(10\Delta t) \tag{2-17}$$

$$C_m = D_m - D_{m+1} \tag{2-18}$$

$$F_m = C_m K_m \tag{2-19}$$

$$Z_m = F_{m-1} - F_m - R_m \quad (2\text{-}20)$$

$$V_m = v_m + Z_m \frac{\Delta t g}{W_m} \quad (2\text{-}21)$$

$$R_m = (D_m - D'_m)K'_m(1 + J_m v_m) \quad (2\text{-}22)$$

$$R_u = \sum_{m=3}^{s} R_m \quad (2\text{-}23)$$

where: V_{Impact} = velocity of the driving hammer at impact;

E_h = rated energy of the driving hammer;

φ = efficiency of the driving hammer;

g = acceleration of gravity;

W_i = weight of pile segment;

D_m = displacement of soil and pile segment in time interval, n;

d_m = displacement of soil and pile segment in time interval, n-1;

V_m = velocity in the time interval, n;

v_m = velocity of pile segment in time interval, n-1;

Δt = time interval;

C_m = Compression in spring in time interval, n;

F_m = force exerted by spring in time interval, n;

K_m = stiffness of spring in time interval, n;

Z_m = accelerating force in time interval n;

R_m = soil resistance acting on the pile segment in time interval, n;

D'_m = soil plastic displacement in time interval, n;

K'_m = stiffness of the soil;

J_m = soil damping constant;

R_u = total ultimate soil resistance during driving; and

s = total number of pile segments in model.

The available output of GRLWEAP is the blow count, axial stresses and energy transfer. From these three outputs, the bearing capacity, stresses at an observed blow count and expected blow count can be determined.

CHAPTER 3: ANALYSIS OF UHPC PILES IN INTEGRAL ABUTMENTS

This chapter focuses on comparing the UHPC and HP 10 x 57 piles. The section behavior of the two piles was evaluated when subjected to different axial loads and then used as input into a lateral load analysis. The goal of the lateral load analysis is to determine the behavior of UHPC piles with respect to steel HP 10 x 57 piles for various conditions associated with integral abutments and assist with the experimental plan for the field testing and long-term monitoring of UHPC piles. This will be conducted via a moment-curvature analysis of the UHPC and HP 10 x 57 piles, and a parametric analysis to compare the pile's performance at five key parameters.

3.1. MOMENT-CURAVATURE RESPONSE

In order to perform the moment-curvature analysis for the UHPC pile section, a Microsoft Excel Moment-Curvature Program written by Vande Voort (2008) from Phase I of the project was modified so that the UHPC pile section could be analyzed about the weak-axis. To calculate the moment-curvature of an HP 10 x 57 steel pile section, an open-source computer program package known as OpenSees (OpenSees 2006) was used. The program has the capabilities of modeling and analyzing the nonlinear response of systems using a wide range of material models, elements, and solution algorithms. The existing script that was developed for the analysis of the HP 10 x 57 pile is included in Appendix A.

3.1.1. Analysis Assumptions

The moment-curvature response program for UHPC piles using Excel is based on the following assumptions which are modeled after Vande Voort (2008):

- Plane sections remain plane;
- Prestress losses occur due only to elastic shortening and shrinkage of UHPC;

- Strands have perfectly bonded to UHPC outside of the transfer regions, so the change in strain in prestressing strands is equal to the change in strain in concrete at the strand location;
- Effective prestressing is applied at the centroid of the section;
- Bending only occurs about the weak flexural axis;
- Initial prestressing does not induce any inelastic strains on the strands; and
- Axial Loads on the pile are applied thought the centroidal axis with no eccentricity.

3.1.2. Section Analysis

The moment-curvature program divides the cross-section into 100 small segments and calculates the stresses and strains for each segment at a given curvature. The stress and strains are then converted into forces and moments. The prestressing, prestressing losses and axial load contribute to the uniform strain in the concrete and are referred to as the zero curvature strains for both UHPC and prestressing steel. The equations used in this Excel worksheet were developed by Vande Voort (2008).

Two equations were used to calculate the prestressing losses. Equations 3-1 and 3-2 were used to obtain the prestressing losses due to elastic shortening of the UHPC member and shrinkage of UHPC material, respectively.

$$\Delta f_{pES} = \frac{f_{pi} A_{ps}}{2A_{ps} + A_c \frac{E_{ci}}{E_p}} \tag{3-1}$$

$$\Delta f_{pSH} = \frac{\varepsilon_{SH} A_c E_p}{A_c + A_{ps} \frac{E_p}{E_c}} \tag{3-2}$$

where: Δf_{pES} = prestress losses due to elastic shortening of UHPC;

f_{pi} = initial prestress applied to prestressing Strands;

A_{ps} = total area of prestressing strands;

A_c = total area of UHPC;

E_{ci} = elastic modulus of UHPC at time of transfer of prestressing;

E_p = elastic modulus of prestressing strands;

Δf_{pSH} = prestress losses due to shrinkage of UHPC;

ε_{SH} = total shrinkage strain of UHPC; and

E_c = elastic modulus of cured UHPC.

Another factor that affects the zero curvature strain is the free shrinkage of the UHPC. The prestressing strands do not undergo the free shrinkage that the UHPC experiences. The result of this difference is a tensile strain induced in the UHPC, which can be characterized by Equation 3-3. The final factor contributing to the zero curvature strain is the strain due to the axial load and can be calculated using Equation 3-4.

$$\Delta\varepsilon_{cSH} = \frac{\varepsilon_{SH} A_{ps}}{A_{ps} + A_c \frac{E_c}{E_p}} \tag{3-3}$$

$$\varepsilon_p = \frac{P}{A_c E_c + A_{ps} E_p} \tag{3-4}$$

where: $\Delta\varepsilon_{cSH}$ = tensile strain in UHPC due to free shrinkage;

ε_p = strain in UHPC or prestressing steel caused by axial load; and

P = applied axial load.

The total initial strains or zero curvature strains can be calculated using Equation 3-5 and Equation 3-6 for the prestressing strands and the UHPC, respectively.

$$\varepsilon_{pZC} = \frac{f_{pi} - \Delta f_{pES} - \Delta f_{pSH}}{E_p} - \varepsilon_p \tag{3-5}$$

$$\varepsilon_{cZC} = -\frac{(f_{pi} - \Delta f_{pES}) A_{ps}}{A_c E_c} + \Delta\varepsilon_{cSH} - \varepsilon_p \tag{3-6}$$

where: ε_{pZC} = strain in prestressing steel at zero curvature; and

ε_{cZC} = strain in UHPC at zero curvature.

After the zero curvature strains are calculated, the tensile and compressive strains due to curvature are calculated. As mentioned previously, the cross-section of the UHPC pile was divided into 100 evenly spaced horizontal segments. The user of the program is required to input the width of each section as well as the location of the prestressing strands. The strain for each of the horizontal segments of the UHPC and prestressing strands are calculated by using Equations 3-7 and 3-8, respectively. The variables in these equations are depicted in Figure 3-1.

$$\varepsilon_{ct} = \varphi y_{cg} + \varepsilon_{cZC} = \varphi\left(y - \frac{\varepsilon_{cZc}}{\varphi}\right) + \varepsilon_{cZC} = \varphi y \tag{3-7}$$

$$\varepsilon_{pt} = \varphi y_{cg} + \varepsilon_{pZC} = \varphi\left(y - \frac{\varepsilon_{cZC}}{\varphi}\right) + \varepsilon_{pZC} = \varphi y - \varepsilon_{cZC} + \varepsilon_{pZC} \tag{3-8}$$

where: ε_{ct} = total strain in UHPC;

φ = curvature about horizontal axis;

y_{cg} = distance from centroid, measured positive downward;

y = distance from neutral axis, measured positive downward; and

ε_{pt} = total strain in prestressing steel.

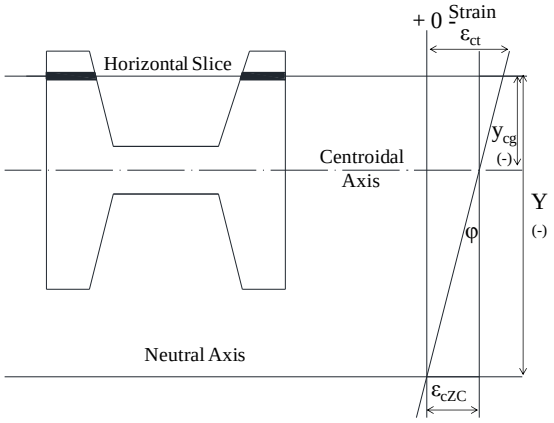

Figure 3-1: Definitions of Distance from Centroid and Distance from Neutral Axis (after Vande Voort 2008)

During each step, the stresses and strains are calculated for each segment of the cross-section using a stress-strain relationship of UHPC and of prestressing strands that are described in Figure 3-2 and Figure 3-3, respectively. The forces and moments are then calculated for each segment of the cross-section by manipulating the strains. The spreadsheet solves a series of equations using the solver to calculate the appropriate curvature and neutral axis for each step. When the correct neutral axis is found for a curvature by satisfying the equilibrium condition, the sum of the moments in the section is equal to the total moment resistance associated with the input curvature (Vande Voort 2008).

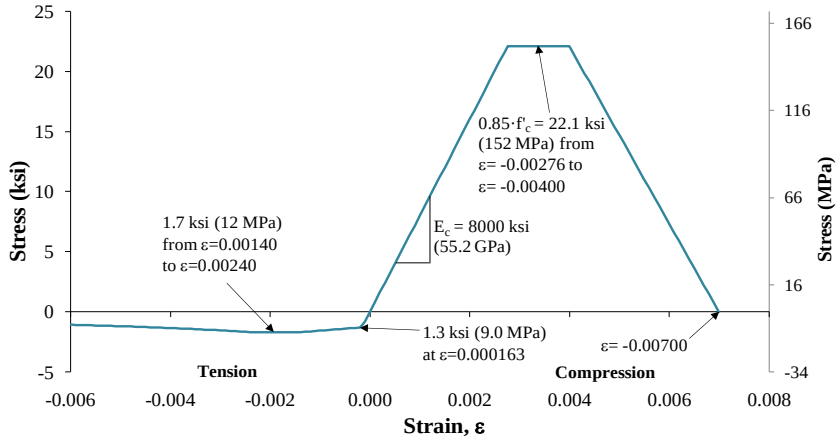

Figure 3-2: Assumed UHPC Monotonic Stress-Strain Behavior (Vande Voort et al. 2008)

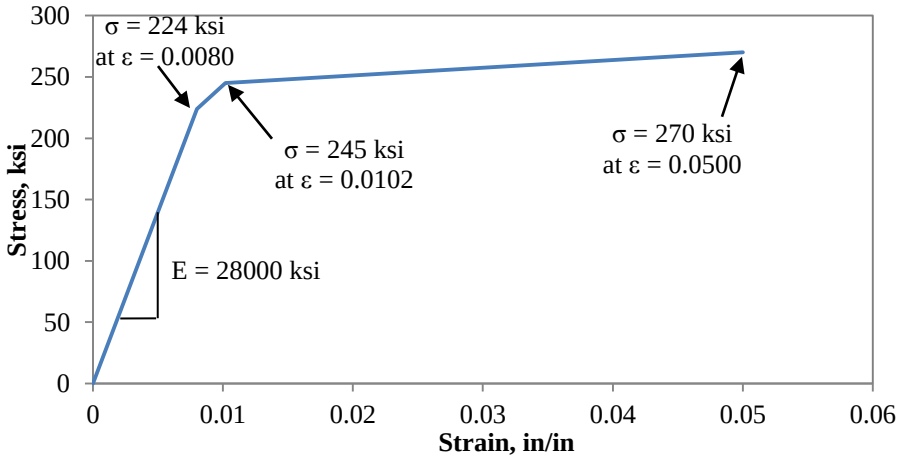

Figure 3-3: Assumed Stress-Strain Behavior for the 0.5-in. 270 ksi Low Relaxation Prestressing Strand (after PCI 2010)

3.1.3. Results

The ultimate curvature for each axial load as defined by the Excel Moment-Curvature Program was determined by using one of the four conditions described by Vande Voort (2008), whichever occurs first:

- The strain in the extreme compression fiber reached the assumed ultimate value of 7000 microstrain;
- The strain in a prestressing strand reached the assumed ultimate value of 50,000 microstrain;
- The moment resistance of the section decreased to 80 percent of its maximum value; or
- The location of the neutral axis depth changed very suddenly, causing a large drop in moment resistance.

Figure 3-4 shows the moment-curvature response of the UHPC pile section in weak-axis bending subjected to various axial loads. As the axial load increases, the ultimate curvature decreases. The maximum moment resistance increases slightly for each load, up to 200 kips and stays the same for the axial load of 300 kips. Figure 3-5 shows the moment-curvature of a UHPC pile in strong-axis bending. Similar to the weak-axis bending, the ultimate curvature for UHPC subjected to strong-axis bending decreases as the axial load increases, but the maximum moment increases as the axial load increases.

To compare the moment-curvature response of the section behavior of a UHPC pile in strong-axis bending and weak axis bending, the response at 100 kip axial load for both was included in Figure 3-6. The results from Vande Voort et al. were used for the UHPC pile section subjected to strong-axis bending. It is worth noting that both the maximum moment resistance and the ultimate curvature are greater for the strong-axis bending. The flexural rigidity and the ultimate moment of a UHPC strong-axis pile are 109 percent greater and 56 percent greater than for a UHPC pile in weak-axis bending, respectively.

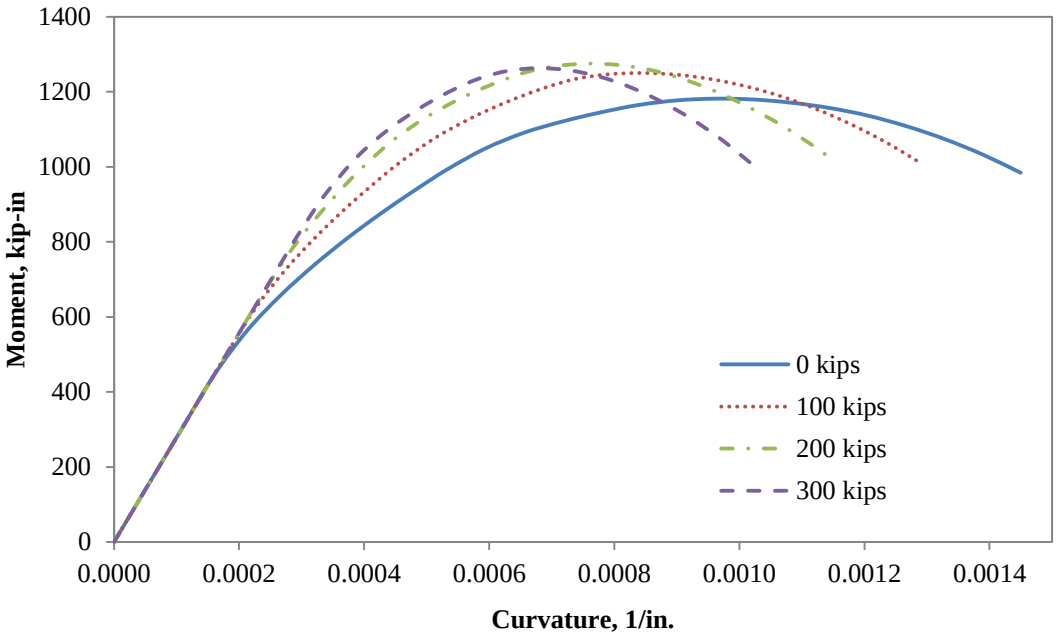

Figure 3-4: Moment-Curvature of the UHPC Pile Section Subjected to Weak-Axis Bending with Varying Axial Loads

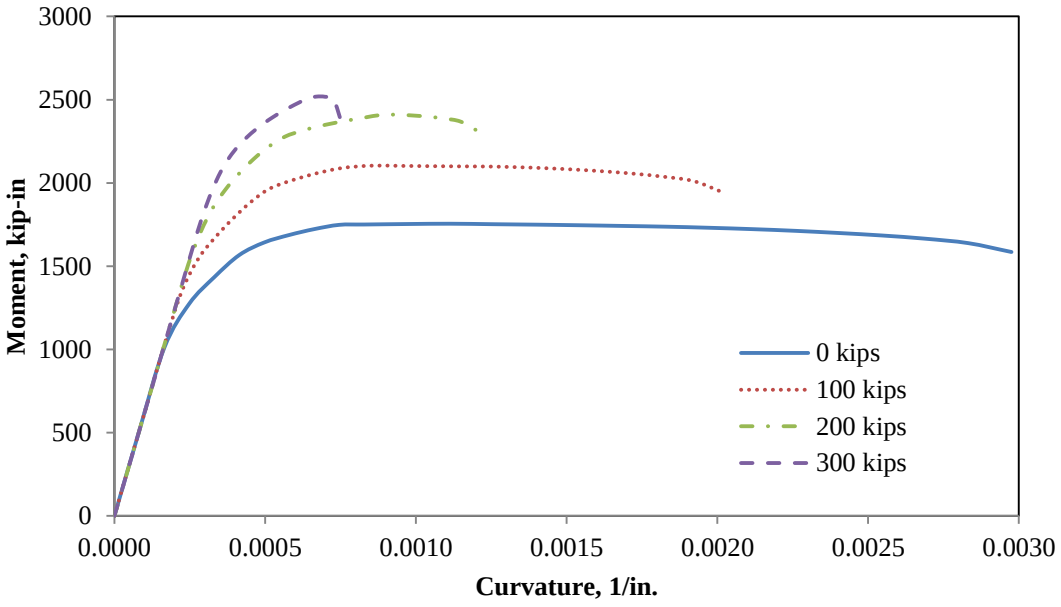

Figure 3-5: Moment-Curvature of the UHPC Pile Section Subjected to Strong-Axis Bending with Varying Axial Loads (after Vande Voort 2008)

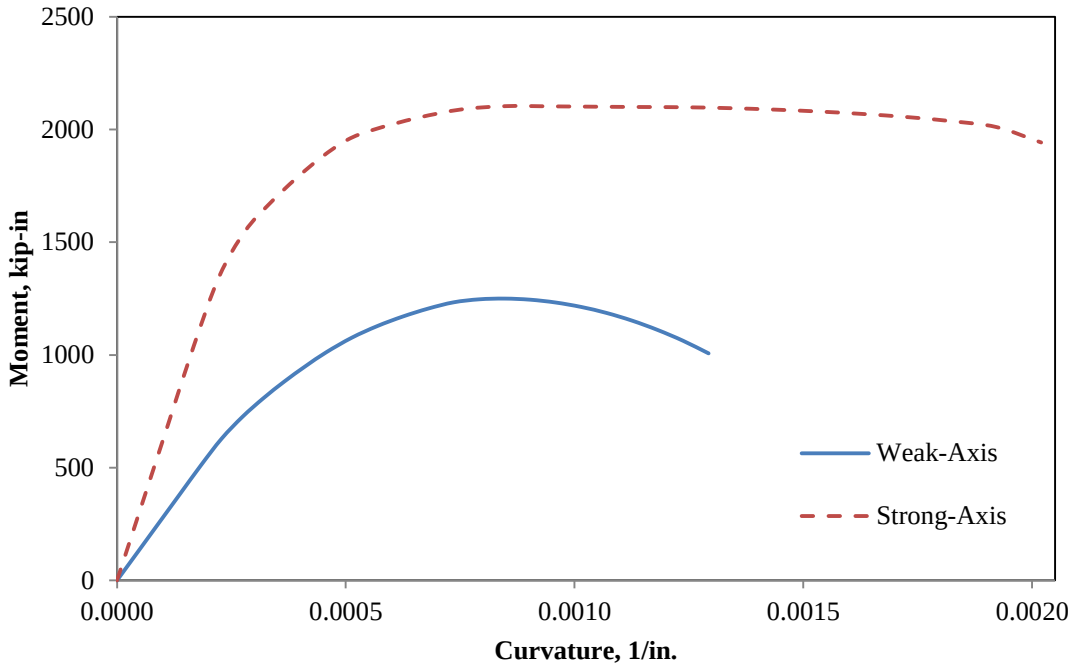

Figure 3-6: Comparison of Moment-Curvature between Strong-Axis and Weak-Axis Bending of the UHPC Pile Sections Subjected to a 100 kip Axial Load

Similarly to the UHPC pile section, the HP 10 x 57 pile section was subjected to the same varying axial loads in both strong-axis and weak-axis bending. The weak-axis piles are given in Figure 3-7 and the strong-axis piles are shown in Figure 3-8. As the axial load increases, the ultimate curvature decreases for both cases, but is more pronounced for the strong-axis piles. The maximum moment resistance decreases very slightly as the axial load is increased on the pile subjected to weak-axis bending. In contrast, the pile in strong-axis bending has a dramatic decrease in the maximum moment resistance for the 200 and 300 kip axial load.

To compare the moment-curvature response of the section behavior of a HP 10 x 57 pile in strong-axis bending and weak axis bending, the response at 100 kip axial load for both is presented in Figure 3-9. It is worth noting that both the maximum moment resistance and the ultimate curvature are greater for the strong-axis bending. The flexural rigidity and the

ultimate moment of a steel pile in strong-axis bending are 191 percent greater and 17 percent less than for the steel pile in weak-axis bending, respectively.

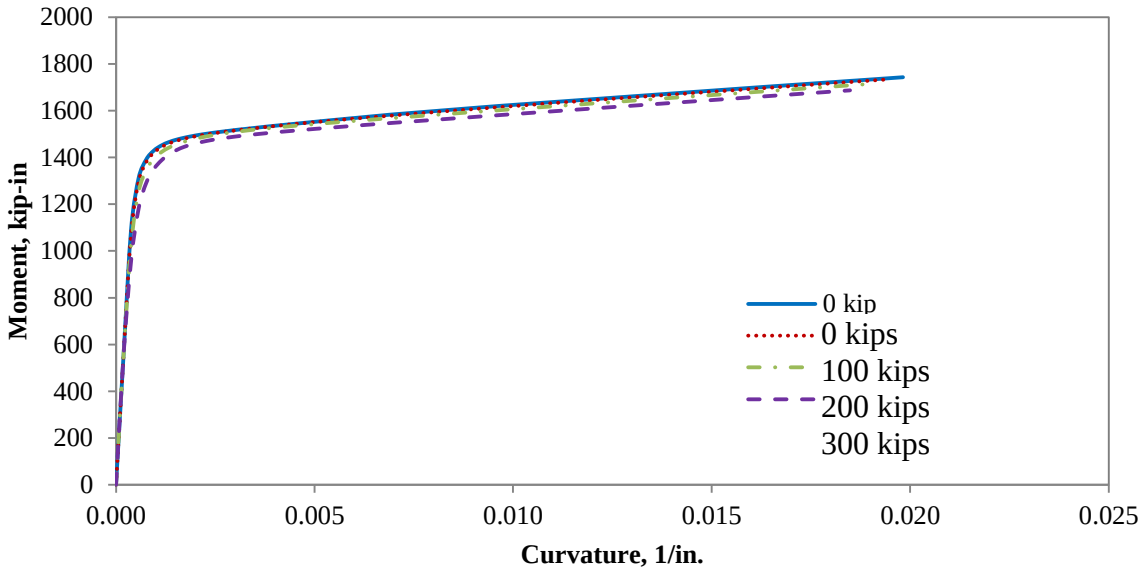

Figure 3-7: Moment-Curvature of the HP 10 x 57 Pile Section Subjected to Weak-Axis Bending with the Varying Axial Loads

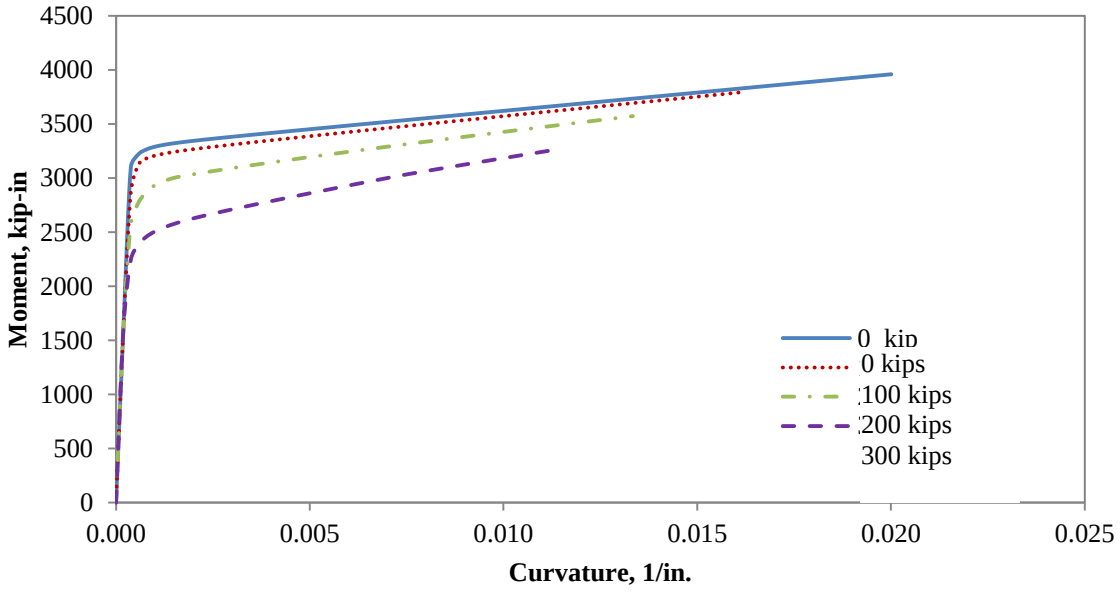

Figure 3-8: Moment-Curvature of the HP 10 x 57 Pile Section Subjected to Strong-Axis Bending with Varying Axial Loads

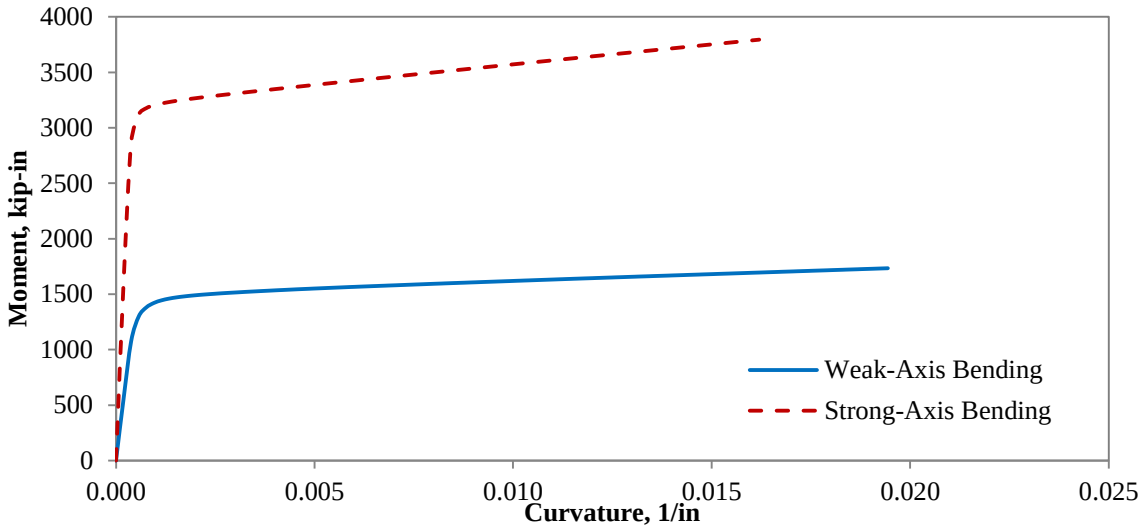

Figure 3-9: Comparison of Moment-Curvature between Strong-Axis and Weak-Axis Bending of the HP 10 x 57 Pile Section Subjected to a 100 kip Axial Load

A comparison between UHPC piles and steel HP 10 x 57 piles is shown for weak-axis bending in Figure 3-10 at an axial load of 100 kips. While the two sections show comparable elastic stiffness, the steel pile exhibits higher moment resistance. Since the piles are primarily used for carrying axial loads in Iowa, the UHPC pile was designed for this purpose. The difference in moment resistance is inconsequential. If the serviceability limit state is defined using the yield strain for the H-pile and keeping the crack width less than 0.0012-in. for UHPC piles, the H-pile section shows and increase in moment resistance of 39 percent. Finally, the inherent ductility of steel produces ultimate curvature significantly higher than that of the UHPC pile section. The level of ductility is not needed for the pile and that shown by the UHPC pile is adequate for piles designed primarily for axial load resistance.

Similar to the weak-axis bending piles, the maximum moment, ultimate curvature, ultimate moment, and stiffness are higher for a strong-axis bending steel HP 10 x 57 pile than a strong-axis bending UHPC pile, as illustrated in Figure 3-11. The differences between UHPC and HP 10 x 57 piles are higher for strong-axis bending than for weak-axis bending due to the differences in stiffness between the two types of piles in strong-axis bending, with the HP 10 x 7 pile's stiffness being 38 percent higher than the UHPC pile. If the serviceability limit state is defined using the yield strain for the H-pile and keeping the crack

width less than 0.0012-in. for UHPC piles, the H-pile section shows and increase in moment resistance of 85 percent.

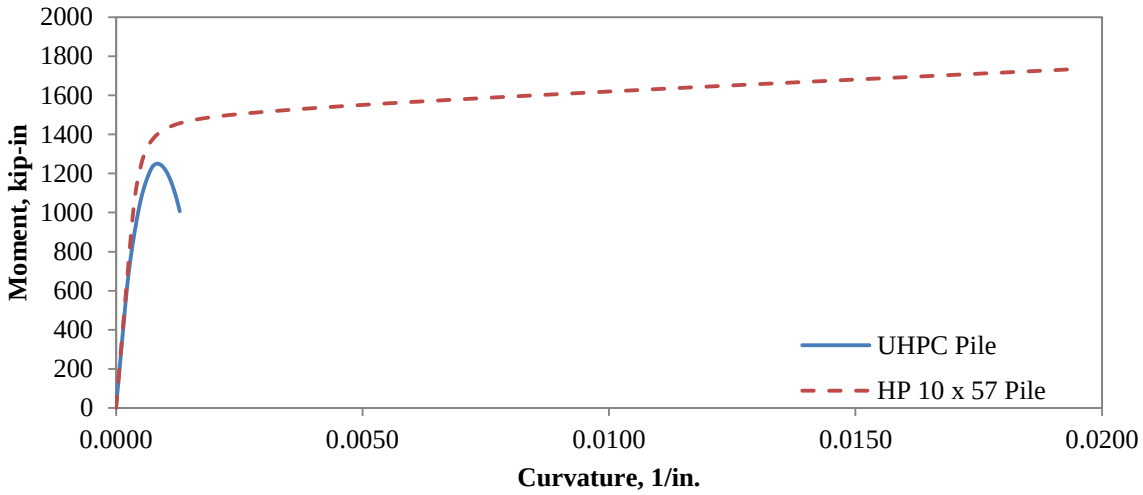

Figure 3-10: Moment-Curvature Response at 100 kip Axial Load Comparing a UHPC Pile and a HP 10 x 57 Pile in Weak-Axis Bending

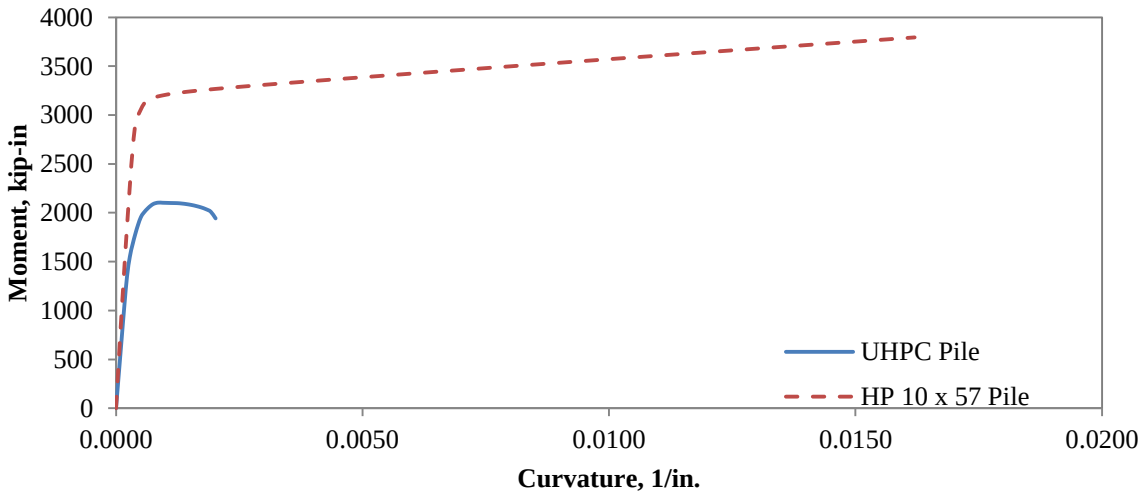

Figure 3-11: Moment-Curvature Response at 100 kip Axial Load Comparing a UHPC Pile and a HP 10 x 57 Pile in Strong-Axis Bending

A moment-curvature analysis of UHPC and HP 10 x 57 piles was compared in strong and weak axis bending for four different axial load cases to better understand the section behavior of piles. The section behavior indicates the effect the piles will have on an integral

abutment. For example, the HP 10 x 57 pile subjected to strong-axis bending has a much higher maximum resisting moment than for a HP 10 x 57 pile subjected to weak-axis bending. As a result from increase in maximum resisting moment, the pile will transfer more forces into the abutment and the deck of the bridge which must be accounted for in the design process to eliminate cracking in the bridge's structural elements.

3.2. PARAMETRIC ANALYSIS

A systematic study was undertaken to examine the lateral load performance of UHPC and HP 10 x 57 piles under various conditions using LPILE^{PLUS} 5.0 to calculate the deflection, bending moment, and shear profiles along the pile were compared for typical integral abutment pile foundation conditions. Five key parameters were investigated to quantify the behavior of UHPC and HP 10 x 57 in this parametric study.

3.2.1. Parameters

The first parametric study compared a UHPC pile to a steel HP 10 x 57 pile by changing various conditions. The key parameters used in the study were soil type, pile head boundary condition, axial load, pile orientation, and displacement. A total of 128 different cases were evaluated for UHPC and steel HP 10 x 57 piles and various combinations of key parameters. The variations included for each parameter are:

- Soil Type: four extreme soil conditions as shown in Table 3-1;
- Pile Head Boundary Condition: fixed and pinned;
- Axial Load: 0 kip, 100 kips, 200 kips, 300 kips;
- Pile Orientation: weak-axis bending and strong-axis bending; and
- Lateral Displacement: 1.00-in and 1.55-in

In Iowa, a 10-ft deep prebore hole is required for abutment piles in integral abutments when the bridge exceeds 130 feet in length (Iowa DOT 2011). As a result, a second study compared the results from the first study to the behavior of a UHPC pile and a HP 10 x 57

pile with a 10-ft prebore hole for some of the conditions used in the first study. A total of 8 cases were evaluated for UHPC and steel HP 10 x 57 piles as given in Table 3-2.

Table 3-1: Soil Properties used for Parametric Analyses

Soil Type	Density* γ (lb/in^3)	Friction Angle* φ (degree)	Cohesion* c (lb/in^2)	Subgrade Modulus* k_s, lb/in^3	Strain at 50%* $\varepsilon_{50\%}$
Loose Sand	0.063	30	-	25	-
Dense Sand	.075	40	-	225	-
Soft Clay	.063	-	3	30	0.020
Very Stiff Clay	.075	-	35	800	0.004

* Kamel et al. (1996), Wang and Reese (1991) and Reese et al. (1956, 1974, 1994)

Table 3-2: Eight Load Cases investigated in the Second Parametric Study Considering a Prebore Hole

Conditions	Axial Load, kips	Soil Type	Lateral Displacement, in.
Fixed Pile Head; Weak-Axis Bending	100	Soft Clay	1.00
			1.55
		Stiff Clay	1.00
			1.55
	200	Soft Clay	1.00
			1.55
		Stiff Clay	1.00
			1.55

3.2.2. Allowable Tensile Strains

The allowable tensile stress versus crack width for UHPC was given in Figure 2-2. Based on components of UHPC, Vande Voort (2008) reported tensile strain limits for the behavior of UHPC corresponding to the stresses in Figure 2-2. Accordingly, 160 microstrain represents the barrier when micro-cracking begins at the extreme tension fiber and 1350 microstrain is when visible cracking begins. The strain limit of the extreme tension fiber to facilitate the fiber to pullout of the UHPC is 2400 microstrain. The model in Figure 2-2 was updated to include the values as shown in Figure 3-12. In comparison, a value of 1700 microstrain was used to determine the first yield of the flanges in the steel HP 10 x 57 piles with an assumed modulus of elasticity of 29,000 ksi and a yield strength of 50 ksi.

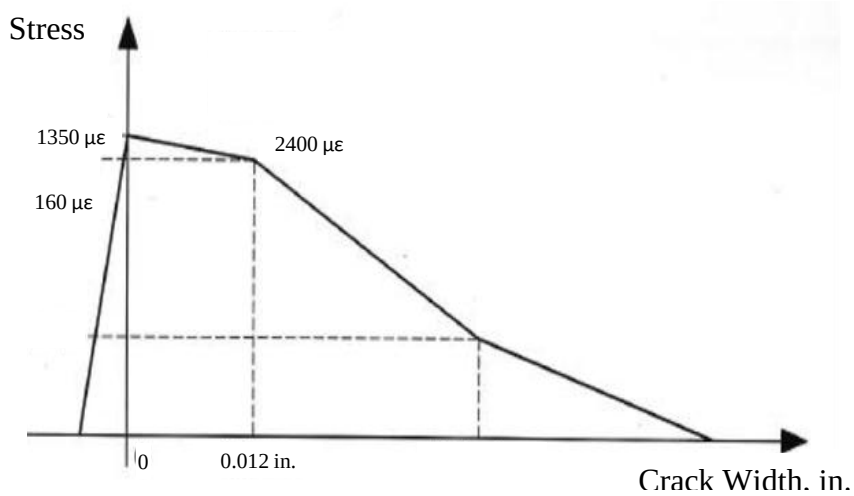

Figure 3-12: Simplified Tensile Strength Law with Tensile Strain Assumptions

3.2.3. Predicted Width and Crack Location along the Piles

The flexural moment resistance at a given section of pile is the sum of the moments a pile is subjected to at a given location. The flexural moment resistance along the length of each pile was calculated using LPILE for a given lateral displacement and was used to predict the extent of cracking the UHPC pile, as well as yielding the HP 10 x 57 pile would experience during lateral loading. For UHPC, micro cracking is considered acceptable, the visible cracking corresponding to 1350 microstrain is considered undesirable and cracking that provides widths greater than 0.012 inches is deemed unacceptable. Yielding of the HP 10 x 57 pile is also considered undesirable; therefore, the visible cracking and yield limits will be compared between the HP 10 x 57 pile and UHPC pile throughout this section to compare the performance of each pile section.

Potential cracking along the length of the UHPC pile was determined by finding the moment corresponding to the defined tensile strain limits for a given axial load. Using the moment-curvature calculations given in Section 3.1, Table 3-3 lists the moments used to determine the onset of cracking for UHPC piles.

Similarly,

Table 3-4 gives the moments where yielding begins in the flanges of steel HP 10 x 57 piles. Notice that as the axial load is increased from 100 kips to 200 kips, the moments at

each of the limits for UHPC increases, while for the steel pile the yielding moment decreases as the axial load increases, giving an advantage for the UHPC pile.

Table 3-3: Assumed Flexural Cracking Moments of UHPC Piles in Weak-Axis Bending

	Moments Corresponding to Strain Limits Given in Figure 3-12, kip-in.		
Axial Load	Micro-Cracking	Visible Cracking	Crack Width > 0.012-in.
100	536	948	1144
200	660	1084	1246

Table 3-4: Estimated Yielding Moments of HP 10 x 57 Piles in Weak-Axis Bending

Pile Type	Axial Load	Yielding Moment, kip-in.
HP 10 x 57	100	840
	200	711

Figure 3-13 through Figure 3-16 illustrate the location and extent of flexural cracking along the length of a UHPC pile as well as the location of yielding for steel HP 10 x 57 piles under various conditions. The boundary conditions are supposed to reflect typical Iowa DOT integral abutment design. As a result, the parameters assumed here include a fixed pile head condition and weak-axis bending.

Figure 3-13 depicts the type and location of damage that would occur if an integral abutment moved 1.0 inch in the longitudinal direction without having a prebore hole around each of the piles. Yielding is present for the top 6 inches of the HP 10 x 57 pile for the 200 kip axial load in the soft clay, but no undesirable cracking occurs for the UHPC pile under the same condition. Both visible cracking and cracks with a width greater than 0.012 inches are present for the UHPC pile, and yield is present in the HP 10 x 57 pile at two different depths.

If the lateral displacement is increased to 1.55 inches in the very stiff clay, the UHPC piles are predicted to have unacceptable crack widths larger than 0.0012 inches. It is important to note that vertical rotations of the abutment are not taken into account during this analysis which would reduce the magnitude of flexural moments on the pile head. Additionally, two locations for yielding in the HP 10 x 57 pile are present for this load case,

resulting in a total of 4 feet of the pile being susceptible to yielding within the flanges. The results of 1.55-in of lateral displacement without a prebore hole are displayed in Figure 3-14.

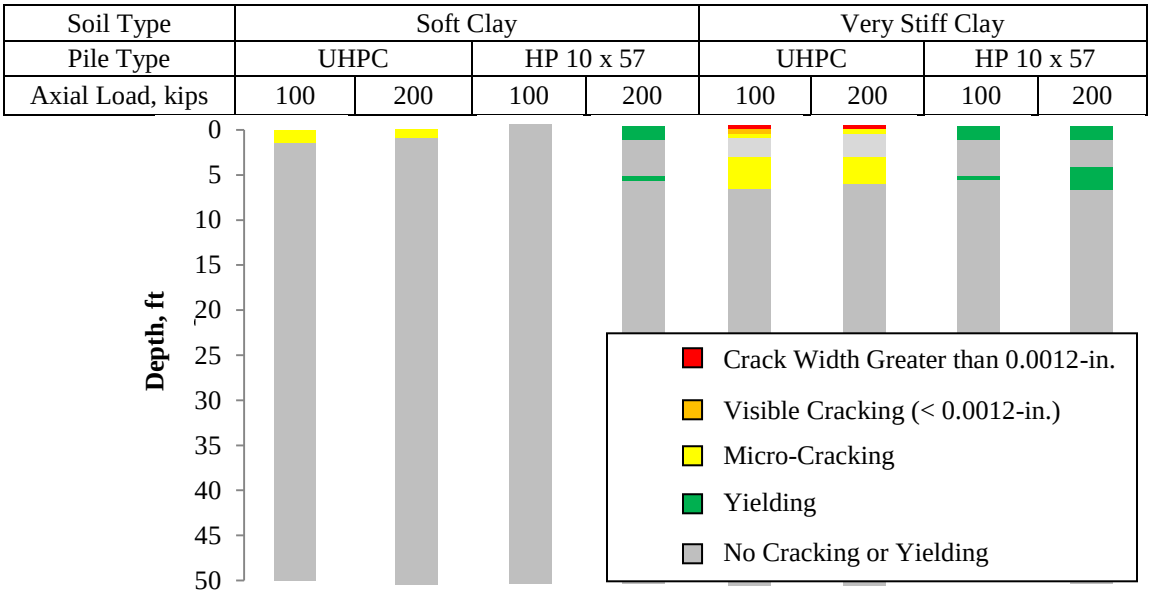

Figure 3-13: Cracking or Yielding along the Length of Piles Subjected to a 1.00 inch of Lateral Displacement without a Prebore Hole

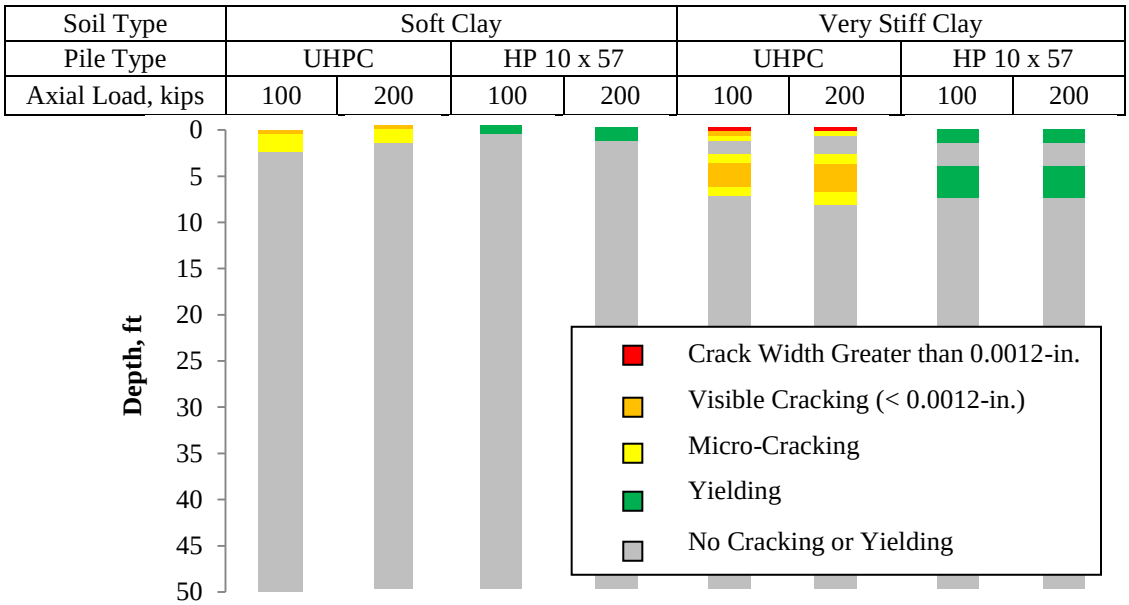

Figure 3-14: Cracking or Yielding along the Length of Piles Subjected to a 1.55 inches of Lateral Displacement without a Prebore Hole

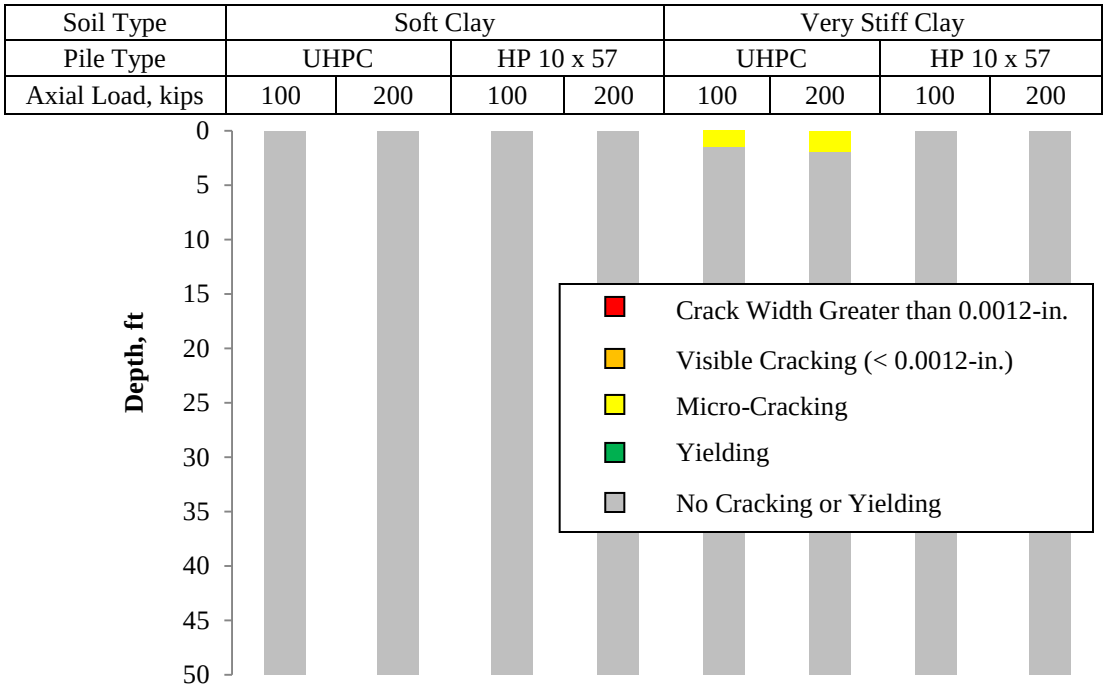

Figure 3-15: Cracking or Yielding along the Length of Piles Subjected to a 1.00 inch of Lateral Displacement with a 10-ft Deep Prebore Hole

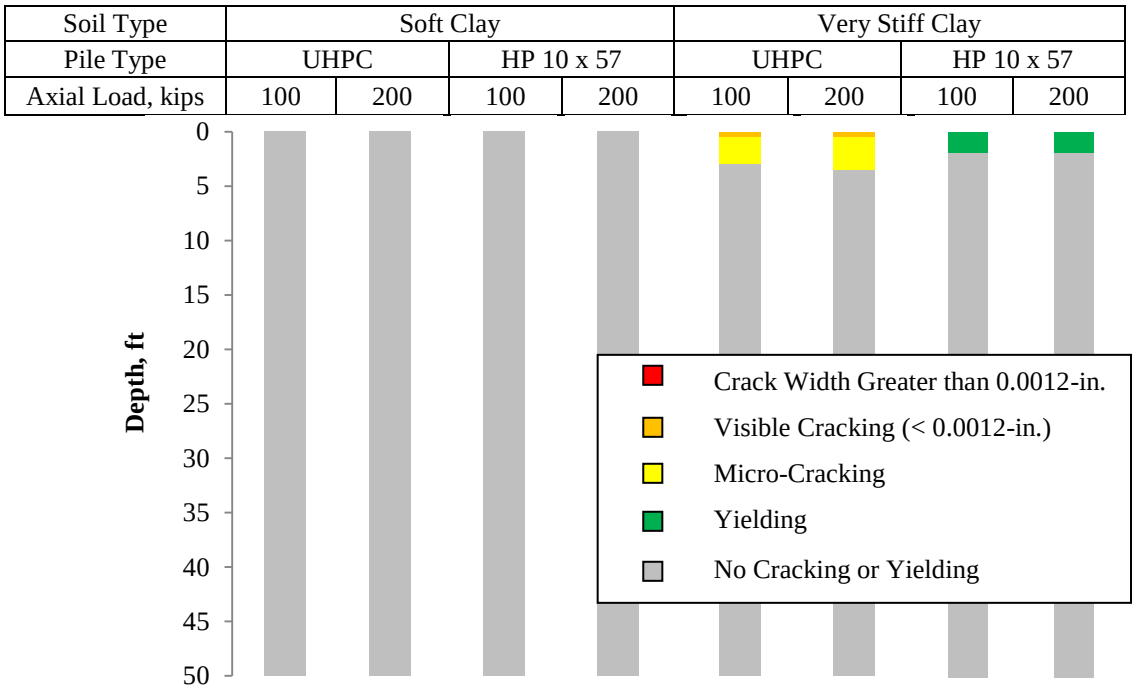

Figure 3-16: Cracking or Yielding along the Length of Piles Subjected to a 1.55 inches of Lateral Displacement with a 10-ft Deep Prebore Hole

Figure 3-13 depicts the expected type and location of damage that would occur if an integral abutment moved 1.0 inches in the longitudinal direction without having a 10-ft prebore hole around each of the pile types. Yielding is present for the top 6 inches of the HP 10 x 57 pile for the 200 kip axial load in the soft clay, but no undesirable cracking is expected for the UHPC pile. Both visible cracking and cracks with a width greater than 0.012 inches are present for the UHPC pile. Yielding is present in the HP 10 x 57 pile at two different depths.

If the lateral displacement is increased to 1.55 inches in the very stiff clay soil condition, the UHPC piles are predicted to have unacceptable crack widths greater than 0.0012 inches. Additionally, two locations for yielding in the HP 10 x 57 pile are present for this load case, resulting in a combined 4 feet of the pile being susceptible to yielding within the flanges. The results of 1.55-in. of lateral displacement without a prebore hole are displayed in Figure 3-14.

A more representative model of an integral abutment pile is to take into account the effects of prebore holes. Typically, the Iowa DOT fills the prebore hole with bentonite or polymer slurry and assumes no lateral resistance from such material. Figure 3-15 displays the reduced amount of cracking and no yielding that is predicted to occur in piles that were installed with a prebore hole at 1.0-in. of lateral displacement. No undesirable cracking or yielding is predicted to occur for either soft clays or very stiff clays.

When piles were subjected to 1.55 inches of lateral displacement with a prebore hole condition, a small amount of visible cracking was found in the UHPC pile as well as yielding in the steel HP 10 x 57 pile as shown in Figure 3-16. When comparing Figure 3-14 to Figure 3-16, it is apparent that the cracking of UHPC piles and yielding of steel piles are noticeably reduced when a 10-ft prebore hole is present.

The point of fixity was also determined for each lateral load case, which was then compared between the UHPC and HP 10 x 57 piles. The point of fixity is the depth at which the pile behaves fixed. This location was determined by identifying the depth at which the piles lateral displacement was less than 0.01 inches.

3.2.4. Results

The pile type, soil type, pile head boundary condition, axial load, pile orientation, and presence of a prebore hole were modeled during the parametric study. The findings from changing these parameters are described in this section.

When comparing the differences in performance between the UHPC pile and the HP 10 x 57 pile while keeping all of the parameters the same, the maximum moments and maximum shear forces induced in both piles are almost identical as shown in Figure 3-17. The steel pile has a slightly higher maximum moment and maximum shear as shown in Figure 3-17, which is caused by the slight difference in flexural rigidity (EI). The HP 10 x 57 pile has a slightly lower EI value than the UHPC pile by 1.0 percent.

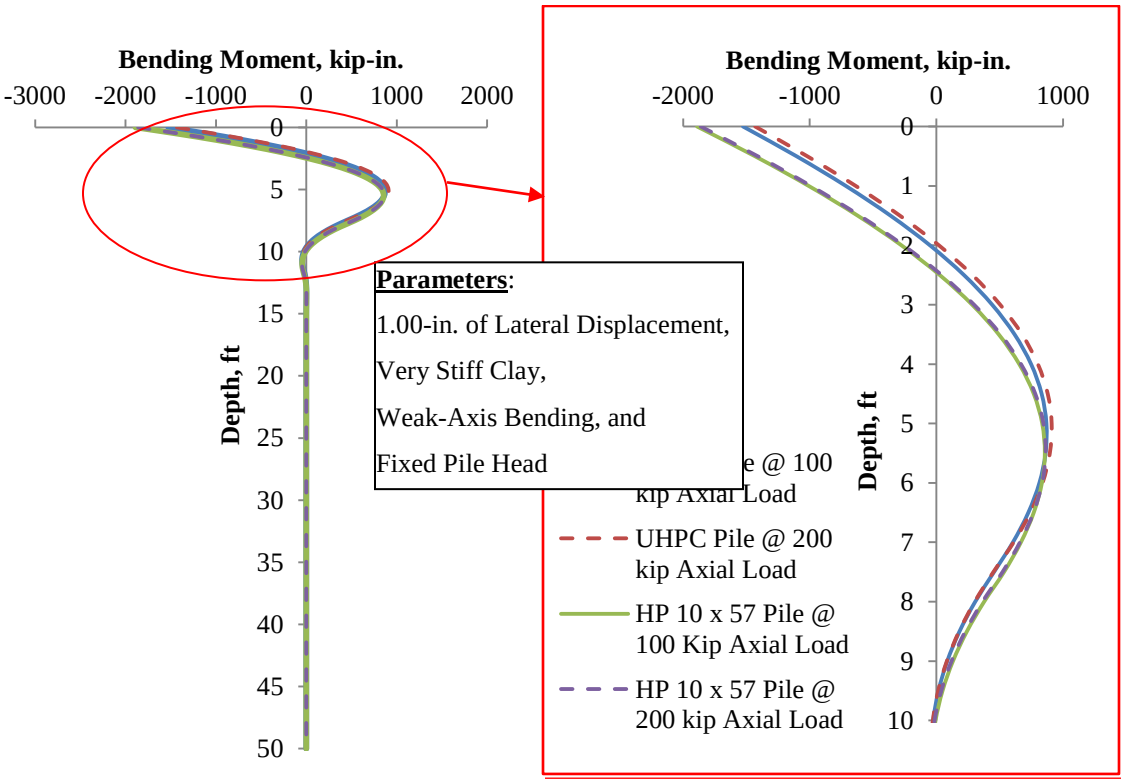

Figure 3-17: Performance Difference between a UHPC pile and an HP 10 x 57 Pile

As the soil becomes softer, the location of the second maximum moment for fixed-pile head conditions is deeper than for stiffer or denser soils. Figure 3-18 illustrates the effect the soil has on the pile's bending moments.

When varying the pile head boundary condition of UHPC and steel HP 10 x 57 piles from fixed to pinned condition the results were very different as can be expected, and are illustrated in Figure 3-19. There are three main differences in performance which are due to: 1) the magnitude of the maximum bending moments and shear forces are greater for the fixed pile head condition as compared to the pinned pile head condition; 2) the location of the second peak moment is much deeper for the pinned pile head condition than that of the fixed pile; and 3) the point of fixity for the pile with a fixed head connection is deeper than for the pinned connection.

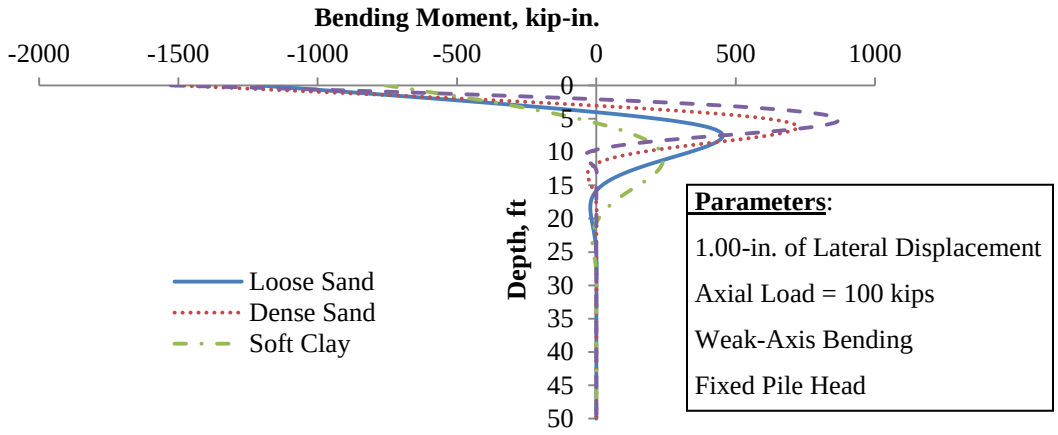

Figure 3-18: Effect of Soil Type on UHPC Pile Behavior

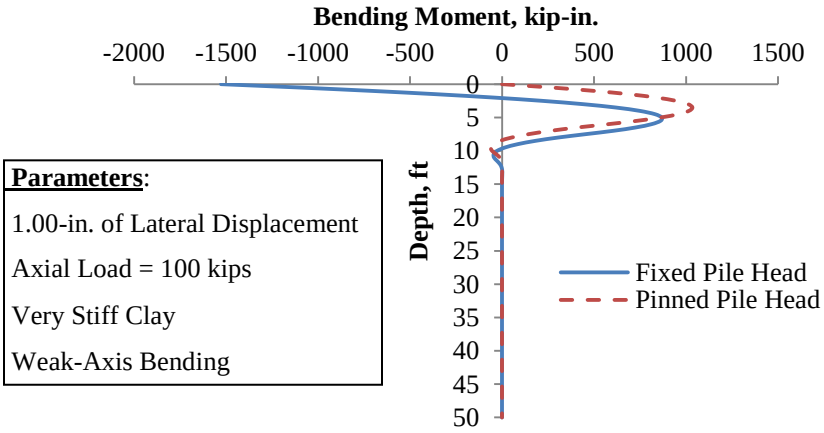

Figure 3-19: Effect of Fixed and Pinned Pile Head Boundary Condition on the Moment Profile for UHPC Piles

Furthermore, it was found that as the axial load was increased, the maximum bending moment and maximum shear forces decrease for the steel HP 10 x 57 piles and the UHPC piles subjected to weak-axis bending, but increased for the UHPC pile subjected to strong-axis bending. For strong-axis HP 10 x 57 piles, the maximum moment increased from 0 kips to 100 kips, but decreases for 200 and 300 kips. Also, the locations of the second maximum moment remains relatively constant, but the magnitude increases as the axial load increases for the weak-axis bending case as shown in Figure 3-20. The point of fixity stays relatively constant as the axial load increases for all the UHPC and HP 10 x 57 piles in all soil types.

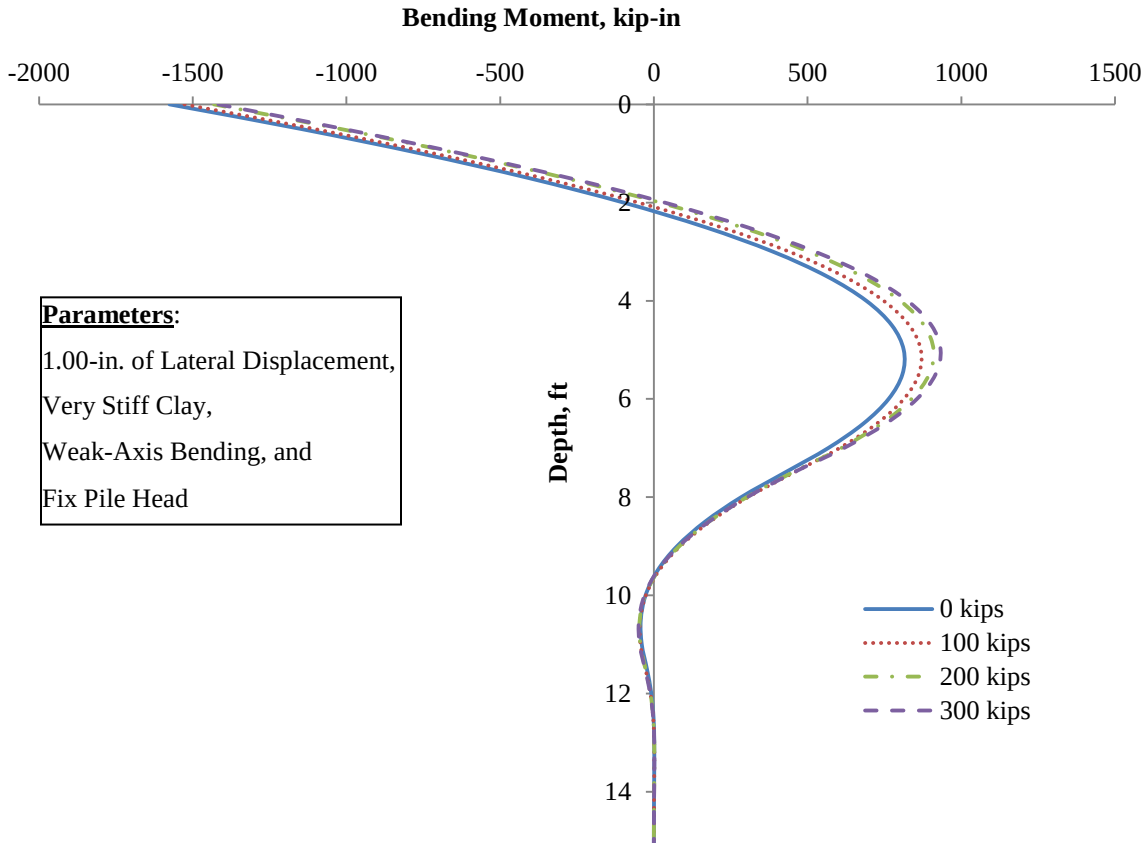

Figure 3-20: Comparison of Bending Moment When Varying the Axial Load for UHPC Piles

As the orientation of the pile was changed from strong-axis to weak-axis, three main differences in performance were evident due to the change in stiffness and are depicted in

Figure 3-21. These differences include: 1) the maximum bending moment and maximum shear force were lower for weak-axis bending; 2) the magnitude and location of the second maximum moment is smaller and closer to the pile head for weak-axis bending; and 3) the depth of fixity is closer to the pile head for weak-axis bending.

The presence of a 10-ft prebore hole around the pile decreased the bending moment shear forces that were imposed on the pile. The depth to the second maximum moment and the depth of fixity are deeper than a pile without a prebore hole, but not as far as would be expected, which is illustrated in Figure 3-22. Also, the maximum shear is not at the pile head for all of the cases where prebore holes were modeled, except for piles in soft clay with a 100 kip axial load. The prebore hole reduced the flexural moment the UHPC pile would be subjected to within the acceptable limits when installed in integral abutments.

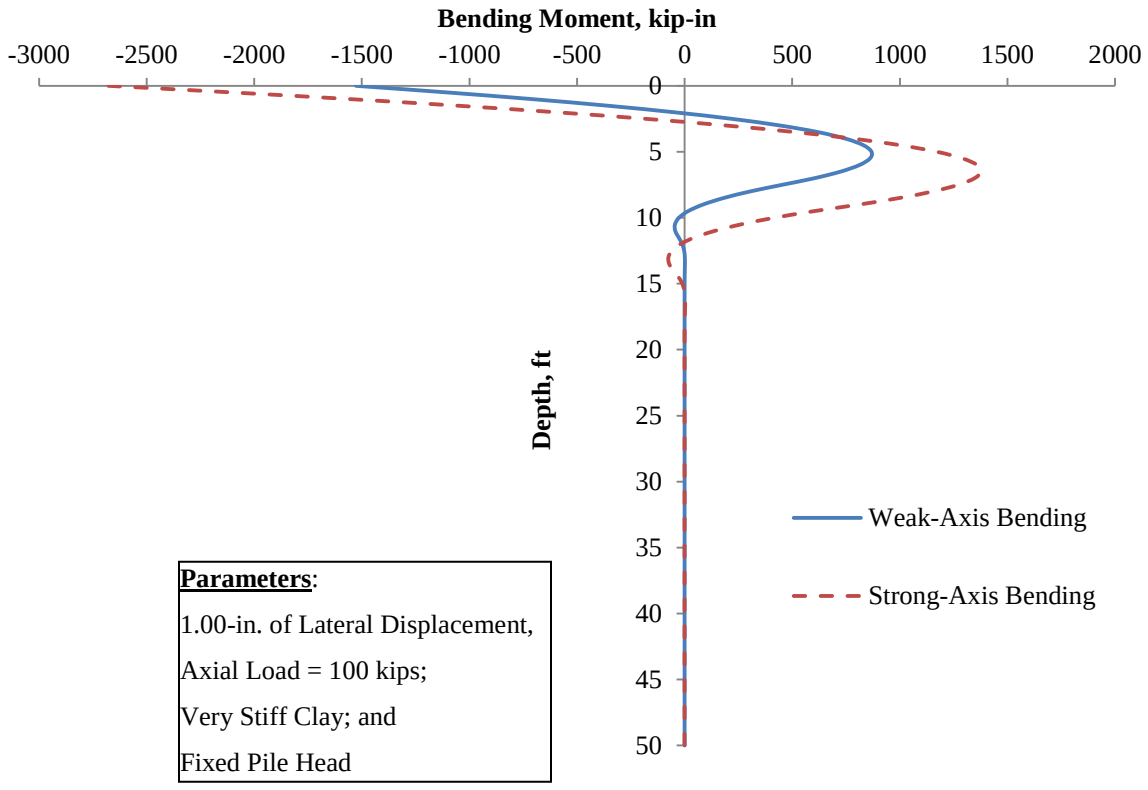

Figure 3-21: Effects of Strong-Axis vs. Weak-Axis Bending for a UHPC Pile

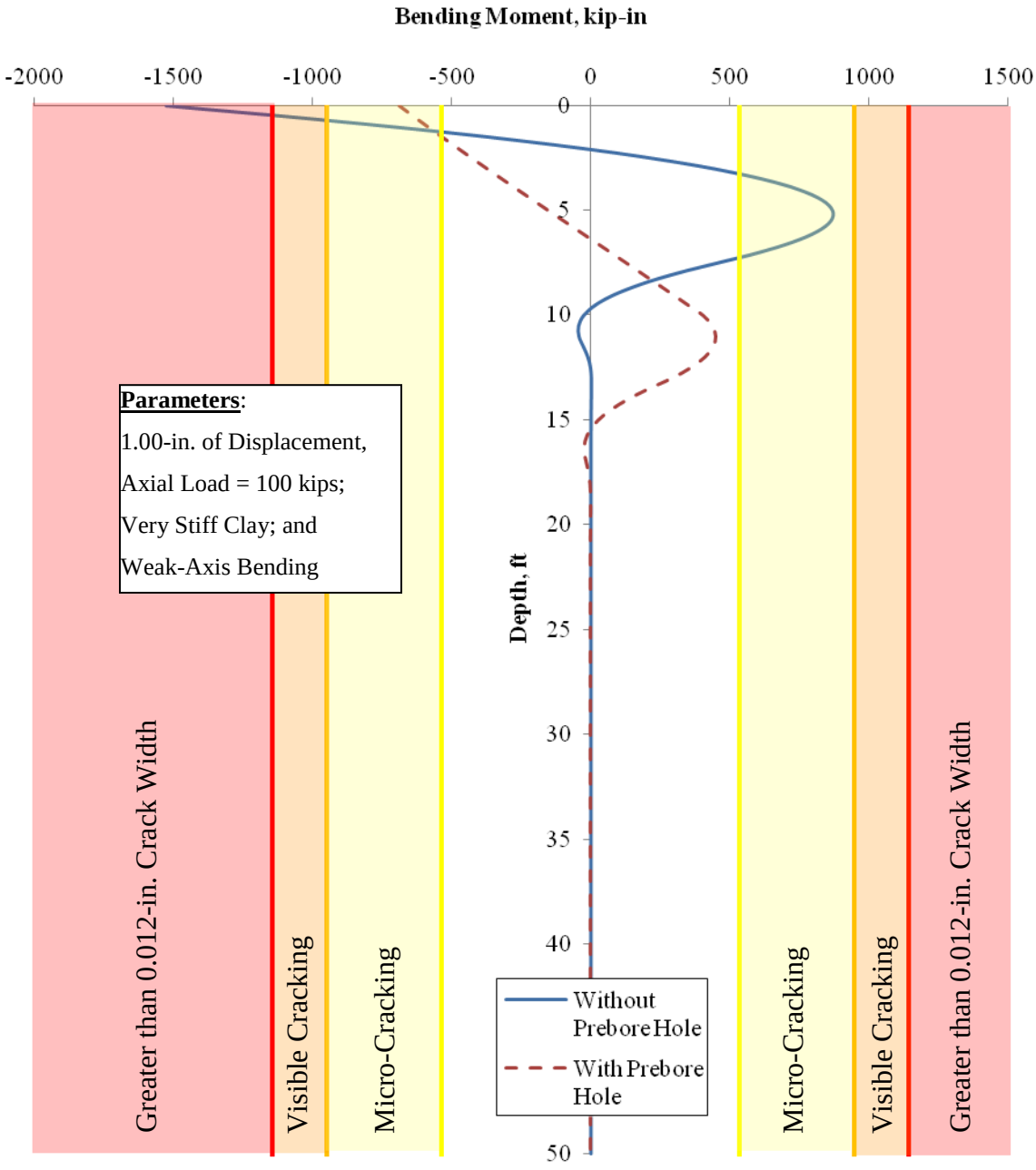

Figure 3-22: Effects of a Prebore Hole on the Imposed Performance of a UHPC Pile

A complete set of the tables from the study can be found in Appendix B, which includes tables of the maximum moments and maximum shear. The depth to the second maximum moments and the depth to the point of fixity are also included.

3.3. EXPERIMENTAL PLAN

The instrumentation, testing plan, and load increments for the field testing and long-term monitoring were based on the results from Phase I of the UHPC project and the parametric analysis conducted in this study.

Phase I of the project identified a need to improve the location and attachment of the PDA equipment to produce better results. Also, a smaller cable was used for the instrumentation so not to make a weak zone within the UHPC pile cross-section during testing and monitoring and the web of the UHPC pile, and rodding the web of the pile during the pouring of UHPC to avoid pocketing within the web of the pile.

The parametric study supports the use of UHPC piles in integral abutments as long as prebore holes are specified. Additionally, the study indicates regions for potential damage and what depth to find it on the pile. A preliminary estimate of the location of instrumentation can be made for the test piles based on the location of the maximum moments.

3.3.1. Field Testing

Two tests were completed in the field. The first field test was a vertical load test which was completed to verify the performance of the UHPC pile and the specified design length of the UHPC production pile since it was 9 feet shorter than the HP 10 x 57 piles used for the bridge. The second test performed was designed with the intention of verifying the performance of the splice detail during driving and lateral loading.

3.3.2. Long-Term Monitoring

The long-term monitoring was designed with the intention of verifying the performance of the UHPC pile subjected to cyclic movement due to the abutments movement caused by thermal effects of an integral abutment. Once completed, the performance will be compared to the steel HP 10 x 57 piles used for the bridge.

CHAPTER 4: PILE-TO-ABUTMENT CONNECTION TESTS

The behavior of a typical pile-to-abutment connection was tested in the laboratory to verify the performance of the abutment, pile and connection. The laboratory tests were designed and completed by using an inverted test setup in comparison to actual field conditions for ease of construction and testing. Full-scale cross-sections for the UHPC and HP 10 x 57 test units and a full-scale section of an abutment were used for the tests. This chapter describes the design, casting, testing, and results of the test specimen SPAC-1 and UPAC-2.

4.1. DESIGN OF TEST UNITS

Three full-scale, 8-ft long UHPC test units and one 8-ft. long steel HP 10 x 57 test unit were designed to test the piles and their connection to abutments using the typical Iowa DOT pile-to-abutment connection detail. The UHPC test units were given the names L7, L8 and L9. The HP 10 x 57 pile was identified as S1, which provided a comparison for the UHPC piles. The HP 10 x 57 pile is a common bridge foundation choice used by the Iowa DOT.

Test units L8 and L9 were cast for future laboratory testing that would focus on the performance of precast pile-to-abutment connections when the pile is subjected to strong-axis bending and to a pile subjected to loading at a 30 degree skew. The focus of this Chapter, however, is on S1 and L7 with each having a cast-in-place abutment cap. Both of these test units were subjected to weak-axis bending for the duration of the test because typical integral abutment piles are oriented to experience weak-axis bending in order to increase lateral flexibility of the bridge foundation.

Typical Iowa DOT abutment details were used as the basis for building the test specimen. Figure 4-1 shows the typical plan view of the abutment details, while Figure 4-2 shows a cross-section view of the abutment and the reinforcement details. The portion of the section modeled in the laboratory is the box found in Figure 4-2 and was rotated 180 degrees for ease of construction and testing, which is shown in Figure 4-3.

The 8-ft length of the test unit was chosen to meet the expectations of the test based on the LPILE analysis in Section 4.4. The test unit was embedded into the abutment cap 24 inches as is commonly used for abutment design. Additionally, 18-in. was needed at the end of the pile to ensure that the prestressing strands were fully developed at the location where the lateral load was applied, thus leaving a maximum lever arm of 54 inches. The cross-section of the test unit was uniform except along the top 18 inches. There was a solid block for the first 9 inches, which was tapered into a H-shaped over the remaining 9 inches as shown in Figure 4-4.

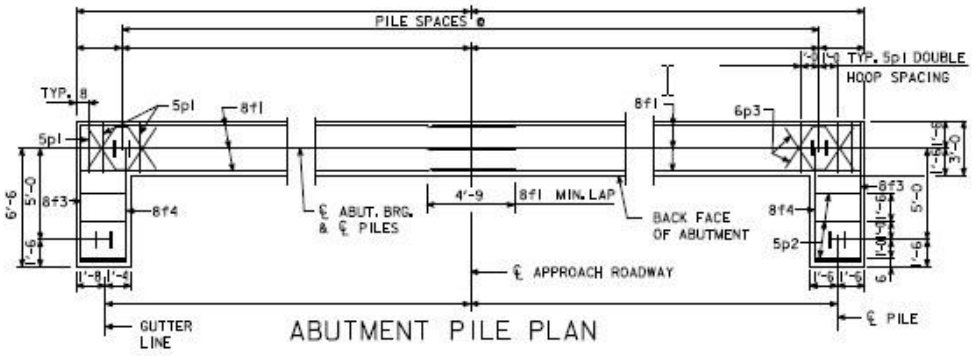

Figure 4-1 Plan View of a Typical Integral Abutment (Iowa DOT 2011)

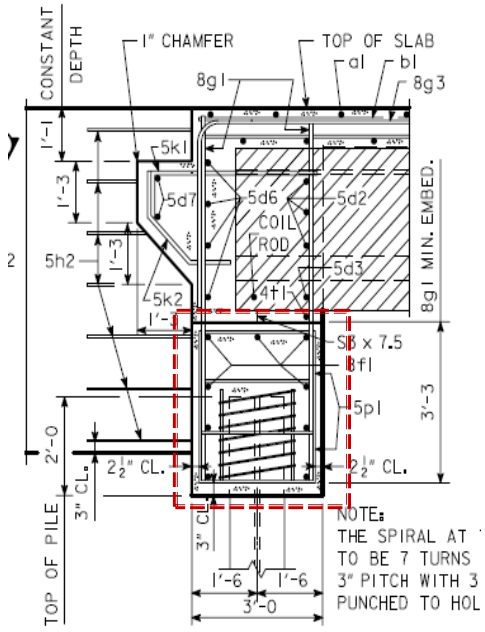

Figure 4-2 Elevation View of a Typical Integral Abutment Detail (Iowa DOT 2011)

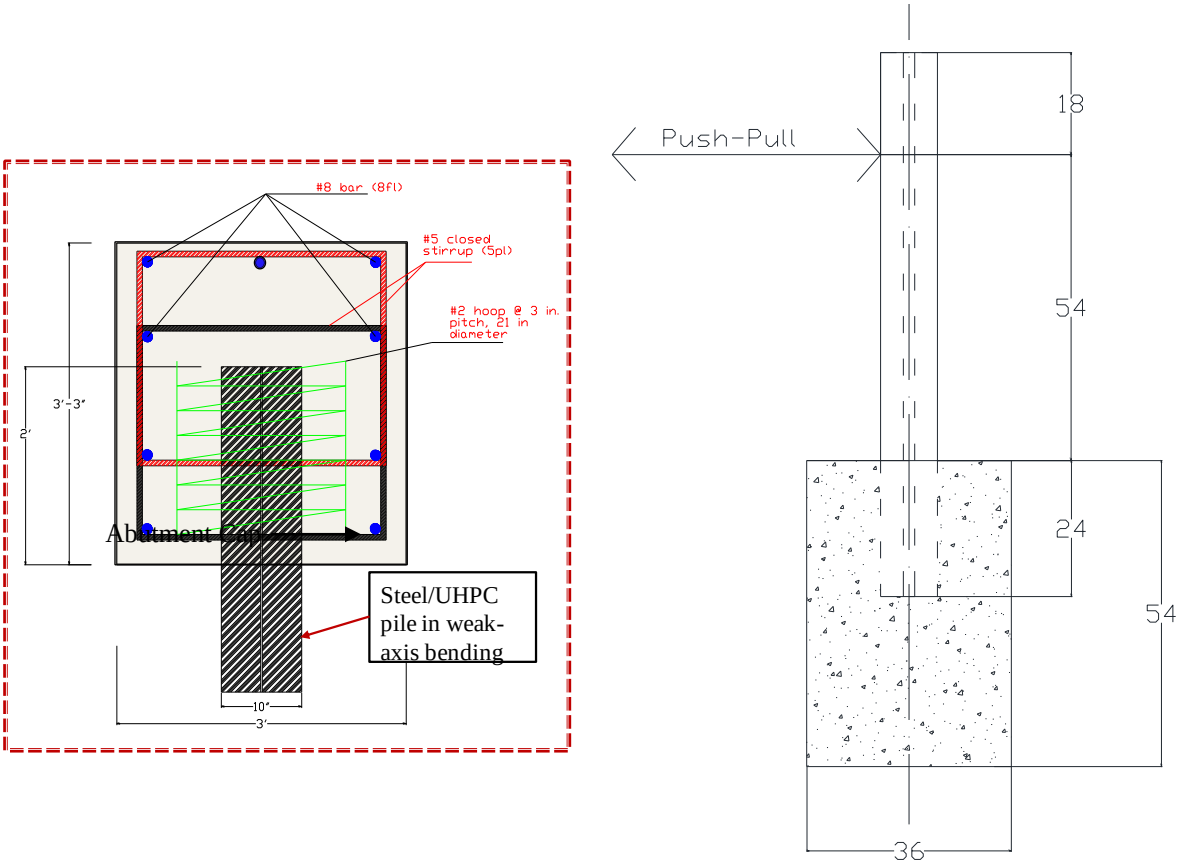

Figure 4-3: Outer Dimensions of the Abutment Block for SPAC-1 AND UPAC-2 (all dimensions in inches)

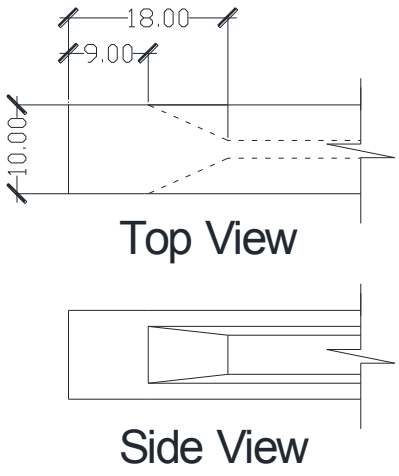

Figure 4-4: Change in Cross-Section of the Top 18 inches on the UHPC Test Unit (all dimensions in inches)

4.2. INSTRUMENTATION SCHEME

The UHPC laboratory test units were instrumented with strain gages on February 8, 2011 at Coreslab Structures, Inc. in Bellevue, Nebraska. The instrumentation scheme for the test units were identical and determined from the LPILE analysis results described in Section 4.4 and the test setup, which is described in Section 4.5.1.

Each test unit had three rotation meters (numbers 1 through 3) and multiple linear variable differential transformers (LVDT) (numbers 4 through 23) were used during the performance evaluation of the test units. Twelve strain gages (numbers 24 through 35) were also used for instrumentation. Table 4-1 lists all of the instrumentation used and the labels for each. The instrumentation was attached to the prestressing strands and the concrete forms at the locations shown in Figure 4-5. In order to attach the LVDTs, nuts were glued to the wood forms at the specified locations to provide a threaded hole as shown in Figure 4-6.

Table 4-1: Instrumentation of UHPC Laboratory Test Pile

ID	Label	ID	Label
1	RM01	**19**	LV16
2	RM02	**20**	LV17
3	RM03	**21**	LV18
4	LV01	**22**	LV19
5	LV02	**23**	LV20
6	LV03	**24**	SGP01
7	LV04	**25**	SGP02
8	LV05	**26**	SGP03
9	LV06	**27**	SGP04
10	LV07	**28**	SGP05
11	LV08	**29**	SGP06
12	LV09	**30**	SGP07
13	LV10	**31**	SGP08
14	LV11	**32**	SGP09
15	LV12	**33**	SGP10
16	LV13	**34**	SGP11
17	LV14	**35**	SGP12
18	LV15		

Additionally, three load cells were used during the tests. One load cell was used to measure the lateral load applied 6-in below the top of the pile, and the other two load cells were used to measure the vertical load applied to the cross beam attached to the top of L7.

Five string-potentiometers were used to measure the lateral displacement of the column. Three of the string-potentiometers were at the point of lateral load application, one at 9-in from the top of the abutment cap, and the final one at 6-in from the abutment cap.

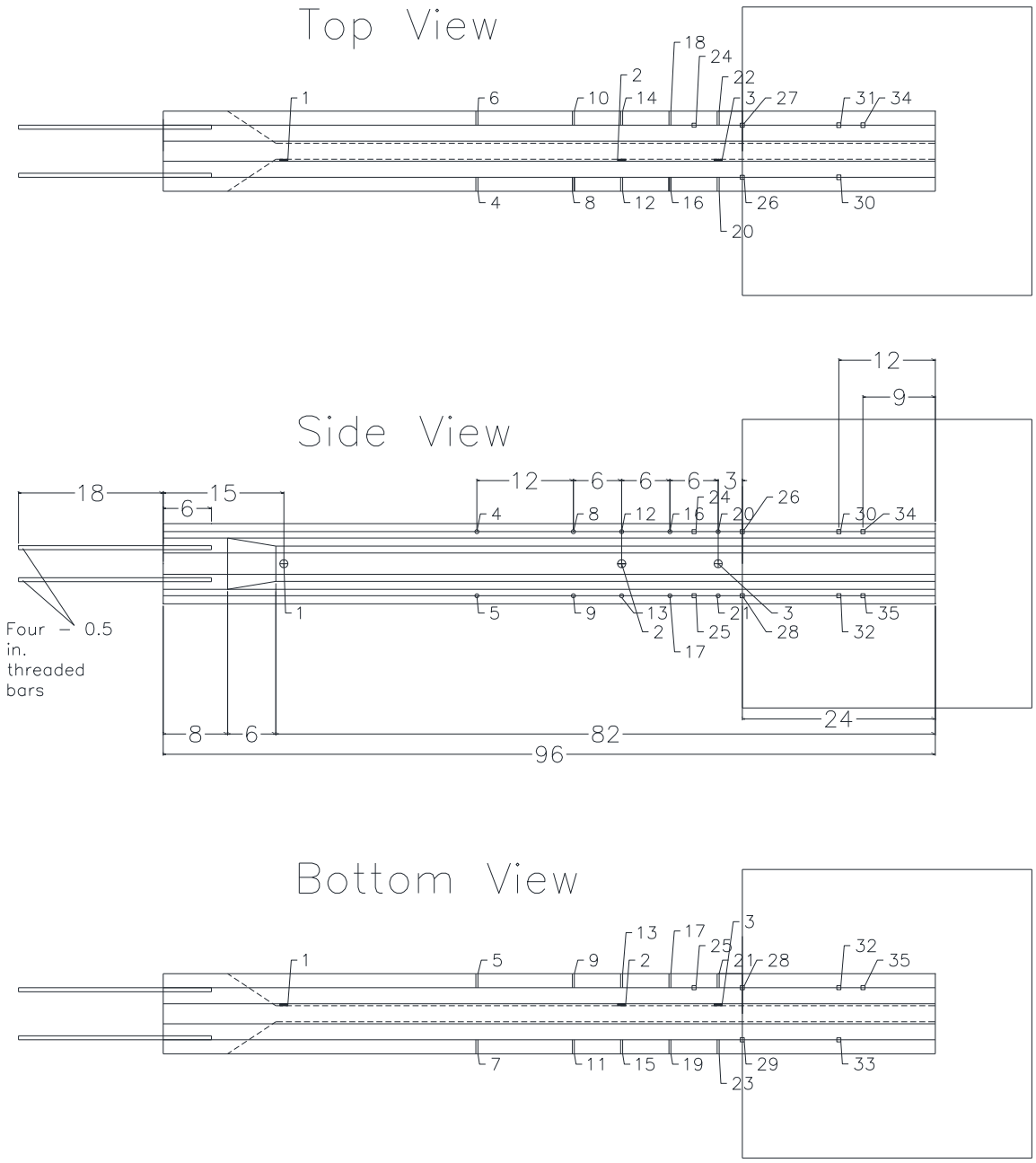

Figure 4-5: Instrumentation Plan used for UHPC Laboratory Test Units

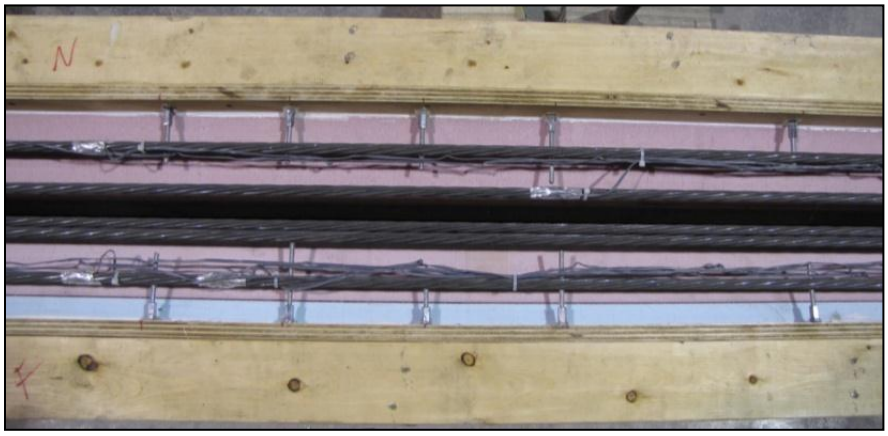

Figure 4-6: Location of Nuts to Fasten LVDTs

4.3. PRECAST FABRICATION

4.3.1. Casting Process

When casting the test units, wooden side forms were used for the UHPC test units and were installed before the ISU research team arrived at the precast plant. The bottom four prestressing strands were arranged in their proper configuration and stressed to their initial prestress of 202.5 ksi, which is approximately 75 percent of their ultimate strength. The strain gages located on the bottom strands were installed as shown in Figure 4-7 following the procedure outlined in Appendix D for TML strain gages. After the bottom row of prestressing strands was instrumented, the Styrofoam inserts were secured to the wood forms with double-sided tape and caulking.

Figure 4-7: Instrumented Bottom Prestressing Strands in the Form

After the Styrofoam was in place, the final six prestressing strands were arranged and stressed to their initial prestress of 202.5 ksi, as shown in Figure 4-8. The rest of the gages were installed to the prestressing strands. Initial readings of the strain gages were taken and the side forms were locked in place. The mixing of the UHPC ensued at the precaster's batch plant in a 4.0 yd^3 mixer.

Figure 4-8: Prestressing Strands Layout at the Anchorage end

After completing the batching of the UHPC mix, the concrete was poured into a bin and transported to the bed by the overhead crane, where it was poured into the forms for all of the UHPC laboratory test units while making sure to rod the web to prevent air pockets. Immediately after the UHPC was poured in the forms, the top surface of the test units was covered with plastic wrap to minimize any moisture loss. A tarp was placed over the UHPC test units and propane heaters were used for the initial curing at 86˚F. Along with the test units, 3-in diameter UHPC cylinders were cast with the pour. The precaster tested cylinders periodically during the initial curing of UHPC to determine the compressive strength of the mix. After reaching a compressive strength of 14 ksi, the prestressing strands were cut at the member ends and the piles were transferred to begin the steam curing was completed.

4.3.2. Details of Test Units Pour

The UHPC laboratory test units were cast at Coreslab Structures, Inc. in Bellevue, Nebraska on February 10, 2011. Figure 4-9 depicts how the test piles were lined up in a

single line along the length of the precast bed to utilize as much of the prestressing strand as possible.

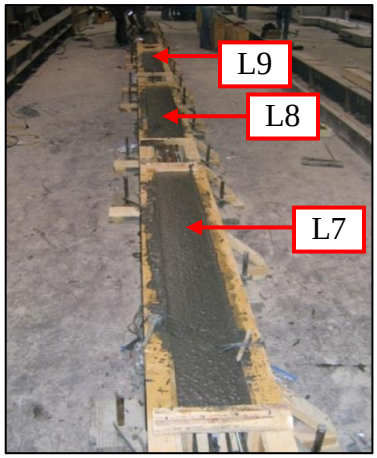

Figure 4-9: Layout of UHPC Test Units

4.3.3. Casting of Pile-to-Abutment Connection Cap

The abutment cap was cast on May 9, 2011 for both SPAC-1 and UPAC-2 in the Iowa State University Structures Laboratory along with the two base blocks. The forms were made out of plywood and had the specified steel reinforcement inside as shown in Figure 4-10. The pile was attached to a steel beam and hung in the desired location with 2 feet of the pile head embedded in the pile cap as shown in Figure 4-11. A drawing of the test specimen is shown previously in Figure 4-3.

Figure 4-10: Abutment Cap Steel Reinforcement Inside of Forms

The 6-yd^3 specified for the 4 ksi strength concrete for the abutment cap was mixed by Iowa State Ready Mix Concrete and transported to the structures laboratory by a concrete truck. Another truck brought the 3-yd^3 of 5 ksi concrete for the base blocks. The concrete truck poured the normal concrete into a bin that was lifted with the overhead crane to the location of the forms. The concrete was then poured and vibrated in a series of steps. Once the abutment cap forms had been filled the surface of the concrete was finished. A similar finish was also completed for the base blocks.

Figure 4-11: Setup used for Casting of the Abutment Cap

4.3.4. Material Properties

4.3.4.1 UHPC

Seven 3-in. diameter cylinders were cast and cured with the UHPC test piles and were tested in compression at the Iowa State University Structures Laboratory using a Universal Compression Machine. The measured strength of the seven cylinders is given in Table 4-2. The design strength of the UHPC mix was 26 ksi, and the results show an average strength of only 20.6 ksi was achieved for the UHPC material. Based on the failure mode, it was suspected the measured strength was not achieved due to the end surface of the test cylinders

not being perfectly horizontal. The elastic modulus for the test piles was calculated using Equation 2-2 from Section 2.3.4 that was developed by Graybeal (2007). The resulting elastic modulus was 6602 ksi as opposed to an expected value of 8000 ksi.

Table 4-2: Measured Compressive Strength of UHPC used in Test Units

Cylinder Number	f'_c, ksi
1	21.4
2	19.8
3	19.1
4	19.4
5	22.7
6	22.8
7	19.1
Average	20.6

4.3.4.2 Abutment Cap

Twenty-four 6-in. diameter cylinders were cast and cured along with the abutment cap, which was tested in compression at the Iowa State University Structures Laboratory. Twelve of the cylinders had the 4 ksi concrete and the other twelve had the 5 ksi concrete. The measured strengths of the cylinders at 3, 7, 14, and 28 days for the abutment cap and base block are given in Table 4-3 and Table 4-4, respectively. The design strength of abutment cap concrete was 4 ksi, and the results show that the 4 ksi average strength for this abutment block and the 5 ksi average strength for the base blocks were achieved before the age of 28 days.

The elastic modulus for the test piles was calculated using Equation 4-1. The resulting elastic modulus for the abutment cap was 3807 ksi and the elastic modulus for the base block was 4137 ksi at 28-day strength.

Table 4-3: Measured Concrete Compressive Strength for Pile-to-Abutment Cap

Cylinder	Concrete Compressive Strength, psi			
	3-day	**7-day**	**14-day**	**28-day**
Test Date:	5/12/2011	5/16/2011	5/23/2011	6/6/2011
1	3720	4279	4236	3930
2	3677	4723	4506	4908
3	3757	4780	4473	4542
Average	3118	4594	4405	4460

Table 4-4: Measured Concrete Compressive Strength of the Base Block

Cylinder	Concrete Compressive Strength, psi			
	3-day	7-day	14-day	28-day
Test Date:	5/12/2011	5/16/2011	5/23/2011	6/6/2011
1	4051	4939	4439	5491
2	3656	4148	5051	4983
3	3857	4649	4768	5331
Average	3855	4794	4910	5268

$$E = 57{,}000\sqrt{f_c'} \text{ (psi)} \qquad \text{(ACI318-05)} \qquad (4\text{-}1)$$

4.4. ANALYSIS

Prior to testing the pile-to-abutment connection, a preliminary analysis was completed to develop the loading protocol for the tests. This section outlines this analysis while Section 4.5.2 presents the loading protocol.

4.4.1. LPILE

LPILE^{PLUS} 5.0 was used to predict the response of abutment piles in weak-axis bending as installed in an integral bridge. The moment-curvature response for UHPC piles and steel HP 10 x 57 piles calculated in Section 3.1 were used for the Type 5 analysis selected within LPILE. A fixed pile head condition was assumed, which is not always the case in the field due to the potential vertical rotation of the abutment, but was used because it would produce conservative results. Also, the 10-ft deep prebore hole filled with bentonite that is commonly required for piles in integral abutments was assumed to provide no lateral resistance to the pile.

4.4.1.1 Predicted Pile Response for Lateral Bridge Movements

Eight different scenarios with appropriate input were analyzed in LPILE to predict the response of the abutment piles for the two different pile types. Table 4-5 describes different

cases which uses different axial loads and lateral displacements. The displacement response was calculated along the length of the pile and compared for each of the cases.

Figure 4-12a and Figure 4-12b illustrate the displacement response of the abutment piles for each of the eight scenarios. It is important to note that the displacements are almost identical when varying the axial load or pile type causing the lines to be on top of one another in the Figure 4-12.

Table 4-5: Eight Cases used to Predict the Response of Integral Abutment Piles

Case	Pile Type	Axial Load, kips	Lateral Displacement, in.
1	**UHPC**	100	1
2			1.55
3		200	1
4			1.55
5	**HP 10 x 57**	100	1
6			1.55
7		200	1
8			1.55

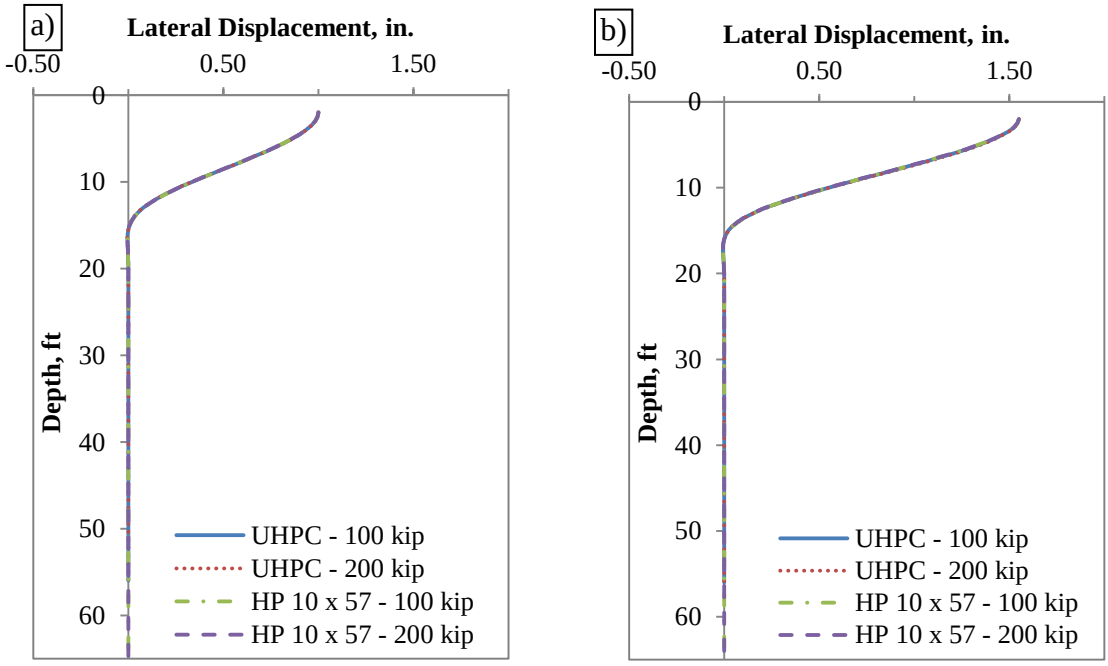

Figure 4-12: Displacement Response of Integral Abutment Piles Subjected to a) 1.00 inch of Lateral Displacement; and b) 1.55 inches of Lateral Displacement

4.4.1.2 Target Laboratory Displacements

To relate the field conditions to the laboratory setup, the maximum displacement was scaled to produce an equivalent laboratory displacement, which is due to the consideration to the short length of the test piles. This was done by subtracting the total displacement, Δ_{total}, by the translation displacement, Δ_t, 54 inches from the pile-to-abutment interface. Figure 4-13a and Figure 4-13b illustrate this process for 1 inch and 1.55 inches of lateral displacement.

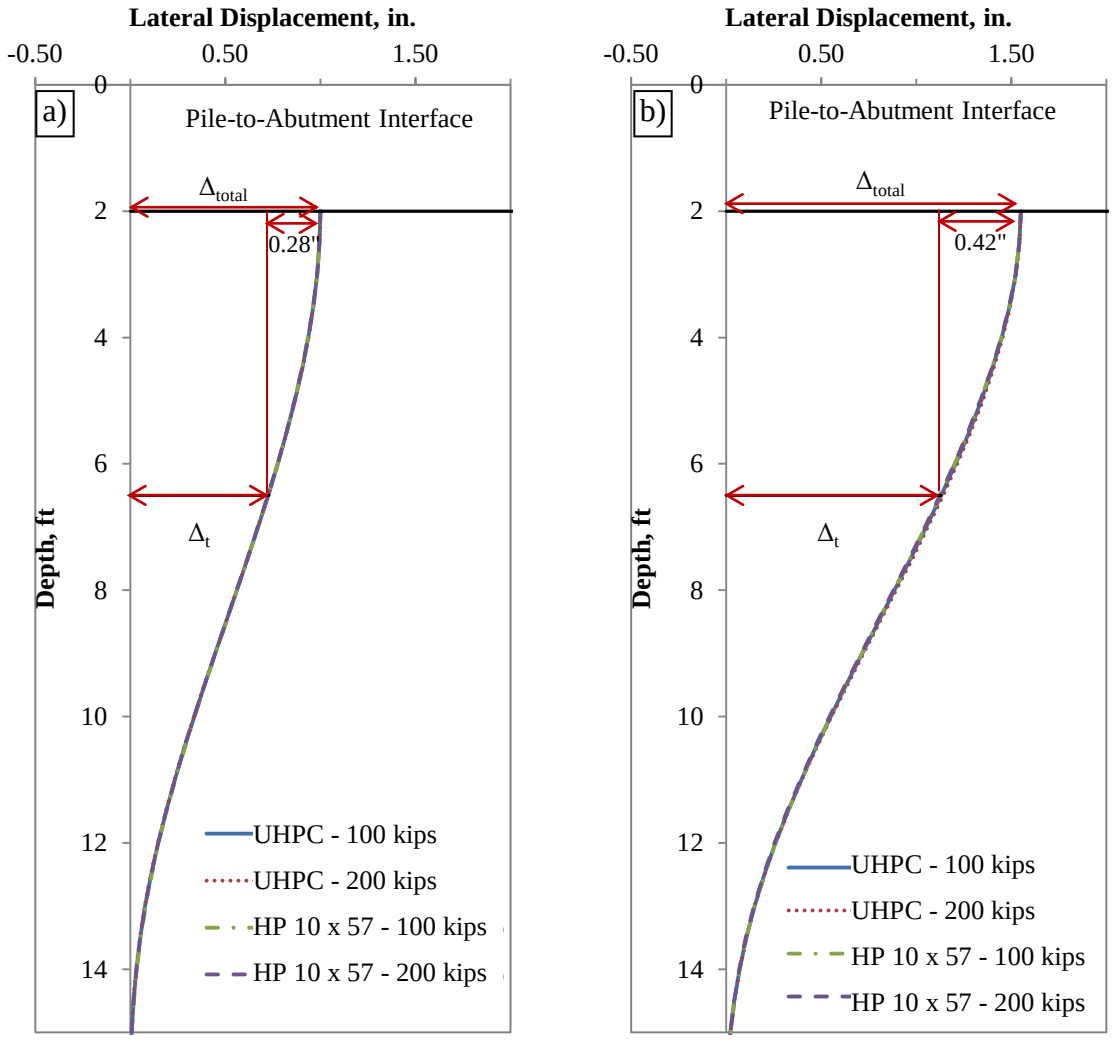

Figure 4-13: Displacement Response of Integral Abutment Piles Subjected to a) 1.00 inch of Lateral Displacement; and b) 1.55 inches of Lateral Displacement

Based on this procedure for each of the scenarios, Table 4-6 lists the displacements for laboratory testing that correspond to the 1.0 inch and 1.55 inches of field displacements. Since the target displacements are very similar, 0.28 inches was used to represent 1 inch of field displacement while 0.42 inches was used to represent 1.55 inches of field displacement.

Table 4-6: Calculated Laboratory Displacements for Each of the Cases

Case	Laboratory Displacements, in.
1	0.27
2	0.42
3	0.27
4	0.41
5	0.28
6	0.42
7	0.28
8	0.42

4.4.2. Cracking and Yielding Limits

From Section 3.2.3, the moments associated with micro-cracking, visible cracking, and maximum crack width were used to calculate the magnitude of lateral force that would need to be applied to the test pile to examine to reach these limits. They were calculated by dividing the moment given in Section 3.2.3 by the 54 inches, where the 54-in. lever arm represented the distance from the applied lateral load to the pile-to-abutment interface. Additionally, the moment for yielding of the steel pile was used for a similar purpose. Table 4-7 lists the calculated lateral forces corresponding to these moments for the test setup described in Section 5.5.1.

Table 4-7: Lateral Load Corresponding to Moment Limits

		Corresponding Strain to Moment Limits, kips			
Pile Type	Axial Load, kips	Micro-Cracking	Visible Cracking	Greater than 0.012-in. Crack Width	Yielding
UHPC	100	9.9	17.6	21.2	-
	200	12.2	20.1	23.1	-
HP 10 x 57	100	-	-	-	20.5
	200	-	-	-	18.4

4.5. WEAK-AXIS PILE-TO-ABUTMENT CONNECTION TESTS

4.5.1. Load Frame and Test Set-up

Figure 4-14 shows the test set up in the laboratory. The abutment cap was raised off of the strong floor by 2 inches to allow the punching of the pile through the cap to be evaluated during the testing. This arrangement was accomplished by using the two concrete base blocks on either side of the pile cap and post-tensioning them together through ducts that were cast into the concrete. An axial load was applied to the test unit by the two actuators shown at the top of Figure 4-14 and the lateral load was applied by a hydraulic actuator.

LVDTs, as shown in Figure 4-15, were used to measure the rotation and displacements at different location along the pile. They were attached to the test unit using an epoxy. Rotation meters were also used to measure the rotation of the test unit at three locations on the pile and were also attached using epoxy. A rotation meter is shown in Figure 4-16. For SPAC-1, TML strain gages were also used at the same locations specified as strain gages for the UHPC test units as shown in Figure 4-5.

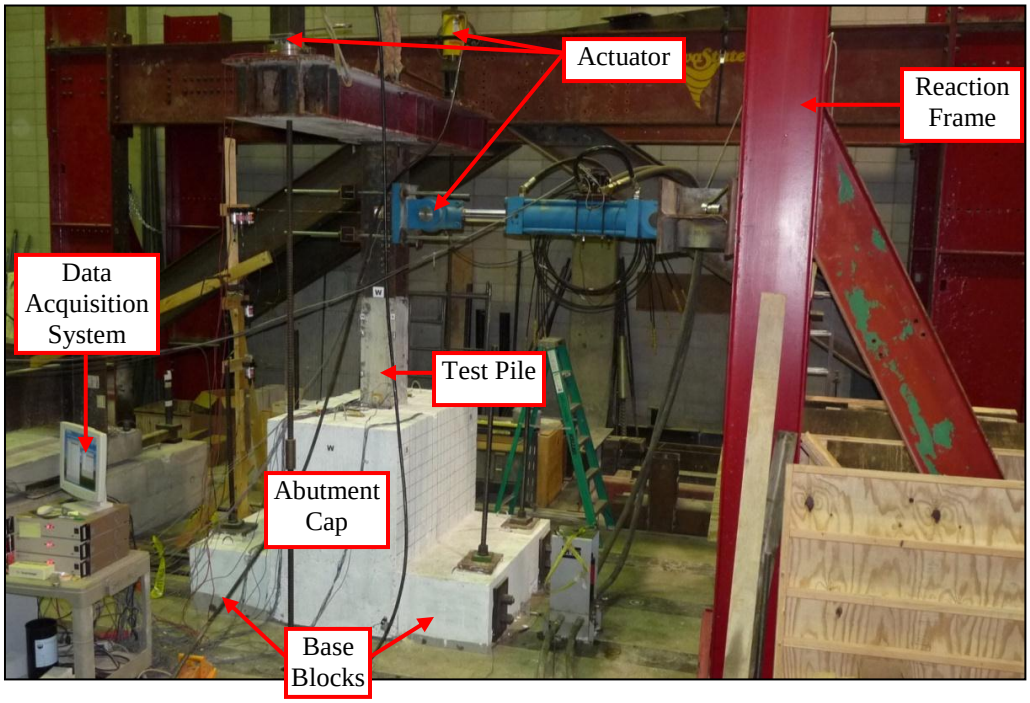

Figure 4-14: Pile-to-Abutment Connection Test Setup

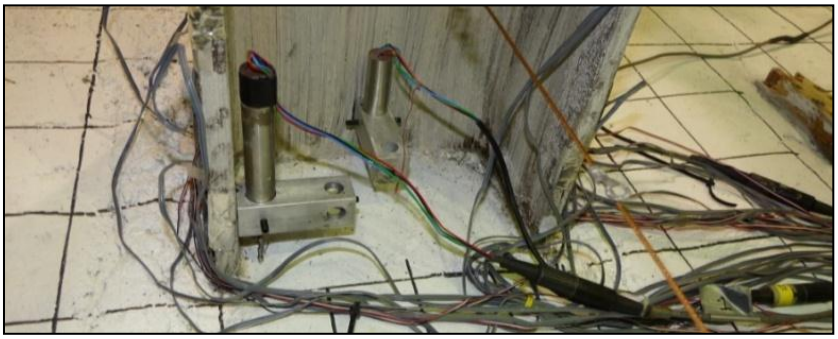

Figure 4-15: LVDTs used Near the Base of the Test Pile during Laboratory Testing

Figure 4-16: A Rotation Meter Attached to the Base of a Test Pile

4.5.2. Test Protocol and Observations

4.5.2.1 SPAC – 1 Connection Test

The steel HP 10 x 57 test pile, SPAC-1, was tested in three phases. Phase I tested SPAC-1 with an axial load of 100 kips on August 8, 2011. The lateral load was initially applied in a force controlled cyclic manner with two cycles per load step. Immediately following Phase I, Phase II increased the axial load on the test pile to 200 kips. Again, the lateral load was applied in a force controlled cyclic manner with 2 cycles per load step. At the beginning of Phase III, the axial load was decreased to 100 kips and the lateral load was applied in a displacement controlled cyclic manner with 3 cycles at each displacement step. All three phases of testing with key forces and displacements are outlined in Table 4-8.

Table 4-8: Loading Protocol used for SPAC-1

Phase	Axial Load, kips	# Cycles per Load Step	Controlling Parameters	Load Steps
I	100	2	Force, kips	±4, ±8, ±12, ±16
II	200	2	Force, kips	±3.5, ±7, ±10.5, ±12
III	100	3	Displacement, in.	±0.5, ±0.75, ±1.0, ±1.5, ±2.0, ±3.0, ±4.0

The cyclic force-displacement response of the HP 10 x 57 test unit during Phase III of SPAC-1 is given in Figure 4-17 along with the measured response envelope established from the first peak cycles. The string-potentiometers located at the point of load application were averaged to give the displacement of the test unit at a given load step. The maximum lateral load applied to S1 was 35.6 kips.

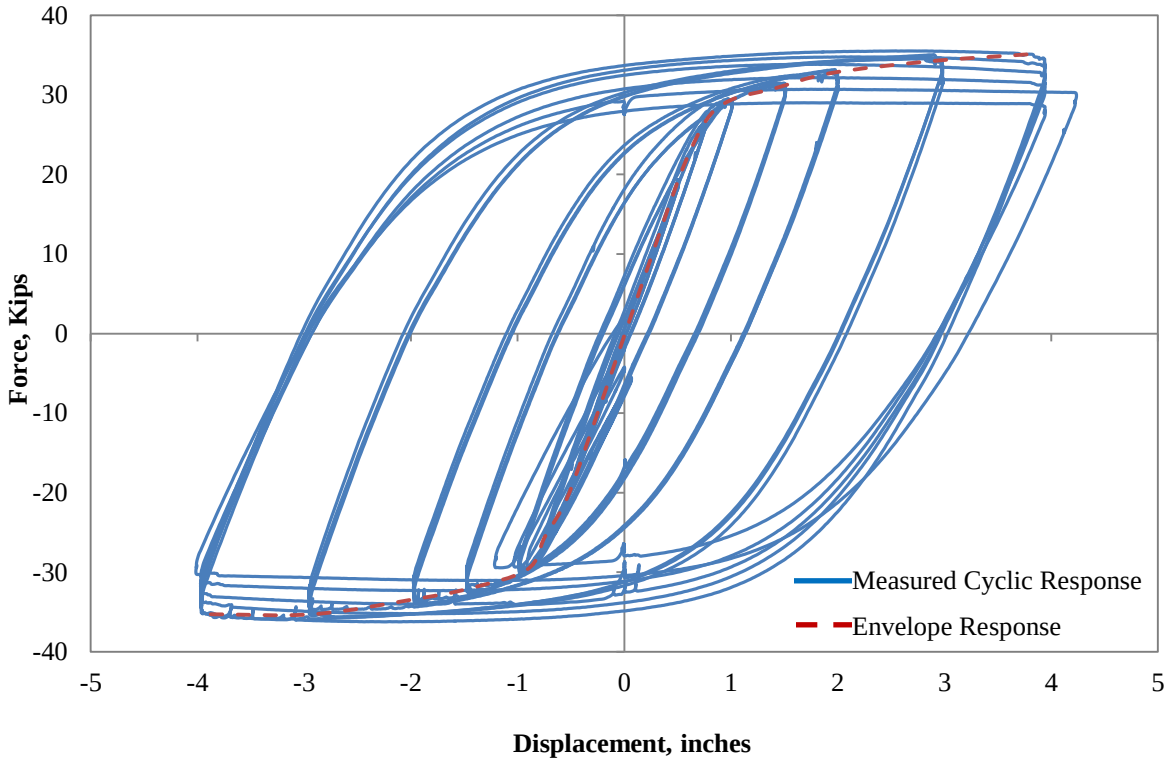

Figure 4-17: Force-Displacement Curve of SPAC-1 Obtainted from Testing

During SPAC-1, yielding was visible on the flanges of the HP 10 x 57 test piles at 26 kips of lateral load with a corresponding lateral displacement of 0.75 inches. Figure 4-18 shows the yielded of the test pile flanges at a lateral load of 29 kips, which has a corresponding displacement of 1.0 inch. A visible gap adjacent to the pile started to open up at the pile-to-abutment interface at 32 kips of lateral load corresponding to 2.0 inches of lateral displacement. Figure 4-19 shows that the gap that was formed during the steel pile test. Also, at this same load step, cracking in the abutment cap were observed.

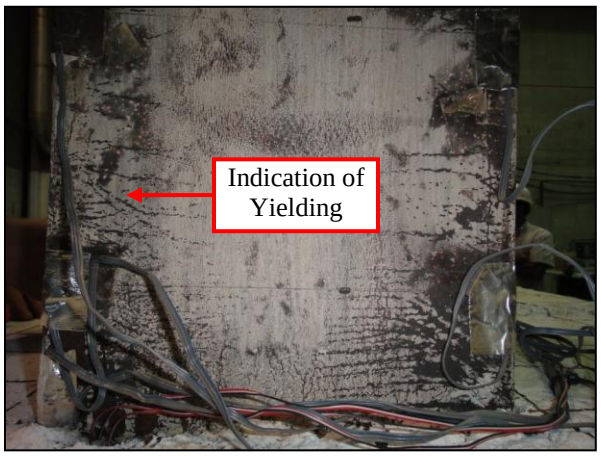

Figure 4-18: Yielding Observed at the Base of the Steel HP 10 x 57 Test Pile during Testing

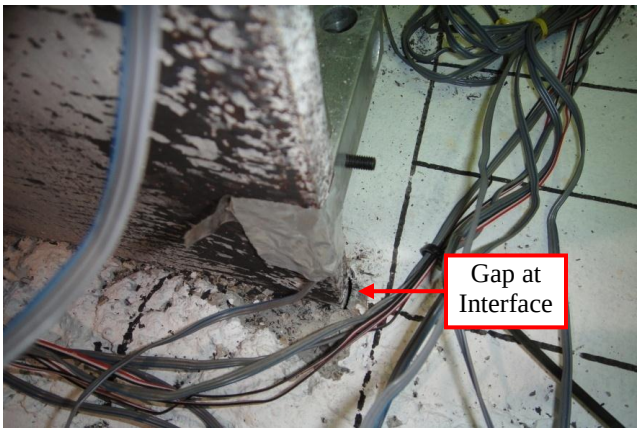

Figure 4-19: HP 10 x 57 Test Pile Rotation at the Pile-to-Abutment Interface

When the lateral displacement became large, buckling of the flanges near the pile-to-abutment interface was visible. Additionally, concrete adjacent to the pile on the top surface

started to spall off the abutment cap when the pile was subjected to 4.0 inches of lateral displacement. Figure 4-20 shows the buckling and spalling of abutment cap concrete after the first cycle of 4 inches of lateral displacement.

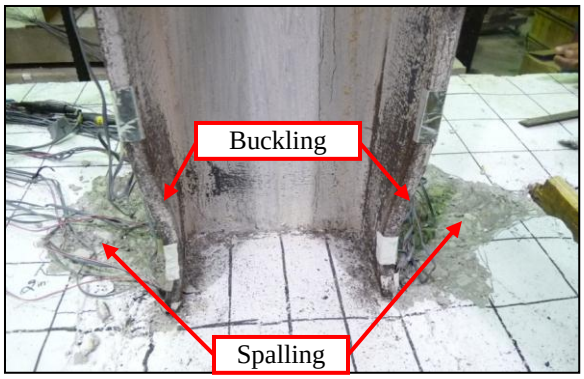

Figure 4-20: Buckling of HP 10 x 57 Steel Pile and Spalling Occurred to the Top Surface of the Abutment Cap

4.5.2.2 UPAC – 2 Connection Test

The first connection test completed for a UHPC pile was UPAC- 2. UHPC test pile, L7, was tested in three phases similar to SPAC-1. Phase I tested UPAC-2 with an axial load of 100 kips on September 13, 2011. The lateral load was applied in a force controlled cyclic manner with 2 cycles at each load step. This was followed by phase II, which used an axial load of 200 kips, but kept the cyclic lateral load force controlled with 2 cycles in each step, which took place on September 14, 2011. The testing was completed with phase III when the axial load was decreased to 100 kips and the cyclic lateral load was displacement controlled with 3 cycles at each displacement. Table 4-9 outlines the loading protocol used for UPAC-2.

The force-displacement curve for Phase III of the UPAC-2 test is shown in Figure 4-21 along with the response envelope established from the first peak cycles. The string potentiometers located at the point of load application were again averaged to give the displacement of the test unit at a given load. The maximum lateral load applied to L7 was 22.8 kips which was 36 percent lower than the lateral load applied to S1. Note that the piles were not designed for any lateral force resistance; instead they were designed for target vertical load resistance. Hence, the reduced lateral load of the UHPC pile should not be of concern.

Table 4-9: Loading Protocol Chosen for UHPC Pile Connection Test, UPAC-2

Phase	Axial Load, kips	# Cycles per step	Control	Load Step
I	100	2	Force, kips	±4, ±8, ±12, ±16
II	200	2	Force, kips	±3.5, ±7, ±10.5, ±12
III	100	3	Displacement, in.	±0.5, ±0.75, ±1.0, ±1.5

Two hairline cracks developed on the test pile during Phase I testing at a 12 kips lateral load near the pile-to-abutment interface as shown in Figure 4-22. Once Phase I was complete, the lateral load was returned to zero and all of the cracks were completely closed. No new cracks were developed during Phase II with the increased axial load and the cracks from Phase I were not visible up to the lateral load of ±12 kips. Minor crushing of UHPC near the base of the pile became visible during Phase III at 1.0 inch of lateral displacement. Figure 4-23 shows the minor crushing of UHPC after cycling though the three 1.0-in. cycles. Throughout all three phases no visible damage occurred to the abutment cap.

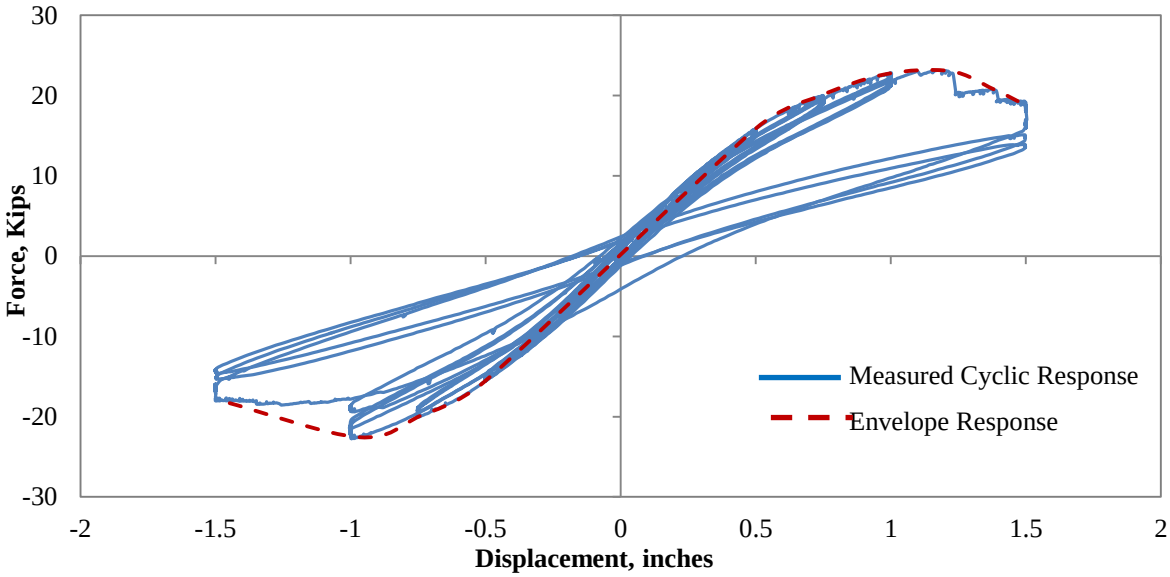

Figure 4-21: Force-Displacement Response during the Testing of UPAC-2

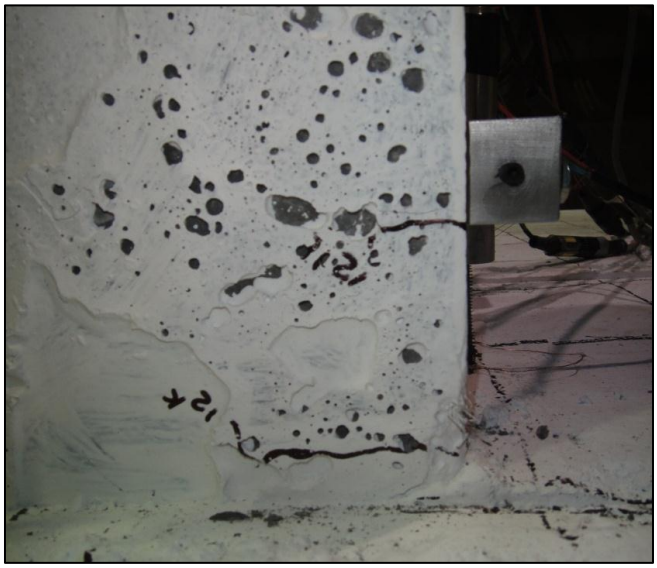

Figure 4-22: Hairline Tensile Cracks that Developed on the UHPC Pile in UPAC-2 at the 12 kip Lateral Load Step with a 100 kip Axial Load

Figure 4-23: Spalled Region of the UHPC Pile Due to Crushing during the UPAC-2 Test after Completing of the 1.0-in. Load Displacement Cycles

4.5.3. Results

Figure 4-24 compares the force-displacement response between UHPC and steel HP 10 x 57 piles up to ±0.5-in. of lateral displacement. The correlation between the laboratory displacements and the full pile service and maximum allowed abutment displacements of an integral bridge are noted in the figure. This section describes the overall response of SPAC-1 and UPAC-2. The complete information from the instrumentation during testing will be available by Garder et al. (2013).

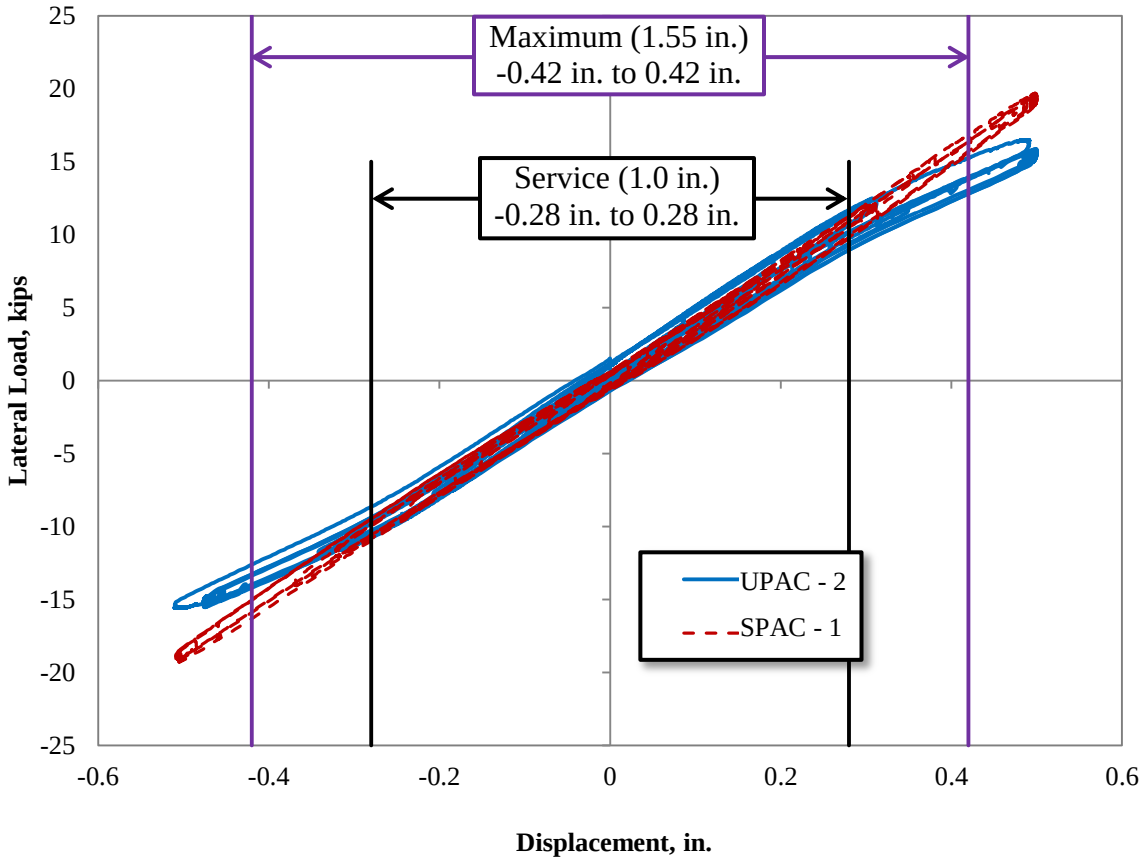

Figure 4-24: Comparison of UHPC and HP 10 x 57 Force-Displacement Response up to 0.5 inches of Lateral Displacement

4.5.3.1 SPAC – 1

From Table 4-7, the lateral load that was expected to cause yielding at a 100 kip axial load is 20.5 kips. The service lateral displacement of 0.28 inches induced a lateral load of

11.3 kips in the push direction and 10.8 kips in the pull direction. Both of these values are well below the yield limit. The maximum displacement of 0.42 inches only induced a 16.9 kip lateral load in the push direction and a 16.4 kip lateral load in the pull direction which are again above the expected yield limit of 15.5 kips for the HP 10 x 57 flanges.

4.5.3.2 UPAC – 2

The predicted start of micro-cracking was induced at a lateral load of 9.9 kips and the predicted start of visible cracking was induced at 17.6 kips. A lateral load of 10.8 kips was required to move the UHPC test unit 0.28 inches in the push direction and 11.5 kips in the pull direction, which indicated micro-cracking should be present in the pile. Additionally, to achieve a lateral displacement of 0.42 inches, a lateral load of 15.3 kips was applied in the push direction and 16.4 kips were applied in the pull direction, which was below the expected limit for visible cracking but increased the extent of micro-cracking.

During testing, two hairline tension cracks developed at 12 kips as shown in Figure 4-22, but were completely closed at 0 kip lateral load and 0 inch lateral displacement and thus they can be considered on the range between micro-cracking and visible cracking. The Iowa DOT deems that hairline cracks were acceptable for UHPC members as long as the widths are negligibly small and are not expected to widen due to repeated loading under the most critical service load conditions (Aaleti et al. 2010).

CHAPTER 5: FIELD TESTING OF UHPC PILES

From the vertical load test in Phase I of the UHPC pile project, the UHPC pile was found to have an 86 percent higher capacity than HP 10 x 57 piles due to the increased toe area. The UHPC production pile for Phase II was designed to be 9 feet shorter than the 65-ft long HP 10x 57 production pile and will be described in Section 6.2. To ensure that the 9-ft reduction in length of the UHPC production pile would have the same capacity as the HP 10 x 57 production pile, a vertical load test was performed on a UHPC test pile with the estimated capacity of 200 kips. A second UHPC test pile was installed with a splice to confirm the performance of the UHPC pile splice during driving, which was followed by a lateral load test to verify the laboratory testing performed on the proposed splicing detail. This chapter describes the design, instrumentation, pouring, installation, and testing of two UHPC test piles at the Sac County Bridge Project site.

5.1. DESIGN OF TEST PILES

The design length of the test piles, anchor piles, and production piles was calculated by following the current Iowa DOT Bridge Design Manual (2011). The predicted design capacity of each of the piles was calculated using DRIVEN (Matthias and Cribbs 1998), CAPWAP (Pile Dynamics, Inc. 2000) and one vertical load test. All of the design calculations are included in Appendix C and Section 5.2 describes the instrumentation of the test piles in detail.

For the vertical load test pile, P3 was designed for a 100 kip design load based on the Iowa DOT SPT values. The soil profile for the location of the vertical load test is given in Section 5.4.2. The required length to achieve the design load of 100 kips, using the Iowa DOT current resistance factors, is 45 feet with 42 feet embedded in the ground. Recently, new resistance factors were calibrated for Iowa (Green et al 2012), which would reduce to a total length of 42 feet with 39 feet embedded into the ground. After the vertical load test was completed, P3 was then used for a lateral load test.

Two 15-ft UHPC pile sections were welded together end to end (P4) at the spice and were used to test the field performance of the splice in both driving and lateral loading. A push-over analysis check was performed using LPILE to make sure that the pile toe would not rotate. The estimated nominal capacity of the P4 using the Blue Book Method was 128 kips and is compared to the other methods in Section 2.5.

The reaction piles were given the names Reaction Pile South (RPS) and Reaction Pile North (RPN). The reaction piles were designed for axial tension by using the Iowa DOT Blue Book method. To give the load frame a capacity of 340 kips, the piles were 80 feet in length with 73 feet embedded into the soil. No instrumentation was installed along the length of the anchor piles, but PDA was run during driving and seven restrikes that were performed on this pile. In axial compression, the current Iowa DOT design practices predicted the capacity of the anchor piles to be 331 kips.

5.2. INSTRUMENTATION SCHEME

The instrumentation used to measure the strains along the length of the UHPC test piles was chosen to be embedded concrete strain gages, as shown in Figure 5-1. The gages were suspended between two prestressing strands at the specified gage locations by wire and installed using the procedure included in Appendix D. Because both P3 and P4 would have lateral loads applied during the lateral load test, the location of the embedded strain gages, as shown in Figure 5-2, were placed on a diagonal at each level of instrumentation to measure the curvature of the piles.

Figure 5-1: Embedded Concrete Strain Gage

Additionally, steel plates were embedded into the web of the UHPC pile to provide a surface to weld a steel pipe that the ShapeAccelArray (SAA) could be inserted into after driving. A total of twelve 2-in. by 4-in. steel plates that are ¼-in. thick with shear studs welded in the center were embedded into the web of P4 on one side for a total length of 20 feet with a typical spacing of 18 inches except over the splice, 36 inches was used. The Styrofoam inserts were cut at the location of the steel plates so that the plate would fit inside of the Styrofoam so not to reduce the area of the web too much as shown in Figure 5-3. The shear stud is the only part of the plate and shear stud combination that would be embedded in the UHPC.

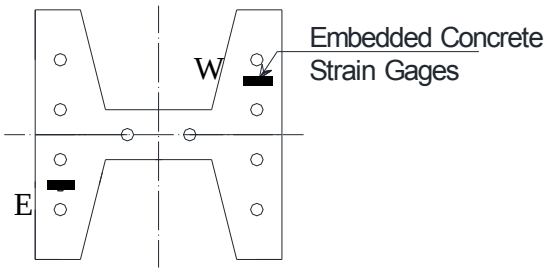

Figure 5-2: Embedded Concrete Strain Gage Location in Plan View

Figure 5-3: Locations of Steel Plates Embedded into P4

During driving, the Pile Driving Analyzer (PDA) equipment was used to measure the driving stresses on P3 and P4 and to predict the capacity of the pile using wave equation

theory. In Figure 5-4, the conduits used to accommodate the PDA instrumentation is illustrated. The strain gages and accelerometers were installed by inserting a bolt through the holes in the web and on the flange.

Notice that the accelerometers were located on the flanges of the pile. This is due to the limited space on the web of the UHPC pile from the tapered flanges. In order to make sure the accelerometers remained flat and tight to the pile, inclined steel brackets were used between each accelerometer and pile. This setup worked very well and valuable data was collected during driving of the UHPC pile. The readings were wirelessly transmitted to the PDA unit provided by the Iowa DOT as shown in Figure 5-5.

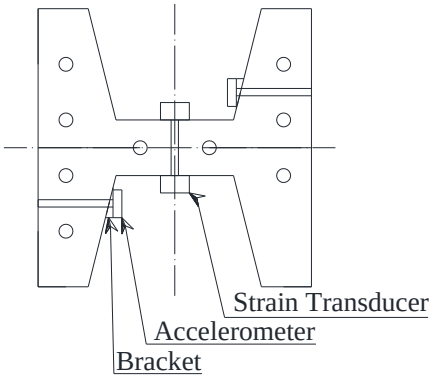

Figure 5-4: Illustration of PDA Instrumentation in Plan View

Figure 5-5: PDA Unit Provided by the Iowa DOT

5.2.1. Test Pile P3

The instrumentation for the vertical load test pile, P3 was installed on November 18, 2011 at Coreslab Structure, Inc. in Bellevue, Nebraska. When the forms were set up for P3, an extra foot was added making the total length of the pile 46 feet in length. Table 5-1 lists the adjusted location and gage label for each of the twenty embedded concrete strain gages. An illustration of the vertical location of the gages is shown in Figure 5-6. Strain gages ISU3-537-E and ISU3-537-W were included on the toe of the drilled shaft to measure the end bearing component of P3 during the vertical load test, but were not recorded during the lateral load test.

Table 5-1: Strain Gage Labels for Test Pile P3

Location from Pile Head, ft	Gage Label	
4	ISU3-48-E	ISU3-48-W
7	ISU3-84-E	ISU3-84-W
9	ISU3-108-E	ISU3-108-W
11	ISU3-132-E	ISU3-132-W
13	ISU3-180-E	ISU3-180-W
20	ISU3-240-E	ISU3-240-W
28	ISU3-335-E	ISU3-335-W
36	ISU3-432-E	ISU3-432-W
43	ISU3-516-E	ISU3-516-W
45.25	ISU3-537-E	ISU3-537-W

5.2.2. Test Pile P4

The instrumentation for the lateral load test pile, P4 was also installed on November 18, 2011 at Coreslab Structure, Inc. in Bellevue, Nebraska. Table 5-2 lists the location and gage labels for all six of the embedded concrete strain gages. Figure 5-7 illustrates the locations of the strain gages as well as the splice, in an elevation view of the pile.

Table 5-2: Strain Gage Labels for Test Pile P4

Location from Pile Head, ft	Gage Label	
4	ISU4-48-E	ISU4-48-W
9	ISU4-108-E	ISU4-108-W
12.83	ISU4-168-E	ISU4-168-W

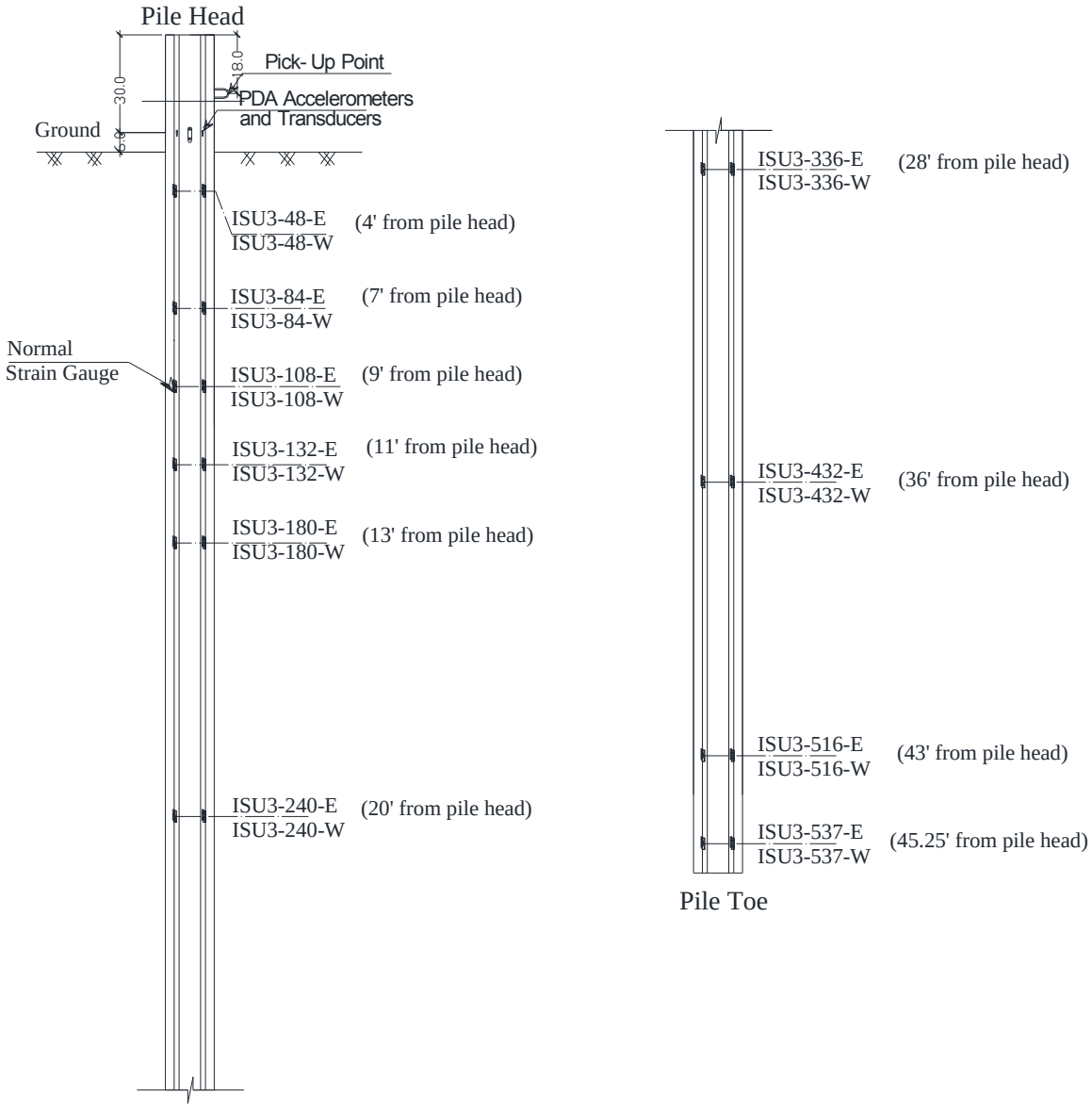

Figure 5-6: An Elevation view of Test Pile P3 Instrumentation

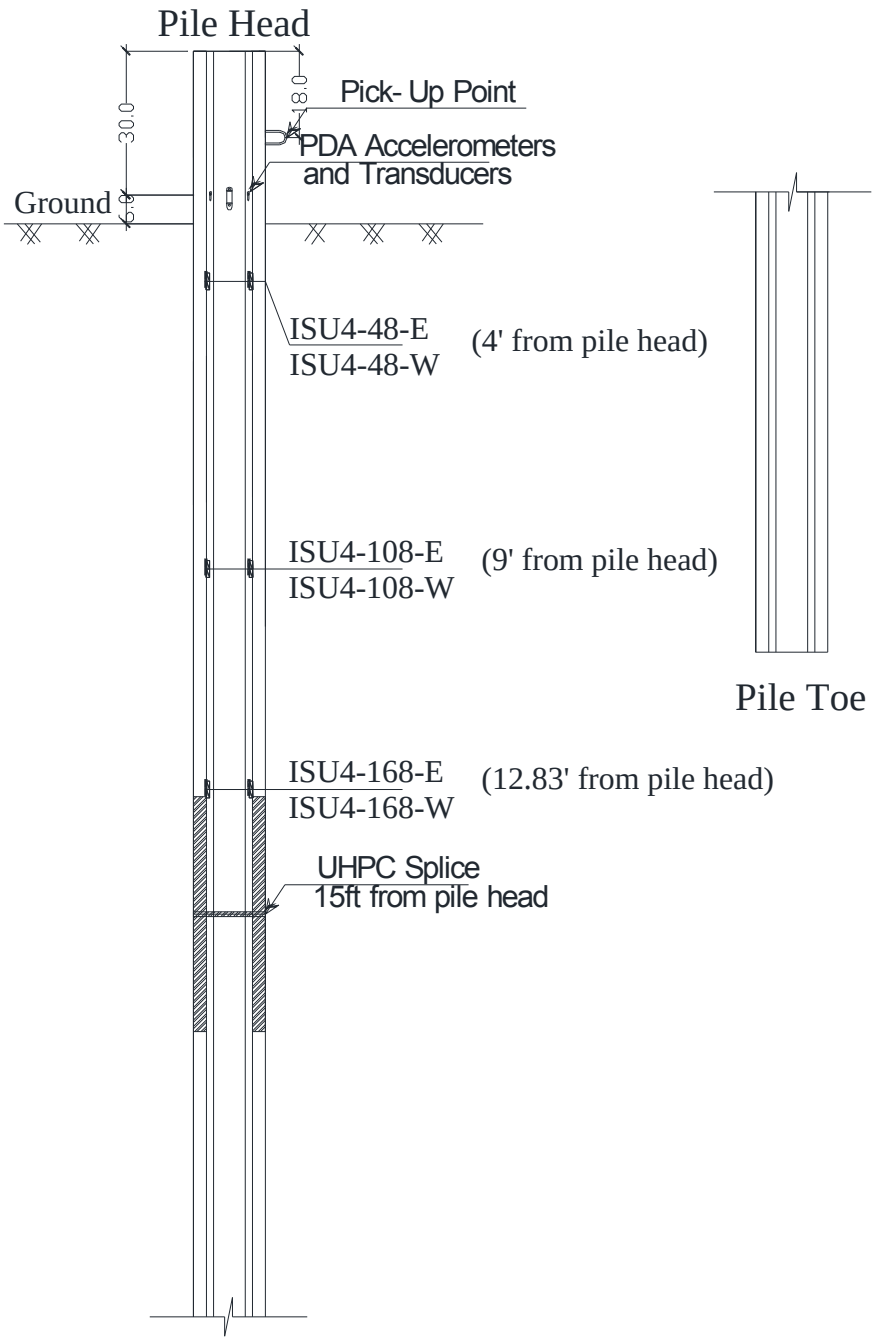

Figure 5-7: An Elevation View of Test Pile P4

5.3. PRECAST FABRICATION

By nature, UHPC induces much greater stresses on the concrete mixer and formwork. Therefore, when mixing UHPC, the mixer will be put under higher demand than that required for normal concrete. The mixer must be able to accommodate higher amounts of shear, minimum blade clearances, and variable speeds (Wipf et al. 2009). As a result, there are limitations on the volume of UHPC that can be mixed at any one time using a typical concrete mixer, which is often only a percentage of the rated capacity. Additionally, when preparing the formwork for UHPC, precautions need to be taken to prevent leaking and lifting of the forms (Wipf et al. 2009). The leaking is prevented by sealing all of the joints and prestressing holes of the formwork, and lifting is prevented by fastening the forms to the precast bed.

5.3.1. Splice Fabrication

The UHPC pile splices were fabricated by Howe Welding in Ames, Iowa, by a certified welder. The ½-inch thick end plates were cut to the same dimensions as the tapered H-section of the UHPC pile, holes were cut into the end plates to accommodate the diameter and location of the prestressing strands, and the edges of the plate were chamfered to allow for welding in the field. Additionally, ¼-inch thick plates were bent to form the angles that were welded to each corner of the splice plate and ½-in. diameter shear studs were welded to the bent plates at the specified locations. Figure 5-8 shows an actual splice and Figure 5-9 illustrates the details of the splice.

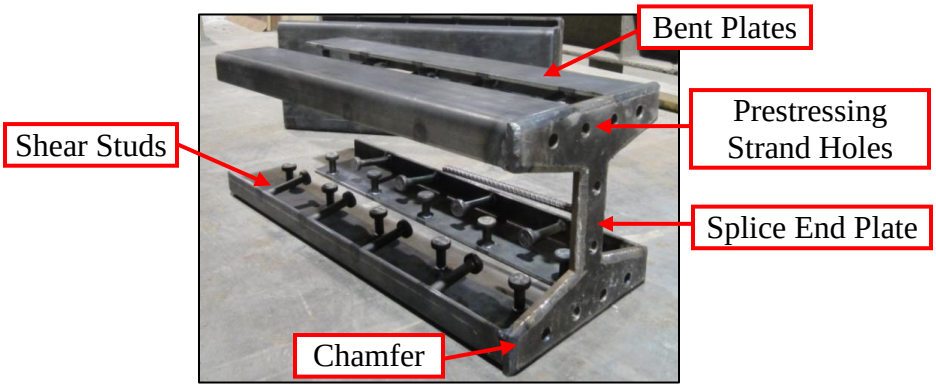

Figure 5-8: Components of UHPC Pile Splice Attachment

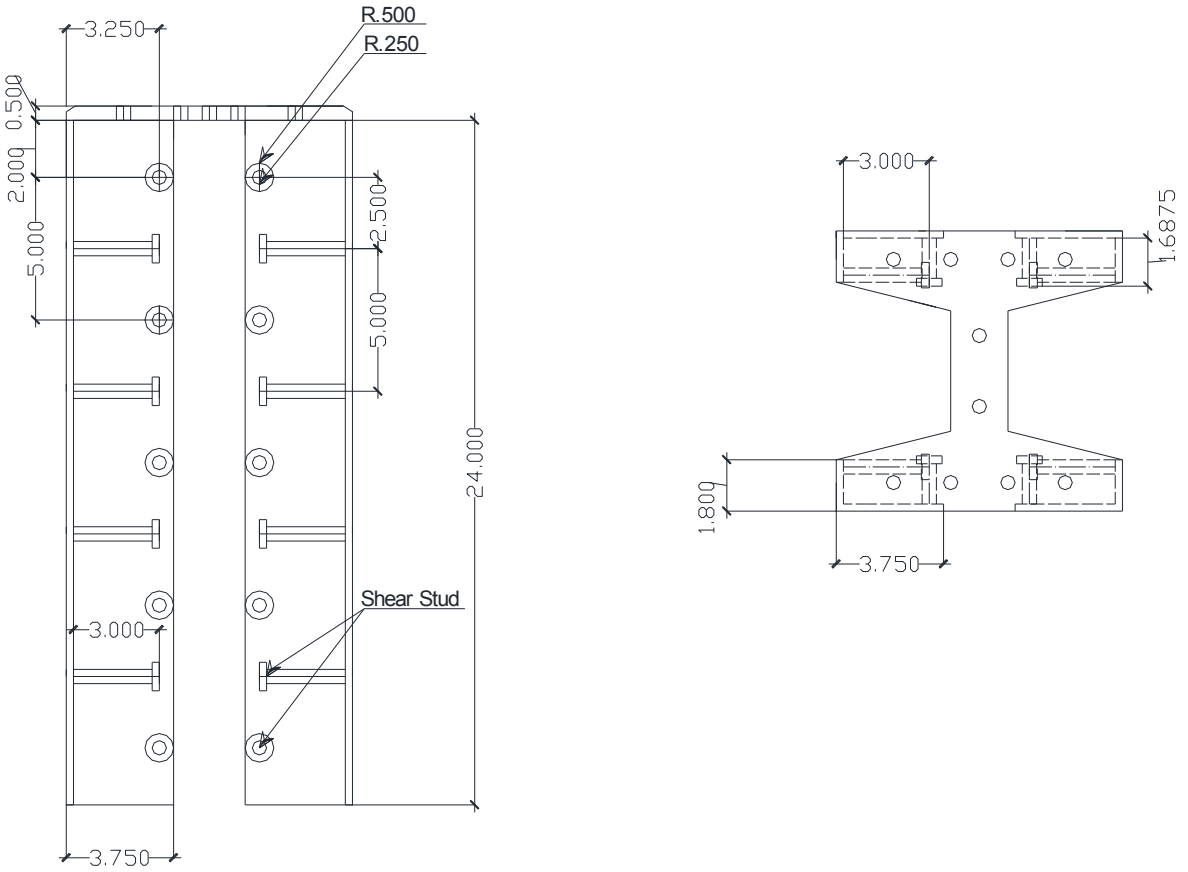

Figure 5-9: Splice Design Details (all units are in inches)

5.3.2. Casting Process

The UHPC field test piles were cast in December of 2011 at Coreslab Structure, Inc. in Bellevue, Nebraska. For the two field test piles, half of the steel side forms with Styrofoam inserts were setup before the research team arrived. While the rest of the formwork was being setup, inserts to accommodate for the PDA equipment, were installed into the Styrofoam inserts as depicted in Figure 5-10.

The two fabricated splices were installed as shown in Figure 5-11. After the splices were installed, all ten of the prestressing strands were arranged and stressed to their initial prestress of 202.5 ksi, which is approximately 75 percent of their ultimate strength. Because one side of the steel forms was left unattached, the strain gages were able to be installed for all of the field test piles and the production pile in the layout shown in Figure 5-12.

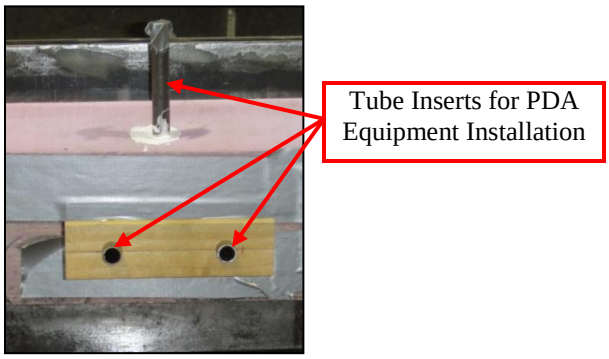

Figure 5-10: Tube Inserts for the PDA Equipment Installed in ISU #3, ISU #4 and UW1-1

Figure 5-11: A UHPC Pile Splice Installed at One of a the UHPC Pile Formwork

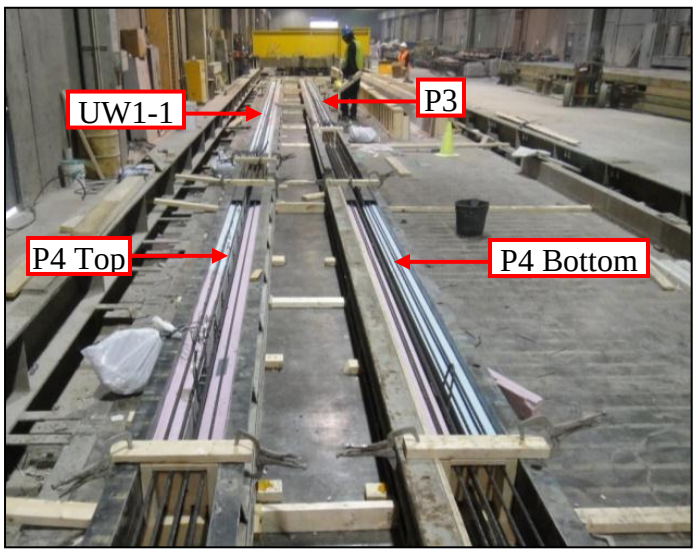

Figure 5-12: Layout of U&HPC Piles P3, P4 and UW1-1

The batching of the UHPC ensued at the precaster's batch plant in a 4.0 yd^3 mixer and approximately 2.75 yd^3 of UHPC was produced for the pour. After completing the batching of the UHPC mix, it was transferred out of the mixer into a large bin as shown in Figure 5-13 and transferred to the bed by the overhead crane. The UHPC was poured into the forms for all of the field test units and production pile as depicted in Figure 5-14. Immediately after the UHPC was poured in the forms, the top surface of the test units and production pile were covered with plastic wrap to prevent moisture loss.

Figure 5-13: Transfer of UHPC from Mixer to Bin

A tarp was placed over the UHPC test units. Propane heaters were used for the initial curing at 86˚F. Along with the test units, twelve 3-in. diameter UHPC cylinders were cast with the pour. The precaster tested cylinders periodically during the initial curing of UHPC to determine the compressive strength of the mix. After reaching a compressive strength of 14 ksi, the prestressing strands were cut at the member ends.

Figure 5-14: Pouring the UHPC from the Bin into the Forms

5.3.3. Details of Field Test Piles Pour

5.3.3.1 P3

Test pile P3 was poured on November 21, 2011 at Coreslab Structures, Inc in Bellevue, Nebraska. The UHPC used for P3 had clumps of cement as shown Figure 5-15. The reason for the clumps is thought to have been caused by the age of the Ductle® material and the lumps came from the bags at the bottom of the pallet used to store the UHPC mix.

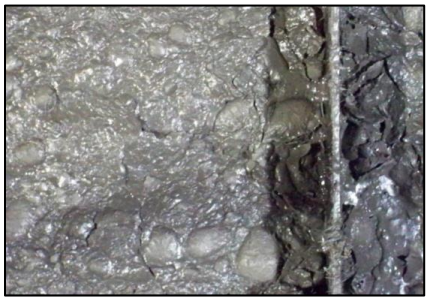

Figure 5-15: Clumps in UHPC after Batching for the 11/21/2011 Pour

Once the concrete was batched and transported to the casting bed, the UHPC was poured into the forms. As the forms began to be filled with UHPC, the formwork shifted and

UHPC leaked out from underneath of the formwork and caused the forms to start floating as shown in Figure 5-16. The concreting was paused to reposition the forms and weigh them down so they would stop floating. To weigh the forms down back into position, rolls of prestressing strands and large concrete blocks were lifted by the crane and placed on top of the formwork. There was a waiting time of about 55 minutes before pouring continued. The UHPC left inside of the forms was raked to join the two layers together.

Figure 5-16: Steel Forms Beginning to Tilt Causing UHPC to Leak

After the forms were stripped, some noticeable defects were found. Figure 5-17 indicates that the Styrofoam portion of the form became unattached and began to float, for one of the form sections. No cracking from the prestressing was found on the top side where

the flange was only 1 inch thick instead of the specified 1.8 inches. It was decided to use P3 for field testing even with the identified defects.

Figure 5-17: Change in the Flange Thickness of P3

5.3.3.2 UHPC Pile P4

Due to the complications that happened during the pour of P3, there was not enough UHPC to complete the pour of P4. Therefore, P4 was poured on November 22, 2011. The forms were reinforced to prevent shifting and floating.

The amount of UHPC that needed to pour P4 was 0.6 yd^3 and was smaller than the minimum amount of concrete required for the 4 yd^3 mixer so the small 1 yd^3 mixer was used at Coreslab. The mixer stopped due to the high demands UHPC subjected the mixer, as suggested by Wipf et al. (2009). Seventy-five percent of the materials were bailed out of the mixer using 5 gallon buckets and the mixer was started again. When all of the material within the mixer became fluid, one 5 gallon bucket at a time was added to the mixture until all of the material was added and mixed.

5.3.4. Steam Curing

After the release of the prestressing strands in P3 and P4, the test piles were steam cured with UW1-1 at 194ºF for 48 hours at the precasting plant. All twenty of the gages in P3 and six gages in P4 were working after the steam curing.

5.3.5. Handling of UHPC Test Piles

For the field test piles, lifting hooks were designed as shown in Figure 5-18 and Figure 5-19. The lifting hook was placed 1.5 feet away from the pile head. Coreslab added an additional hook at the pile toe for easy storage and transportation out of the precast bed and to the construction site.

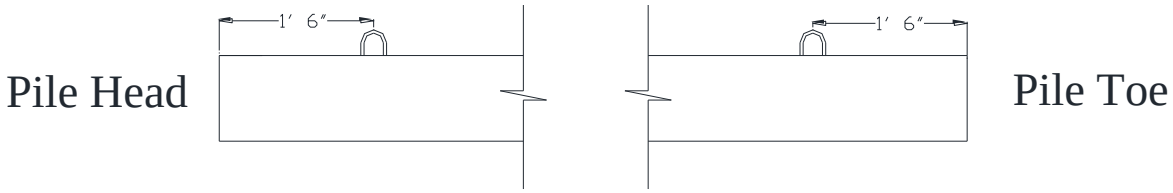

Figure 5-18: Location of Pickup Points

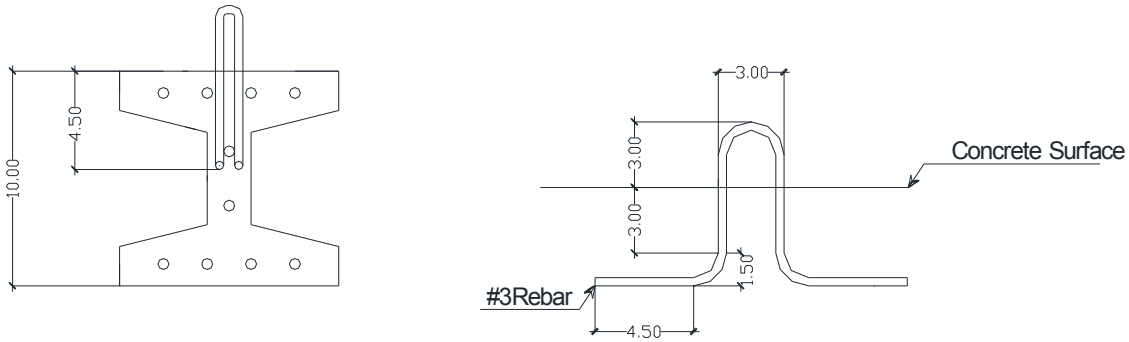

Figure 5-19: Original Pickup Point Design for Field Installation

5.3.6. Material Properties

5.3.6.1 Prestressing Strands

Three 5-ft sections of the 270 ksi low-relaxation prestressing strands were cut from the prestressing strand role used for the test piles and the first production pile. The three strands were tested in uniaxial tension at Iowa State University until reaching the yield stress. Figure 5-20 shows the stress-strain response of the specimens. The continuous lines are where the strain was directly measured and recorded by the data acquisition system, and the dashed lines are where the strain was calculated by taking the change in length of the specimen divided by the original length. The average yield stress was found to be 250.5 ksi and the average modulus of elasticity is 29,449 ksi.

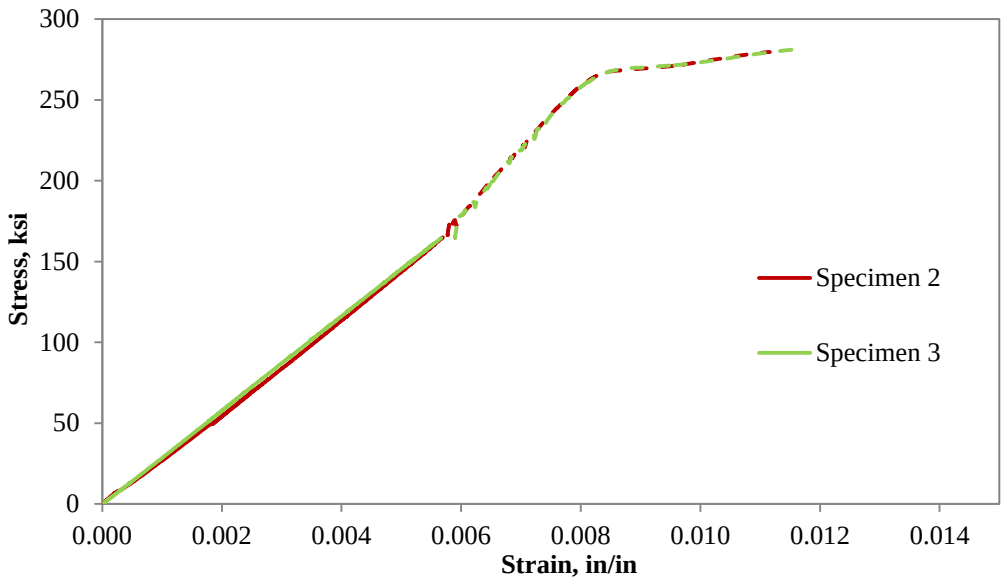

Figure 5-20: Stress-Strain Response of Prestressing Steal used in P3, P4 and UW1-1

5.3.6.2 UHPC

The 3-in. diameter cylinders were cast and cured with the UHPC test piles and were tested in compression by Coreslab Structures, Inc. The measured strength of six of the cylinders is given in Table 5-3. The design strength of 26 ksi for the UHPC mix was, achieved. The elastic modulus for the test piles was calculated using Equation 2-2 from Section 2.3.4. The resulting elastic modulus was 7502 ksi.

Table 5-3: UHPC Compressive Strength at 46 days for UHPC Piles P3, P4 and UW1-1

Cylinder #	f'_c, ksi
1	26.9
2	25.9
3	26.9
4	26.6
5	27.3
6	26.0
Average	**26.6**

5.4. DRIVING OF UHPC TEST PILES

5.4.1. Test Site

The site for testing piles P3 and P4 was located on the same side of the bridge as the production UHPC pile would be installed to verify the capacity of the shortened UHPC production pile with respect to the production steel HP 10 x 57 piles. Figure 5-21 shows the approximate location relative to the Sac County Bridge.

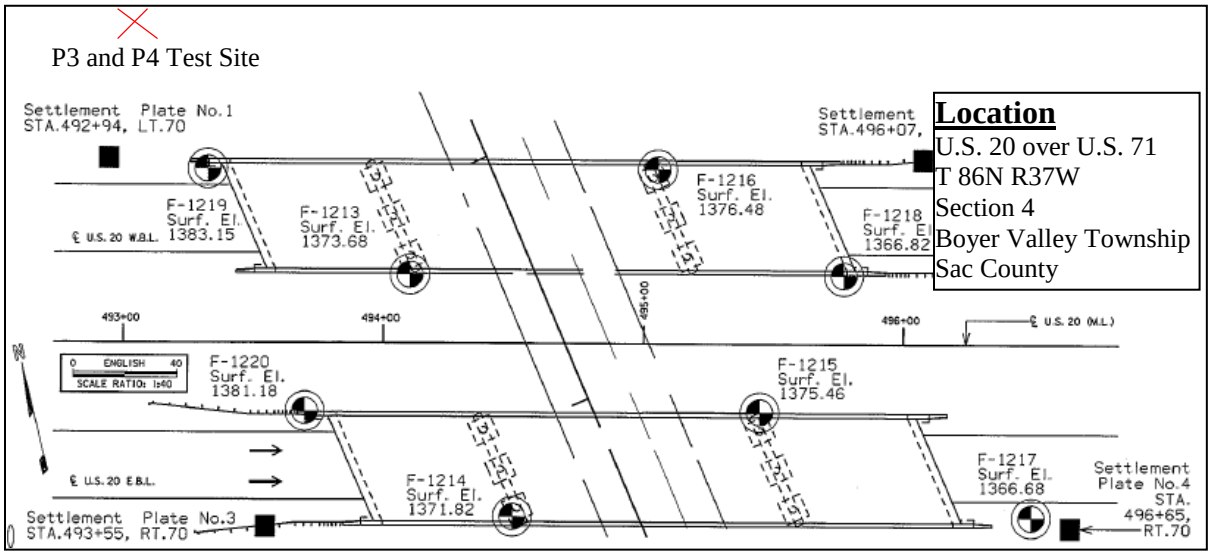

Figure 5-21: Location of Test Pile

5.4.2. Soil Profile

One Standard Penetration Test (SPT) and one Cone Penetration Test (CPT) were conducted by the Iowa State Research team at the location of the test piles. The SPT test was performed by TEAM Services on August 4, 2011, and the CPT test was performed by Geotechnical Services, Inc. on August 10, 2011.

The soil at the Sac County Bridge site consists of cohesive clay and silty clay. The water table was located at a depth of approximately 20.50 feet according to the Iowa DOT soil report for borehole F-1219 near the west abutment of the westbound bridge. Figure 5-22 shows the soil classification reported by the Iowa DOT based on SPT and the classification by TEAM Services based on the CPT test.

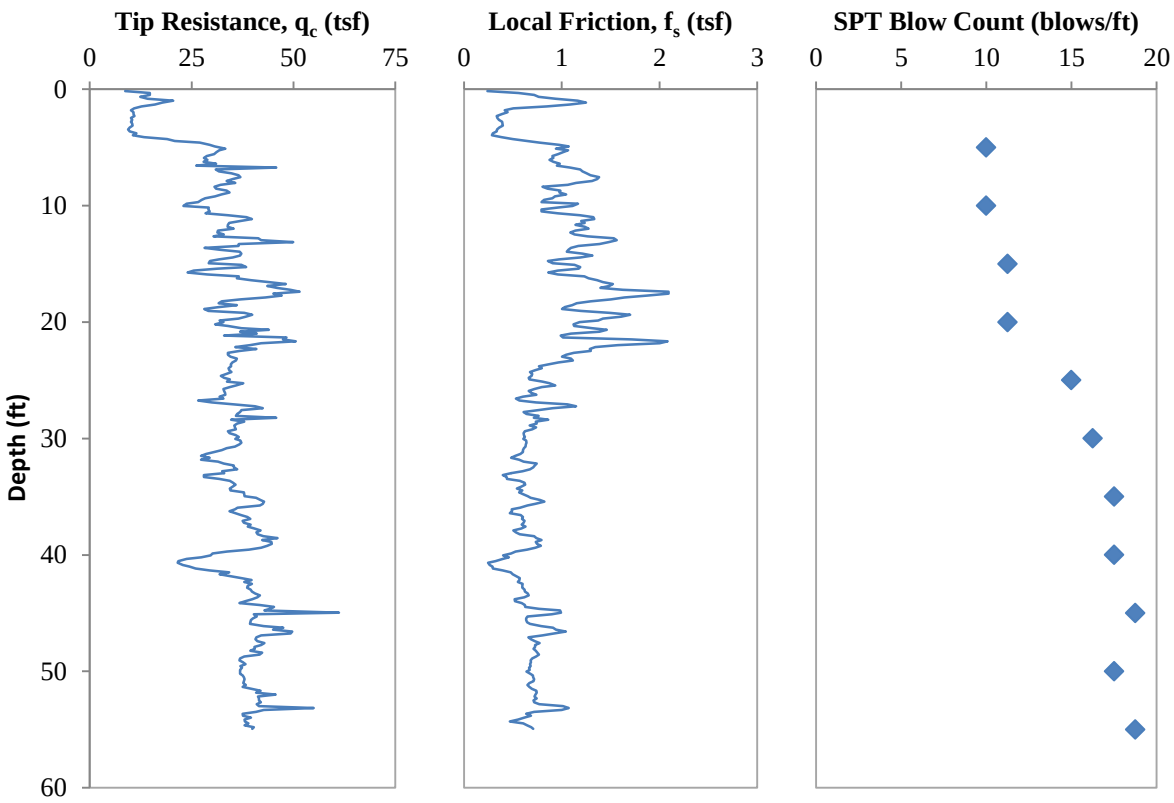

Figure 5-22: CPT and SPT Data at the Test Pile Location at the Sac County Bridge Site

Table 5-4 shows the undrained shear strength and friction angle for each soil layer, which was calculated from the CPT test results. The undrained shear strength and friction angle for each layer was calculated using by using an empirically based approach described by Lunne et al. (1997).

Table 5-4: Undrained Shear Strengths and Friction Angles Calculated from CPT Data

Soil Classification	Depth to Bottom of Layer, ft	Undrained Shear Strength, psi	Friction Angle, Degrees
Clay	4.43	11.52	34.9
Clayey Silt to Silty Clay	10.66	28.02	35.8
Clayey Silt to Silty Clay	16.4	31.07	34.9
Clayey Silt to Silty Clay	17.88	41.66	35.8
Silty Clay to Clay	19.03	33.07	34.6
Sandy Silt to Clayey Silt	55.12	31.45	32.9

5.4.3. Driving System

The HP 12 x 53 anchor piles were driven first, followed by driving of P3 and then P4 at the locations indicated in Figure 5-23. A 4-in thick plywood cushion with horizontal grain was used while driving P3 and P4. Even though the driveability analysis described in the following section indicated UHPC pile stresses during driving would be well within the allowable stress values with no pile cushion at the maximum hammer stroke, the pile cushion was used for the UHPC piles as a precautionary measure.

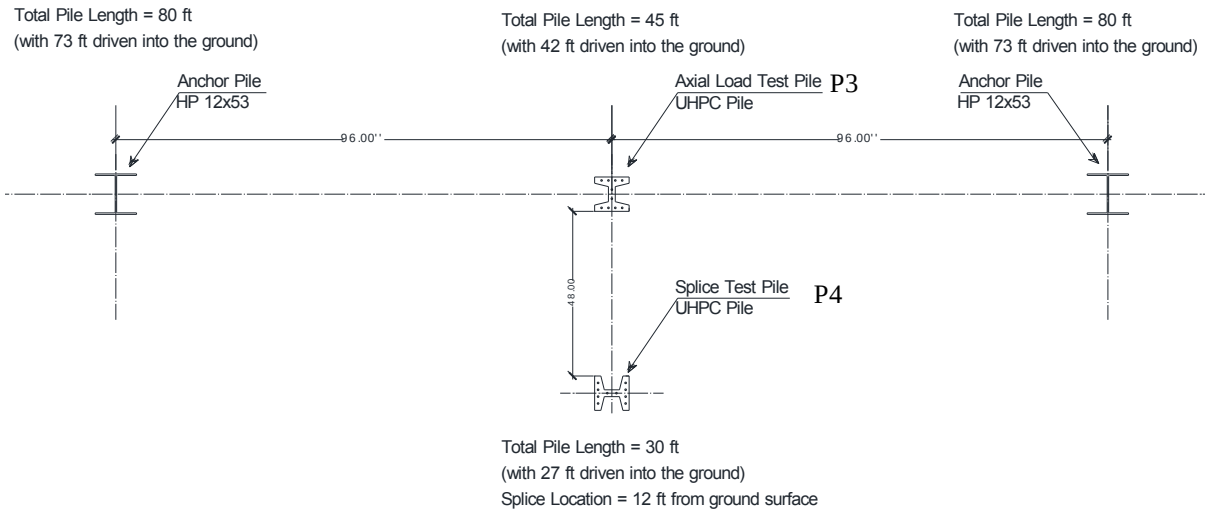

Figure 5-23: Location of Test Piles P3 and P4 in Plan View

5.4.4. Driveability Analysis

In addition to the mentioned hammer properties in Section 5.4.3, an elastic modulus of 530 ksi and a coefficient of restitution of 0.8 were assumed for the hammer cushion. The elastic modulus and the coefficient of restitution for the plywood pile cushions used on the UHPC piles were assumed to be 30 ksi and 0.4, respectively by following the Iowa DOT guidelines (Dirks and Kam 2003). The percent shaft resistance on the UHPC test piles and steel anchor piles was calculated using the undrained shear strength and friction angles calculated for the average CPT results in the FHWA computer program DRIVEN (Matthias and Cribbs 1998). The driveability analysis was conducted using GRLWEAP, and the maximum predicted stresses during driving for the UHPC and steel piles are shown in Table

5-5, which shows that both the tensile and compressive driving stress measured for the test piles were well within the limits for UHPC.

Table 5-5: Predicted Maximum Stresses during Driving of the UHPC Test Piles and Steel Anchor Piles

Pile		Maximum Stress, ksi
		Predicted
RPS	Compressive Stress	29.4
	Tensile Stress	1.7
RPN	Compressive Stress	29.4
	Tensile Stress	1.7
P3	Compressive Stress	7.2
	Tensile Stress	0.1
P4	Compressive Stress	5.9
	Tensile Stress	0.0

5.4.5. Driving Process

The first 40 feet of RPS was driven at the Sac County test site on December 6, 2011. The second 40 feet of RPS and both sections of RPN were driven on December 7, 2011. P3 and P4 were both driven on December 8, 2011. PDA equipment was used to monitor the driving of the HP 12 x 53 anchor piles, P3 and P4. Five restrikes were performed on the RPS, RPN, P3, and P4 at 5 minutes, 1 hour, 1 day, 3 days, and 7 days after the end of drive (EOD).

5.4.5.1 Steel Anchor Piles

The PDA equipment was bolted to the anchor piles while the pile was lying on the ground. In order to bolt the PDA equipment to the pile, five 3/8-in. diameter holes had to be drilled in the steel. Once completed, the steel piles were lifted into position by cutting a hole in the web and passing a crane hook through it. The pile was lifted to a vertical position while a second crane had the hammer leads. The steel piles were positioned inside of the hammer leads at the correct location and the helmet was placed on the top of the steel pile. When the leads, hammer and pile were in place, the ram of the hammer was lifted manually by the crane and dropped.

Since the anchor piles were specified to be 80 feet in length, two 40-ft sections were spliced together for the anchor pile. After the first 40-ft section was installed, the second 40-

ft section was picked up by the crane and the two piles were spliced together by a butt-weld shown in Figure 5-24. Once the welding was completed, the hammer was placed back on the pile and driving was resumed.

At the end of drive, both of the anchor piles, RPS and RPN, experienced minimal local buckling or bending of the flanges near the pile head. The top 12 inches were cut off as planned after the restrikes were performed to provide a level and even surface for the load frame to rest on.

Figure 5-24: Steel HP 12 x 53 Butt-Weld Splice

5.4.5.2 UHPC Test Piles

Before P4 was installed, the two 15 foot long pieces were welded together horizontally on the ground as shown in Figure 5-25a. Once the splice was complete, the steel pipe for the SAA equipment was welded to the web of P4 so that it could be driven alongside of the test pile as shown in Figure 5-25b.

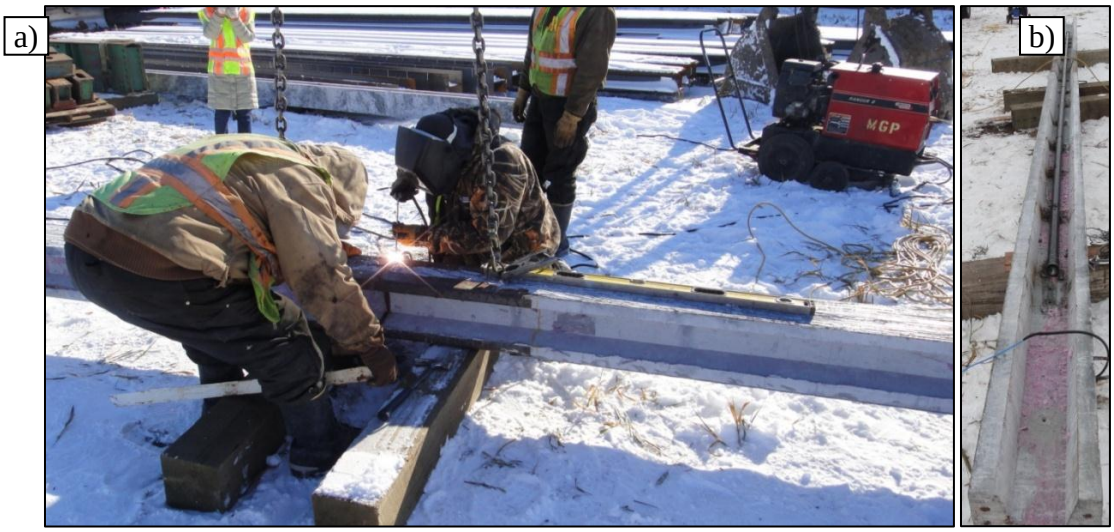

Figure 5-25: a) Splicing of P4 Horizontally on the Ground; and b) After Installing the Steel Pipe for the SAA Equipment to P4

The lifting hook cast into the UHPC piles was designed to allow the piles to be raised into position with a lifting chain, similar to steel piles. The lifting hook was not used for the UHPC test piles. Instead, a lifting strap was used to hold the head of the pile and insert the UHPC pile into the hammer leads lifted with the second crane.

The installation of the UHPC test piles was similar to that of the steel anchor piles. The low soil resistance at the beginning of driving required the ram to be raised manually several times before the hammer was able to develop enough combustion pressure to run continuously. PDA equipment monitored the driving of P3 and P4. During driving of P3 with 38 feet already installed into the soil, the bolt holding the accelerometer to the pile sheared off as the foot of the leads slid along the pile. Driving was stopped temporarily to reattach the accelerometer with a new bolt. Precautions were taken from then on to ensure that the leads did not slide along the pile.

A 4-in. plywood pile cushion was used for the UHPC test piles, but both P3 and P4 punched through the pile cushion shortly after driving had begun. Instead of replacing the cushion with a new cushion, the pile was driven with essentially no cushion based on the experience in Phase I (Vande Voort et al. 2008). There was slight damage to P3 and no visible damage to P4 as shown in Figure 5-26 and Figure 5-27, respectively. The reason for the damage to P3 was the pile head was not perfectly centered under the helmet. It is also important to note that the P3 tilted slightly during driving.

Figure 5-26: Slight Damage observed to P3 Pile Head after Driving the Pile in Place

Figure 5-27: No Visible Damage on Pile P4 Head after Driving

Strain readings were taken for each pile after driving. All of the strain gages in P3 and P4 were working after driving, giving an overall instrumentation success rate of 100 percent. Strains remained virtually unchanged from measurements taken shortly before driving, indicating minimal residual stresses in the piles. Overall, the UHPC test piles performed extremely well during driving.

5.4.6. Pile Driving Analyzer (PDA) Results

5.4.6.1 Steel Anchor Piles

The PDA confirmed that both anchor piles were not damaged during driving based on the shape of the force and velocity waved recorded at the pile head. The maximum compressive stress developed in RPS during driving was 28.5 ksi, and the maximum tensile stress was 1.2 ksi. The driveability analysis reported in Section 5.4.4, calculated the compressive stress with an error of 3.2 percent. The tension stress was underestimated by the driveability analysis but was still well below the allowable tensile stresses of 45 ksi for the south anchor pile. The CAPWAP results calculated total capacity of RPS to be 369.3 kips with a Case damping factor of 0.242.

RPN had a maximum compressive stress during driving of 30.8 ksi, and the maximum tensile stress was 1.7 ksi. The driveability analysis reported in Section 5.4.4,

calculated the compressive stress with an error of 4.5 percent. The driveability analysis predicted the maximum tensile stress with 0 percent error. The PDA results gave a total capacity of the RPN of 373 kips with a Case damping factor of 0.219.

5.4.6.2 UHPC Test Piles

P3 had a maximum measured compressive stress during driving of 5.4 ksi, and the maximum measured tensile stress was 0.2 ksi which was measured by the PDA equipment attached near the pile head as shown in Figure 5-28. The driveability analysis reported in Section 5.4.4 over predicted the compressive stress with an error of 33 percent. The tension stress was underestimated by the driveability analysis by 0.1 ksi and was still well below the allowable tensile stress of 5.40 ksi for the UHPC pile. The PDA results gave a total capacity of P3 of 278.6 kips with a Case damping factor of 0.266.

Figure 5-28: Attached PDA Equipment during the Installation of P3

P4 had a maximum compressive stress during driving of 5.7 ksi, and the maximum tensile stress was 0.1 ksi. The driveability analysis reported in Section 5.4.4, calculated the compressive stress with an error of 26.3 percent. The tension stress was underestimated by the driveability analysis again only by 0.1 ksi and was still well below the allowable tensile stress of 5.4 ksi for the UHPC pile. The PDA results gave a total capacity of P4 of 170.1 kips with a Case damping factor of 0.083.

5.5. VERTICAL LOAD TEST

5.5.1. Load Frame and Test Setup

The vertical load test was performed on P3 on December 16, 2011. Top and profile views of the test frame are shown in Figure 5-29 and Figure 5-30, respectively. After the seven day restrike, the top 12 inches was cut off of the anchor piles and two shorter HP 10 x 57 pieces were welded to each of the anchor piles. The main reaction beam was lifted and placed on the protruding flanges of the piles shorter side pieces. The 3-in. diameter rods were lowered through the holes in the height adjusters and clamping beams and through the spaces between each side pile piece web and each corresponding anchor pile web. Finally, sleeved rod nuts were tightened against the bottom plate directly underneath each side pile piece. The completed load frame is shown in Figure 5-31.

A hydraulic jack was used to apply a vertical load on P3 and imposed an equal and opposite load upward on the main reaction beam. The main reaction beam reacted upward against the clamping beams and transferred to the 3-in. diameter rods on either side of the main reaction beam. The rods reacted against the plates on the bottoms of each side pile piece, and the welds transferred the vertical load from the side pile pieces to the anchor piles and then to the soil. The anchor piles were subjected to axial tension throughout the test.

The load capacity of the test frame was controlled by the friction capacity of the anchor piles. Using a safety factor of two on the capacity of the anchor piles, the maximum load that could be applied to P3 was 340 kips. If the friction capacity of the anchor piles was not exceeded first, the load test frame could be used to apply a load of 680 kips to P3 which would be controlled by the tension capacity of the 3-in. diameter rods.

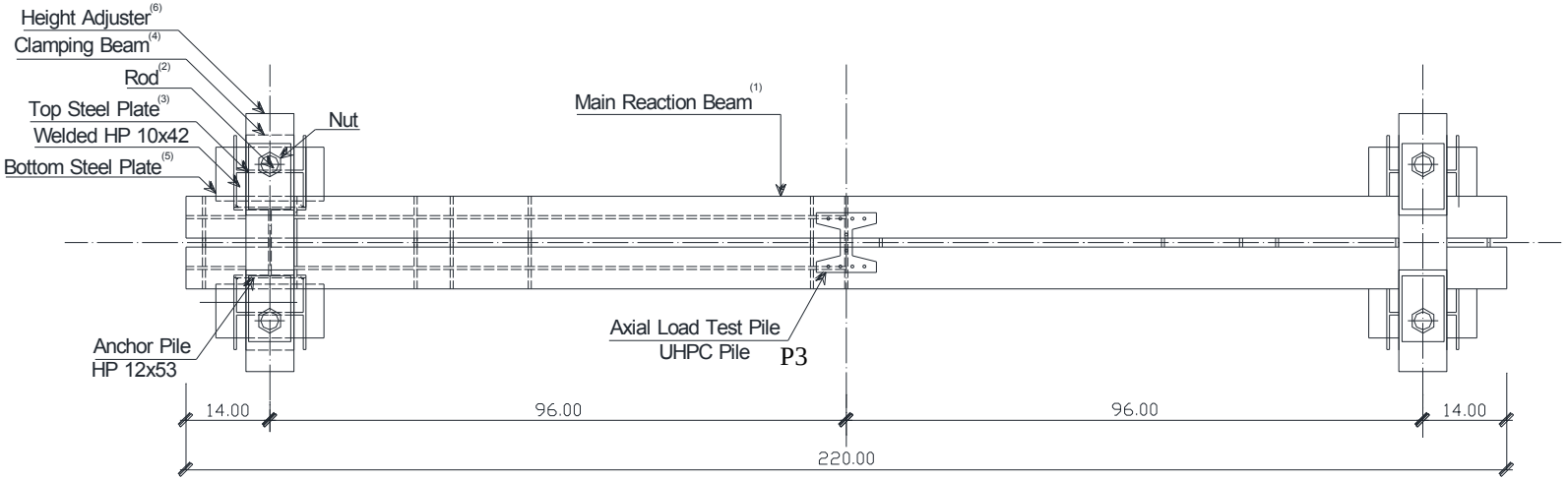

Figure 5-29: Top View of Vertical Load Test Setup (all dimensions are in inches)

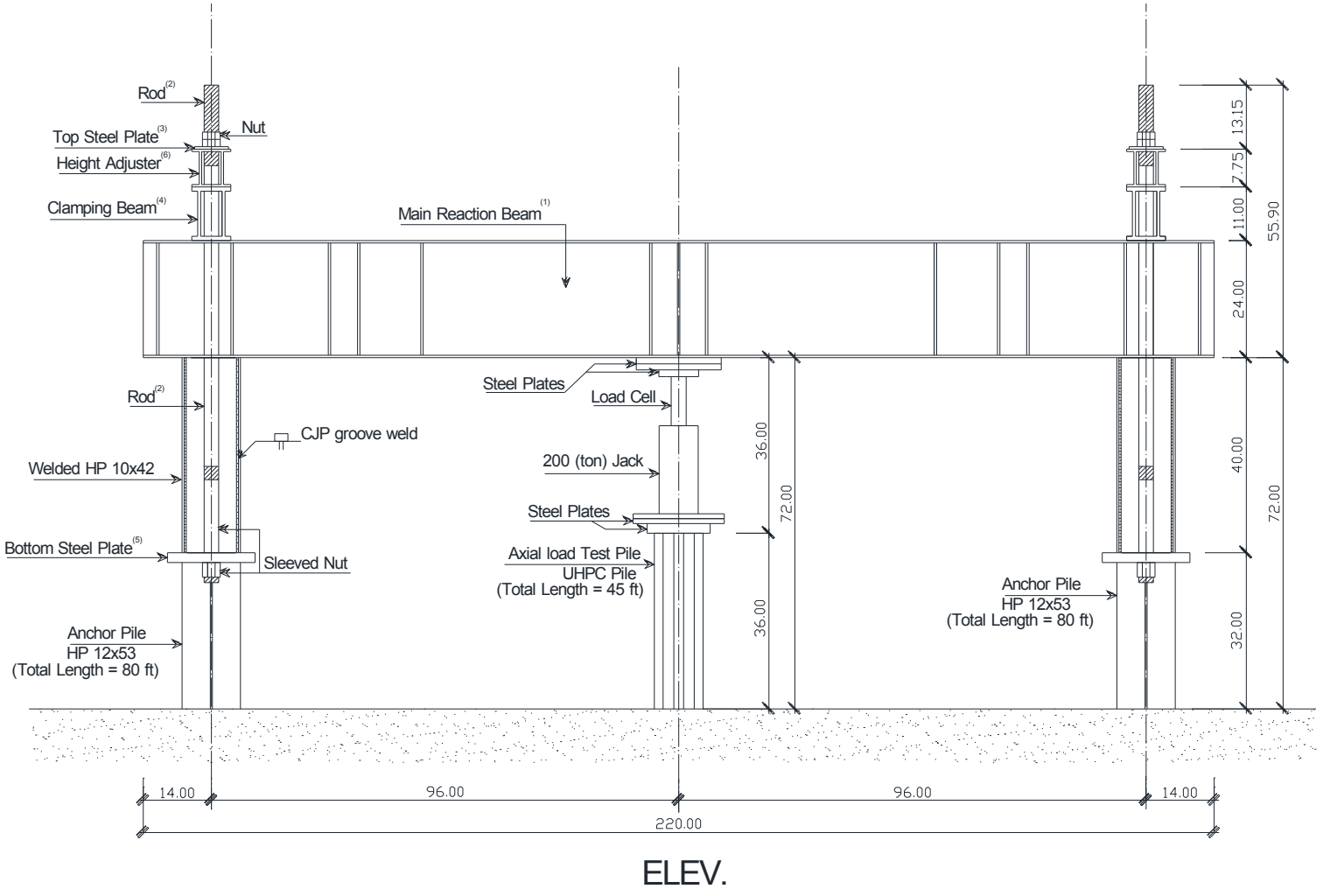

Figure 5-30: Elevation View of Vertical Load Test Reaction Frame

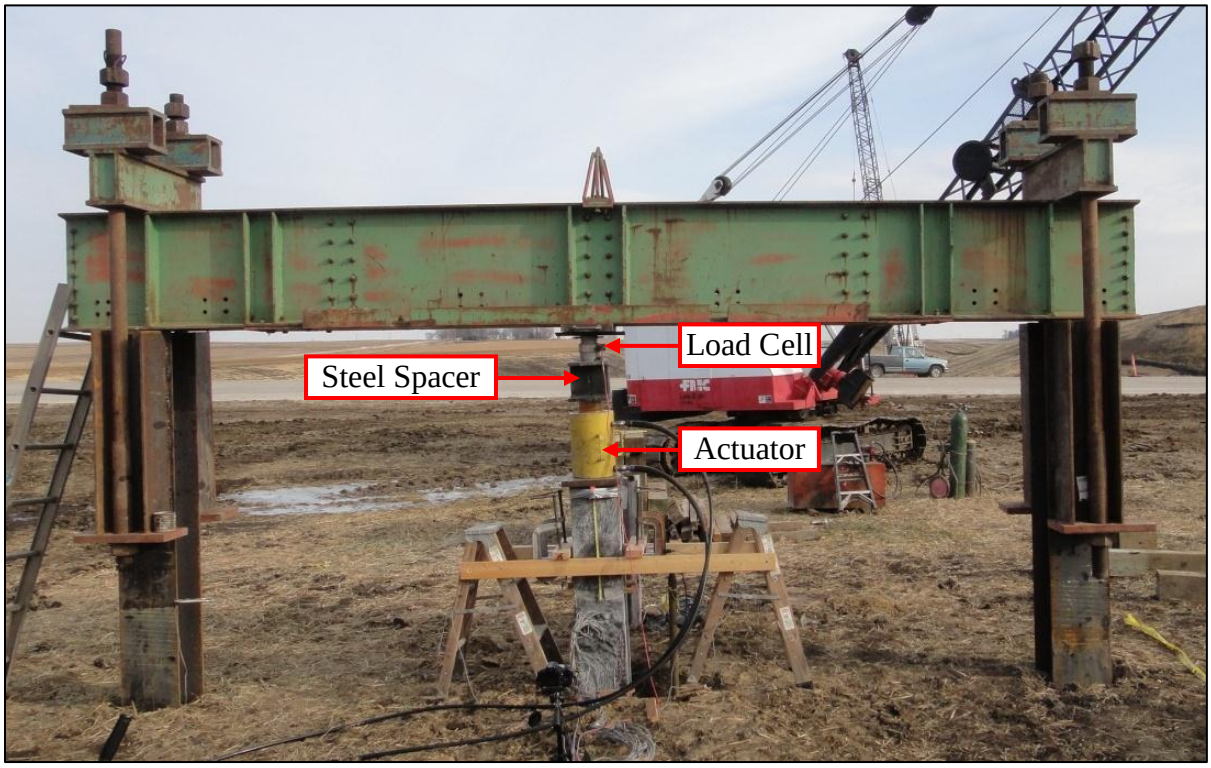

Figure 5-31: Completed Axial Load Test Set-up

A 200 ton hydraulic jack was used to apply the vertical load on P3, and a 400 kip load cell was used to measure the applied load as shown in Figure 5-32. Four 10-in. stroke displacement transducers were used to measure the vertical displacement at the top of P3 (see Figure 5-33). These transducers were mounted on 2x4-in. wooden reference beams, which were supported approximately 6 inches away from the pile on either side by attaching to short ladders. This set-up allowed for the pile displacement to be measured independent of the load test frame. The displacement transducers were attached to the top of the pile using eye-hooks screwed into wooden pieces and glued with epoxy to the test pile in the field.

All embedded concrete strain gages in P3 were functioning and were zeroed before the load test began. The gages were used to calculate strains at various depths throughout the pile. Data from the load cell, deflection transducers, and strain gages were collected using a Megadac data acquisition system as shown in Figure 5-34.

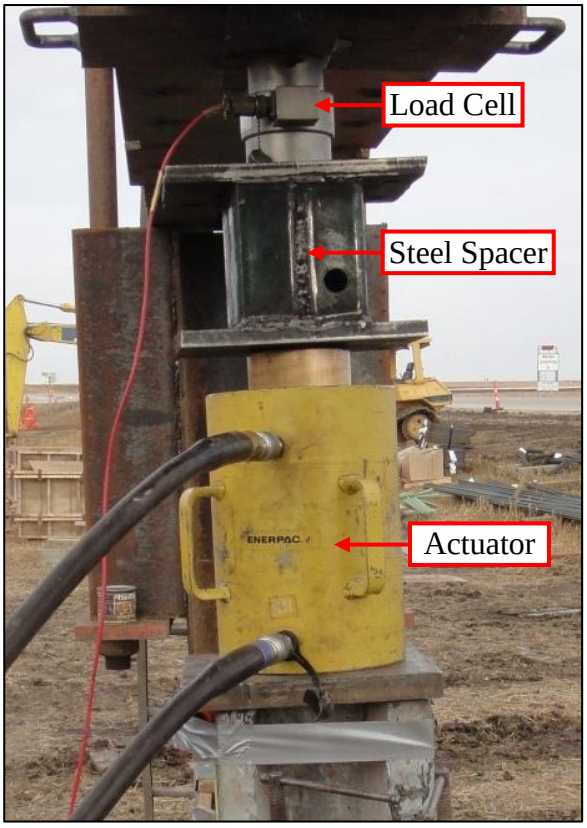

Figure 5-32: Vertical Load Testing Equipment

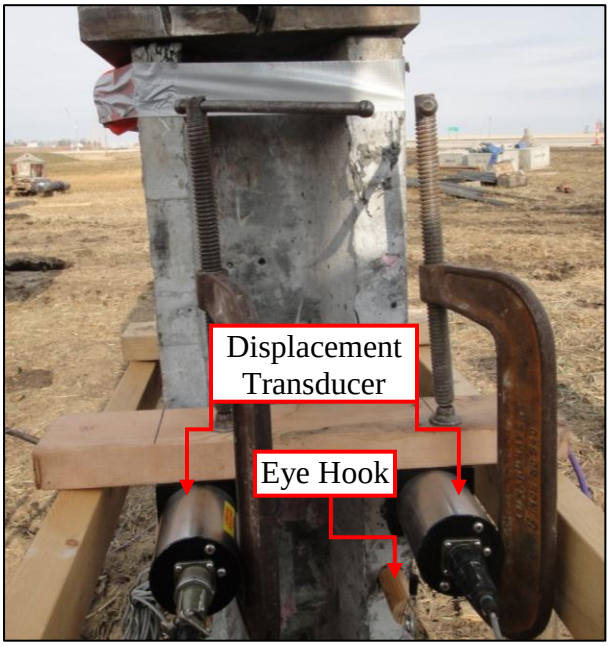

Figure 5-33: Displacement Transducers

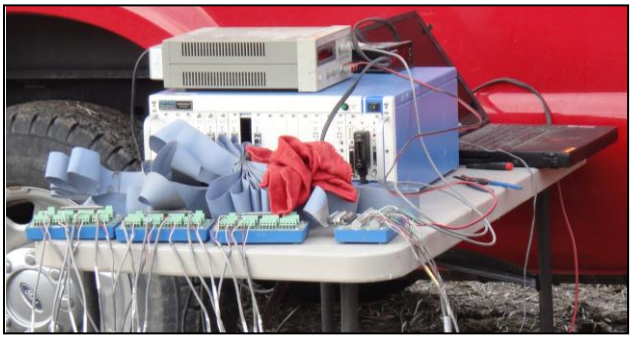

Figure 5-34: Data Acquisition System

5.5.2. Test Procedure

The vertical load test was complete following "Procedure A: Quick Test" as outlined in ASTM D 1143/D 1143 M - 07. Accordingly, the test pile was loaded in five percent increments up to the anticipated failure load. The load was kept relatively constant during each load step until deflection readings had stabilized, which was specified as a minimum of 5 to 15 minutes for each step. Deflection, strain, and load measurements were recorded electronically every second. To estimate when failure occurred, the load-displacement behavior of P3 was monitored at each load step by hand. The Davisson failure criterion (1972) was used to determine the ultimate capacity of the pile and terminate the vertical load test. P3 was unloaded in five equal steps.

The vertical load test on P3 was performed on December 16, 2011 at the Sac County site near the west abutment of the westbound bridge. The calculated failure loads for P3 was approximately 200 kips according the Iowa DOT Blue Book Method and 216 kips from the DRIVEN computer software. The undrained shear strengths from averaged CPT results was used as input for the soil conditions within DRIVEN. A maximum load of 200 kips was planned for the test. The actual loading sequence of P3 is given in Table 5-6.

The anchor piles did not show noticeable movement at the planned maximum load of 200 kips, so the load on P3 was increased further in the same loading increments of 10 kips until a final load of 300 kips. After the final load was reached the pile was unloaded in 30 kip increments.

Table 5-6: Vertical Load Test Step for P3

Approximate % of Predicted Failure Load	Load Applied (kips)	Load Duration (min)
5	10	15
10	20	15
15	30	15
20	40	10
25	50	5
30	60	5
35	70	5
40	80	5
45	90	5
50	100	5
55	110	5
60	120	5
65	130	5
70	140	5
75	150	5
80	160	5
85	170	5
90	180	5
95	190	5
100	200	5
Overloading	210	5
Overloading	220	5
Overloading	230	5
Overloading	240	5
Overloading	250	5
Overloading	260	5
Overloading	270	5
Overloading	280	5
Overloading	290	5
Overloading	297	5
Unloading	270	5
Unloading	240	5
Unloading	210	5
Unloading	180	5
Unloading	150	5
Unloading	120	5
Unloading	90	5
Unloading	60	5
Unloading	30	5
Unloading	0	-

5.5.3. Observations and Test Results

5.5.3.1 Load-Displacement

The load-displacement behavior of P3 is given in Figure 5-35. P3 was loaded to a maximum value of 297.25 kips and underwent a maximum displacement of 0.65 inches of

downward displacement during this load step. The test pile continued its downward displacement for the first unloading step and reached a maximum downward displacement of 0.71 inches.

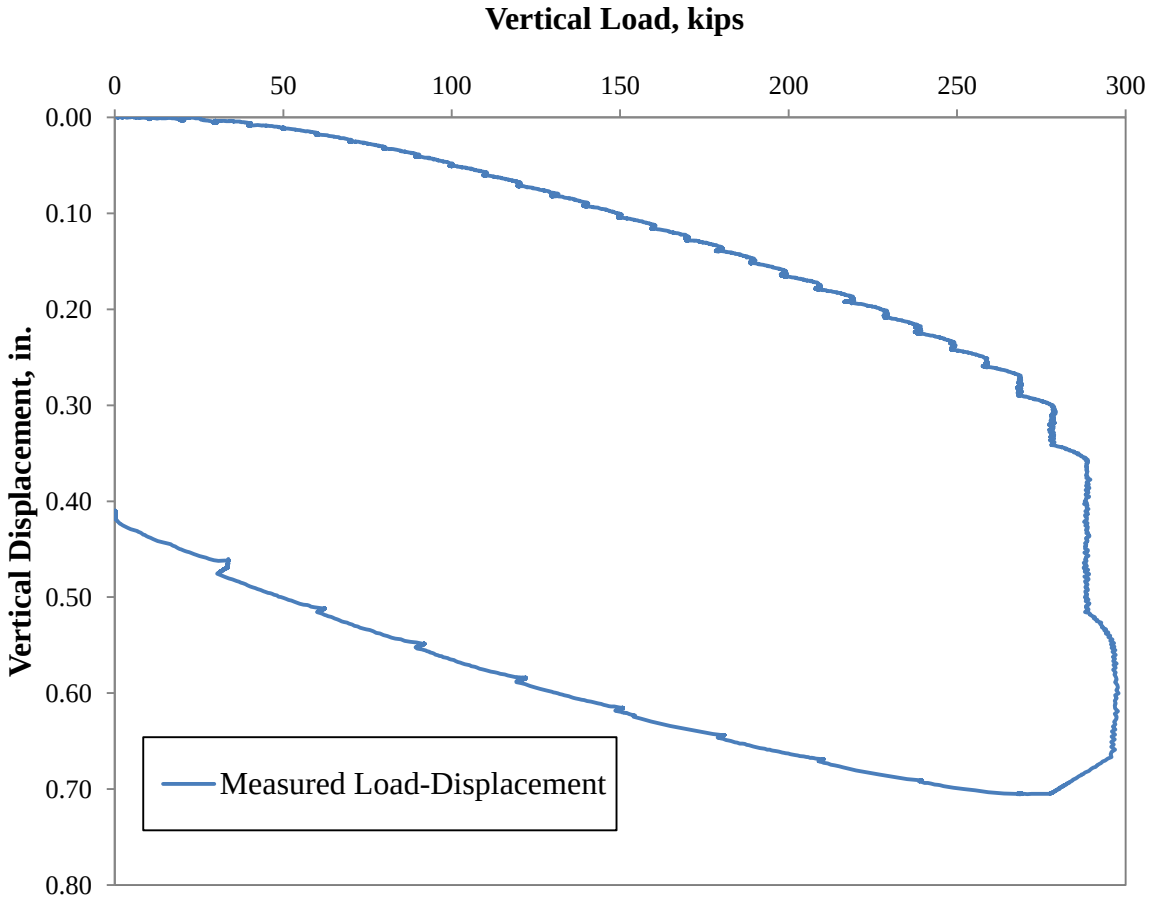

Figure 5-35: Observed Load-Displacement Behavior for the Vertical Load Test of P3

After unloading P3, a time interval of 3 minutes passed. The test pile experienced a permanent vertical displacement of 0.42 inches. The relationship between load and displacement can be represented by connecting the average load and average displacement for each load step as illustrated in Figure 5-36. The pile axial stiffness was calculated using Equation 4-1 and is shown in Figure 5-36, along with the Davisson Failure Criterion Line which was calculated using Equation 4-2 (Davisson 1972). The load at the point where the Davisson Failure Criterion crosses the measured load-displacement curve is capacity of the pile. The results from the vertical load test found the capacity of P3 to be 297 kips.

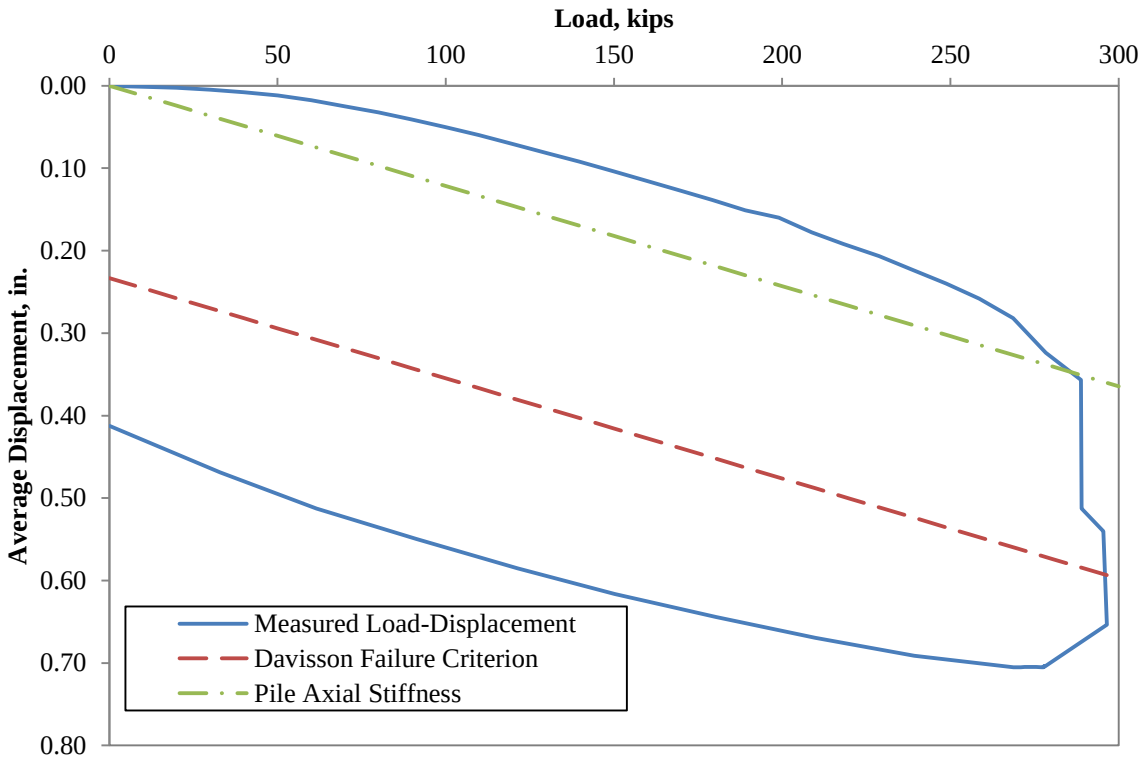

Figure 5-36: Load-Displacement Behavior Established from the Maximum Load Points and Davisson Failure Criterion for the Vertical Load Test of P3

$$\Delta_k = \frac{PL}{AE} \tag{4-1}$$

where: P = axial load, kips
L = length of pile, in.
A = cross-sectional area, in^2
E = modulus of elasticity, ksi

$$\Delta_{Davisson} = \frac{PL}{AE} + 0.15 + \frac{D}{120} \tag{4-2}$$

where: D = diameter of pile, in.

5.5.3.2 Load Transfer

The strain gages embedded along the length of P3 provided information about the skin friction along the pile. Figure 5-37 shows the average calculated load transfer along the

length of the pile from the measured strains. The maximum vertical load applied to P3 was 297.25 kips but from the force transfer the strain gages are only measuring a maximum load of 220 kips at the strain gages located 4 feet from the pile head which is right at the ground surface so it should have minimal soil effects.

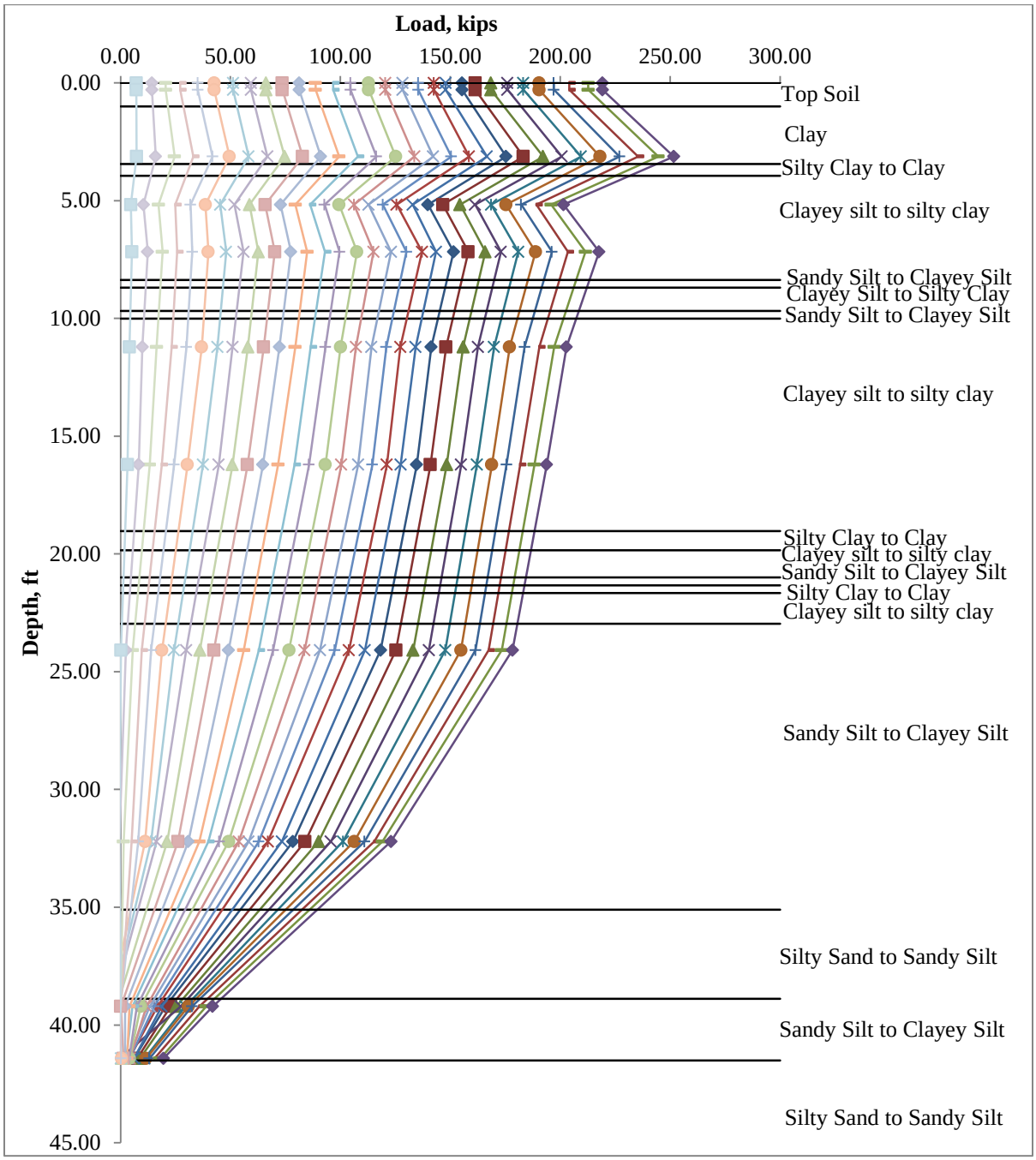

Figure 5-37: Measured Force Transfer Response of P3 during the Vertical Load Test

There are some possible reasons that the load transfer curve does not match the measured applied load. One such reason could be due to the prefabrication process. The embedded strain gages were hung between two prestressing strands as shown in Figure 5-38. When UHPC was poured, the gages could have tilted in the y-direction or shifted in the x-direction, causing the gage to be subjected to bending. Also, when the gage shifts the distance from the gage to the neutral axis changes from the specified distance and could be different for every gage.

Figure 5-38: Suspended Embedded Strain Gages

As mentioned in Section 5.3.3.1, there were some defects in the pile from the prefabrication process. One of the defects is an inconsistent flange thickness near the pile head which could cause a change in stiffness and an unsymmetrical cross-section.

There was also an issue with the test set-up and installation of P3. Test pile, P3 was installed very close to two push-in pressure cells as shown in Figure 5-39. To install a push-in pressure cell, a 4-in. diameter hole is drilled and the push-in pressure cell is pushed to the specified depth. The depth of one of the push-in pressure cell is 15 feet and the other is 20 feet from the ground surface. The effect of having this so close to the pile is it reduces the

skin resistance along the pile, which can cause an eccentricity due to the non-uniform forces resisting the vertical load. In addition to the push-in pressure cells, a void filled with water around P3 was formed due to driving as shown in Figure 5-40. The depth of the void was measured to be 5 feet deep from the ground surface.

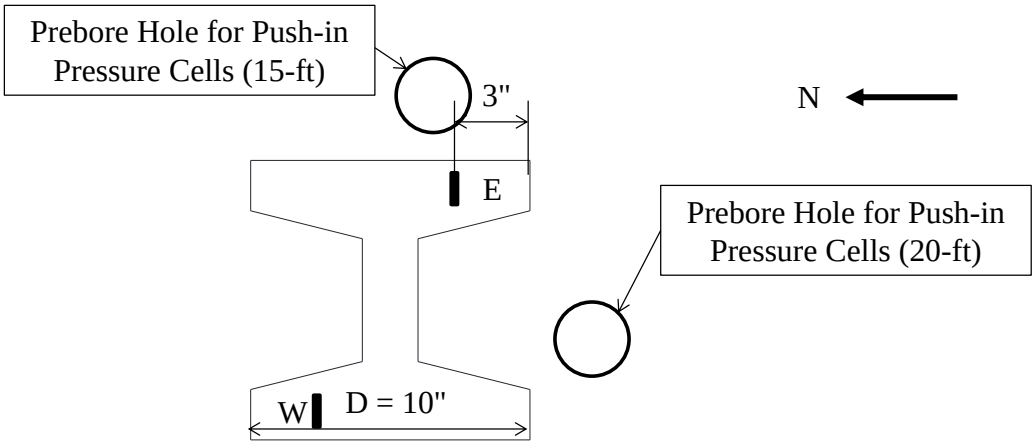

Figure 5-39: Location of Push-in Pressure Cells

Figure 5-40: Void that Formed from Installation of P3

After the installation was complete, it was noticed that the pile was installed at an angle in both the x-axis and y-axis direction. Figure 5-41a and b show the tilt of P3 in the strong-axis and weak-axis direction. The angle causes load that is measured by the load cell to be the resultant force of two force components, vertical (P_v) and horizontal (P_h) as illustrated in Figure 5-42a and b. A moment is induced due to the horizontal force.

Figure 5-41: Tilt of P3 after Driving in the a) Weak-Axis Direction; and b) Strong-Axis Direction

There was an issue during the testing which is that the actuator was not placed exactly on the center of the pile. This causes the vertical force to be applied with an eccentricity. There was an eccentricity in the x-axis and y-axis directions which are also shown in Figure 5-41a and b, respectively.

To ensure that the measured applied load was accurate, the load cell was tested on April 23, 2012 with the Universal Compression Machine in the Iowa State University Laboratory. The load cell had a 100 kip compression load applied to it and measured 99.9 kips, which results in an error of 0.1 percent.

Figure 5-42: Components of Applied Load during Vertical Load Test in the a) Weak-Axis Direction; and b) Strong-Axis Direction

Using estimated unit skin friction values the load transfer curve was corrected to reflect the actual load that was applied to the pile head. Figure 5-43 shows the measured loads along the length of the pile as solid lines and the corrected portions of the load transfer are shown as a dashed line. Only the 100, 200 and 300 kip load steps are shown in this figure.

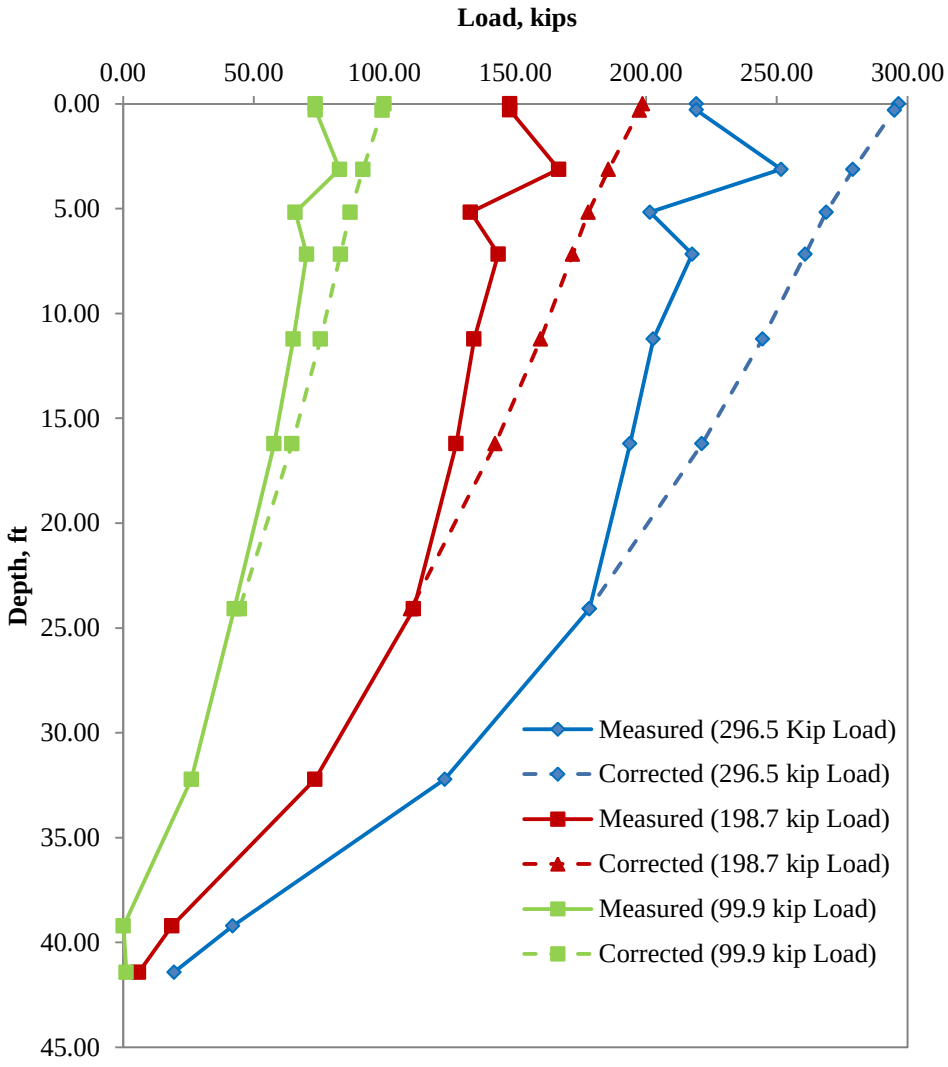

Figure 5-43: Measured and Corrected Load-Transfer Curves for Three Load Steps

5.6. LATERAL LOAD TEST

5.6.1. Test Setup

The UHPC test piles, P3 and P4 underwent a lateral load test on December 19, 2011. For the test, P3 was in strong-axis bending and P4 was in weak-axis bending and included a splice at 15 feet from the pile head. The elevation view of the setup for the designed lateral load test is shown in Figure 5-44. The field measurements identified that P3 had 3.83 feet exposed above the ground surface, and P4 had 2.98 feet exposed above the ground surface after driving and the specified restrikes.

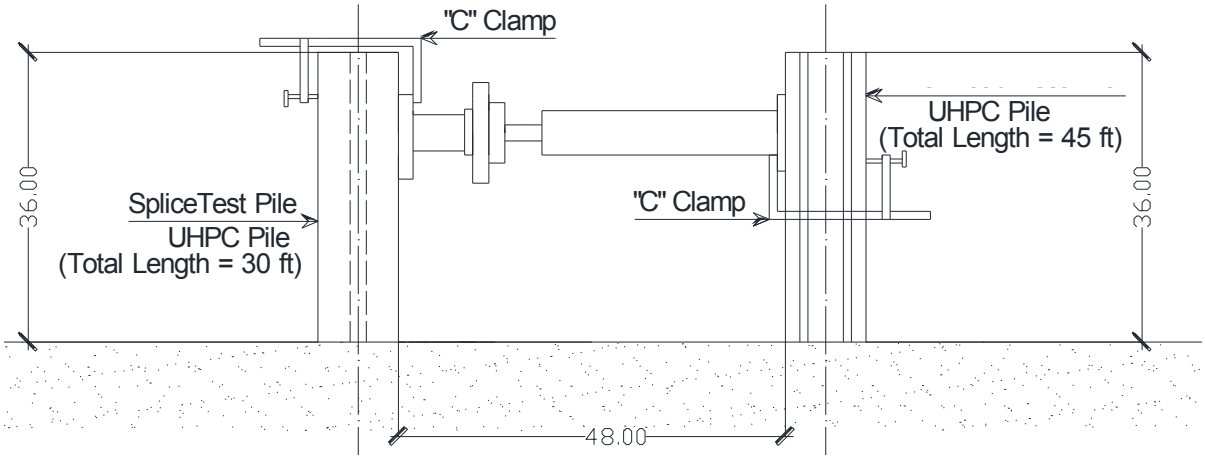

Figure 5-44: Elevation View of Lateral Load Test Setup

A 100 kip actuator was used to apply the lateral load to P3 and P4 simultaneously. The actuator was clamped to P3 14.5 inches below the pile head and a steel spacer was clamped to P4 8 inches from the pile head. A 300 kip load cell was used to measure the applied load, which was positioned in line with the actuator and steel spacer. The actuator, load cell and steel spacer are identified in Figure 5-45.

Two 10-in. displacement transducers were used to measure the lateral displacement at the top of each pile. The transducers were completely extended at the beginning of the test and were mounted to 2x4-in. wooden reference beams, which were supported approximately 1 foot from each of the pile on short ladders. The transducers were connected to the top of the pile using eye-hooks screwed into wooden pieces glued to the pile head, as shown in Figure 5-46. The UHPC test piles were measured independently from each other as illustrated in Figure 5-47.

A new piece of equipment was purchased to measure the displacement along the length of P4 which is called the SAA. The SAA was inserted into a steel tube that was welded to the embedded plates. The SAA ran along the east side of P4 as illustrated in Figure 5-47 for 20 feet. Three dimensional displacements and rotations were read starting 34 ¼ inches from the pile head. The x-axis of the SAA was lined up with the lateral force direction.

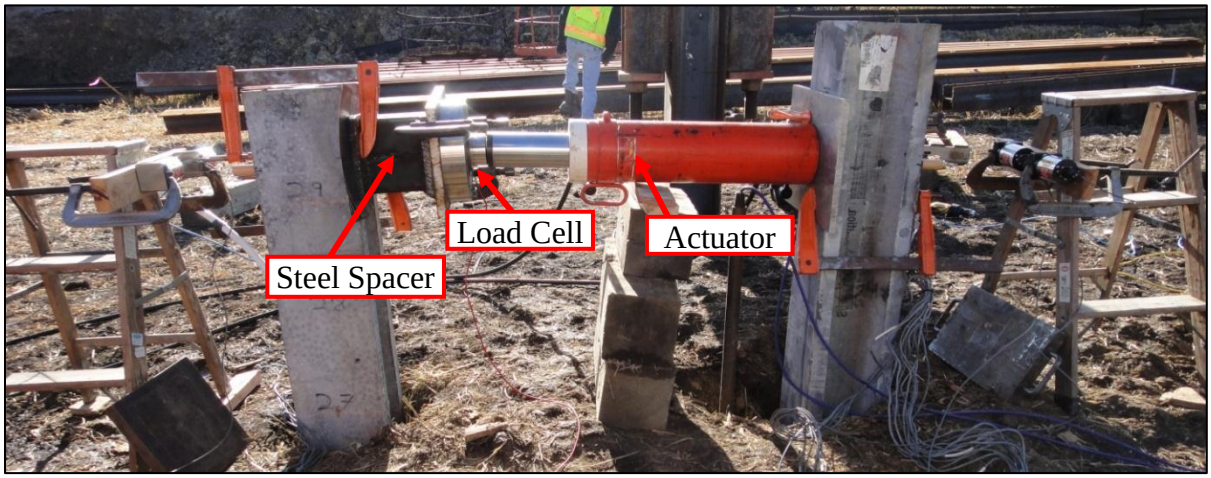

Figure 5-45: Setup used for the Lateral Load Test

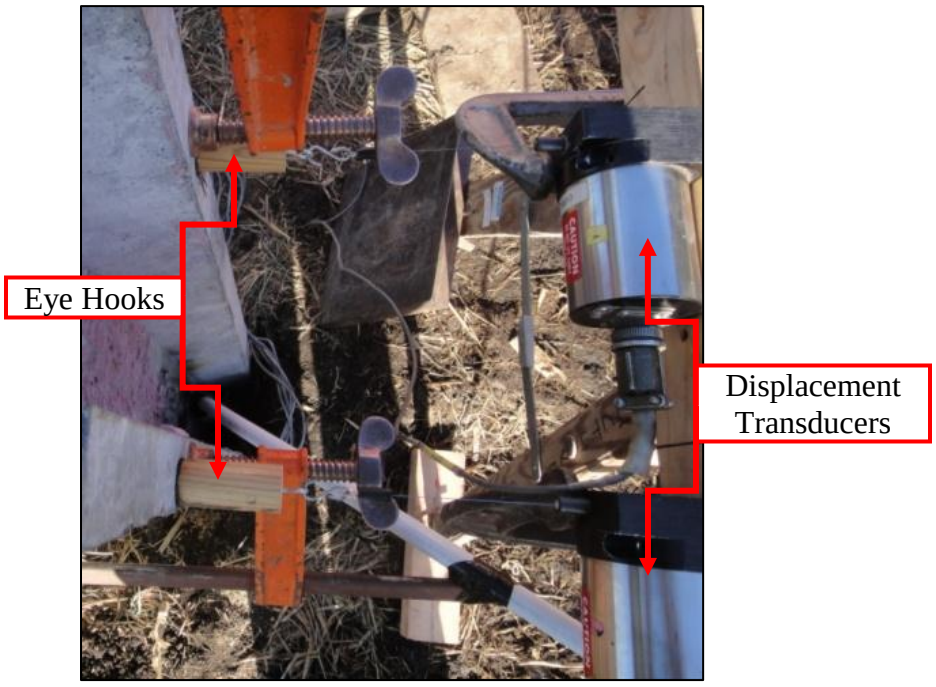

Figure 5-46: Displacement Transducers and Eye-Hooks Mounted to P4

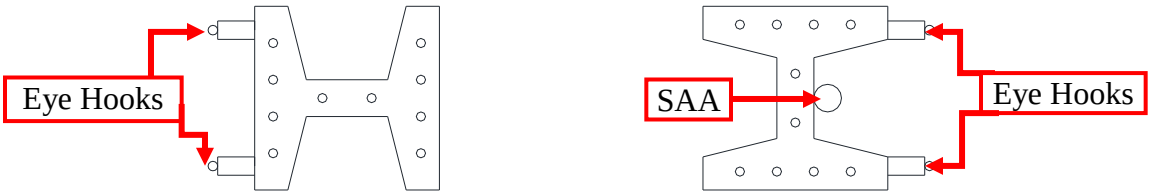

Figure 5-47: Illustration of Eye Hook and SAA Instrumentation Location

Throughout the length of pile P3, the top 9 levels or a total of 18 embedded concrete gages had strain measurements recorded, while P4 had only three levels of gages or six embedded concrete gages providing strain measurements only along the upper portion of the P4. Data from the load cell, deflection transducers, and strain gages were collected using the Megadac data acquisition system and the data from the SAA instrument was collected using the CR-1000 data logger.

5.6.2. Test Procedure

The lateral load test was completed following "Procedure A: Standard Loading" of ASTM 3966-07. The procedure recommends applying a design load of 200% of the proposed pile lateral design load unless failure occurs first. Table 5-7 details the load steps used during the lateral load test. A design load of 10 kips was used for the test.

To apply the lateral load to the UHPC test piles, a manual hydraulic jack was used to for the test. During each load step, the load was kept relatively constant until deflection measurements had stabilized for a minimum duration of 10 minutes or a maximum duration of 20 minutes required by ASTM 3966-07. Deflection, strain, and load readings were electronically recorded once every second.

Table 5-7: Lateral Load Sequence

% of Design Load	Load Duration (min)
0	10
25	10
50	15
75	20
100	20
125	20
150	20
170	20
180	20
190	20
200	60
150	10
100	10
50	10
0	-

5.6.3. Observations and Test Results

The first part of the lateral load sequence used to test the UHPC piles is shown in Table 5-8 which consisted of force controlled load steps. For the remaining cycles, the piles were displacement controlled based off the measurements taken from test pile P4 and is outlined in Table 5-9. Between each cycle the UHPC test piles were unloaded to 0 kips of lateral load.

Table 5-8: Force-Control Loading Sequence during Cycle 1 of the Lateral Load Test

Lateral Load, kips	Load Duration (min)
2.5	10
5.0	10
7.5	15
10.0	20
12.5	20
15.0	23
17.0	23
18.0	21
19.0	21
20.0	24
15.0	10
10.0	10
5.0	10
0.0	-

Table 5-9: Displacement Controlled Loading Sequence during Load Step 2 through 4 of the Lateral Load Test

Load Step	Lateral Displacement, in.	Lateral Load, kips
2	4	6.1
3	7	9.5
4	10	16.2

The actual applied loads varied slightly from those shown in Table 5-8. Since the manual hydraulic pump was used, the loads were applied very slowly. A combination of minor leakage in the hydraulic system and soil creep caused the applied load at each load step to drop slightly over the duration of each load step. The magnitude of the load reduction increased with increasing load step duration and applied load.

5.6.3.1 P3

P3 was tested in strong-axis bending during the lateral load test. The force-displacement curve is given for P3 in Figure 5-48. The maximum load P3 was subjected to is 20.6 kips corresponding to 1.7 inches of lateral displacement. Test pile, P3 had a 0.08-in. residual displacement after the pile had been unloaded for the first cycle and a total residual displacement of 0.03 inches after all of the cycles had been completed.

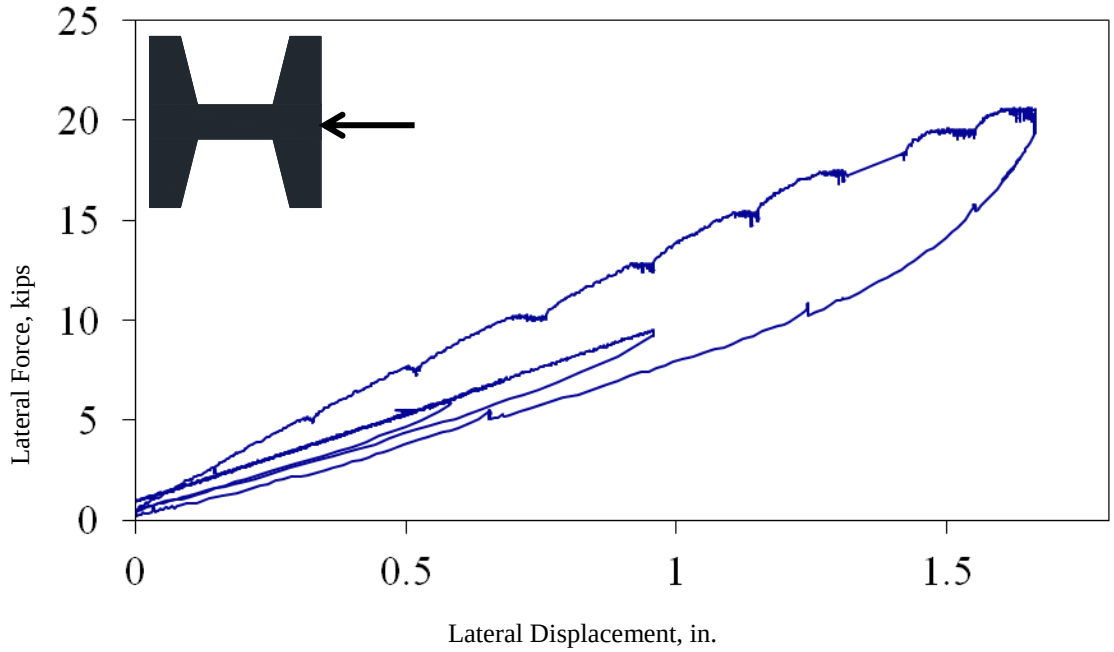

Figure 5-48: Force-Displacement Response of P3 during Lateral Load Test

The tensile strain and compressive strain measurements along the length of the P3 were obtained from the embedded concrete strain gages. The information from the gages was used to calculate the bending moment while the pile was subjected to lateral loading. Two gages on the tension side of P3 stopped working during the lateral load test. Figure 5-49 shows the measured tensile strain compared to the measured compressive strain at the top six levels of strain gages in P3.

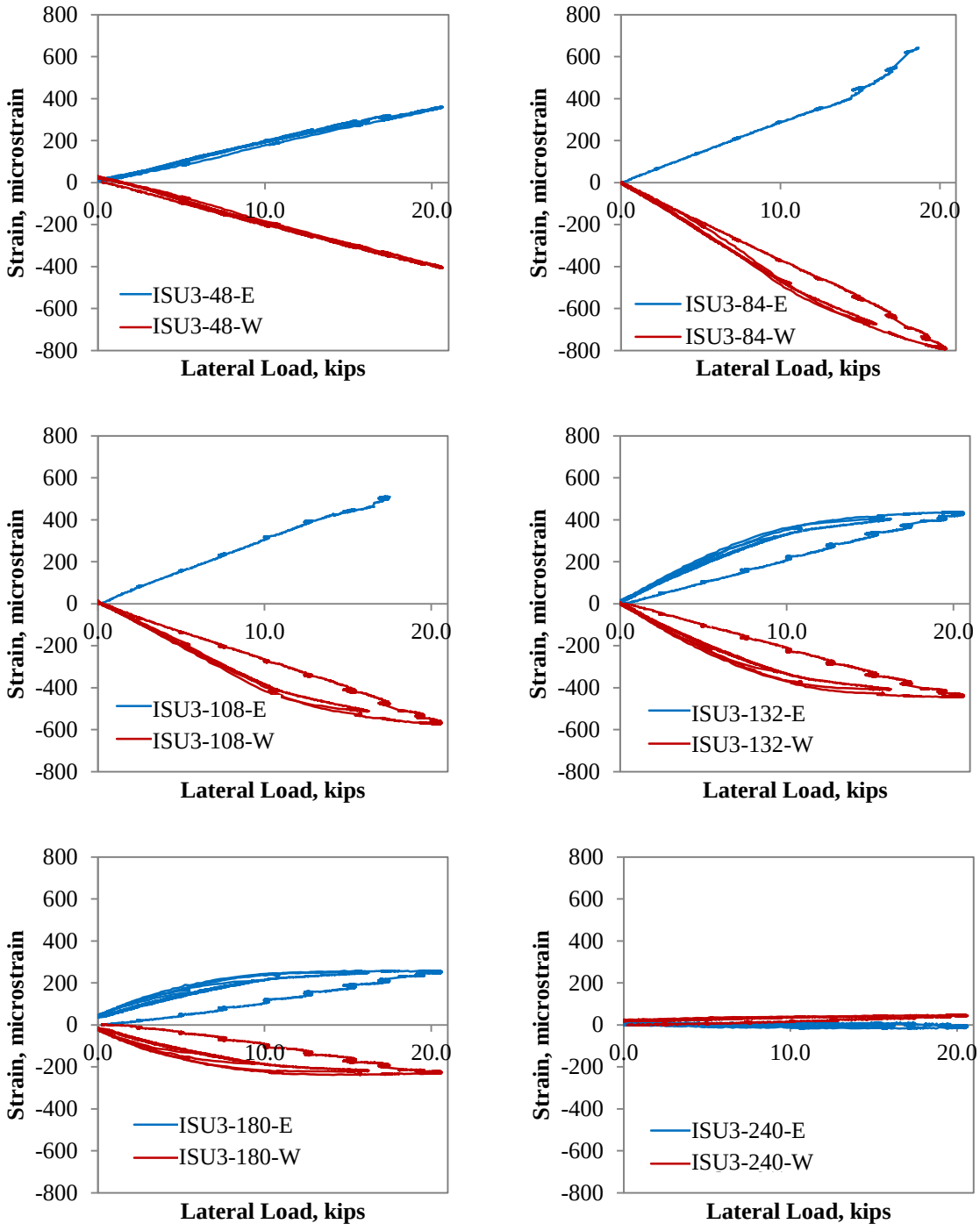

Figure 5-49: Measured Compression Strain Compared to Measured Tension Strain for Top Six Levels of Strain Gages from P3 during the Lateral Load Test

Table 5-10 identifies the lateral load and strain reading when the embedded concrete gages stopped working. The broken gages were identified by a large, sudden jump of two orders of magnitude in the strain value. The information after the gages stopped working was discarded.

Table 5-10: P3 Gages that Stopped Working during Lateral Load Test

Gage	Lateral Load, kips	Strain, microstrain
P3-108-E	17.2	511
P3-84-E	18.7	643

5.6.3.2 P4

The test pile, P4, was tested in weak-axis bending, and exhibited a greatly reduced stiffness as compared to P3 as expected due to the orientation of P3. Figure 5-50 shows the force-displacement curve for P4. The maximum load that P4 was subjected to was 20.6 kips corresponding to 8.3 inches of lateral displacement during the first cycle. The maximum displacement that P4 was subjected to was 10 inches of lateral displacement. There was noticeable heaving of the soil on one side of P4 during the lateral load test, as shown in Figure 5-52. P4 had a 0.95-in. residual displacement after the first cycle and a 2.35-in. residual displacement after the pile had been unloaded for the final time.

The tensile strain and compressive strain measurements along the depth of the P4 were obtained from the embedded concrete strain gages. The information from the gages was used to calculate the bending moment along the length of the pile while the pile was subjected to lateral loading. Figure 5-51 shows the tensile strain compared to the compressive strain at various strain gage levels and the location where the strain gage stopped working is identified.

The gages embedded in P4 that stopped working during the lateral load test are identified in Table 5-11. Again, the procedure to identify the gages that stopped working was to identify time when an unrealistically large sudden jump in strain was recorded. The data after the load were the gages were identified as unreliable was disregarded during the analysis.

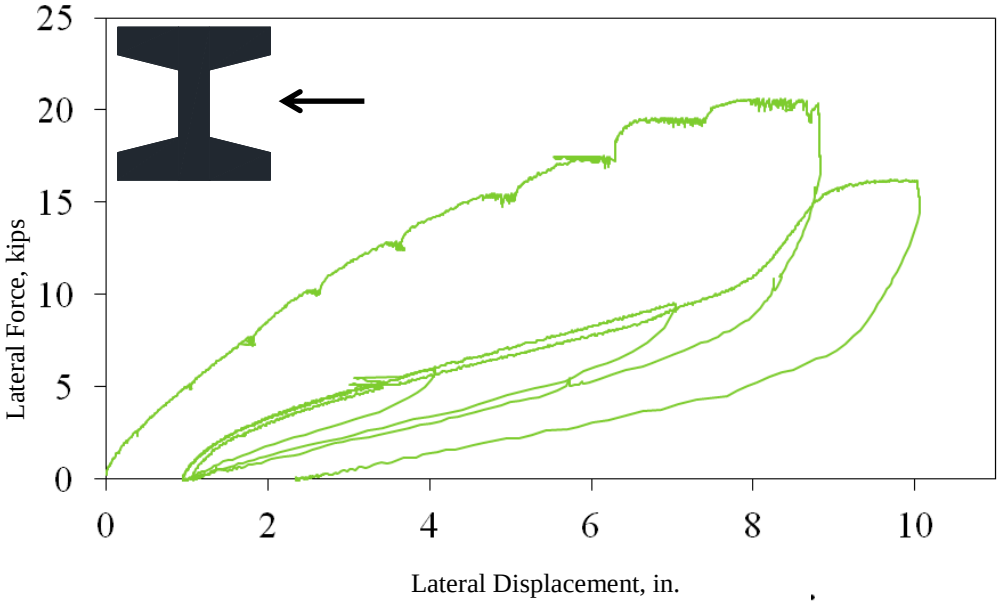

Figure 5-50: Force-Displacement Response of P4 during Lateral Load Test

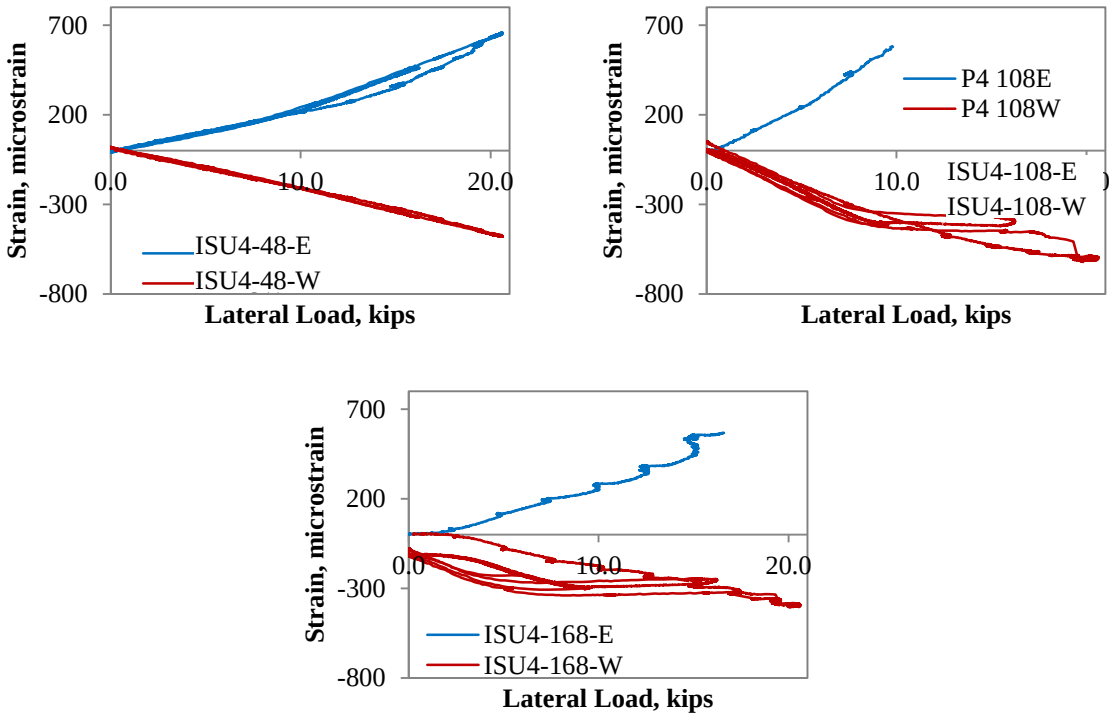

Figure 5-51: Measured Compression Strains Compared to Measured Tension Strains for All Three Levels of Strain Gages in P4 during the Lateral Load Test

Table 5-11: P4 Gages that Stopped Working during Lateral Load Test

Gage	Lateral Load, kips	Strain, microstrain
P4-108-E	9.8	581
P4-168-E	16.5	566

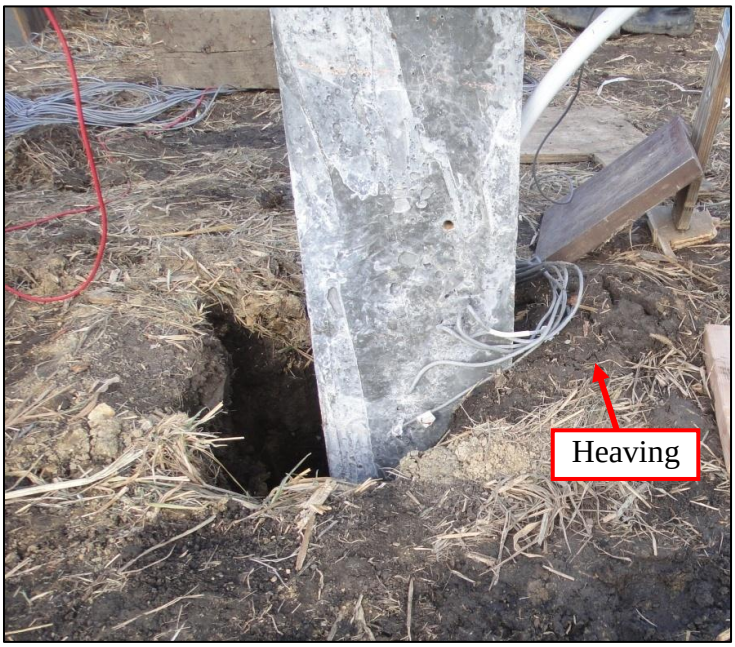

Figure 5-52: Heaving of Soil during Lateral Load Test of P4

5.6.4. Excavation of Test Pile P4

The visual evaluation of the splice performance in P4 during the lateral load test was done by excavating the soil down to the location of the splice as shown in Figure 5-53. The contractor tried to pull P4 out of the ground using a crane, but had to terminate this plan because the crane was starting to tip. As a result, the excavation was completed on January 5, 2012 and only went 12 feet below the ground surface to the location of the splice.

A fairly large crack was discovered 9 feet from the pile head on the tension side of P4, which corresponded to the maximum moment location predicted in LPILE as described in Section 5.6.5. Figure 5-54 depicts the crack on the north-west corner of P4. No damage was observed to the splice.

Figure 5-53: Excavation of Soil Surrounding P4

Figure 5-54: A Flexural Crack Found at a distance of 9 ft. from the Ground Surface on P4 due to the Lateral Load Test

5.6.5. LPILE Analysis

LPILE^{PLUS} 5.0 was used to analyze the force-displacement behavior of P3 and P4 during the lateral load test. The average undrained shear strengths calculated from the CPT test pile data and the moment-curvature response calculated for strong-axis and weak-axis bending at 0 kips axial load were used as input values into LPILE. Figure 5-55 compares the measured force-displacement curve for P3 compared to the predicted response calculated in LPILE and the adjusted LPILE response. Additionally, the predicted, adjusted and measured responses of P4 are shown in Figure 5-56.

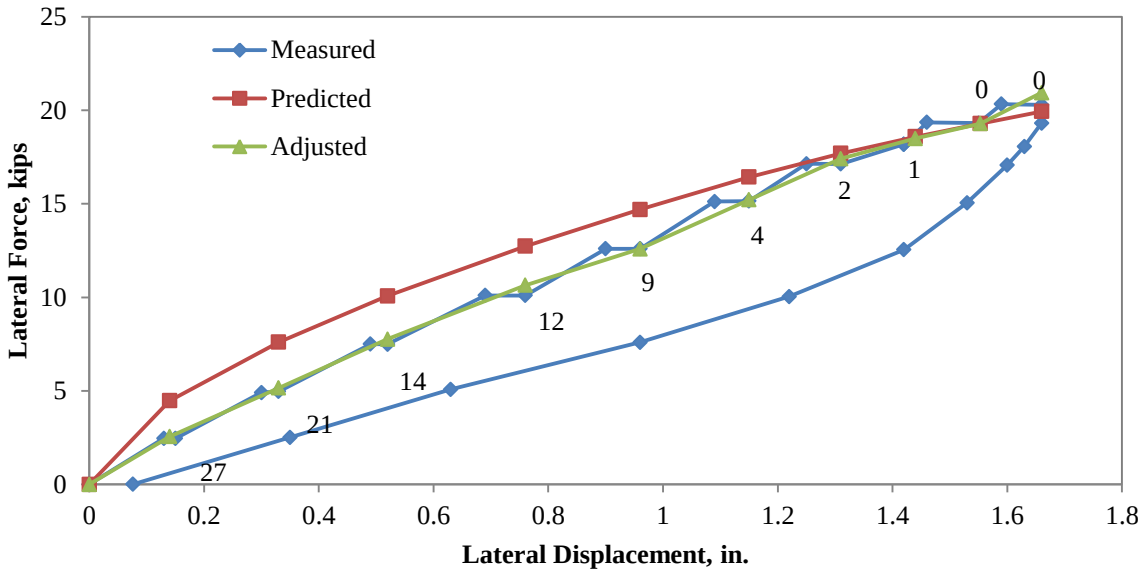

Figure 5-55: Predicted, Adjusted and Measured Force-Displacement Response of P3 during Lateral Load Test

The predicted curve was calculated using the CPT data from the test pile location as the soil input into LPILE. During driving a noticeable gap was discovered around both UHPC test piles. To account for the gap, an adjusted curve was calculated to take into account the changing gap as the pile displaces during the lateral load test. Figure 5-55 and Figure 5-56 include the depth of gap for each load step in inches next to the force-displacement point.

The corresponding moments to the predicted and adjusted displacements were calculated to compare with the average measured moments of P3 and P4. The average measured moments were calculated from the tension and compression strains, which were then averaged. Figure 5-57 and Figure 5-58 compare the moments calculated from the predicted and adjusted models for the 12.5 kip load step for P3 and P4, respectively. Appendix E has figures illustrating the predicted, adjusted and average measured moments along the length of P3 and P4, for all of the load steps in the lateral load test.

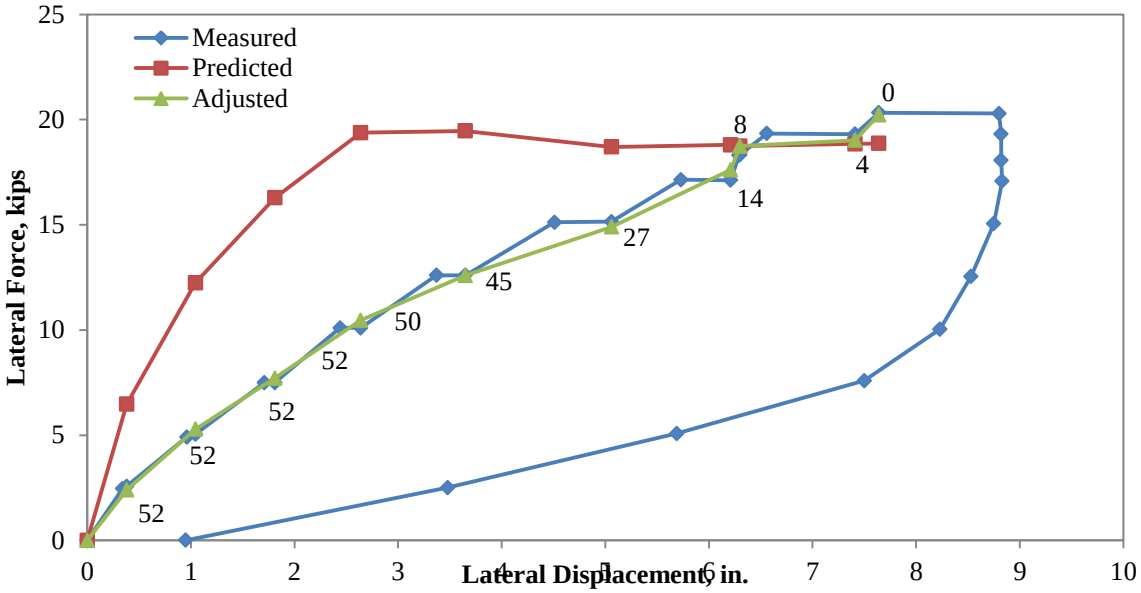

Figure 5-56: Predicted, Adjusted and Measured Force-Displacement Curve for P4 Subjected to the Lateral Load Test

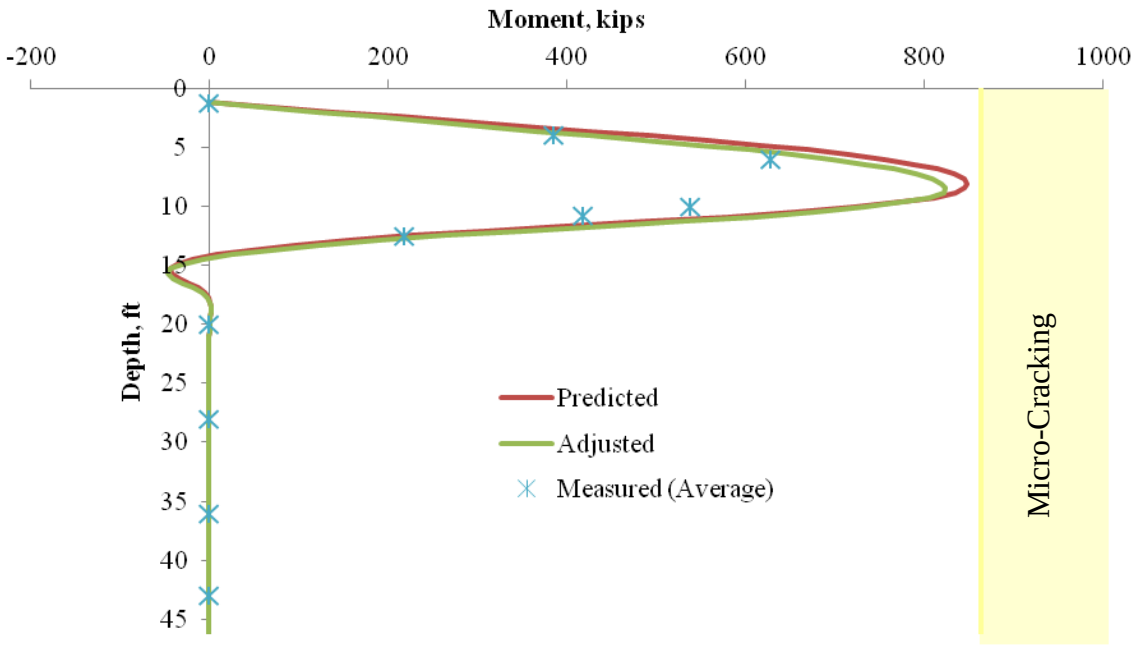

Figure 5-57: Predicted, Adjusted and Average Measured Moments along the Length of P3 at the 12.5 kip Load Step during the Lateral Load Test

Due to the small stains measured at the strain gage levels 20 feet from the pile head and lower, drift at these locations were insignificant. Figure 5-60 shows a strain gage located approximately 28 feet from the pile head as an example of the drift. For Figure 5-57 the drift was taken into consideration and the average measured moment was corrected. P3 was predicted to perform well for a 12.5 kips lateral load, but P4 was predicted to have cracks greater than 0.012 inches in width based on the corresponding moment as calculated in Section 3.2.2.

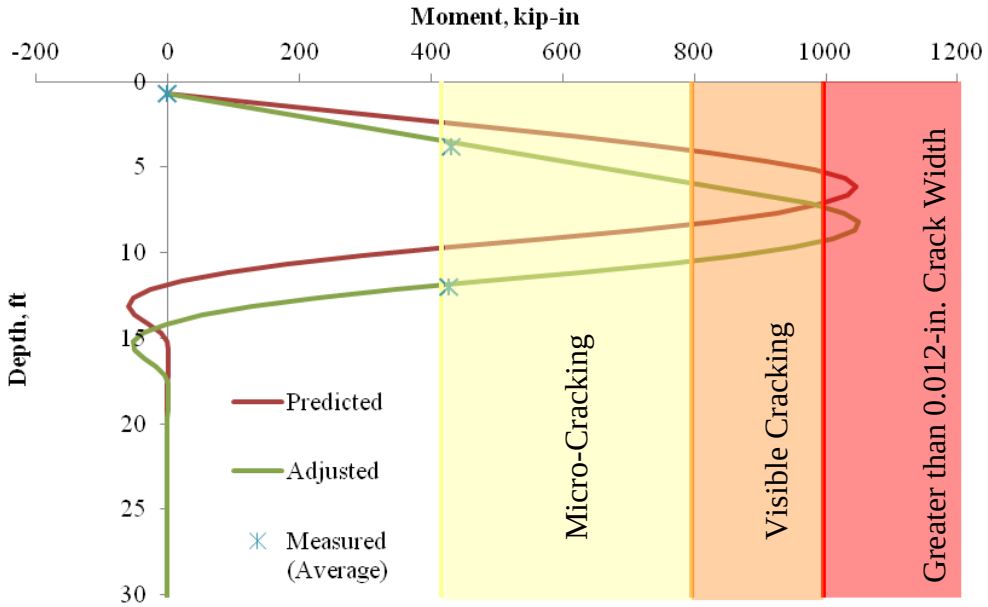

Figure 5-58: Predicted, Adjusted and Average Measured Moments along the Length of P4 at the 12.5 kip Load Step during the Lateral Load Test

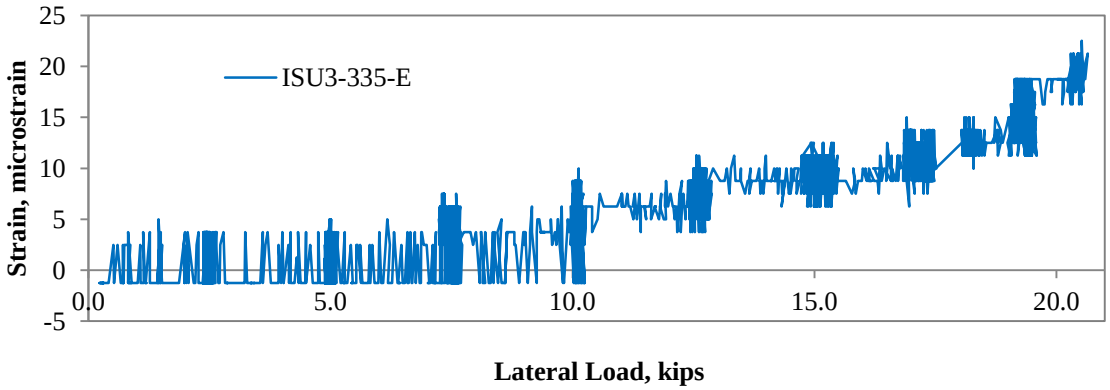

Figure 5-59: Drift in Embedded Concrete Strain Gage

For each of the load steps, the displacements measured by the SAA were compared to the displacements calculated in the adjusted LPILE model. Figure 5-60 compares the predicted, adjusted and measured displacements during the 12.5 kip load step of the lateral load test for P4 and shows that the adjusted LPILE model predicts the performance of P4 very well. All of the other displacement comparisons can be found in Appendix E.

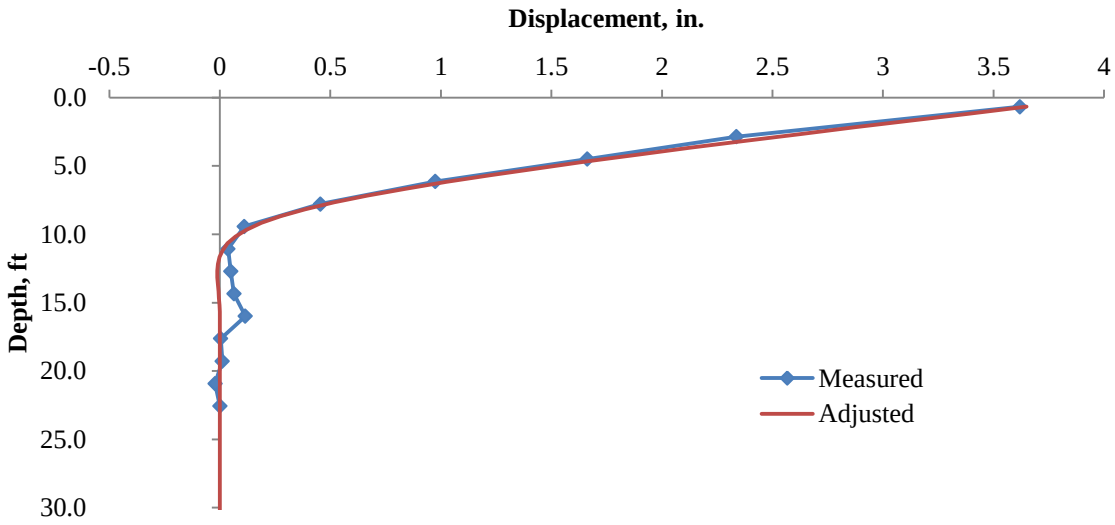

Figure 5-60: Measured Displacements Compared to Adjusted Displacements at the 12.5 kip Load Step during the Lateral Load Test

5.6.6. Splice Performance

Since the splice was located 15 feet from the pile head on P4, it was subjected to 52.4 kip-in bending moment and 0.08 inches of lateral displacement as shown in Figure 5-58 and Figure 5-60, respectively. The predicted shear profile along the length of P4 for the 12.5 kip lateral load step is given in Figure 5-61 and indicates the splice was subjected to a shear force of 1.2 kips.

As mentioned in Section 5.6.4, no visible damage from driving or the lateral load test was found on or near the splice after excavation. The splice was subjected to compressive stresses of 5.7 ksi and a tensile stress of 0.1 ksi during driving. Due to a miscommunication between design and installation, the splice was driven to 12 feet below the ground surface instead of the required 9-ft embedment. The drawings in the chapter were changed to reflect

the in situ condition. As a result, the splice was only subjected to 2.6 kips of shear, 52.4 kip-in of bending moment, and 0.1-in of lateral displacement.

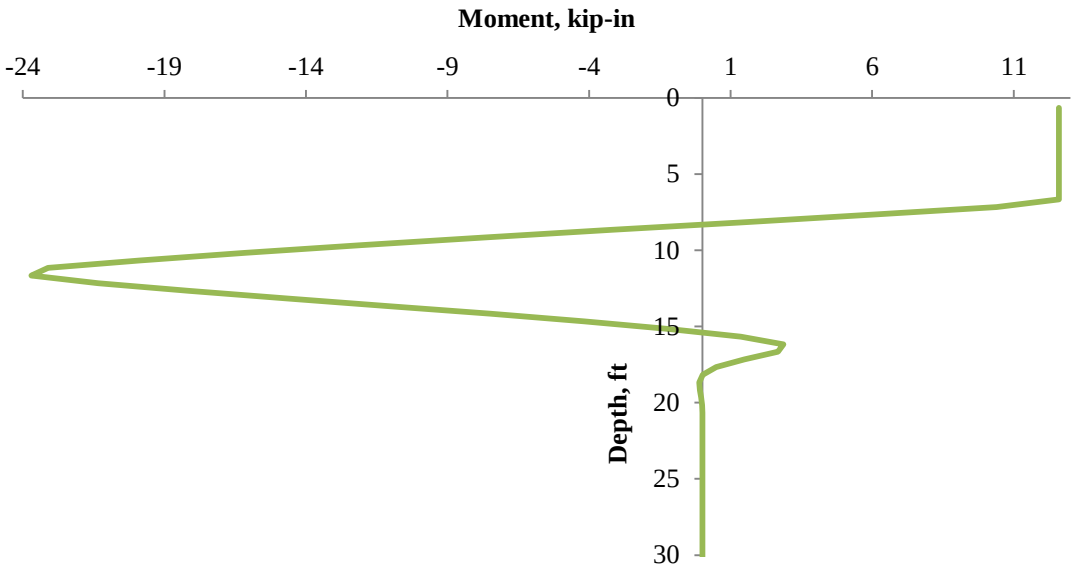

Figure 5-61: Adjusted Shear along P4 during 12.5 kip Load Step of Lateral Load Test

P4 was subjected to a maximum shear force of 2.6 kips during the lateral load test. In the laboratory, a similar splice was subjected to additional shear and bending tests. The splice proved to be very robust with a reserve shear capacity of 45 kips, which exceeds the maximum shear demand from the lateral load field test of 20.6 kips by 118 percent (Sritharan et al. 2012). When considering the field test with the laboratory results, the performance of the splice in the field can be expected to meet the required shear and moment demands even under extreme field conditions.

CHAPTER 6: INSTRUMENTATION AND INSTALLATION OF INSTRUMENTED PRODUCTION PILES

Following successful development of the UHPC pile and its connections, the performance of a UHPC production pile in a constructed bridge over a period of time was the next step. The overall goal of this exercise was to determine the suitability of UHPC piles in integral bridge foundations as well as the ability of these piles to sustain cyclic lateral movements resulting from time dependent movements including those due to thermal effects. This task was investigated as part of this project by replacing a steel HP 10 x 57 pile with an equivalent UHPC pile during construction of a new bridge. This chapter presents the details about the selection of the bridge, location of the UHPC pile, reference steel piles, and instrumentation and installation of both of the UHPC and the three H-piles. At the time of writing, no data has been gathered from the piles since the bridge is still under construction. The data collected from monitoring of the pile will be reported in the future by Garder et al. (2013).

6.1. BRIDGE SITE

A suitable new or replacement bridge site for installing the UHPC production pile, identified as UW1, was selected using the following criteria: 1) must use an integral abutment; 2) the length should be in excess of 200 feet; and 3) foundation soil type should be less favorable for pile movement. The Sac County Bridge was chosen as the site for the UHPC production pile (UW1) because the bridge's geometry, soil conditions and construction timeline met the criteria being sought. The site is just north of Early, Iowa, at the intersection of U.S. 20 over U.S. 71.

6.1.1. Bridge Geometry

The bridge is a 223-ft long and 40-ft wide with a 24 degree skew. The bridge consists of three spans and the span lengths are 55′-9", 106′-6", and 60′-9" from west to east. HP 10 x 57 steel piles were designed to support the two abutments and the two bridge piers.

6.1.2. Soil Conditions

SPT test information was obtained from the Iowa DOT on the abutment with the UHPC production pile. The ID number for the SPT borehole that was used for design of the HP 10 x 57 production piles was F-1219. A CPT test was performed on the west abutment of the westbound bridge by Geotechnical Services, Inc. on August 10, 2011 at the request of the ISU research team to better classify the soil profile for the location of the UHPC production pile. The soil consists of cohesive clay and silty clay with a water table located at a depth of approximately 20.50 ft according to the Iowa DOT soil report for borehole F-1219.

The soil classification reported by the Iowa DOT based on SPT is shown in Figure 6-1 and is compared with the CPT results. Table 6-1 summarizes the undrained shear strength and friction angle for each soil layer, which is calculated by using an empirically based approach described by Lunne et al. (1997) and taking the average of for each soil layer.

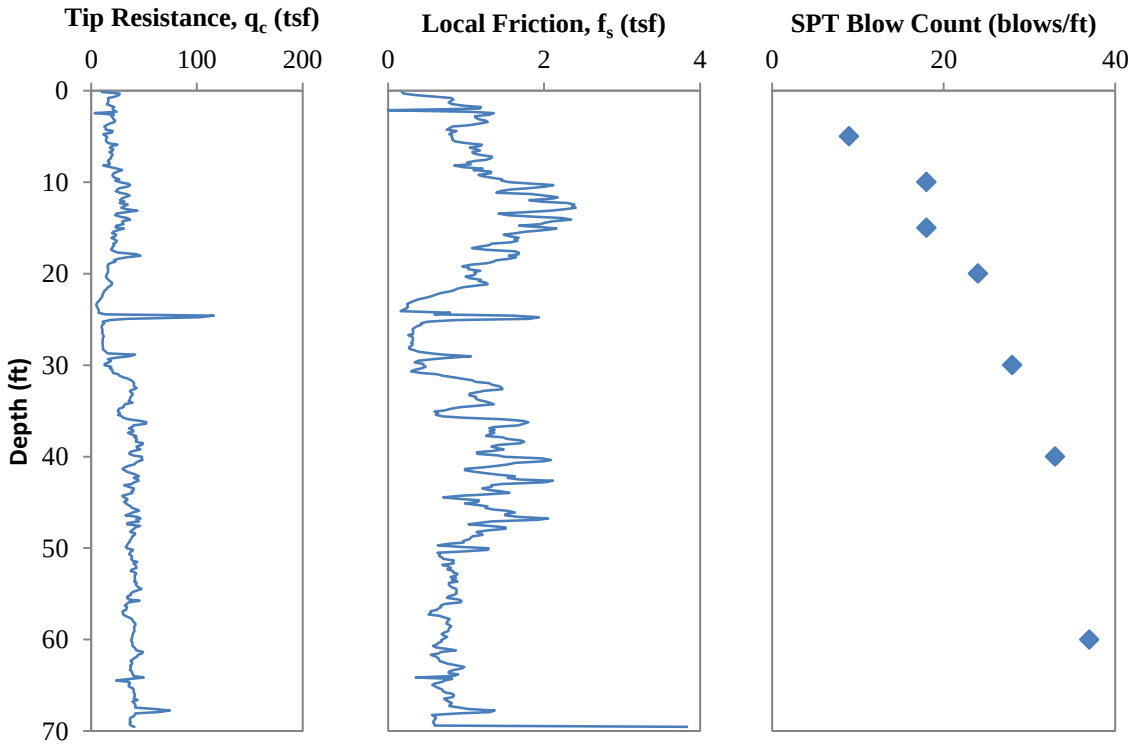

Figure 6-1: CPT and SPT Results for the West Abutment of the Westbound Bridge at the Sac County Site

Table 6-1: Undrained Shear Strengths and Friction Angles Calculated from the CPT Data for the West Abutment

Soil Classification	Depth to Bottom of Layer, ft	Undrained Shear Strength, psi	Friction Angle, Degrees
Clay	25.75	19.27	33.0
Silty Clay to Clay	28.54	8.87	27.9
Sandy Silty to Clayey Silt	33.46	25.23	31.8
Clayey Silt to Silty Clay	38.39	31.59	32.8
Clayey Silt to Silty Clay	48.23	33.84	32.8
Sandy Silt to Clayey Silt	69.72	32.18	31.9

6.2. DESIGN OF PRODUCTION PILES

The designed steel HP 10 x 57 piles were designed for 100 kips of vertical load using the Iowa DOT Blue Book Method outlined in Section 2.5. The production pile, UW1, was to replace one of the HP 10 x 57 piles on the west abutment of the westbound bridge. As a result, UW1 was also designed for a 100 kip vertical load. The predicted design capacity of each of the piles was also calculated by using DRIVEN 1.0 (Matthias and Cribbs 1998) and CAPWAP (PDI 2000). The location of all the instrumented bridges is given in Figure 6-2. All of the design calculations based on the Blue Book Method are included in Appendix C.

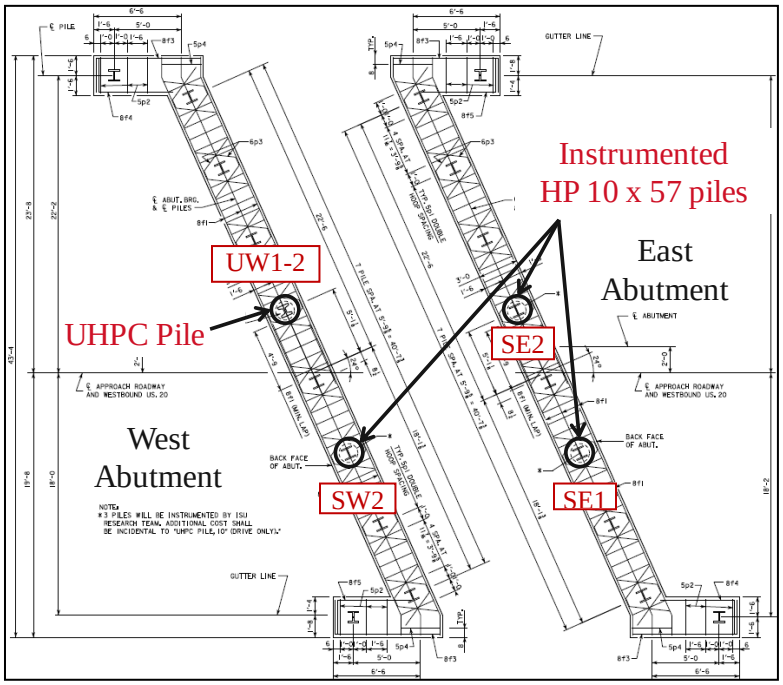

Figure 6-2: Location of Instrumented Production Piles

6.2.1. HP 10 x 57 Production Piles

The HP 10 x 57 pile on the west abutment (SW2) was designed for a vertical load capacity of 100 kips, resulting in a total length of 65-ft with 62-ft embedded below the ground surface. Using the new LRFD resistance factors recommended by Green et al. (2012) to achieve the same design load, the total length of the pile would only need to be 60-ft. The amount new resistance factors shorten the pile was 7.7 percent.

The two instrumented HP 10 x 57 piles on the east abutment, SE1 and SE2, had a design length of 85 ft with an embedment of 82 ft for the same 100 kip design load, but using the new LRFD resistance factors (Green et al. 2012) the pile could be shortened by 5.9 percent for a total length of 80-ft.

6.2.2. UHPC Production Pile

UW1 was designed with a total length of 55 ft and a 53 ft embedment below ground surface for a 100 kip design load. Unlike steel HP 10 x 57 piles, the top 12 inches of UHPC piles does not need to be cut off because there is no buckling taking place, resulting in saved material. As a comparison, the new resistance factors calibrated by Abdelsalam et al. (2012) for H-piles were used to calculate the design length of UW1 which resulted in a total pile length of 52-ft with 50-ft embedded below the ground surface. The new resistance factors would only result in shortening the UHPC pile by 3 ft or 5.5 percent.

To accommodate PDA equipment an extra foot was added to the design of UW1 to make the total length 56-ft. This resulted in easier disassembly of the PDA equipment at the end of drive and reassembly for the restrikes because the PDA equipment was installed 30 inches from the pile head.

6.3. INSTRUMENTATION SCHEME

The instrumentation used for the first UHPC production pile (UW1-1) was the same embedded concrete gages as described in Section 5.2 and shown in Figure 5-1. A second production pile (UW1-2) was needed because UW1-1 was dropped from the crane due to the use of inadequate hook and poor handling in the field and deemed unusable as a production

pile (described in Section 6.5). Due to the limited amount of time to gather instrumentation for the second production pile (UW1-2), two different types of concrete embedment gages were used along this pile. The two types of gages are shown in comparison in Figure 6-3. For the steel piles, weldable strain gages were used as shown in Figure 6-4. All of the production piles had two gages at each level that were on the diagonal to measure the curvature of the pile during the expansion and contraction of the integral bridge due to thermal movements.

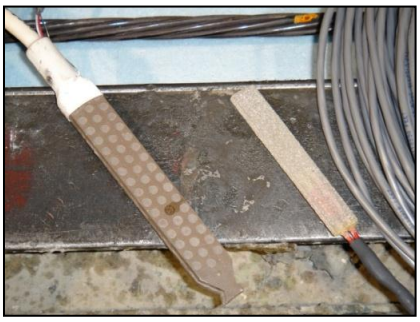

Figure 6-3: Embedded Concrete Strain Gages for UW1-2

Figure 6-4: Weldable Steel Strain Gages used to Monitor the Steel HP 10 x 57 Production Piles

6.3.1. First UHPC Production Pile

The concrete gages for UW1-1 were installed November 18, 2011 at Coreslab Structures, Inc in Bellevue, Nebraska using the procedure given in Appendix C for embedded concrete strain gages. Table 6-2 lists the gage labels and the location from the pile head for each of the twelve gages. The gage locations are also illustrated in an elevation view in Figure 6-5.

Table 6-2: Location and Labels of Strain Gages in UHPC Production Pile UW1

Location from Pile Head, ft	Gage Label	
4	UW1-48-E	UW1-48-W
12	UW1-144-E	UW1-144-W
18	UW1-216-E	UW1-216-W
30	UW1-360-E	UW1-360-W
43	UW1-516-E	UW1-516-W
54.25	UW1-668-E	UW1-668-W

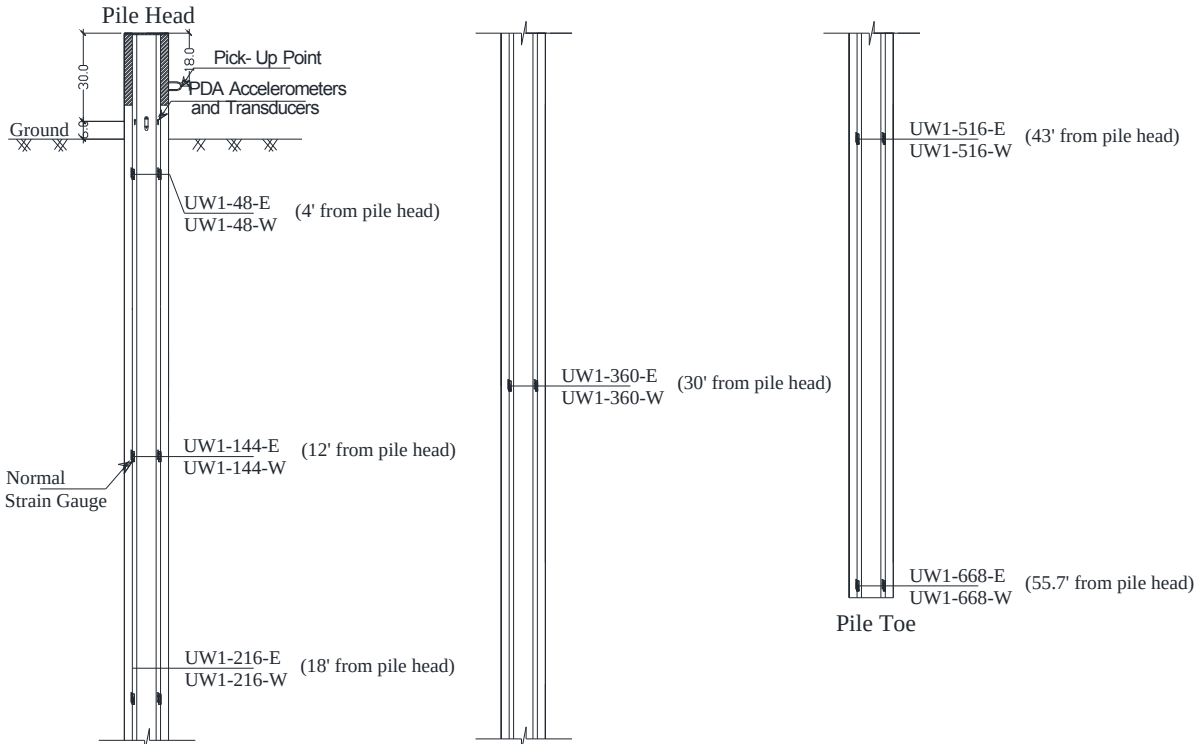

Figure 6-5: An Elevation View of UW1 Showing the Location of Instrumentation

6.3.2. Second UHPC Production Pile (UW1-2)

The instrumentation for UW1-2 was also installed at Coreslab Structures, Inc. in Bellevue, Nebraska but on February 13, 2012 with the same instrumentation scheme as for UW1-1. The only difference between the two piles is that UW1-2 did not include a splice at the pile head. There was no need to include the splice because the UHPC production pile capacity had been verified by the vertical load test described in Section 5.5 at the site near the west abutment which is where UW1-2 would be located.

6.3.3. HP 10 x 57 Production Piles

PDA was performed on all of the instrumented steel HP 10 x 57 production piles. The cross-section view of the location of the strain gages and accelerometers is given in Figure 6-6. Notice that the accelerometers are on opposite sides of the web of the pile as was done by Ng et al. (2011). The data gathered by the PDA equipment was wirelessly transmitted to the PDA unit, same as for the UHPC test piles.

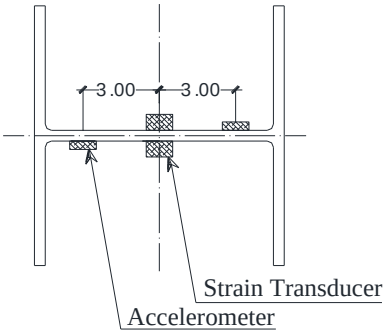

Figure 6-6: Location of PDA Instrumentation on HP 10 x 57 Piles at a Cross-Section 18 inches from the Pile Head

To instrument the steel H-piles, weldable gages were used to measure the strain in the steel along the length of the pile. In order to secure the gages, a tack welder, shown in Figure 6-7, was used for gage installation. The procedure for installing the weldable strain gages is outlined in Appendix D. The cross-section of the instrumented steel HP 10 x 57 piles is shown in Figure 6-8, which also shows how the ends of the angle welded to the pile to protect the instrumentation was closed at the end.

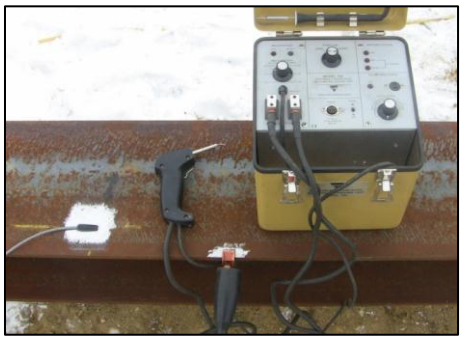

Figure 6-7: Tack Welding Machine

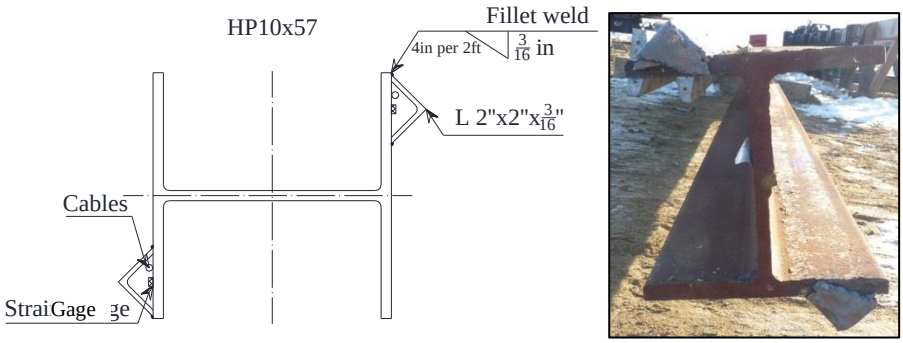

Figure 6-8: Cross-Section View of HP 10 x 57 Pile Showing the Strain Gage Location

6.3.3.1 SW2

SW2 was instrumented on January 23, 2012 using the procedure outlined in Appendix D for the weldable strain gages. Twelve gages were installed along the length of the pile at six levels with two gages at each level. Table 6-3 lists the strain gage label and location from the pile head and Figure 6-9 illustrates the location of PDA and strain gages in elevation view.

Table 6-3: Location and Labels of Strain Gages in Steel Production Pile SW2

Location from Pile Head, ft	Gage Label	
4	SW2-48-E	SW2-48-W
12	SW2-144-E	SW2-144-W
18	SW2-216-E	SW2-216-W
33	SW2-396-E	SW2-396-W
49	SW2-588-E	SW2-588-W
64.5	SW2-774-E	SW2-774-W

6.3.3.2 SE1 and SE2

SE1 and SE2 were instrumented on March 7, 2012 using the procedure outlined in Appendix D for the weldable strain gages. Six gages were installed along the length of the pile at three levels with two gages at each level. The reason for the reduced number of strain gages is that the piles on the east abutment are 85 feet in length. The east abutment piles were to be spliced at 40 feet from the pile head and it would be difficult to run cables from the portion of HP 10 x 57 below the splice. Table 6-4 lists the strain gage labels and location from the pile head for SE1 and

Table 6-5 for SE2. Figure 6-10 illustrates the location of PDA and strain gages in elevation view for SE1 and SE2, respectively.

Table 6-4: Location and Labels of Strain Gages in Steel Production Pile SE1

Location from Pile Head, ft	Gage Label	
4	SE1-48-E	SE1-48-W
12	SE1-144-E	SE1-144-W
16	SE1-192-E	SE1-192-W

Table 6-5: Strain Gage Labels for SE2

Location from Pile Head, ft	Gage Label	
4	SE2-48-E	SE2-48-W
12	SE2-144-E	SE2-144-W
16	SE2-192-E	SE2-192-W

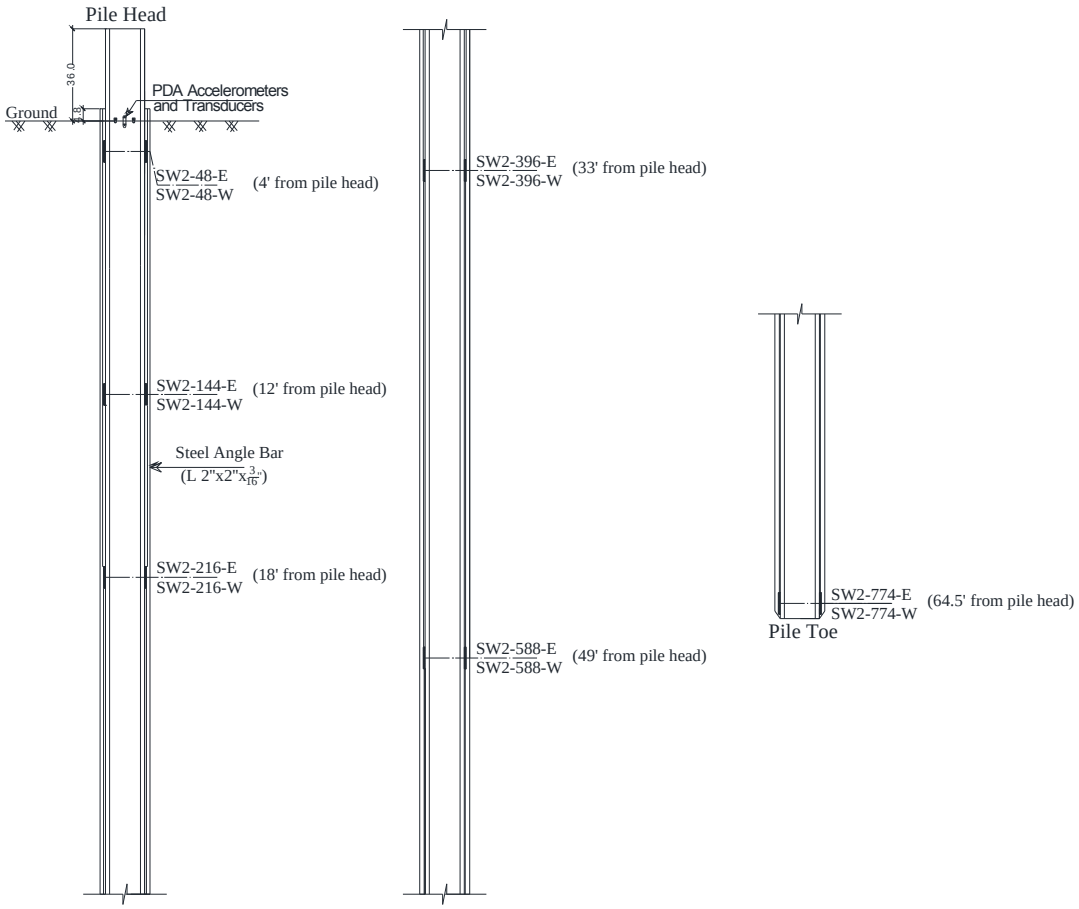

Figure 6-9: An elevation View of SW2 Showing the Locations of Instrumentation

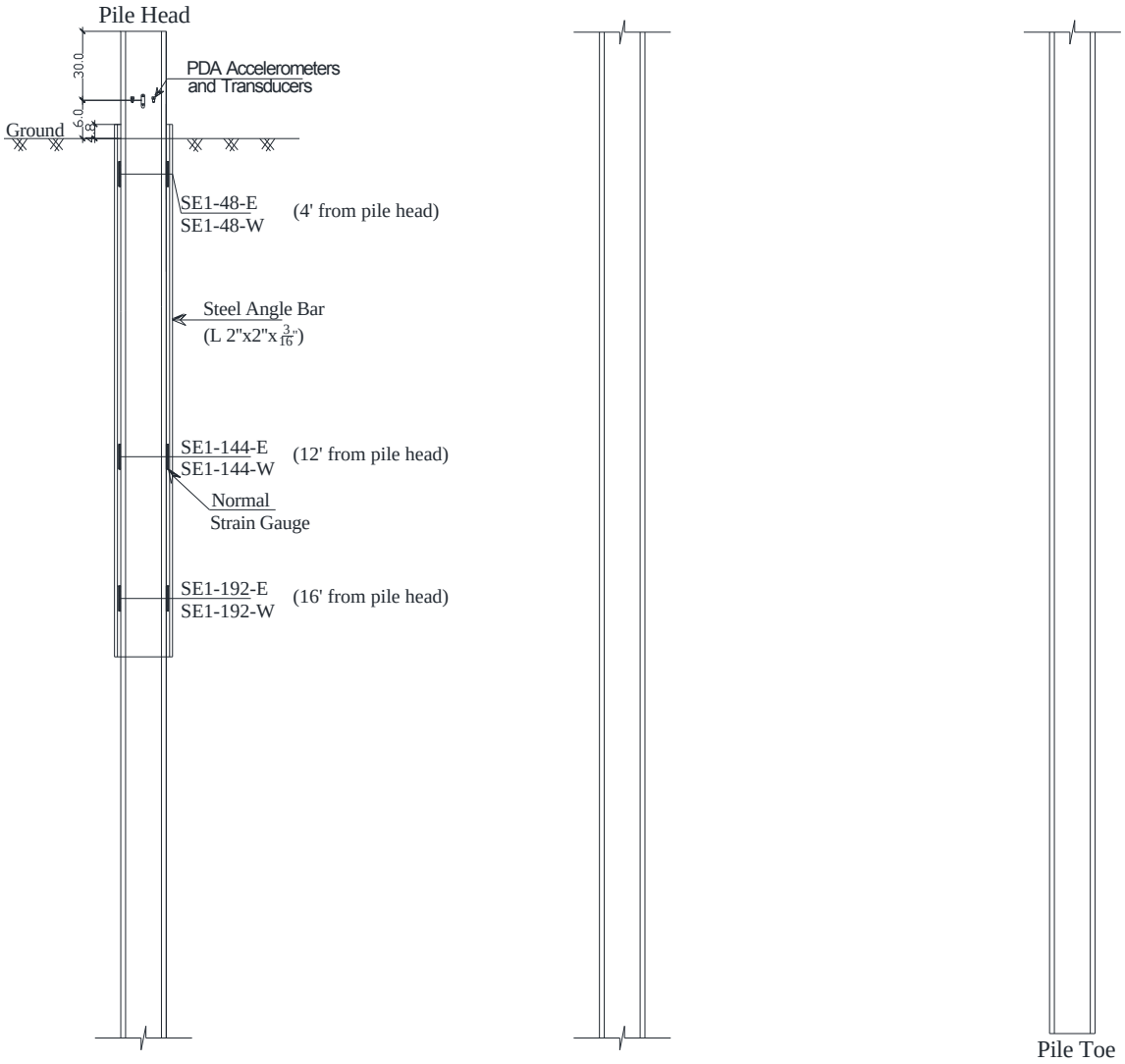

Figure 6-10: An Elevation View of SE1 and SE2 Showing the Locations of Instrumentation

6.4. FABRICATION OF UHPC PILES

6.4.1. Splice Fabrication

The splice for UW1-1 was fabricated by Howe Welding in Ames, Iowa by a certified welder along with the splices for the test piles. The fabrication is outlined in Section 5.3.1.

No splice was fabricated for UW1-2 due to the verification of capacity through the vertical load test.

6.4.2. Casting Process

The UHPC production piles were cast at Coreslab Structures, Inc. in Bellevue, Nebraska. UW1-1 was cast along with the test piles, P3 and P4 in December of 2011. A second production pile was needed due to complications in the field that are discussed in Section **Error! Reference source not found.**, and is attributed to the third cast date in ebruary 2012.

6.4.2.1 UW1-1

The casting process, steam curing and materials properties were the same for UW1-1 as for P3 as outlined in Section 5.3 because they were cast from the same batch. The layout of the production pile is shown in Figure 5-12.

6.4.2.2 UW1-2

The casting process and steam treatment were the same as outlined in Section 5.3 for UW1-2. One side of the steel forms was left off while all ten prestressing strands were arranged and stressed to their initial prestress of 202.5 ksi. Because the side of the forms was left off, twelve strain gages were able to be installed along the pile length. No inserts were added for the PDA equipment since it was just as easy to drill through the UHPC with a 3/8 in. diameter concrete drill. After the instrumentation was complete the forms were closed as shown in Figure 6-11 by lifting the steel side with the overhead crane and then locked into place.

The UHPC was mixed using the precaster's 4.0 yd^3 mixer at the batch plant. A total of 1 yd^3 of Ductal® was used for the pour. After completing the batching of the UHPC mix, it was poured into a large bin and transported by a fork lift to the building where the UHPC forms were located. The UHPC was then poured into the forms. Once the pour was complete, the top surface of UW1-2 was covered with plastic wrap to prevent moisture loss as shown in Figure 6-12 as before.

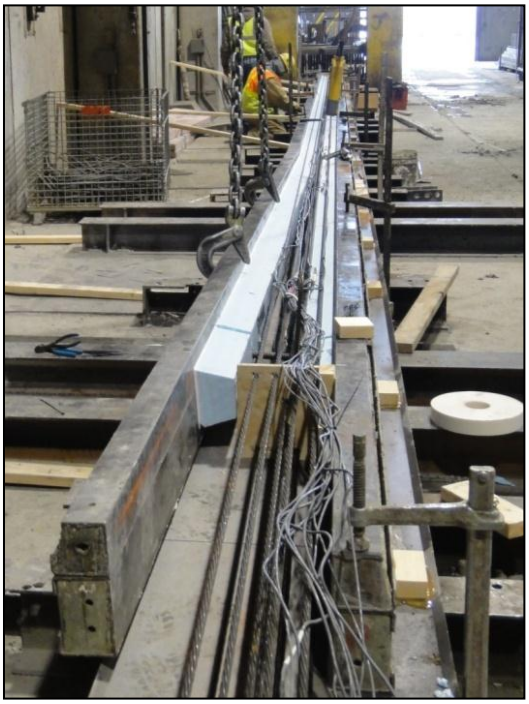

Figure 6-11: Closing the Side Forms before Casting UW1-2

Figure 6-12: Plastic Wrap Cover for UW1-2 at the End of Casting

6.4.3. Details of First UHPC Production Pile Pour

The pour of UW1-1 was on November 21, 2011, the same day as the pour for P3 and P4. The same batch of UHPC was used, therefore the UHPC was lumpy and the formwork also moved and concrete leaked out of the formwork as mentioned in Section 5.3.3.1. Concreting paused halfway and a waiting time of about 55 minutes before pouring continued

took place. After the forms were stripped there were a few imperfections along the length of UW1-1, however the pile was deemed acceptable.

6.4.4. Details of Second UHPC Production Pile Pour

The pour of UW1-2 took place on February 14, 2012. The dry ingredients of the UHPC were broken up in the mixer before the liquids were added. Once the clumps were broken down the water and admixtures were added to the mix in the proper order. The UHPC had a good consistency and everything went well for the pour.

6.4.5. Steam Curing and Instrumentation Performance

After the release of the prestressing strands in UW1-1, it was steam cured with P3 and P4 at 194ºF for 48 hours at the precasting plant. All twelve of the gages in UW1-1 were working after the steam curing. The same process for steam curing was used for UW1-2. All twelve of the gages in UW1-2 were working after the steam curing was complete.

6.4.6. Handling of UHPC Production Piles

Due to the failure of the pick-up point hook on UW1-1, a new pick-up point detail was designed for the UW1-2. A 1-in. diameter high strength threaded rod was embedded into the web at the location of the previous pick-up point hook by the pile head as shown in Figure 6-13. Core slab also inserted bent prestressing strands 1.5 feet away from the pile head and the pile toe, to provide easy transportation pick-up points at the precast plant.

The idea behind the pickup point is at the construction site, a cable loop is slipped over the threaded rod followed by a washer and a nut to keep the cable in place during installation. Figure 6-14 shows that the tread size of the nut is much smaller than the thread size of the threaded rod. To ensure safety that the cable loop would not slip off the threaded rod when picking up the pile, an additional washer was welded to the threaded rod, which is shown in Figure 6-15.

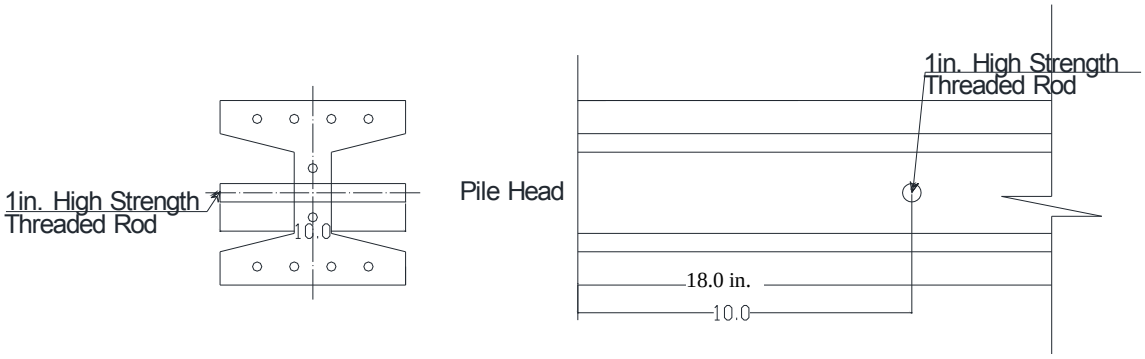

Figure 6-13: Revised Pick-up Point Design

Figure 6-14: Proposed Pick-up Point

a) b)

Figure 6-15: a) Welding the 2nd Washer to the Threaded Rod; and b) Pick-up Point After Welding

6.4.7. Material Properties

6.4.7.1 Prestressing Strands

The material properties for the prestressing strands of UW1-1 are the same as for P3 and P4 because it was cast at the same time as the two test piles. Section 5.3.6.1 gives the average yield strength of the strands which was 250.5 ksi and the average modulus of elasticity of 29,449 ksi.

For the prestressing strand roll used for UW1-2, three 5-ft sections of the 270 ksi low-relaxation prestressing strands were cut. The three strands were tested in uniaxial tension at Iowa State University. The ultimate strength of the ½-in. strands was 295 ksi before failing the strand fractured in tension. The yield strength of the strands were found to be 256 ksi.

6.4.7.2 UHPC

The 3-in. diameter cylinders that were cast out of the same batch as UW1-2 were tested in compression by Coreslab Structure, Inc. The average compressive strength of the UW1-2 was 28.1 ksi. The design strength of the mix was 26 ksi, and the results in Table 6-6 show that the 26 ksi average strength was achieved. The elastic modulus for UW1-2 was calculated using Equation 2-2 from Section 2.3.4 that was developed by Graybeal (2007). The modulus of elasticity of UW1-2 was calculated to be 7711 ksi.

Table 6-6: Average Compressive Strength Measured for the UW1-2 Pile

Cylinder Number	f'_c, ksi
1	27.5
2	28.4
3	28.5
	Average = 28.1

6.5. DRIVING OF PRODUCTION PILES

6.5.1. Driveability Analysis

A driveability analysis was conducted using GRLWEAP (PDI 2005) and the same hammer, cushion, and soil parameters as for the UHPC test piles which are given in Section 5.4.4. The percent shaft resistance that UW1-2, SW2, SE1, and SE2 are subjected to during

driving was calculated using the undrained shear strength and friction angles calculated for the average CPT results in the FHWA computer program DRIVEN (Matthias and Cribbs 1998). The maximum predicted and measured stresses during driving for the UHPC and steel production piles are shown in Table 6-7. The measured maximum stresses were calculated from the PDA analysis.

Table 6-7: Predicted and Measured Stresses in Production Piles during Driving

Pile		Maximum Stress, ksi		Percent Difference, %
		Predicted	Measured	
SW2	Compressive Stress	27.0	25.9	+ 4.2
	Tensile Stress	1.7	1.8	- 5.6
SE1	Compressive Stress	30.8	27.3	+ 12.8
	Tensile Stress	1.8	1.3	+ 38.5
SE2	Compressive Stress	30.8	28	+ 10.0
	Tensile Stress	1.8	0.7	+ 157
UW1-2	Compressive Stress	7.6	4.8	+ 58.3
	Tensile Stress	0.2	0	N/A

All of the predicted maximum stresses were over predicted when compared to the measured maximum stresses from the PDA, except for the maximum tensile stress of SW2. The reason for the very maximum tensile stress percent difference for SE1 and SE2 is due to the fact that the tensile stress were so low that a small change in stress results in a big percent difference. All of the compressive stresses and tensile stresses for all of the production piles were well within the allowable driving stress limits given in Section 2.3.6.

6.5.2. Driving Process

The same driving system as described in Section 5.4.3 was used to drive the steel HP 10 x 57 piles and UW1-2. Figure 6-16 illustrates the layout of the abutment piles within the abutment. The details of installation for each of the instrumented production piles are described in this section.

SW2 was driven into the west abutment of the westbound bridge on January 26, 2012. The only usable restrike for SW2 was one on March 19, 2012 approximately 53 days after the end of drive (EOD). The reason for the postponed restrike is the PDA transmitters had to be replaced because it was damaged when UW1-1 fell.

Figure 6-16: Layout of Abutment Piles

6.5.2.1 Steel Production Piles

The PDA equipment was bolted to the HP 10 x 57 piles while lying on the ground as described in Section 5.4.5.1. Once completed, the steel piles were lifted into position by using the pickup point shown in Figure 6-17. The pile was lifted to a vertical position and set into the 10-ft deep prebore hole. The crane was unhooked from the steel pile to pick up the hammer leads and positioned them on the top of the steel pile. When the leads, hammer and pile were in place the ram of the hammer was lifted manually by the crane and dropped. SE1 and SE2 had a design length of 85 feet and were spliced 40 feet from the pile head using a similar method as described for the spliced anchor piles in Section 5.4.5.1.

Figure 6-17: Steel HP 10 x 57 Production Pile Pickup Point

6.5.2.2 UHPC Production Pile

PDA was performed during the installation of UW1-2. The way the strain gages and accelerometers were attached to the pile was the same as for the test piles which is shown in Figure 5-4. The data gathered by the PDA equipment was wirelessly transmitted to the PDA unit by the same process as for the UHPC test piles.

The new pickup point designed for UW1-2 worked very well. To reduce the amount of stresses on the UHPC pile, the pile was picked-up by the new pickup point at the pile head and the inserted prestressing strand hook at the toe of the pile. Once the pile was lifted off the ground, the crane operator rotated the pile to the vertical position in the air as shown in Figure 6-18. The installation was very similar to a steep H-pile, except one of the crew members had to be sent to the top of the UHPC pile to release the pile from the crane.

Figure 6-18: Stages in Lifting UW1-2

A 4-in. plywood pile cushion was used to protect the UHPC pile head, but UW1-2 punched through the pile cushion shortly after driving had begun. Instead of replacing the cushion with a new cushion, the pile was driven with essentially no cushion. There was slight damage to the pile head corners of UW1-2 as shown in Figure 6-19. The reason for the damage to UW1-2 was the pile head was not perfectly centered under the helmet. It is also important to note that the UW1-2 was slightly tilted after driving and on the back side of the prebore hole as shown in Figure 6-20 which might reduce the effectiveness of the prebore hole.

Figure 6-19: Damage to the Pile Head of UW1-2

Figure 6-20: UW1-2 after Installed in the Prebore Hole

6.6. ESTIMATED CAPCITY

6.6.1. UW1-2

As a comparison of the different methods used to design deep foundations, Table 6-8 lists the estimated nominal capacity of UW1-2 using the Iowa DOT current design procedures, DRIVEN and CAPWAP. The predicted capacity using DRIVEN was 8 percent higher than for the Iowa DOT current design method, and 6.5 percent higher than the Iowa

DOT current design method when using CAPWAP. The CAPWAP analysis was completed using a Case damping factor of 0.166.

Table 6-8: UW1 Nominal Capacity Calculated by Various Methods

Method	Estimated Nominal Capacity, kips
Iowa DOT Current	200
DRIVEN	216
CAPWAP (3-day) *	212.9

* Further gain is expected due to setup (Ng et al. 2011)

The vertical load test that was performed on P3, which was 10 feet shorter than UW1-2 produced a vertical capacity of 296.5 kips. P3 and UW1-2 are comparable in length because the 10-ft reduction in length of P3 was to account for the prebore hole of UW1-2. The vertical load test was performed eight days after the EOD, while the CAPWAP predicted capacity of UW1-2 was from a restrike three days after EOD. The difference in the amount of time after EOD for measuring or predicting the nominal capacity could account a portion of the 39 percent difference in capacity due to the effect of setup in clays (Ng et al. 2011).

6.6.2. SW2

The results of the calculated nominal capacity of the different types of design methods are given in Table 6-9. DRIVEN calculates an estimated nominal capacity 6.2 percent higher than the current Iowa DOT method. Interestingly, CAPWAP estimated the nominal capacity of SW2 to be 318.6 kips by using a Case damping factor of 0.245, which was 59.3 percent higher than the current Iowa DOT method. One thing to note is that the final restrike, which was used to estimate the nominal capacity of SW2, took place 53 days after the end of drive instead of the specified 3-days. The reason for the delay was the two PDA transmitters were broken and two new transmitters had to be ordered.

Table 6-9: SW2 Nominal Capacity Calculated by Various Methods

Method	Estimated Nominal Capacity, kips
Iowa DOT Current	200
DRIVEN	212.3
CAPWAP (53-day)	318.6

6.6.3. SE1 and SE2

Using the Iowa DOT current design method the predicted capacity of SE1 was 200 kips. The calculated nominal capacity from the CAPWAP analysis estimates the nominal capacity of SE1 to be 286.9 kips by using a Case damping factor of 0.335. The CAPWAP analysis predicted a value 43.5 percent higher than the capacity estimated by the Iowa DOT's current design method.

Similar to SE1, SE2 has a predicted nominal capacity of 200 kips from the Iowa DOT current design method, but the CAPWAP analysis estimates the capacity to be 271.2 kips by using a Case damping factor of 0.277. This results in a 35.6 percent increase.

6.7. ESTIMATED INITIAL COST COMPARISON

For the Sac County Bridge Replacement Project. It was suggested by the Iowa DOT to use an average price of $35 per linear foot for the material and installation. The fabrication cost of UHPC piles, as recommended by industry, is $2500 per cubic yard. There are 0.015 cubic yards of UHPC in every linear foot of the pile. This would give a material and fabrication cost of $37.50 per linear foot. From the RS Means (2009) the labor and equipment cost in Iowa for pile installation is $7.47 per linear foot with an additional $5.50 per linear foot for overhead and profit costs for the crew and equipment given in Table 6-10. The price per linear foot of UHPC is estimated to be approximately $50.47.

Table 6-10: Crew and Equipment for Labor Cost Estimate

Crew	Equipment
1 Pile Driver Foreman	1 Crawler Crane
4 Pile Drivers	1 90-ft. Lead
2 Equipment Operators (Crane)	1 Diesel Hammer
1 Equipment Operator (Oiler)	

Clearly, UHPC piles are more expensive per linear foot than the HP 10 x 57 piles used for the Sac County Bridge Project. Table 6-11 lists the number and length HP 10 x 57 piles used in both the westbound and eastbound bridges. Similarly, Table 6-12 lists the

number and corresponding length of UHPC piles needed to support the two bridges based on the current Iowa DOT Blue Book Method.

Table 6-11: Total Length of HP 10 x 57 Piles Needed for Sac County Bridge Project

Bridge	Location	Number of Piles	Length/Pile, ft	Total Length, ft
Westbound	West Abutment	10	65	650
	Pier 1	27	50	1350
	Pier 2	27	55	1485
	East Abutment	10	85	850
Eastbound	West Abutment	10	65	650
	Pier 1	27	50	1350
	Pier 2	27	55	1485
	East Abutment	10	85	850
			Sum	8670

Table 6-12: Total Length of UHPC Piles Needed for Sac County Bridge Project

Bridge	Location	Number of Piles	Length/Pile, ft	Total Length, ft
Westbound	West Abutment	10	55	550
	Pier 1	27	40	1080
	Pier 2	27	45	1215
	East Abutment	10	85	850
Eastbound	West Abutment	10	55	550
	Pier 1	27	40	1080
	Pier 2	27	45	1215
	East Abutment	10	80	800
			Sum	7290

Based on the total length of HP 10 x 57 piles the cost of the foundation at $35 per linear foot the total would be $303,450. The UHPC pile foundation would cost a total of $367,926. For just the initial cost estimate UHPC pile are approximately 21 percent more expensive. For the Sac County Bridge Project, the price for UHPC material and prefabrication costs needs to be reduced to $1910 per cubic yard to have the same total foundation cost as for the steel HP 10 x 57 piles which is a reduction of 31 percent. One thing

to note is that this estimate does not take into account the increased durability and reduced maintenance costs associated with UHPC piles. For a more accurate cost comparison, a total life cycle cost analysis should be done with due consideration to increased life span of the UHPC piles.

CHAPTER 7: SUMMARY AND CONCLUSIONS

7.1. SUMMARY OF RESEARCH

This research presented herein is part of the second phase of an extensive study on the development and field installation of UHPC piles, which has focused on the design, precast fabrication, installation, and performance verification in the field. During Phase I of the project, the design of the UHPC pile cross-section was optimized and the section behavior in strong-axis bending was predicted and verified through laboratory testing followed by a vertical and a lateral load test in the field. Specifically, this study 1) investigated the performance of a UHPC pile as part of an integral bridge using analytical models; 2) tested the typical pile-to-abutment connection detail in the laboratory by subjecting the connection to a combination of axial and lateral cyclic loading; 3) conducted a field vertical load test to failure; 4) performed a lateral load test in the field on an spliced UHPC pile; and 5) instrumented and installed a production UHPC pile as part of a bridge foundation to compare its driving behavior and performance to a comparable steel H-pile.

A brief introduction to the history and background of the challenges associated with traditional concrete and steel piles in the United States along with an introduction to Phase I of the UHPC pile project was given in Chapter 1, which focused on the way UHPC members with enhanced engineering and durability properties could be used as a extending bridge foundation service life. A review of published studies describing the composition, microstructure, durability, material properties, applications, practice for splicing piles in the field, pile-to-abutment connection details, integral abutment issues relevant to this study, and analysis procedures for evaluating driveability and lateral load performance of piles were given in Chapter 2. Chapter 3 focused on an analysis of UHPC piles in integral abutments by describing the section behavior of UHPC and HP 10 x 57 piles in weak-axis bending and strong-axis bending, and a parametric study on the lateral load behavior of UHPC piles with the appropriate axial load using the calculated section behavior. The fabrication and casting of the UHPC test units and abutment cap were described in Chapter 4, which also describes the weak-axis bending HP 10 x 57 test unit lateral load test and weak-axis bending UHPC

test unit lateral load test. A description of the fabrication and casting process, installation, vertical load test, and lateral load test for the UHPC test piles is given in Chapter 5. Chapter 6 describes the fabrication and casting process of the UHPC Production pile, the installation and instrumentation of three instrumented HP 10 x 57 piles and the UHPC production pile.

7.2. CONCLUSIONS

This study provided a complete analysis of the design, fabrication and installation of UHPC piles in comparison to steel HP 10 x 57 piles. The conclusions drawn from the pile analysis, production, handling, installation, feasibility, and performance of the pile in the laboratory and field are described in this section.

7.2.1. Pile Analysis

The parametric study of the UHPC pile in comparison with the HP 10 x 57 pile proved that the UHPC pile could be a viable option for supporting integral abutment bridges. At higher axial loads, such as 200 kips, it was found that the UHPC pile resisted cracking even at large target lateral displacements of 1.0 inches and 1.55 inches as previously specified in Section 3.2 as compared to a 100 kip axial load. In comparison, HP 10 x 57 piles resisted yielding at the same target displacements. The strength benefits associated with increasing axial loads on UHPC piles supported their use in integral abutments.

The lateral load analysis conducted in LPILE supported the use of prebore holes for both UHPC piles and HP 10 x 57 piles, which is currently required by the Iowa DOT for bridges over 130 feet in length. The benefit of the prebore holes was found to minimize or prevent cracking of UHPC piles and yielding of H-piles to an acceptable level during the cyclic expansion and contraction of the bridge due to thermal movements.

7.2.2. Production, Handling and Installation of UHPC Piles

The newly design pickup point for UHPC piles described in Section 6.4.6, which used a 1-in. diameter high strength threaded rod, washers and a nuts, proved to be successful but somewhat labor intensive since a crew member had to be lifted by the crane to unhook the pile from the crane head before driving could begin. A release mechanism similar to that

used for steel H-piles needs to be established as it will increase the efficiency during installation of UHPC piles in the field. After the pile was positioned to be vertical, the UHPC pile could be set in the prebore hole in the same way as an HP 10 x 57 pile. The benefit of the new pickup point was to have the pile hang in the vertical position as straight as possible to provide easy insertion into the prebore hole, which was successful in the field.

During installation, a void in the soil opened up near the web on both sides of the UHPC piles. The void of the 46-ft test pile had a depth of approximately 5 feet, while the void of the 30-ft test pile was 3 feet deep. This possibly indicates the occurrence and depth of the void to be related to the embedment length of the pile. Another likely parameter that may affect the size and occurrence of the void could be the soil condition at the site of installation. Analysis of UHPC piles should take this void into account when establishing the vertical load capacity and lateral load performance as the void can have some limited influence on the pile performance.

In some cases minimal damage to the UHPC pile head was seen in the field after driving. The 30-ft test pile did not have any visible damage to the pile head after installation. The longer 46-ft and 56-ft UHPC piles sustained minor damage to the corners of the pile head. This was believed to be due to not placing of the hammer on the center of the pile head during installation, which should be given attention in the field.

7.2.3. Feasibility of using UHPC Piles in Integral Abutments

The test of the pile-to-abutment connection confirmed that the current Iowa DOT design of integral abutments with steel piles was robust and would accommodate UHPC piles as well. Even though two hairline tension cracks with negligibly small widths developed at 12 kips of lateral load during testing in the laboratory, they were considered acceptable based on previous experience with testing and used of UHPC members.

During the UHPC vertical load test in the field, the UHPC test pile reached an ultimate capacity of 297 kips, which was 49 percent greater than the estimated nominal capacity of 200 kips. The capacity measured during the field testing confirmed that a 16 percent shorter UHPC production pile compared to the HP 10 x 57 piles was appropriate for the Sac County Bridge.

The UHPC lateral load piles were tested to a maximum lateral load of 20.6 kips with a corresponding lateral displacement of 8.3 inches for the weak-axis pile. The weak-axis pile failed 3 ft. above the splice. The soil was excavated around the 30-ft test pile where a significant tension crack was discovered at approximately the location of expected maximum moment. Under design lateral movements of 1.55 inches of lateral displacement, the UHPC piles performed well and indicated no damage.

7.2.4. Performance of Pile Splice

The splice located on P4, 15 feet from the pile head, performed very well during installation. No visible damage from driving or the lateral load test was found on or near the splice after excavation. Based on field testing and completed additional laboratory tests, the performance of the splice in the field can be expected to meet the required shear, moment demands and tensile demands.

7.3. FUTURE RESEARCH

To ensure quality production of UHPC piles without any defects, consistent tolerances and procedures need to be developed. The tolerances for imperfections should include limits on shrinkage cracking along the pile, air voids within the web of the pile, and inconsistence dimensions of the flanges and other applicably quality issues that are used today for precast concrete piles.

The prebore hole may not be as effective as intended during design. Future research with regards to lateral load tests on UHPC piles installed in prebore holes filled with bentonite may be used to verify their performance. For a reference, a similar pile test without a prebore hole may be used.

It is common to have battered piles in bridge piers. To increase the broad use of the UHPC piles, use of battered UHPC piles as well as their connections to pile caps and abutments should be investigated and their performance should be evaluated in the field.

Additional sizes of the tapered H-section UHPC pile should be investigated to make the product feasible for various soil and structural conditions. Having a variety of sizes

would increase the efficiency and frequency of use of UHPC piles. Steel piles are increasing in size to meet the demands for efficient, higher capacity foundations and in order to provide a comparable solution, a larger sized UHPC pile might be necessary. With increased web and flange dimension in larger UHPC sections, the production efficiency of UHPC piles will likely increase.

To reduce the relatively high cost of UHPC piles, the UHPC material, design, fabrication, installation, and increased life cycle need to be investigated or improved from current knowledge. Integrating the life cycle cost and expected maintenance cost reduction for the UHPC members into the analysis will help realize the true costs of the UHPC piles. In order to improve the design procedures for UHPC piles, additional vertical load tests need to be performed to more accurately predict the ultimate pile capacity. In doing so, the length of UHPC piles can be optimized and overall foundation costs may be reduced. At the fabrication stage, it is essential to develop easier to use steel forms to cast multiple UHPC piles and shorten the time the piles need to be on the precast bed to gain strength in order to streamline the production process. Improved installation procedures and an improved pickup point also need to be developed.

REFERENCES

Aaleti, S., S. Sritharan, D. Bierwagen, and B. Moore. (2011). Precast UHPC Waffle Bridge Deck Panels and Connections for Accelerated Bridge Construction. *PCI National Bridge Conference,* Salt Lake City, Utah.

Aaleti, S., S. Sritharan, M. Rouse, and T. Wipf. (2010). Structural Characterization of UHPC Waffle Deck Panels and Connections. Final Report. Ames, Iowa: Iowa State University – Institute for Transportation.

AbdelSalam, S.S., K.W. Ng, S. Sritharan, M.T. Suleiman, and M. Roling. (2012). Development of LRFD Procedures for Bridge Pile Foundations in Iowa – Volume III: Recommended Resistance Factors with Consideration of Construction Control and Setup. Final Report. Ames, IA: Iowa State University – Center for Transportation Research and Education.

Abendroth, R.E. and L.F. Greimann. (2005). Field Testing of Integral Abutments. Final Report. Iowa DOT Project HR-399. Ames, IA: Iowa State University – Center for Transportation Research and Education.

Abendroth, R.E., L.F. Greimann, and M.D. LaViolette. (2007). An Integral Abutment Bridge with Precast Concrete Piles. Final Report. Ames, IA: Iowa State University – Center for Transportation Research and Education.

American Association of State Highway and Transportation Officials (AASHTO). (2007). *AASHTO LRFD Bridge Design Specifications, 4th edition*.

American Association of State Highway and Tronsportation Officials (AASHTO). (2005). Grand Challenges: A Strategic Plan for Bridge Engineering. AASHTO SUbcommitte on Bridges and Structures, June.

American Concrete Institute (ACI). (2005). *Building Code Requirements for Structural Concrete (ACI 318-05).* ACI, Farmington Hills, Michigan.

American Petroleum Institute (1993). Recommended Practice on Planning, Designing, and Constructing Fixed Offshore Platforms – Load and Resistance Factor Design – 1st Edition. API RP 2A-LRFD.

Arsoy, S., R.M. Barker, and J.M. Duncan. (2002). Experimental and Analytical Investigations of Piles and Abutments of Integral Bridges. Final Report. Charlottesville, VA: Virginia Transportation Research Council.

Association Française de Génie Civil (AFGC). (2002). Ultra High Performance Fibre-Reinforced Concretes, Interim Recommendations. *AFGC Publication*, France.

Behloul, M. (2006). Ductal® PRestressed Girders for a Traffic Bridge in Mayenne, France. *7th International Conference on Short & Medium Span Bridges, Quebec, Canada.*

Behloul, M., R. Ricciotti, R.F. Ricciotti, P. Pallot, and J. Leboeuf. (2008). Ductal® Pont du Diable Footbridge, France. *Tailor Made Concrete Structures.* Walreven & Stoelhorst.

Blais, P.Y. and M. Couture. (1999). Precast, Prestressed Pedestrian Bridge – World's First Reactive Powder Concrete Structures. *PCI Journal*. pp 60-71.

Bonczar, C., S.F. Breña, S. Civjan, J. DeJong, B. Crellin, and D. Crovo. (2005). Field Data and FEM Modeling of the Orange-Wendell Bridge, FHWA Conference – Integral Abutment and Jointless Bridges, Baltimore, Maryland.

Brown, D.A., O'Neill, M.W., Hoit, N., McVay, M., El Naggar, M.H., and Chakraborty, S. (2001). Static and Dynamic Lateral Loading of Pile Groups, NCHRP Report 461, Transportation Research Board – National Research Council, Washington, DC, 60.

Bustamante, M. and Gianeselli, L. (1982). Pile Bearing Capacity Prediction by Means of Static Penetrometer CPT. *Proceedings of the Second European Symposium on Penetration testing, Amsterdam*, 493-500.

CDOT. (2009). CDOT Bridge Design Manual, Retrieved February 2012, from CDOT Bridge Manuals: http://www.coloradodot.info/library/bridge/bridge-manuals.

Chanvillard G. and S. Rigaud. (2003). Complete Characterization of Tensile Properties of Ductal® UHPFRC According to the French Recommendations. *Proceeding of the Fourth Internation RILEM Workshop, Ann Arbor, Michigan.* Pp 21-34.

Cheyrezy, M. and M. Behloul. (2001). Creek and Shrinkage of Ultra-High Performance Concrete. *Creep, Shrinkage and Durability Mechanisms of Concrete and other Quasi-Brittle materials – Proceddings of the Sixth International Conference CONCREEP-6@MIT*, Cambridge, MA, USA, 20-22 August. Ed. By Ulm, F.-J., Bažant, S.P., and F.H. Wittmann. Elsevier: 526-538.

Davisson, M.T. (1972). High Capacity Piles. *Proceedings,* Lecture Series, Innovations in Foundation Construction, ASCE, Illinois Section.

Decker, J.B., K.M. Rollins and J.C. Ellsworth. (2008). Corrosion Rate Evaluation and Prediction for Piles Based on Long-Term Field Performance. *Journal of Geotechnical and Geoenvironmental Engineering*, ASCE, Vol. 134, No. 3: 341-351.

Dicleli, M. and S.M. Albhaisi. (2003) Effect of Cyclic Thermal Loading on Performance of Steel H-Piles in Integral Bridges with Stub-Abutments. *Journal of Constructional Steel Research.* Vol. 60: 161-182.

DilMillio, A. (1998). A Quarter Centery of Geotechnical Research. FHWA-RD-98-139. March 2012. http://www.fhwa.dot.gove/engineering/geotech/pubs/century/index.cfm.

Dirks, K. and P. Kam. (2003). Foundation Soils Information Chart – Pile Foundation. Iowa Department of Transportation, Office of Road Design, Ames, Iowa.

Dugat, J., N. Roux, G. Bernier. (1996). Mechanical Properties of Reactive Powder Concretes. *Materials and Structures*, May, Vol. 29: 233-240.

Ductal. (2012). Structural. March 2012. < http://www.ductal-lafarge.com/wps/portal/ductal/2-Structural>.

Duncan, J.M. and S. Arsoy. (2003). Effect of Bridge-Soil Interactions on Behavior of Piles Supporting Integral Bridges, *TRB 2003 Annual Meeting*, Paper No. 03-2633, Washington, D.C.

Ehsani, M., M. Farahani, and E. Raatz. (2012). Repair of Columns with FRP Laminates. *Structure*®. March 2012. <http://www.structuremag.org/article.aspx?articleID=1379>.

Ensoft, Inc. (2004). LPILE Plus 5.0. Ensoft, Inc.

Federal Highway Administration (FHWA). (2011). Focus – Ultra High Performance Concrete: Taking Concrete to New Levels. March 2012. < www.fhwa.dot.gov/publications/focus/10jul/05.cfm>.

Freyermuth, C. (2009). Service Life and Sustainability of Concrete Bridges. *Aspire.*12-15.

Frosch, R.J., Wenning, M., Chovichien, V. (2005). The In-Service Behavior of Integral Abutment Bridges: Abutment Pile Response, FHWA Conference - Integral Abutment and Jointless Bridges, Baltimore, Maryland.

Garder, J., Aaleti, S., Sritharan, S., and Ng. K. (2013). Connection Details and Field Implementation of UHPC Piles. Final Report. Yet to be published. Ames, IA: Iowa State University – Center for Transportation Research and Education.

Girton, D.D., Hawkinson, T.R., and Greimann, L.F. (1991). Validation of Design Recommendations for Integral-Abutment Piles, *Journal of Structural Engineering*, ASCE, Vol. 117, No. 7, July 1991, pp. 2117-2134.

Gowripalan, N. and R.I. Gilbert. (2000). Design Guidelines for Ductal Prestressed Concrete Beams. *VSL (Aust) Pty Ltd*.

Graybeal, B. (2005). Characterization of the Behavior of Ultra-High Performance Concrete. pHD dissertation, University of Maryland.

Graybeal, B. (2007) Compressive Behavior of Ultra-High-Performance Fiber-Reinforced Concrete. *ACI Materials Journal*, pp 146-152.

Graybeal, B. (2009). Structural Behavior of a 2nd Generation UHPC Pi-Girder. FHWA-HRT-09-068. Federal Highway Administration. McLean, VA.

Green D., Ng, K.W., Dunker, K., and Sirtharan, S. (2012). Development of LRFD Design Procedures for Bridge Pile Foundations in Iowa – Design Guide and Track Examples. Final Report Vol. IV. *Institute for Transportation,* Iowa State University, Ames, IA.

GRL Engineers. (2001). Pile Driving Wave Equation Workshop – Course Notes. March 21, Iowa State University, Ames, Iowa.

Grünewald, S. (2004). Performance-Based Design of Self-Compacting Fibre Reinforced Concrete. Delft University Press, Delft, The Netherlands.

Hetényi, M. (1946). Beams on Elastic Foundation. University of Michigan Press, Ann Arbor, Michigan.

Hoffman, S. and H. Weiher. (2012). Innovative Design of Bridge Bearings by the use of UHPFRC. *Proceedings of the 3rd International Symposium on UHPC and Nanotechnology for High Performance Construction Materials, Kassel, Germany. March 7-9*: 973-980.

Hannigan, C.G, C.G. Goble, C.E. Likins, and F. Rausche. (2006). Design and Construction of Driven Piles Foundations – Volume I. Report No. FHWA-NHI-05-042. Washington: Federal Highway Administration (FHWA).

Hannigan, C.G, C.G. Goble, C.E. Likins, and F. Rausche. (2006). Design and Construction of Driven Piles Foundations – Volume II. Report No. FHWA-NHI-05-043. Washington: Federal Highway Administration (FHWA).

Hassiotis, S. (2007). Data Gathering and Design Details of an Integral Abutment Bridge. 18th Engineering Mechanics Division Conference of ASCE, Blacksburg,Virginia.

Huang, J., French, C., and Shield, C. (2004). Behavior of Concrete Integral Abutment Bridges. Final Report. Minneapolis, MN: University of Minnesota - Department of Civil Engineering.

Iowa DOT. (2011). Iowa LRFD Bridge Design Manual, Retrieved February 2012, from Iowa DOT Design Policies: www.iowadot.gov/bridge/manuallrfd.htm.

Iowa's Deficient Bridges – Strategies to Improve and Maintain the Condition of Iowa's Bridges. (2008)

Japan Society of Civil Engineers (JSCE). (2008). Recommendations for Design and Construction of High Performance Fiber Reinforced Cement Composites with Multiple Fine Cracks (HPFRCC). *Concrete Committee – Concrete Engineering Series 82, Japan.*

Jungwirth, J., and A. Muttoni. (2004). Structural Behavior of Tension Members in UHPC. École Polytechnique Fédérale de Lausanne, *IS-Benton.* April. http://ibeton.epfl.ch/Publications/2004/Jungwirth04b.pdf

Kamel, M.R., J.V. Benak, M.K. Tadros, and M. Jamshidi. (1996). Prestressed Concrete Piles in Jointless Bridges. *PCI Journal*, 56-67.

Kim, B.S., S. Kim, Y.J. Kim, S.Y. Park, K.T. Koh, and C. Joh. (2012). R&D Activities and Application of Ultra High Performance Concrete to Cable Stayed Bridges. *Proceedings of the 3rd International Symposium on UHPC and Nanotechnology for High Performance Construction Materials, Kassel, Germany. March 7-9*: 865-872.

Lunne, T., P.K. Robertson, and J.J.M. Powell. (1997). Cone Penetration Testing in Geotechnical Practice. Blackie Academic & Professional. London, UK.

Ma, J., and H. Schneider. (2002). Properties of Ultra-High-Performance Concrete. *Zeipzig Annual Civil Engineering Report (LACER),* no. 7: 25-32.

Ma, J., M. Orgass, F. Dehn, D. Schmit, and N.V. Tue. (2004). Comparative Investigations on Ultra-High Perforamnce Concrete with and without Coarse Aggregates. *Proceedings of the International Symposium on Ultra-High Performance Concrete, Kassel, Germany Sept. 13-15*: 205-212.

MaineDOT. (2003). MaineDOT Bridge Design Guide, Retrieved February 2012, from MaineDOT Bridge Design Guide: www.maine.gov/mdot/technical-publications/brdesignguide.php.

MassDOT. (2009). LRFD Bridge manual, Retrieved February 2012, from Mass DOT Bridge Downloads: www.mhd.state.ma.us/default.asp?pgid=bridge/bridgemanual_02&sid=about.

Matthias, D. and M. Cribbs. (1998). Driven 1.0: A Microsoft Windows Based Program for Determining Ultimate Vertical Static Pile Capacity (User's Manual). FHWA-SA-98-074, May.

McKenna, F., G.L. Fenves, F.C. Filippou, S. Mazzoni, M. Scott, B. Jeremic, A. Elgamal, P. Arduino, P. McKenzie, G.G. Deierlein, and K. Law. (2006). OpenSees 2.3.2. Available from <http://opensees.berkeley.edu/index.php>.

Measurand Shape Advantage. (2011). ShapeAccelArray (SAA) Installation Guide.

Menn, C. (1990). Prestressed Concrete Bridges. Germeny. Birkhäuser Verlag AG Basel.

Meyerhof, G.G. (1976). Bearing Capacity and Settlement of Pile Foundations. American Society of Civil Engineers, ASCE, *Journal of Soil Mechanics and Foundations Division*, Vol. 85, SM6, December, 1-29.

Minnesota DOT. (2011). LRFD Bridge Design Manual, Retrieved February 2012, from Minnesota DOT Bridge Manuals: www.dot.state.mn.us/bridge/manuals/.

Moser, R., B. Holland, L. Kahn, P. Singh, and K. Kurtis. (2011) Durability of Precast Prestressed Concrete Piles in Marine Environment: Reinforcement Corrosion and Mitigation Part 1. Final Report. Project No. 07-30. Georgia Department of Transportation.

Naaman, A.E and K. Wille. (2012). The Path to Ultra-High Performance Fiber Reinforced Concrete (UHP-FRC): Five Decades of Progress. *Proceedings of the 3rd International Symposium on UHPC and Nanotechnology for High Performance Construction Materials, Kassel, Germany. March 7-9*: 3-15.

Ng. K.W., M.T. Suleiman, M. Roling, S.S. AbdelSalam, and S. Sritharan. (2011). Development of LRFD Design Procedures for Bridge Piles in Iowa – Field Testing of Steel H-Piles in Clay, Sand, and Mixed Soils and Data Analysis (Volume II). Final Report. Ames, IA: Iowa State University – Center for Transportation Research and Education.

Nordlund, R.L. (1963). Bearing Capacity of Piles in Cohesionless Soils. American Socitety of Civil Engineers, ASCE, *Journal of the Soil Mechanics and Foundations Division*, SM3, 1-35.

Nottingham, L.C. (1975). Use of Quasi-Static Friction Cone Penetrometer to Predict Load Capacity of Displacement Piles. Ph.D. dissertation to the Department of Civil Engineering, University of Florida, 552.

NYSDOT. (2011). Bridge Manual – 1st Edition with Addendum #2, from NYSDOT Design Policies: www.dot.ny.gov/divisions/engineering/structures/manuals/bridge-manual-usc.

Oesterle R.G. and Lotfi, H.R. (2005). Transverse Movement in Skewed Integral Abutment Bridges, FHWA Conference - Integral Abutment and Jointless Bridges, Baltimore, Maryland.

OpenSees. (2006). The Open System for Earthquake Engineering Simulation. April 2012. http://opensees.berkeley.edu/OpenSees/home/about.php.

Ozyildirim, C. (2011). Evaluation of Ultra-High-Performance Fiber-Reinforced Concrete. Final Report. Charlottesville, VA: Virginia Center for Transportation Innovation & Research.

Perry, V.H. and P.J Seibert. (2011). Working with Ductal Ultra-High Performance Concrete. *Concrete Plant International, North America Edition, February 2011*.

Pile Dynamics, Inc (PDI). (2005). *GRLWEAP – Wave Equation Analysis of Pile Driving, Procedures and Models*, Cleveland, OH.

Pile Dynamics, Inc (PDI). (2000). CAPWAP for Windows Manual. Cleveland, Ohio: Pile Dynamics, Inc.

Portland Cement Association (PCA). (2012). Ultra High-Performance Concrete Case Study. March 2012. < http://www.cement.org/bridges/br_case_jakway.asp>.

Precast/Prestressed Concrete Institute (PCI). (2010). *PCI Design Handbook: Precast and Prestressed Concrete*, Seventh Edition, PCI, Chicago, IL.

Randl, N., A. Pichler, W. Schneider, and J. Juhart. (2012). Study on the Application of UHPC for Precast Tunnel Segments. *Proceedings of the 3rd International Symposium on UHPC and Nanotechnology for High Performance Construction Materials, Kassel, Germany. March 7-9*: 981-988.

Reese, L.C., Wang, S.T., Isenhower, W.M., and Arréllaga, J.A. (2004). Computer Program LPILE Plus Version 5.0 Technical Manual: A Program for the Analysis of Piles and Drilled Shafts Under lateral Loads. Ensoft, Inc., Austin, Texas.

Reese, L.C., Cox W.R., and Koop F.D. (1974). Analysis of Laterally Loaded Piles in Sand, Offshore Technical Conference, Dallas, Texas, Paper No. OTC 2080

Reese, L.C. and H. Matlock. (1956). Non-dimensional Solutions for Laterally Loaded Piles with Soil Modulus Proportional to Depth. *Proceedings from the 8th Texas Conference on Soil Mechanics and Foundation Engineering.*, Austin, Texas.

Resplendino, J. (2012). State of the Art of Design and Construction of UHPFRC Structures in France. *Proceedings of the 3rd International Symposium on UHPC and Nanotechnology for High Performance Construction Materials, Kassel, Germany. March 7-9*: 27-41.

Rhode Island DOT. (2007). Rhode Island LRFD Bridge Design Manual, Retrieved February 2012, from Rhode Island Government: http://www.ri.gov/search/?q=bridge+design+manual

Richard, P., and Cheyrezy, M. (1995). Composition of Reactive Powder Concretes. *Cement and Concrete Research*, Oct., Vol. 25, No. 7: 1501-1511.

Romanoff, M. (1962). Corrosion of Steel Pilings in Soils. *NBS Monograph No. 58*, National Bureau of Standards, U.S> Department of Commerce, Washington, D.C.

RS Means – Heavy Construction Cost Data. (2009). Kinston, MA: Construction and Consultants. Print.

Scheydt, J.C. and H.S. Müller. (2012). Microstructure of Ultra High Performance Concrete (UHPC) and its Impact on Durability. *3rd International Symposium on UHPC and Nanotechnology for High Performance Construction Materials, Kassel, Germany, March 7-9*: 349-356.

Smith, E.A. (1960). Pile-Driving Analysis by the Wave Equation. *Journal of the Soil Mechanics and Foundations Division, Proceedings from the American Society of Civil Engineers.* pp. 35-61.

Sritharan, S., B. Bristow, and V. Perry. (2003). Characterizing an Ultra-High Performance Material for Bridge Applications under Extreme Loads. *Proceedings of the 3rd International Symposium on High Performance Concrete,* Orlando, Florida.

Sritharan, S., S. Aaleti, D. Bierwagen, J. Garder, and A. Abu-Hawash. (2012). Current Research on Ultra High Performance Concrete (UHPC) for Bridge Applications in Iowa. *Proceedings of the 3rd International Symposium on UHPC and Nanotechnology for High Performance Construction Materials, Kassel, Germany, March 7-9*: 857-864.

Standard Test Methods for Deep Foundations under Lateral Loads. (2007). ASTM D 3966-07, in *Annual Book of ASTM Standards,* vol. 04.08.

Standard Test Methods for Deep Foundations Under Static Axial Compressive Load. (2007). ASTM D1143/D1143M-07, in *Annual Book of ASTM Standards,* vol 04.08.

Tang, M.C. (2004). High Performance Concrete – Past, Present, and Future. Ultra High Performance Concrete (UHPC). *Proceedings of the International Symposium on Ultra High Performance Concrete, Kassel, Germany, Sept. 13-15*: 3-9.

Tomlinson, M.J. (1994). Pile Design and Construction Practice. Fourth Edition, Pitman Advanced Publishing Program.

Vande Voort, T.L., M.T. Suleiman, and S. Sritharan. (2008). Design and Performance Verification of UHPC Piles for Deep Foundations. Final Report. Ames, IA: Iowa State University – Center for Transportation Research and Education.

VTrans. (2008). Integral Abutment Bridge Design Guidelines, Retrieved February 2012, from VTrans Structures Section: www.aot.state.vt.us/progdev/sections/structures62011.htm.

Walraven J.C. (2002). From Design of Structures to Design of Materials. Innovations and Developments in Concrete Materials and Construction. *Proceedings of the International Conference Held at the University of Dundee, Scotland, UK on 9-11 Sept. London:* 805-818.

Wang, S.T. and Reese, L.C. (1993). COM624P-Laterally Loaded Pile Analysis Program for Microcomputer, Version 2.0, US Department of Transportation, FHWA-SA-91-048.

Wipf, T.J., B.M. Phares, S. Sritharan, B.E. Degen, and M.T. Giesmann. (2009). Design and Evaluation of Single-span Bridge Using Ultra-High Performance Concrete. Final

Report. Ames, IA: Iowa State University – Center for Transportation Research and Education.

Wong, I.H. and K.H. Law. (1999). Corrosion of Steel H Piles in Decomposed Granite. *Journal of Geothechnical and Geoenvironmental Engineering.* Vol. 126. No. 6: 529-532.

Young, W.F., J. Boparai, V. Perry, B.I. Archibald, and S. Salib. (2012). Whiteman Chreek Bridge – A Synthesis of Ultra High Performance Concrete and Fiber Reinforced Polymers for Accelerated Bridge Construction. *Proceedings of the 3rd International Symposium on UHPC and Nanotechnology for High Performance Construction Materials, Kassel, Germany, March 7-9*: 849-856.

APPENDIX A

Opensees script used to calculate the moment-curvature response of steel HP x 57 piles in strong-axis and weak-axis bending for various axial loads.

```
### UHPC PILE PROJECT_PHASE 2
### ----------
##--------- Written by Sriram Aaleti date: 26th August 2010 ----------
#----------
wipe;

##---------- Simulation Parameters----------
set specimen HP10by57;
set orientation weakaxis; # other option is weakaxis/strongaxis
##set orientation strongaxis; # other option is weakaxis/strongaxis
#### CHANGE ORIENTATION TO STRONGAXIS OR WEAKAXIS FOR ANALYSIS IN BOTH DIRECTIONS

#---------- unit definition----------
set in 1.; # define basic units
set sec 1.; # define basic units
set kip 1.; # define basic units
set ft [expr 12.*$in]; # define engineering units
set ksi [expr $kip/pow($in,2)];
set psi [expr $ksi*1000.];
set in2 [expr $in*$in]; # inch^2
set in4 [expr $in*$in*$in*$in]; # inch^4
set PI [expr 2*asin(1.0)]; # define constants
set g [expr 32.2*$ft/pow($sec,2)]; # gravitational acceleration
set Ubig 1.e10; # a really large number
set Usmall [expr 1/$Ubig]; # a really small number
set cm [expr $in/2.54]; # SI centimeter unit
# --------- end of unit definition ----------

##################----------
# ## ---------- Defining the procedures for the cross section (steel pile) ----------
#################----------

# input parameters
# secID - section ID number
# matID - material ID number
# d = nominal depth
# tw = web thickness
# bf = flange width
# tf = flange thickness
# nfdw = number of fibers along web depth
# nftw = number of fibers along web thickness
# nfbf = number of fibers along flange width
# nftf = number of fibers along flange thickness

####----------Weak axis bending definition----------
proc Wsection_weak {secID matID d tw bf tf nfdw nftw nfbf nftf} {
set dw [expr $d - 2 * $tf]
set z1 [expr -$d/2]
set z2 [expr -$dw/2]
set z3 [expr $dw/2]
set z4 [expr $d/2]
set y1 [expr $bf/2]
```

```
set y2 [expr $tw/2]
set y3 [expr -$tw/2]
set y4 [expr -$bf/2]
#
section Fiber $secID {
patch quad $matID $nftf $nfbf $y1 $z3 $y1 $z4 $y4 $z4 $y4 $z3
patch quad $matID $nfdw $nftw $y2 $z2 $y2 $z3 $y3 $z3 $y3 $z2
patch quad $matID $nftf $nfbf $y1 $z1 $y1 $z2 $y4 $z2 $y4 $z1

# # # patch quad $matID $nfbf $nftf $y1 $z3 $y4 $z3 $y4 $z4 $y1 $z4
# # # patch quad $matID $nftw $nfdw $y2 $z2 $y3 $z2 $y3 $z3 $y2 $z3
# # # patch quad $matID $nfbf $nftf $y1 $z1 $y4 $z1 $y4 $z2 $y1 $z2
}
}

####----------Strong axis bending definition----------
proc Wsection_strong {secID matID d tw bf tf nfdw nftw nfbf nftf} {
set dw [expr $d - 2 * $tf]
set y1 [expr -$d/2]
set y2 [expr -$dw/2]
set y3 [expr $dw/2]
set y4 [expr $d/2]
set z1 [expr -$bf/2]
set z2 [expr -$tw/2]
set z3 [expr $tw/2]
set z4 [expr $bf/2]
#
section Fiber $secID {
patch quad $matID $nftf $nfbf $y1 $z1 $y2 $z1 $y2 $z4 $y1 $z4
patch quad $matID $nfdw $nftw $y2 $z2 $y3 $z2 $y3 $z3 $y2 $z3
patch quad $matID $nftf $nfbf $y3 $z1 $y4 $z1 $y4 $z4 $y3 $z4

# # # # patch quad $matID $nfbf $nftf $y1 $z1 $y1 $z4 $y2 $z4 $y2 $z1
# # # # patch quad $matID $nftw $nfdw $y2 $z2 $y2 $z3 $y3 $z3 $y3 $z2
# # # # patch quad $matID $nfbf $nftf $y3 $z1 $y3 $z4 $y4 $z4 $y4 $z1
}
}

####----------

set ndm 2; # 2-D problem
set ndf 3;
model basic -ndm $ndm -ndf $ndf
logFile screendump.dat

########----------
###---------- defining the dimensions of the section HP 10x57 ----------
########----------

set tflange [expr 0.57*$in]; #flange thickness
set tweb [expr 0.57*$in]; # web thickness
set bflange [expr 10.2*$in];#flange width
set dpile [expr 9.99*$in];#depth of the section
```

```
######## ----------------------------------------------------------------------------------------------------------
## ---------------------------------- Defining the material properties ----------------------------------------------
######## ----------------------------------------------------------------------------------------------------------
set Grade50 1
set Fy [expr 50.*$ksi];
set Es [expr 29000.*$ksi];
set bratio 0.004;
uniaxialMaterial Steel01 $Grade50 $Fy $Es $bratio
##uniaxialMaterial Steel02 $Grade50 $Fy $Es $bratio 15 0.925 0.15 0 5 0 5;

## Defining the nodes
node 1 0 0
node 2 0 0

## boundary conditions
fix 1 1 1 1
fix 2 0 1 0

######----------------------------------------------------------------------------------------------------------########
######-------------------------DEFINING THE FIBER SECTION-----------------------------------------------######
----------------------------------------------------------------------------------------------------------------------

set HP_10b57 1;
 if {$orientation == "strongaxis"} {
            puts " Strong axis cross section in section defination"
            Wsection_strong 1 1 $dpile $tweb $bflange $tflange 80 8 24 8
}

 if {$orientation == "weakaxis"} {
            puts " Weak axis cross section in section defination"
            Wsection_weak 1 1 $dpile $tweb $bflange $tflange 15 8 80 8
}
#################### ----------------------------------------------------------------------------------------------

geomTransf PDelta 1;
# Define element
element zeroLengthSection 1 1 2 1;

#######----------------------------------------------------------------------------------------------------------------#####
###--------------------------------- Create recorder ----------------------------------------------------------------
###############----------OUTPUT DATA ------------------------------------------------------------------------------

set kword $orientation;
recorder Node -file momcurv_$kword.out -time -node 2 -dof 3 disp

if {$orientation == "strongaxis"} {
puts " recoreders for stronf axis bending"
recorder Element -file flangeComp_$kword.out -time -ele 1 section fiber [expr 0.5*$dpile] 0 $Grade50 stressStrain;##strain in the compression flange
recorder Element -file flangeTension_$kword.out -time -ele 1 section fiber -[expr 0.5*$dpile] 0 $Grade50 stressStrain;##strain in the tension flange
```

```
}

if {$orientation == "weakaxis"} {
puts "recorder for weak axis bending"
recorder Element -file flangeComp_$kword.out -time -ele 1 section fiber [expr 0.5*$bflange] [expr 0.5*$dpile] $Grade50 stressStrain;##strain in the compression flange
recorder Element -file flangeTension_$kword.out -time -ele 1 section fiber -[expr 0.5*$bflange] [expr 0.5*$dpile] $Grade50 stressStrain;##strain in the tension flange
}

#######-------------------------------------------------------------------------------------------------------------------------------------##
#####-------------------------------------------------------------------------------------------------------------------------------------
# Define constant axial load
set P 300; ##p is the axial load
pattern Plain 1 "Constant" {
 load 2 $P 0.0 0.0
 }
# Define analysis parameters
integrator LoadControl 0 1 0 0
set tolerence 1.0e-8;
set nItr 1000;
system SparseGeneral -piv
test NormDispIncr $tolerence $nItr 1
##test NormUnbalance $tolerence $nItr 1
numberer Plain
constraints Plain
algorithm KrylovNewton
analysis Static

analyze 1

### Define reference load
pattern Plain 2 "Linear" {
 load 2 0.0 0.0 1.0
}

# Maximum curvature from Anndrianna
set maxK 0.15246063
set numIncr 800
set dK [expr $maxK/$numIncr]

# Use displacement control at node 2 for section analysis
integrator DisplacementControl 2 3 $dK

# Perform the section analysis
analyze $numIncr
```

APPENDIX B

The maximum moment and shear predicted along the length of a pile and the second maximum moment and shear along the length of the same pile are given with their corresponding locations.

Table B-1: Maximum Moment and Maximum Shear for Trials 1a through 64a

Parameters: (1) HP 10 x 57; (2) Weak-Axis Bending; (3) 1.00-in. of Lateral Displacement; and (4) No Prebore Hole				
Axial Load, kips	Soil Type	Pile Head Boundary Condition	Maximum Moment, kip-in	Maximum Shear, kips
0	Loose Sand	Fixed	1215.9	27.7
		Pinned	491.5	11.7
	Dense Sand	Fixed	1579.3	45.8
		Pinned	726.6	20.4
	Soft Clay	Fixed	768.2	14.2
		Pinned	303.0	6.9
	Very Firm Glacial Clay	Fixed	1902.5	80.3
		Pinned	973.4	44.9
100	Loose Sand	Fixed	1211.0	26.8
		Pinned	502.8	10.6
	Dense Sand	Fixed	1569.7	44.5
		Pinned	736.0	19.0
	Soft Clay	Fixed	767.3	13.6
		Pinned	317.8	6.1
	Very Firm Glacial Clay	Fixed	1889.6	78.8
		Pinned	984.0	43.2
200	Loose Sand	Fixed	1201.4	25.8
		Pinned	514.8	9.5
	Dense Sand	Fixed	1548.0	43.1
		Pinned	744.4	17.6
	Soft Clay	Fixed	766.0	13.0
		Pinned	333.3	5.2
	Very Firm Glacial Clay	Fixed	1860.1	77.1
		Pinned	989.8	41.3
300	Loose Sand	Fixed	1186.3	24.7
		Pinned	527.3	8.4
	Dense Sand	Fixed	1513.3	41.4
		Pinned	751.6	16.2
	Soft Clay	Fixed	764.8	12.3
		Pinned	349.4	4.3
	Very Firm Glacial Clay	Fixed	1815.0	75.0
		Pinned	993.5	39.4

Table B-2: Maximum Moment and Maximum Shear for Trials 65a through 128a

Parameters: (1) HP 10 x 57; (2) Weak-Axis Bending; (3) 1.55-in. of Lateral Displacement; and (4) No Prebore Hole				
Axial Load, kips	Soil Type	Pile Head Boundary Condition	Maximum Moment, kip-in	Maximum Shear, kips
0	Loose Sand	Fixed	1515.5	33.7
		Pinned	700.5	15.1
	Dense Sand	Fixed	1772.4	52.2
		Pinned	965.7	25.1
	Soft Clay	Fixed	997.0	17.6
		Pinned	410.6	8.8
	Very Firm Glacial Clay	Fixed	2000.4	89.7
		Pinned	1199.3	52.9
100	Loose Sand	Fixed	1505.7	32.2
		Pinned	715.8	13.4
	Dense Sand	Fixed	1758.3	50.3
		Pinned	978.7	23.0
	Soft Clay	Fixed	995.5	16.7
		Pinned	433.7	7.6
	Very Firm Glacial Clay	Fixed	1988.1	87.5
		Pinned	1215.6	50.3
200	Loose Sand	Fixed	1484.9	30.7
		Pinned	730.2	11.7
	Dense Sand	Fixed	1731.3	48.1
		Pinned	987.9	20.8
	Soft Clay	Fixed	991.7	15.8
		Pinned	457.9	6.3
	Very Firm Glacial Clay	Fixed	1966.4	85.1
		Pinned	1227.1	47.5
300	Loose Sand	Fixed	1452.3	28.9
		Pinned	743.9	9.9
	Dense Sand	Fixed	1691.1	45.7
		Pinned	993.1	18.4
	Soft Clay	Fixed	984.6	14.8
		Pinned	483.2	5.0
	Very Firm Glacial Clay	Fixed	1934.0	82.4
		Pinned	1227.8	44.4

Table B-3: Maximum Moment and Maximum Shear for Trials 129a through 192a

Parameters: (1) HP 10 x 57; (2) Strong-Axis Bending; (3) 1.00-in. of Lateral Displacement; and (4) No Prebore Hole				
Axial Load, kips	Soil Type	Pile Head Boundary Condition	Maximum Moment, kip-in	Maximum Shear, kips
0	Loose Sand	Fixed	2490.7	45.4
		Pinned	953.0	18.6
	Dense Sand	Fixed	3240.9	76.4
		Pinned	1496.1	33.6
	Soft Clay	Fixed	1376.5	19.7
		Pinned	533.9	9.7
	Very Firm Glacial Clay	Fixed	3663.7	115.7
		Pinned	1862.0	64.0
100	Loose Sand	Fixed	2507.0	44.8
		Pinned	963.6	17.7
	Dense Sand	Fixed	3301.6	76.2
		Pinned	1506.6	32.5
	Soft Clay	Fixed	1385.3	19.2
		Pinned	566.9	9.1
	Very Firm Glacial Clay	Fixed	3728.1	115.5
		Pinned	1877.3	62.8
200	Loose Sand	Fixed	2478.2	43.8
		Pinned	974.4	16.8
	Dense Sand	Fixed	3216.4	74.3
		Pinned	1517.3	31.4
	Soft Clay	Fixed	1375.9	18.8
		Pinned	563.3	8.4
	Very Firm Glacial Clay	Fixed	3502.6	111.8
		Pinned	1885.4	61.5
300	Loose Sand	Fixed	2356.2	41.9
		Pinned	985.7	15.8
	Dense Sand	Fixed	2830.9	68.7
		Pinned	1528.1	30.3
	Soft Clay	Fixed	1376.0	18.3
		Pinned	579.3	7.7
	Very Firm Glacial Clay	Fixed	3083.7	105.5
		Pinned	1870.6	59.6

Table B-4: Maximum Moment and Maximum Shear for Trials 193a through 256a

Parameters: (1) HP 10 x 57; (2) Stong-Axis Bending; (3) 1.55-in. of Lateral Displacement; and (4) No Prebore Hole				
Axial Load, kips	Soil Type	Pile Head Boundary Condition	Maximum Moment, kip-in	Maximum Shear, kips
0	Loose Sand	Fixed	3095.9	55.7
		Pinned	1395.0	24.5
	Dense Sand	Fixed	3802.9	89.8
		Pinned	2041.1	42.3
	Soft Clay	Fixed	1842.6	24.8
		Pinned	720.2	12.2
	Very Firm Glacial Clay	Fixed	4072.1	132.0
		Pinned	2322.6	75.9
100	Loose Sand	Fixed	3144.6	55.0
		Pinned	1411.7	23.1
	Dense Sand	Fixed	3730.1	87.7
		Pinned	2060.8	40.7
	Soft Clay	Fixed	1825.3	23.4
		Pinned	754.9	11.1
	Very Firm Glacial Clay	Fixed	3980.4	129.6
		Pinned	2354.5	74.3
200	Loose Sand	Fixed	3076.9	53.3
		Pinned	1429.6	21.8
	Dense Sand	Fixed	3435.9	82.7
		Pinned	2063.0	38.8
	Soft Clay	Fixed	1842.2	23.5
		Pinned	766.4	10.3
	Very Firm Glacial Clay	Fixed	3701.6	124.6
		Pinned	2350.3	72.0
300	Loose Sand	Fixed	2718.7	48.8
		Pinned	1448.1	20.4
	Dense Sand	Fixed	2985.3	75.3
		Pinned	2010.2	36.0
	Soft Clay	Fixed	1832.9	22.7
		Pinned	790.8	9.3
	Very Firm Glacial Clay	Fixed	3240.8	116.3
		Pinned	2241.0	67.5

Table B-5: Maximum Moment and Maximum Shear for Trials 1b through 64b

Parameters: (1) UHPC; (2) Weak-Axis Bending; (3) 1.00-in. of Lateral Displacement; and (4) No Prebore Hole				
Axial Load, kips	Soil Type	Pile Head Boundary Condition	Maximum Moment, kip-in	Maximum Shear, kips
0	Loose Sand	Fixed	1140.8	26.6
		Pinned	475.5	11.4
	Dense Sand	Fixed	1418.8	42.9
		Pinned	690.3	19.7
	Soft Clay	Fixed	738.0	13.9
		Pinned	294.8	6.8
	Very Firm Glacial Clay	Fixed	1575.2	74.2
		Pinned	919.1	43.5
100	Loose Sand	Fixed	1212.5	26.6
		Pinned	488.1	10.4
	Dense Sand	Fixed	1509	43.5
		Pinned	728.2	18.9
	Soft Clay	Fixed	757.3	13.4
		Pinned	309.4	6.0
	Very Firm Glacial Clay	Fixed	1526.9	72.9
		Pinned	986.6	43.3
200	Loose Sand	Fixed	1258.6	26.3
		Pinned	500.1	9.2
	Dense Sand	Fixed	1530.8	42.9
		Pinned	749.1	17.7
	Soft Clay	Fixed	762.1	12.9
		Pinned	324.5	5.1
	Very Firm Glacial Clay	Fixed	1430.7	70.5
		Pinned	1034.8	42.5
300	Loose Sand	Fixed	1279.9	25.7
		Pinned	512.6	8.1
	Dense Sand	Fixed	1448.4	40.6
		Pinned	762.4	16.4
	Soft Clay	Fixed	761.9	12.2
		Pinned	340.3	4.2
	Very Firm Glacial Clay	Fixed	1416.5	69.2
		Pinned	1065.9	41.4

Table B-6: Maximum Moment and Maximum Shear for Trials 65b through 128b

Parameters: (1) UHPC; (2) Weak-Axis Bending; (3) 1.55-in. of Lateral Displacement; and (4) No Prebore Hole				
Axial Load, kips	Soil Type	Pile Head Boundary Condition	Maximum Moment, kip-in	Maximum Shear, kips
0	Loose Sand	Fixed	1359.2	31.6
		Pinned	668.6	14.6
	Dense Sand	Fixed	1247.4	44.1
		Pinned	907.7	24.0
	Soft Clay	Fixed	947.0	17.2
		Pinned	400.0	8.7
	Very Firm Glacial Clay	Fixed	1440.7	79.5
		Pinned	1123.6	51.0
100	Loose Sand	Fixed	1438.8	31.4
		Pinned	706.8	13.3
	Dense Sand	Fixed	1270.4	43.6
		Pinned	976.4	23.1
	Soft Clay	Fixed	991.1	16.6
		Pinned	423.0	7.4
	Very Firm Glacial Clay	Fixed	1466.5	79.2
		Pinned	1093.8	46.7
200	Loose Sand	Fixed	1442.8	30.1
		Pinned	731.1	11.7
	Dense Sand	Fixed	1280.9	42.6
		Pinned	1037.4	21.8
	Soft Clay	Fixed	1015.6	15.9
		Pinned	446.3	6.2
	Very Firm Glacial Clay	Fixed	1478.7	78.2
		Pinned	1020.0	41.3
300	Loose Sand	Fixed	1169.4	25.6
		Pinned	750.3	10.0
	Dense Sand	Fixed	1264.9	40.9
		Pinned	1075.1	20.1
	Soft Clay	Fixed	1026.8	15.1
		Pinned	471.7	4.8
	Very Firm Glacial Clay	Fixed	1447.8	73.6
		Pinned	1010.4	36.9

Table B-7: Maximum Moment and Maximum Shear for Trials 129b through 192b

Parameters: (1) UHPC; (2) Strong-Axis Bending; (3) 1.00-in. of Lateral Displacement; and (4) No Prebore Hole				
Axial Load, kips	Soil Type	Pile Head Boundary Condition	Maximum Moment, kip-in	Maximum Shear, kips
0	Loose Sand	Fixed	1767.6	36.4
		Pinned	761.2	15.9
	Dense Sand	Fixed	2080.4	57.8
		Pinned	1135.0	27.8
	Soft Clay	Fixed	1119.7	17.6
		Pinned	440.1	8.6
	Very Firm Glacial Clay	Fixed	2329.7	93.1
		Pinned	1400.3	54.7
100	Loose Sand	Fixed	2003.9	38.3
		Pinned	798.7	15.3
	Dense Sand	Fixed	2434.8	62.4
		Pinned	1226.4	28.0
	Soft Clay	Fixed	1169.0	17.5
		Pinned	467.7	8.1
	Very Firm Glacial Clay	Fixed	2677.4	98.4
		Pinned	1566.8	56.7
200	Loose Sand	Fixed	2141.8	39.0
		Pinned	809.7	14.3
	Dense Sand	Fixed	2702.8	64.9
		Pinned	1243.3	26.9
	Soft Clay	Fixed	1168.9	17.0
		Pinned	482.6	7.4
	Very Firm Glacial Clay	Fixed	2978.7	101.6
		Pinned	1624.2	56.3
300	Loose Sand	Fixed	2205.1	39.0
		Pinned	820.9	13.3
	Dense Sand	Fixed	2856.4	65.9
		Pinned	1254.8	25.7
	Soft Clay	Fixed	1168.6	16.5
		Pinned	499.0	6.6
	Very Firm Glacial Clay	Fixed	29327	100
		Pinned	1645.8	55.2

Table B-8: Maximum Moment and Maximum Shear for Trials 193b through 256b

Parameters: (1) UHPC; (2) Strong-Axis Bending; (3) 1.55-in. of Lateral Displacement; and (4) No Prebore Hole				
Axial Load, kips	Soil Type	Pile Head Boundary Condition	Maximum Moment, kip-in	Maximum Shear, kips
0	Loose Sand	Fixed	2000.2	42.5
		Pinned	1083.1	20.4
	Dense Sand	Fixed	2205.0	64.1
		Pinned	1452.8	33.3
	Soft Clay	Fixed	1434.1	21.7
		Pinned	594.4	10.9
	Very Firm Glacial Clay	Fixed	2434.6	103.3
		Pinned	1661.7	63.2
100	Loose Sand	Fixed	2339.4	45.2
		Pinned	116.3	19.9
	Dense Sand	Fixed	2513.5	68.9
		Pinned	1670.2	34.7
	Soft Clay	Fixed	1557.5	21.9
		Pinned	635.1	10.1
	Very Firm Glacial Clay	Fixed	2722.6	108.6
		Pinned	1916.7	65.8
200	Loose Sand	Fixed	2593.9	46.6
		Pinned	1185.7	18.5
	Dense Sand	Fixed	2815.1	72.1
		Pinned	1770.2	34.3
	Soft Clay	Fixed	1577.2	21.3
		Pinned	659.0	9.1
	Very Firm Glacial Clay	Fixed	2973.1	111.8
		Pinned	2073.0	66.6
300	Loose Sand	Fixed	2735.0	46.9
		Pinned	1202.8	17.1
	Dense Sand	Fixed	2774.5	70.5
		Pinned	1812.0	33.0
	Soft Clay	Fixed	1577.8	20.5
		Pinned	684.1	8.0
	Very Firm Glacial Clay	Fixed	3001.5	111.1
		Pinned	2169.5	66.2

Table B-9: Maximum Moment and Maximum Shear for Trials 257 through 264

Parameters: (1) Weak-Axis Bending; (2) 1.00-in. of Lateral Displacement; (3) Fixed Pile Head; and (4) 10-ft Prebore Hole				
Pile Type	Axial Load, kips	Soil Type	Maximum Moment, kip-in	Maximum Shear, kips
UHPC	100	Soft Clay	363.6	3.1
		Very Stiff Clay	686.9	13.2
	200	Soft Clay	358.2	2.9
		Very Stiff Clay	682.7	13.3
HP10x57	100	Soft Clay	377.6	3.2
		Very Stiff Clay	705.6	13.5
	200	Soft Clay	371.9	2.9
		Very Stiff Clay	698.1	13.7

Table B-10: Maximum Moment and Maximum Shear for Trials 265 through 272

Parameters: (1) Weak-Axis Bending; (2) 1.55-in. of Lateral Displacement; (3) Fixed Pile Head; and (4) 10-ft Prebore Hole				
Pile Type	Axial Load, kips	Soil Type	Maximum Moment, kip-in	Maximum Shear, kips
UHPC	100	Soft Clay	520.2	4.3
		Very Stiff Clay	956.8	17.1
	200	Soft Clay	511.9	3.8
		Very Stiff Clay	979.2	10.7
HP10x57	100	Soft Clay	539.6	4.4
		Very Stiff Clay	963.7	17.3
	200	Soft Clay	531.5	3.9
		Very Stiff Clay	950.8	17.5

Table B-11: Depth to 2nd Maximum Bending Moment and Shear Forces and Depth of Fixity for Trials 1a through 64a

Parameters: (1) HP 10 x 57 Pile; (2) Weak-Axis Bending; (3) 1.00-in of Lateral Displacement; and (4) No Prebore Hole					
Axial Load, kips	Boundary Condition	Soil Type	Location from GS of 2nd Maximum, ft		Depth of Fixity, ft
			Bending Moment	Shear	
0	Pinned	Loose Sand	17.0	9.0	17.5
		Dense Sand	12.5	7.5	12.0
		Soft Clay	20.0	11.5	19.5
		Very Stiff Clay	9.5	6.0	9.0
	Fixed	Loose Sand	7.5	11.0	19.0
		Dense Sand	6.5	8.5	13.5
		Soft Clay	11.0	15.5	22.5
		Very Stiff Clay	5.5	8.0	10.0
100	Pinned	Loose Sand	16.5	8.5	17.5
		Dense Sand	12.5	7.5	12.0
		Soft Clay	20.0	11.0	19.5
		Very Stiff Clay	9.5	6.0	9.0
	Fixed	Loose Sand	7.5	10.5	19.0
		Dense Sand	6.5	8.5	13.5
		Soft Clay	11.0	15.5	22.5
		Very Stiff Clay	5.5	8.0	10.0
200	Pinned	Loose Sand	16.5	8.5	17.5
		Dense Sand	12.0	7.5	12.0
		Soft Clay	19.5	10.5	19.5
		Very Stiff Clay	9.5	6.0	9.0
	Fixed	Loose Sand	7.5	10.5	19.0
		Dense Sand	6.5	8.5	13.5
		Soft Clay	11.0	15.0	23.0
		Very Stiff Clay	5.5	7.5	10.0
300	Pinned	Loose Sand	16.5	8.0	17.0
		Dense Sand	12.0	7.0	12.0
		Soft Clay	19.5	10.0	20.0
		Very Stiff Clay	9.5	6.0	9.0
	Fixed	Loose Sand	7.5	10.5	19.0
		Dense Sand	6.0	8.5	13.0
		Soft Clay	11.0	14.5	23.0
		Very Stiff Clay	5.5	7.5	10.0

Table B12: Depth to 2nd Maximum Bending Moment and Shear Forces and Depth of Fixity for Trials 65a through 128a

Parameters: (1) HP 10 x 57 Pile; (2) Weak-Axis Bending; (3) 1.55-in of Lateral Displacement; and (4) No Prebore Hole					
Axial Load, kips	Boundary Condition	Soil Type	Location from GS of 2nd Maximum, ft		Depth of Fixity, ft
			Bending Moment	Shear	
0	Pinned	Loose Sand	17.0	9.0	18.0
		Dense Sand	12.5	7.5	12.5
		Soft Clay	21.5	12.5	21.5
		Very Stiff Clay	10.0	6.5	9.5
	Fixed	Loose Sand	8.0	11.0	19.5
		Dense Sand	6.5	9.0	13.5
		Soft Clay	12.0	16.5	25.0
		Very Stiff Clay	5.5	8.0	11.0
100	Pinned	Loose Sand	17.0	9.0	18.0
		Dense Sand	12.5	7.5	12.5
		Soft Clay	21.5	11.5	21.5
		Very Stiff Clay	10.0	6.5	9.5
	Fixed	Loose Sand	8.0	11.0	19.5
		Dense Sand	6.5	8.5	13.5
		Soft Clay	11.5	16.5	25.0
		Very Stiff Clay	5.5	8.0	10.5
200	Pinned	Loose Sand	16.5	8.5	18.0
		Dense Sand	12.5	7.5	12.5
		Soft Clay	21.0	11.0	22.0
		Very Stiff Clay	10.0	6.0	9.5
	Fixed	Loose Sand	7.5	10.5	19.5
		Dense Sand	6.5	8.5	13.5
		Soft Clay	11.5	16.0	25.0
		Very Stiff Clay	5.5	8.0	10.5
300	Pinned	Loose Sand	16.5	8.5	18.0
		Dense Sand	12.0	7.0	12.5
		Soft Clay	21.0	10.5	22.0
		Very Stiff Clay	10.0	6.0	9.5
	Fixed	Loose Sand	7.5	10.5	19.5
		Dense Sand	6.0	8.5	13.5
		Soft Clay	11.5	15.5	25.0
		Very Stiff Clay	5.5	7.5	10.5

Table B-13: Depth to 2nd Maximum Bending Moment and Shear Forces and Depth of Fixity for Trials 129a through 192a

Parameters: (1) HP 10 x 57 Pile; (2) Strong-Axis Bending; (3) 1.00-in of Lateral Displacement; and (4) No Prebore Hole					
Axial Load, kips	Boundary Condition	Soil Type	Location from GS of 2nd Maximum, ft		Depth of Fixity, ft
			Bending Moment	Shear	
0	Pinned	Loose Sand	20.5	11.0	21.5
		Dense Sand	15.0	9.0	15.0
		Soft Clay	26.0	14.5	25.5
		Very Stiff Clay	12.5	8.0	11.5
	Fixed	Loose Sand	9.5	13.5	23.0
		Dense Sand	7.5	10.5	16.5
		Soft Clay	14.5	20.5	29.5
		Very Stiff Clay	7.0	10.0	13.5
100	Pinned	Loose Sand	20.5	10.5	21.5
		Dense Sand	15.0	9.0	15.0
		Soft Clay	24.5	14.5	23.5
		Very Stiff Clay	12.5	8.0	11.5
	Fixed	Loose Sand	9.5	13.5	23.5
		Dense Sand	7.5	10.5	16.5
		Soft Clay	14.5	20.0	27.5
		Very Stiff Clay	7.0	10.0	13.5
200	Pinned	Loose Sand	20.5	10.5	21.5
		Dense Sand	15.0	9.0	15.0
		Soft Clay	25.5	14.0	25.5
		Very Stiff Clay	12.5	8.0	11.5
	Fixed	Loose Sand	9.5	13.0	23.5
		Dense Sand	7.5	10.5	16.0
		Soft Clay	14.5	20.0	29.5
		Very Stiff Clay	7.0	10.5	13.5
300	Pinned	Loose Sand	20.5	10.5	21.5
		Dense Sand	15.0	8.5	15.0
		Soft Clay	25.5	13.5	25.5
		Very Stiff Clay	12.5	8.0	11.5
	Fixed	Loose Sand	9.0	13.0	23.5
		Dense Sand	7.5	9.5	16.0
		Soft Clay	14.5	19.5	29.5
		Very Stiff Clay	7.0	9.5	13.0

Table B-14: Depth to 2nd Maximum Bending Moment and Shear Forces and Depth of Fixity for Trials 193a through 256a

Parameters: (1) HP 10 x 57 Pile; (2) Strong-Axis Bending; (3) 1.55-in of Lateral Displacement; and (4) No Prebore Hole					
Axial Load, kips	Boundary Condition	Soil Type	Location from GS of 2nd Maximum, ft		Depth of Fixity, ft
			Bending Moment	Shear	
0	Pinned	Loose Sand	21.0	11.0	22.5
		Dense Sand	15.5	8.5	15.5
		Soft Clay	28.0	16.0	28.5
		Very Stiff Clay	13.0	8.5	12.5
	Fixed	Loose Sand	9.5	13.5	24.5
		Dense Sand	7.5	10.5	17.0
		Soft Clay	15.5	22.0	32.5
		Very Stiff Clay	7.5	10.5	14.5
100	Pinned	Loose Sand	21.0	11.0	22.5
		Dense Sand	15.5	9.0	15.5
		Soft Clay	26.5	15.5	26.5
		Very Stiff Clay	13.0	8.5	12.5
	Fixed	Loose Sand	9.5	13.5	24.5
		Dense Sand	7.5	10.5	17.0
		Soft Clay	15.5	21.5	31.0
		Very Stiff Clay	7.5	10.5	14.5
200	Pinned	Loose Sand	21.0	11.0	22.0
		Dense Sand	15.0	9.0	15.5
		Soft Clay	27.5	15.0	28.0
		Very Stiff Clay	13.0	8.5	12.5
	Fixed	Loose Sand	9.5	13.0	24.5
		Dense Sand	7.5	10.5	16.5
		Soft Clay	15.5	21.0	32.5
		Very Stiff Clay	7.0	10.0	14.5
300	Pinned	Loose Sand	20.5	10.5	22.0
		Dense Sand	15.0	8.5	15.5
		Soft Clay	27.5	14.5	28.0
		Very Stiff Clay	13.0	8.0	12.5
	Fixed	Loose Sand	9.5	13.0	24.0
		Dense Sand	7.5	10.0	16.5
		Soft Clay	15.5	21.0	32.5
		Very Stiff Clay	7.0	10.0	14.0

Table B-15: Depth to 2nd Maximum Bending Moment and Shear Forces and Depth of Fixity for Trials 1b through 64b

Parameters: (1) UHPC Pile; (2) Weak-Axis Bending; (3) 1.00-in of Lateral Displacement; and (4) No Prebore Hole					
Axial Load, kips	Boundary Condition	Soil Type	Location from GS of 2nd Maximum, ft		Depth of Fixity, ft
			Bending Moment	Shear	
0	Pinned	Loose Sand	16.5	8.5	17.5
		Dense Sand	12.0	7.5	12.0
		Soft Clay	20.0	11.5	19.5
		Very Stiff Clay	9.5	6.0	8.5
	Fixed	Loose Sand	7.5	10.5	19.0
		Dense Sand	6.0	8.5	13.0
		Soft Clay	11.0	15.5	22.5
		Very Stiff Clay	5.0	7.5	9.5
100	Pinned	Loose Sand	16.5	8.5	17.0
		Dense Sand	12.0	7.5	12.0
		Soft Clay	19.5	11.0	19.5
		Very Stiff Clay	6.0	9.5	9.0
	Fixed	Loose Sand	7.5	10.5	19.0
		Dense Sand	6.0	8.5	13.0
		Soft Clay	11.0	15.0	22.5
		Very Stiff Clay	5.0	7.5	10.0
200	Pinned	Loose Sand	16.5	8.5	17.0
		Dense Sand	12.0	7.0	12.0
		Soft Clay	19.5	10.5	19.5
		Very Stiff Clay	9.5	6.0	9.0
	Fixed	Loose Sand	7.5	10.5	19.0
		Dense Sand	6.0	8.5	13.5
		Soft Clay	11.0	15.0	22.5
		Very Stiff Clay	5.0	7.5	10.0
300	Pinned	Loose Sand	16.0	8.0	17.0
		Dense Sand	12.0	7.0	12.0
		Soft Clay	19.0	10.0	19.5
		Very Stiff Clay	9.5	6.0	9.0
	Fixed	Loose Sand	7.5	10.5	19.0
		Dense Sand	6.0	8.5	13.0
		Soft Clay	11.0	14.5	22.5
		Very Stiff Clay	5.0	7.5	10.0

Table B-16: Depth to 2nd Maximum Bending Moment and Shear Forces and Depth of Fixity for Trials 65b through 128b

Parameters: (1) UHPC Pile; (2) Weak-Axis Bending; (3) 1.55-in of Lateral Displacement; and (4) No Prebore Hole					
Axial Load, kips	Boundary Condition	Soil Type	Location from GS of 2nd Maximum, ft		Depth of Fixity, ft
			Bending Moment	Shear	
0	Pinned	Loose Sand	17.0	9.5	18.0
		Dense Sand	12.5	7.5	12.5
		Soft Clay	21.5	12.0	21.5
		Very Stiff Clay	10.0	6.5	9.5
	Fixed	Loose Sand	7.5	11.0	19.5
		Dense Sand	6.0	8.5	13.5
		Soft Clay	11.5	16.5	24.5
		Very Stiff Clay	5.0	7.5	10.5
100	Pinned	Loose Sand	17.0	9.0	18.0
		Dense Sand	12.5	7.5	12.5
		Soft Clay	21.0	11.5	21.5
		Very Stiff Clay	9.5	6.0	9.0
	Fixed	Loose Sand	7.5	11.0	19.5
		Dense Sand	6.0	8.5	13.5
		Soft Clay	11.5	16.0	25.0
		Very Stiff Clay	5.0	7.5	10.5
200	Pinned	Loose Sand	16.5	8.5	18.0
		Dense Sand	12.5	7.5	12.5
		Soft Clay	21.0	11.0	21.5
		Very Stiff Clay	9.5	6.0	9.5
	Fixed	Loose Sand	7.5	10.5	19.5
		Dense Sand	6.0	8.5	13.5
		Soft Clay	11.5	15.5	25.0
		Very Stiff Clay	5.0	7.5	11.0
300	Pinned	Loose Sand	16.5	8.5	17.5
		Dense Sand	12.5	7.5	12.5
		Soft Clay	20.5	10.5	21.5
		Very Stiff Clay	9.0	5.5	8.5
	Fixed	Loose Sand	7.5	10.0	19.0
		Dense Sand	6.0	8.5	13.5
		Soft Clay	11.5	15.5	25.0
		Very Stiff Clay	5.0	7.5	10.5

Table B-17: Depth to 2nd Maximum Bending Moment and Shear Forces and Depth of Fixity for Trials 129b through 192b

Parameters: (1) UHPC Pile; (2) Strong-Axis Bending; (3) 1.00-in of Lateral Displacement; and (4) No Prebore Hole					
Axial Load, kips	Boundary Condition	Soil Type	Location from GS of 2nd Maximum, ft		Depth of Fixity, ft
			Bending Moment	Shear	
0	Pinned	Loose Sand	19.5	10.0	20.0
		Dense Sand	14.0	8.5	14.0
		Soft Clay	23.5	13.5	23.0
		Very Stiff Clay	11.0	7.0	10.5
	Fixed	Loose Sand	8.5	12.5	21.5
		Dense Sand	7.0	9.5	15.0
		Soft Clay	13.0	18.5	27.0
		Very Stiff Clay	6.0	9.0	11.5
100	Pinned	Loose Sand	19.5	10.0	20.0
		Dense Sand	14.0	8.5	14.0
		Soft Clay	24.0	13.5	23.5
		Very Stiff Clay	11.5	7.5	10.5
	Fixed	Loose Sand	9.0	12.5	22.0
		Dense Sand	7.0	9.5	15.0
		Soft Clay	13.5	18.5	27.5
		Very Stiff Clay	6.5	9.0	12.5
200	Pinned	Loose Sand	19.5	10.0	20.0
		Dense Sand	14.0	8.5	14.0
		Soft Clay	23.5	13.0	23.5
		Very Stiff Clay	11.5	7.5	11.0
	Fixed	Loose Sand	9.0	12.5	22.0
		Dense Sand	7.0	10.0	15.5
		Soft Clay	13.5	18.5	27.5
		Very Stiff Clay	6.5	9.5	12.5
300	Pinned	Loose Sand	19.0	9.5	20.0
		Dense Sand	14.0	8.5	14.0
		Soft Clay	23.5	12.5	23.5
		Very Stiff Clay	11.5	7.5	11.0
	Fixed	Loose Sand	9.0	12.5	22.0
		Dense Sand	7.5	10.0	15.5
		Soft Clay	13.5	18.0	27.5
		Very Stiff Clay	6.5	9.5	12.5

Table B-18: Depth to 2nd Maximum Bending Moment and Shear Forces and Depth of Fixity for Trials 193b through 256b

Parameters: (1) UHPC Pile; (2) Strong-Axis Bending; (3) 1.55-in of Lateral Displacement; and (4) No Prebore Hole					
Axial Load, kips	Boundary Condition	Soil Type	Location from GS of 2nd Maximum, ft		Depth of Fixity, ft
			Bending Moment	Shear	
0	Pinned	Loose Sand	19.5	10.5	21.0
		Dense Sand	14.0	8.5	14.5
		Soft Clay	25.5	14.5	25.5
		Very Stiff Clay	11.5	7.5	11.0
	Fixed	Loose Sand	8.5	12.5	22.5
		Dense Sand	7.0	9.5	15.5
		Soft Clay	14.0	20.0	29.5
		Very Stiff Clay	6.0	9.0	12.5
100	Pinned	Loose Sand	19.5	10.5	21.0
		Dense Sand	14.5	8.5	14.5
		Soft Clay	25.5	14.0	26.0
		Very Stiff Clay	12.0	7.5	11.5
	Fixed	Loose Sand	9.0	12.5	22.5
		Dense Sand	7.0	10.0	15.5
		Soft Clay	14.5	20.0	30.0
		Very Stiff Clay	6.5	9.5	13.0
200	Pinned	Loose Sand	19.5	10.0	21.0
		Dense Sand	14.5	8.5	14.5
		Soft Clay	25.5	13.5	26.0
		Very Stiff Clay	12.5	8.0	12.0
	Fixed	Loose Sand	9.0	12.5	23.0
		Dense Sand	7.0	10.0	16.0
		Soft Clay	14.5	19.5	30.5
		Very Stiff Clay	6.5	9.5	13.5
300	Pinned	Loose Sand	19.5	10.0	21.0
		Dense Sand	14.5	8.5	14.5
		Soft Clay	25.0	13.0	26.0
		Very Stiff Clay	12.5	8.0	12.0
	Fixed	Loose Sand	9.0	12.5	23.0
		Dense Sand	7.0	10.0	16.0
		Soft Clay	14.5	19.0	30.5
		Very Stiff Clay	6.5	9.5	13.5

Table B-19: Depth to 2nd Maximum Bending Moment and Shear Forces and Depth of Fixity for Trials 257 through 264

Parameters: (1) Weak-Axis Bending; (2) 1.00-in of Lateral Displacement; (3) Fixed Pile Head; and (4) No Prebore Hole					
Pile Type	Axial Load, kips	Soil Type	Location from GS of 2nd Maximum, ft		Depth of Fixity, ft
			Bending Moment	Shear	
UHPC	100	Soft Clay	15.0	19.0	25.0
		Very Soft Clay	11.0	13.5*	13.5
	200	Soft Clay	15.0	18.5*	25.0
		Very Soft Clay	11.0	13.5*	13.0
HP 10x57	100	Soft Clay	15.0	19.0	25.5
		Very Soft Clay	11.0	13.5*	13.5
	200	Soft Clay	15.0	19.0*	25.5
		Very Soft Clay	11.0	13.5*	13.5

*The depth of the maximum shear force

Table B-20: Depth to 2nd Maximum Bending Moment and Shear Forces and Depth of Fixity for Trials 265 through 272

Parameters: (1) Weak-Axis Bending; (2) 1.55-in of Lateral Displacement; (3) Fixed Pile Head; and (4) No Prebore Hole					
Axial Load, kips	Boundary Condition	Soil Type	Location from GS of 2nd Maximum, ft		Depth of Fixity, ft
			Bending Moment	Shear	
UHPC	100	Soft Clay	15.5	20.0	28.0
		Very Soft Clay	11.5	14.0*	15.5
	200	Soft Clay	15.5	19.5*	27.5
		Very Soft Clay	11.0	14.0*	16.0
HP 10x57	100	Soft Clay	15.5	20.0	27.5
		Very Soft Clay	11.5	14.0*	15.5
	200	LS	15.5	19.5*	27.5
		DS	11.5	17.0*	16.0

*The depth of the maximum shear force

APPENDIX C

Test pile and production pile design calculations are included here using the procedures from Section 2.5.

C.1: DESIGN CALCULATIONS FOR UHPC TEST PILE P3

C.1.1: Current Iowa DOT Practice to Determine Pile Design Length

Step 1: Idealize the Soil Layers

Table C-1: Idealized Soil Layers for P3

Layer	N-Value	Thickness	fs, kip/ft (Iowa DOT 2011)
Above Ground	-	3	0
Firm Glacial Clay	9	6	3.2
Very Firm Glacial Clay	24	24	3.2
Very Firm Glacial Clay	34	L	4.8

Step 2: Calculate the Nominal Capacity

A nominal capacity of 200 kips is used to calculate the design length of P3 to verify the piles design for the integral abutments.

Step 3: Calculate End Bearing

$$Q_p = 60kip \times \frac{100in^2}{144in^2} = 41.7kips$$

Step 4: Calculate Side Friction

$$Q_s = 6ft \times 3.2\frac{kip}{ft} + 24ft \times 3.2\frac{kip}{ft} + L \times 4.8\frac{kip}{ft} = 96 + 4.8L$$

Step 5: Calculate L

$$200kips = 41.7 + 96 + 4.8L$$

$$L = 13ft$$

Step 6: Calculated Required Depth of Pile

$$Design\ Length = 3ft + 6ft + 24ft + 13ft = 46 \approx 45ft$$

C.1.2: New Resistance Factors to Predict Nominal Capacity

Step 1: Idealize the Soil Layers

Use Table B-1 for the idealized soil layers.

Step 2: Calculate the Nominal Capacity

$$P_n = \frac{1.45 \times 100kip}{0.8} = 183\ kips$$

Step 3: Calculate End Bearing

$$Q_p = 60kip \times \frac{100in^2}{144in^2} = 41.7kips$$

Step 4: Calculate Side Friction

$$Q_s = 6ft \times 3.2\frac{kip}{ft} + 24ft \times 3.2\frac{kip}{ft} + L \times 4.8\frac{kip}{ft} = 96 + 4.8L$$

Step 5: Calculate L

$$183kips = 41.7 + 96 + 4.8L$$

$$L = 9.4ft$$

Step 6: Calculated Required Depth of Pile

$$Design\ Length = 3ft + 6ft + 24ft + 9.4ft = 42ft$$

C.2: DESIGN CALCULATIONS FOR UHPC TEST PILE P4

C.2.1: Current Iowa DOT Practice

Step 1: Idealize the Soil Layers

Table C-2: Idealized Soil Layers for P4

Layer	N-Value	Thickness	fs, kip/ft (Iowa DOT 2011)
Above Ground	-	3	0
Firm Glacial Clay	9	6	3.2
Very Firm Glacial Clay	24	21	3.2

Step 2: Calculate End Bearing

$$Q_p = 60kip \times \frac{100in^2}{144in^2} = 41.7kips$$

Step 3: Calculate Side Friction

$$Q_s = 6ft \times 3.2\frac{kip}{ft} + 21ft \times 3.2\frac{kip}{ft} = 86.4kips$$

Step 4: Calculate Nominal Capacity

$$P_n = 41.7kips + 86.4kips = 128kips$$

C.3: DESIGN CALCULATIONS FOR STEEL HP 12 X 53 ANCHOR PILES RPS AND RPN

C.3.1: Current Iowa DOT Practice for Uplift

Step 1: Idealize the Soil Layers

Table C-3: Idealized Soil Layers for RPS and RPN

Layer	N-Value	Thickness	fs, kip/ft (Iowa DOT 2011)
Cutoff	-	1	0
Above Ground	-	6	0
Fill	-	0.4	0
Firm Glacial Clay	9	6	3.2
Very Firm Glacial Clay	24	24	3.2
Very Firm Glacial Clay	34	L	4.8

Step 2: Calculate Factored Uplift

$$Uplift = \frac{1.7 \times 100kips}{0.6} = 283kips$$

Step 3: Calculated Side Friction

$$Q_s = 6ft \times 3.2\frac{kip}{ft} + 24ft \times 3.2\frac{kip}{ft} + L \times 4.8\frac{kip}{ft} = 96 + 4.8L$$

Step 5: Calculate L

$$283kips = 96 + 4.8L$$

$$L = 40ft$$

Step 6: Calculated Required Depth of Pile

$$Design\ Length = 1ft + 6ft + 0.4ft + 6ft + 24ft + 40ft = 77 = 80ft$$

C.3.2: Current Iowa DOT Practice for Downward Load

Step 1: Idealize the Soil Layers

Table B-3 is used to idealize the soil layers.

Step 2: Calculate End Bearing

$$Q_p = 2ksi \times 15.5in^2 = 31kips$$

Step 3: Calculate Side Friction

$$Q_s = 6ft \times 3.2\frac{kip}{ft} + 24ft \times 3.2\frac{kip}{ft} + 42.6 \times 4.8\frac{kip}{ft} = 300kips$$

Step 4: Calculate Nominal Capacity

$$P_n = 31kips + 300kips = 331kips$$

C.4: DESIGN OF UHPC PRODUCTION PILE UW1

C.4.1: Current Iowa DOT Practice

Step 1: Idealize the Soil Layers

Table C-4: Idealized Soil Layers for UW1

Layer	N-Value	Thickness	fs, kip/ft (Iowa DOT 2011)
Abutment	-	2	0
Prebore Hole	-	10	0
Fill	-	0.4	0
Firm Glacial Clay	9	6	3.2
Very Firm Glacial Clay	24	24	3.2
Very Firm Glacial Clay	34	L	4.8

Step 2: Calculate the Nominal Capacity

A nominal capacity of 200 kips is used to calculate the design length of P3 to verify the piles design for the integral abutments.

Step 3: Calculate End Bearing

$$Q_p = 60kip \times \frac{100in^2}{144in^2} = 41.7kips$$

Step 4: Calculate Side Friction

$$Q_s = 7ft \times 3.2\frac{kip}{ft} + 22ft \times 3.2\frac{kip}{ft} + L \times 4.8\frac{kip}{ft} = 92.8 + 4.8L$$

Step 5: Calculate L

$$200kips = 41.7 + 92.8 + 4.8L$$

$$L = 13.6ft$$

Step 6: Calculated Required Depth of Pile

$$Design\ Length = 2ft + 10ft + 0.4ft + 7ft + 22ft + 13.6ft = 55ft$$

C.4.2: New Resistance Factors

Step 1: Idealize the Soil Layers

Use Table B-4 for the idealized soil layers.

Step 2: Calculate the Nominal Capacity

$$P_n = \frac{1.45 \times 100kips}{0.8} = 183\ kips$$

Step 3: Calculate End Bearing

$$Q_p = 60kip \times \frac{100in^2}{144in^2} = 41.7kips$$

Step 4: Calculate Side Friction

$$Q_s = 6ft \times 3.2\frac{kip}{ft} + 24ft \times 3.2\frac{kip}{ft} + L \times 4.8\frac{kip}{ft} = 96 + 4.8L$$

Step 5: Calculate L

$$183kips = 41.7 + 96 + 4.8L$$

$$L = 9.4ft$$

Step 6: Calculated Required Depth of Pile

$$Design\ Length = 2ft + 10 + 0.4ft + 6ft + 24ft + 9.4ft = 52ft$$

C.5: DESIGN OF STEEL HP 10 X 57 PRODUCTION PILE SW2

C.5.1: Current Iowa DOT Practice

Step 1: Idealize the Soil Layers

Table C-5: Idealized Soil Layers for SW2

Layer	N-Value	Thickness	fs, kip/ft (Iowa DOT 2011)
Cutoff	-	1	0
Abutment	-	2	0
Prebore Hole	-	10	0
Fill	-	0.4	0
Firm Glacial Clay	9	6	2.8
Very Firm Glacial Clay	24	24	2.8
Very Firm Glacial Clay	34	L	4.0

Step 2: Calculate the Nominal Capacity

$$P_n = \frac{1.45 \times 6ksi \times 16.8in^2}{0.725} = 201.6 = 200kips$$

Step 3: Calculate End Bearing

$$Q_p = 2ksi \times 16.8in^2 = 33.6kips$$

Step 4: Calculate Side Friction

$$Q_s = 7ft \times 2.8\frac{kip}{ft} + 22ft \times 2.8\frac{kip}{ft} + L \times 4.0\frac{kip}{ft} = 81.2 + 4.0L$$

Step 5: Calculate L

$$200kips = 33.6 + 81.2 + 4.0L$$

$$L = 21.3ft$$

Step 6: Calculated Required Depth of Pile

$$Design\ Length = 1ft + 2ft + 10ft + 0.4ft + 7ft + 22ft + 21.3ft = 63.7$$

$$Design\ Length = 65ft$$

C.5.2: New Resistance Factors

Step 1: Idealize the Soil Layers

Use Table B-5 for the idealized soil layers.

Step 2: Calculate the Nominal Capacity

$$P_n = \frac{1.45 \times 6ksi \times 16.8in^2}{0.8} = 183\ kips$$

Step 3: Calculate End Bearing

$$Q_p = 2ksi \times 16.8in^2 = 33.6kips$$

Step 4: Calculate Side Friction

$$Q_s = 6ft \times 2.8\frac{kip}{ft} + 24ft \times 2.8\frac{kip}{ft} + L \times 4.0\frac{kip}{ft} = 84 + 4.0L$$

Step 5: Calculate L

$$183kips = 33.6 + 84 + 4.0L$$

$$L = 16.4ft$$

Step 6: Calculated Required Depth of Pile

$$Design\ Length = 1ft + 2ft + 10ft + 0.4ft + 6ft + 24ft + 16.4ft = 60ft$$

C.6: DESIGN OF STEEL HP 10 X 57 PRODUCTION PILE SE1 AND SE2

C.6.1: Current Iowa DOT Practice

Step 1: Idealize the Soil Layers

Table C-6: Idealized Soil Layers for SE1 and SE2

Layer	N-Value	Thickness	fs, kip/ft (Iowa DOT 2011)
Cutoff	-	1	0
Abutment	-	2	0
Prebore Hole	-	10	0
Fill	-	17	0
Soft Sand Silty Clay	4	7	0.8
Firm Glacial Clay	17	23	2.8
Firm Glacial Clay	24	L	4.0

Step 2: Calculate the Nominal Capacity

$$P_n = \frac{1.45 \times 6ksi \times 16.8in^2}{0.725} = 201.6 = 200kips$$

Step 3: Calculate End Bearing

$$Q_p = 2ksi \times 16.8in^2 = 33.6kips$$

Step 4: Calculate Side Friction

$$Q_s = 7ft \times 0.8\frac{kip}{ft} + 23ft \times 2.8\frac{kip}{ft} + L \times 4.0\frac{kip}{ft} = 70 + 4.0L$$

Step 5: Calculate L

$$200kips = 33.6 + 70 + 4.0L$$

$$L = 24.1ft$$

Step 6: Calculated Required Depth of Pile

$$Design\ Length = 1ft + 2ft + 10ft + 17ft + 7ft + 23ft + 24.1ft = 84.1$$

$$Design\ Length = 85ft$$

C.6.2: New Resistance Factors

Step 1: Idealize the Soil Layers

Use Table B-6 for the idealized soil layers.

Step 2: Calculate the Nominal Capacity

$$P_n = \frac{1.45 \times 6ksi \times 16.8in^2}{0.8} = 183\ kips$$

Step 3: Calculate End Bearing

$$Q_p = 2ksi \times 16.8in^2 = 33.6kips$$

Step 4: Calculate Side Friction

$$Q_s = 7ft \times 0.8\frac{kip}{ft} + 23ft \times 2.8\frac{kip}{ft} + L \times 4.0\frac{kip}{ft} = 70 + 4.0L$$

Step 5: Calculate L

$$183kips = 33.6 + 70 + 4.0L$$

$$L = 19.9ft$$

Step 6: Calculated Required Depth of Pile

$$Design\ Length = 1ft + 2ft + 10ft + 17ft + 7ft + 23ft + 20ft = 80ft$$

APPENDIX D

Instrumentation Installation Procedure for the test units, test piles and production piles.

D.1: PROCEDURE FOR INSTALLING TML STRAIN GAUGES

1. Grind down the surface of the prestressing strand at the desired location of installation with sand paper
2. Clean the bonding surface with a clean cloth and acetone
3. Apply the bonding adhesive to the back of the gage base. Place the gage on the guide mark and then place on the polyethylene sheet. Press down on the gage constantly
4. After curing is complete, remove the polyethylene sheet, and raise the gage leads with a pair of tweezers
5. Protect the gage by covering it with a water proofing agent, followed by Butyl rubber, and finally aluminum tape (See Figure D-1)
6. Attach the cable to the prestressing strand close to the gage making sure to leave some slack in case the cable is pulled
7. Continue to attach the cable periodically along the prestressing strand until the point where the cable will exit. Make sure to spread the cables throughout the cross-section to ensure no weak points such as bonding problems between the UHPC and prestressing strands

Figure D-1: TML Strain Gauge after the Aluminum Foil was Applied

D.2: PROCEDURE FOR INSTALLING WELDABLE STRAIN GAGES

1. Grind down the surface of the H-pile at the specified gage locations
2. Align the strain gage with the transition end pointing towards the pile head
3. Tack the gage with 1 weld at each side of the align marks on the strain gage
4. Continue welding the gage in place. The first line of welds should be adjacent to the hermetic sealant 1/6-in on center. The sequence of welds should be:
5. Vertically down from the right side alignment mark looking at the gage from transition end
6. Vertically up from the right side alignment mark
7. Vertically down from the left side alignment mark
8. Vertically up from the left side alignment mark
9. Horizontally across the top of the gage
10. Complete the tack welding by adding a second row of tack welds between and 1/32-in outboard of the first row
11. Cover with butyl rubber
12. Cover with aluminum tape
13. Weld 3/8-in nuts at various locations along the pile
14. Tie the strain gage cables together
15. Wrap the cable with aluminum foil to protect the cables during welding of the protective angle (See Figure D-2)
16. Secure the cables to the nuts welded onto the pile with zip ties
17. Weld the steel angle over the cables 4-in every 24-in, but adjusting the location of the weld when near the location of a gage

Figure D-2: Installed Weldable Strain Gage

D.3: PROCEDURE FOR INSTALLING EMBEDDED CONCRETE STRAIN GAGES

1. Twist wire around the bottom of the strain gage, which is nearest to the attached cable, leaving excess wire on both sides
2. Twist wire around the top of the strain gages, leaving excess wire on both sides
3. Align the strain gages with the transition end pointing toward the head of the pile
4. Twist the excess wire from steps 1 and 2 around the adjacent prestressing strands (see Figure D-3)
5. String the cables along the prestressing strands using zip ties, until at the pile head. Make sure to spread the cables out so a weak point does not develop in the cross-section of the pile

Figure D-3: Strung Embedded Concrete Strain Gage

APPENDIX E

The comprehensive results from the lateral load tests are given in this appendix which includes: 1) the predicted, adjusted and average measured moments along P3 and P4; 2) the adjusted and measured displacements along the length of P4; and 3) the adjusted shear force along the length of P4.

E.1: PREDICTED, ADJUSTED AND AVERAGE MEASURED MOMENTS ALONG THE LENGTH OF P3

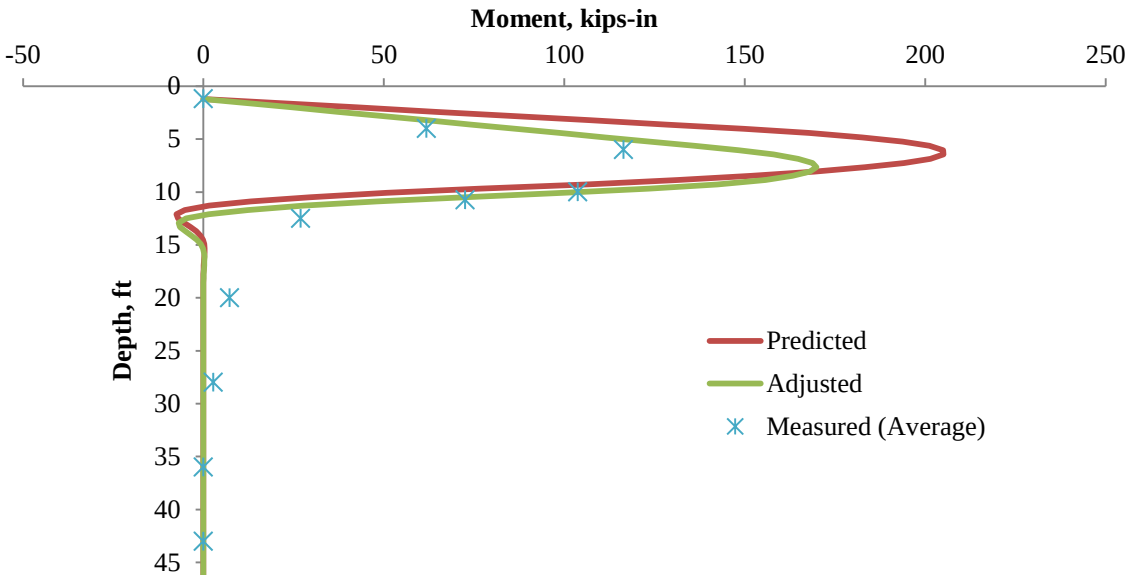

Figure E-1: Predicted, Adjusted and Average Measured Moments along the Length of P3 at the 2.5 kip Load Step during the Lateral Load Test

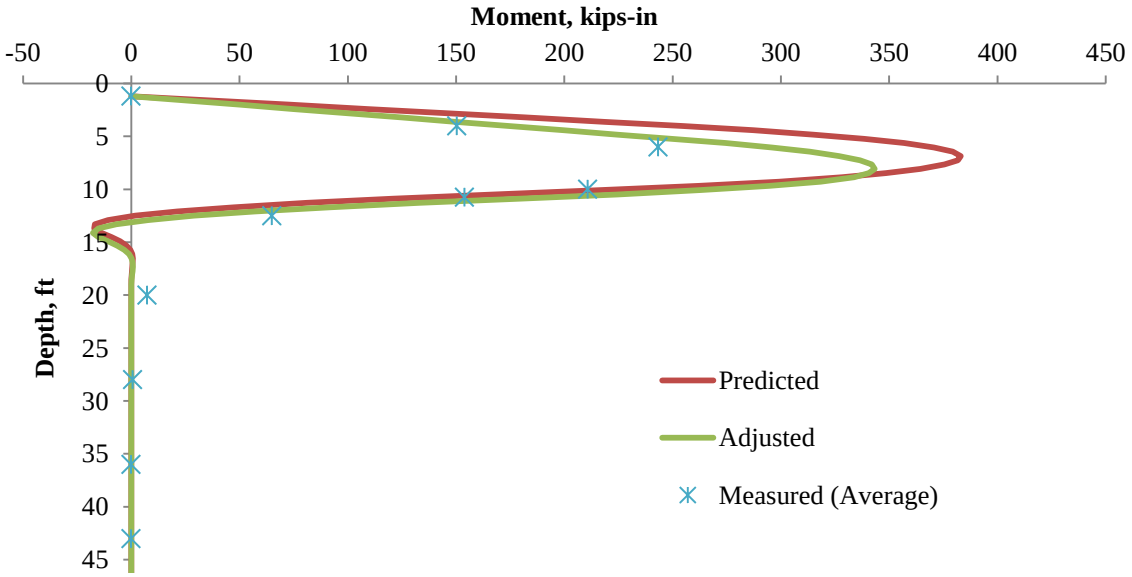

Figure E-2: Predicted, Adjusted and Average Measured Moments along the Length of P3 at the 5.0 kip Load Step during the Lateral Load Test

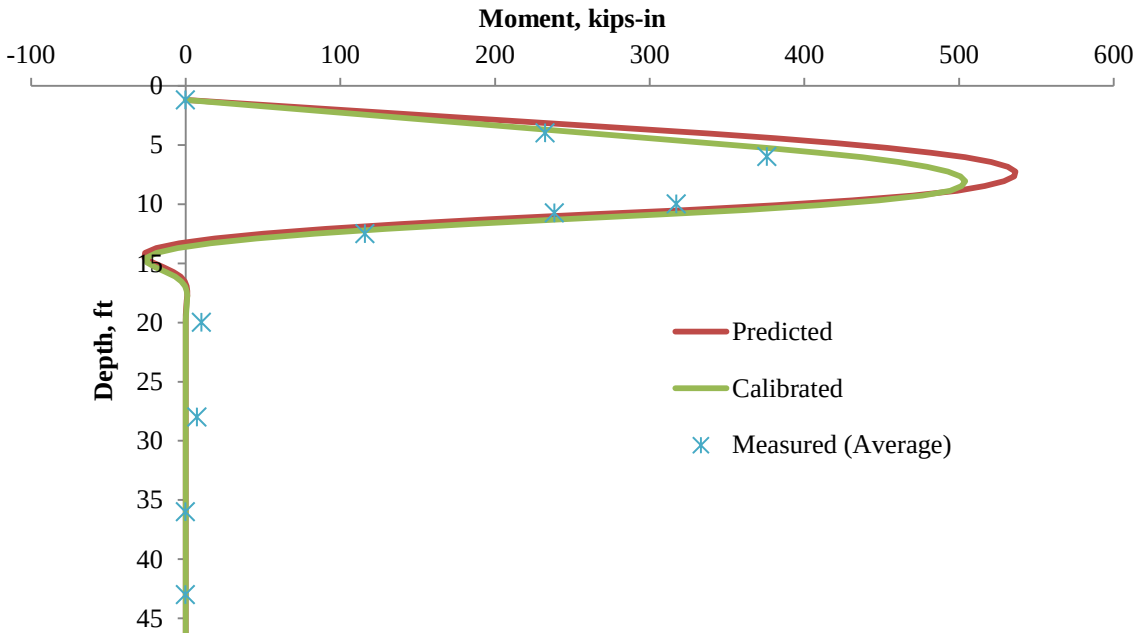

Figure E-3: Predicted, Adjusted and Average Measured Moments along the Length of P3 at the 7.5 kip Load Step during the Lateral Load Test

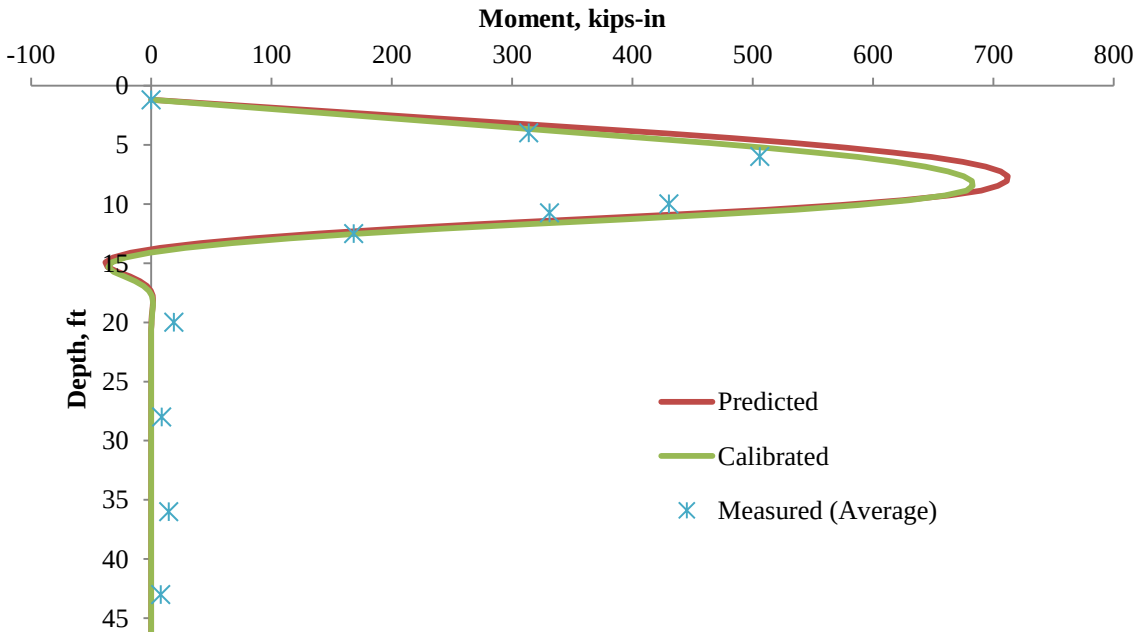

Figure E-4: Predicted, Adjusted and Average Measured Moments along the Length of P3 at the 10.0 kip Load Step during the Lateral Load Test

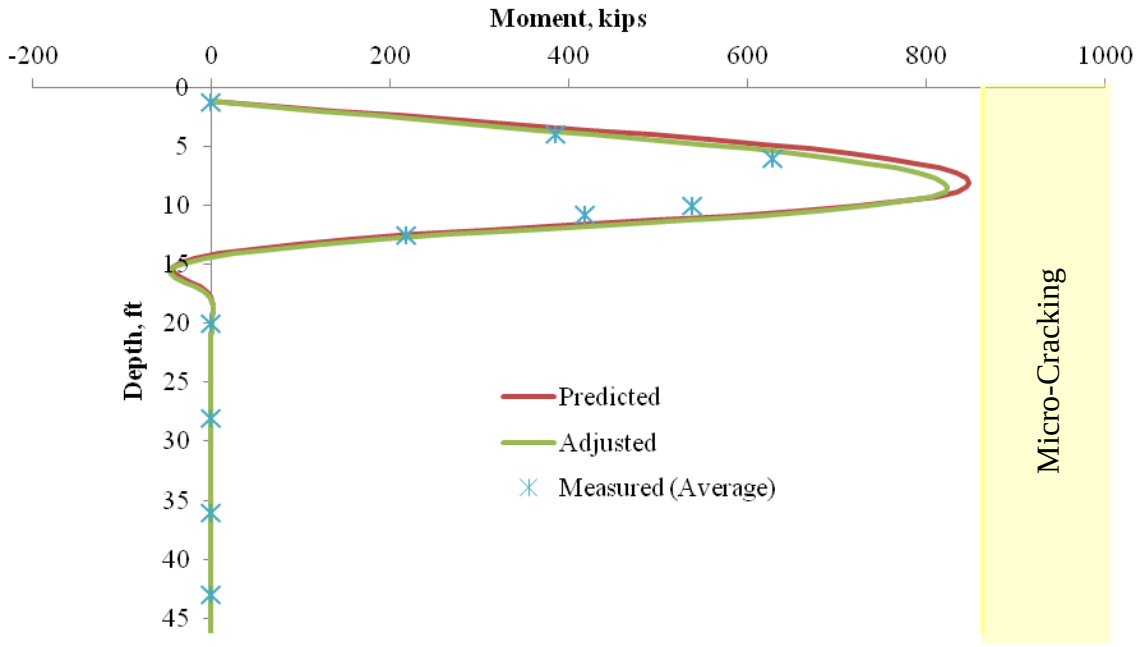

Figure E-5: Predicted, Adjusted and Average Measured Moments along the Length of P3 at the 12.5 kip Load Step during the Lateral Load Test

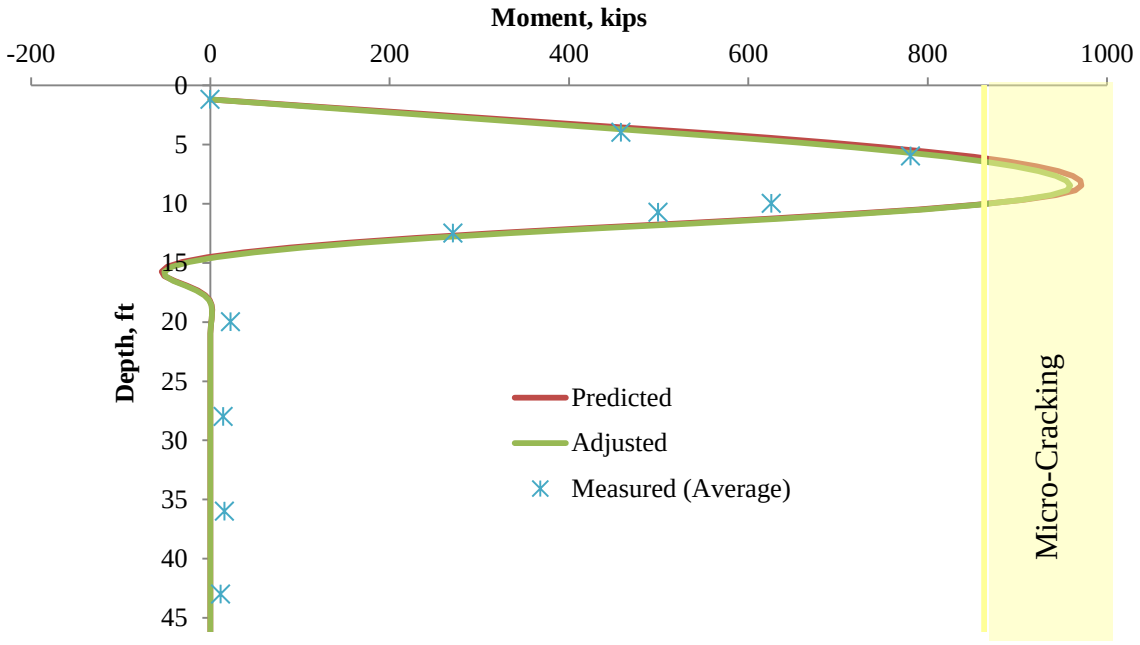

Figure E-6: Predicted, Adjusted and Average Measured Moments along the Length of P3 at the 15.0 kip Load Step during the Lateral Load Test

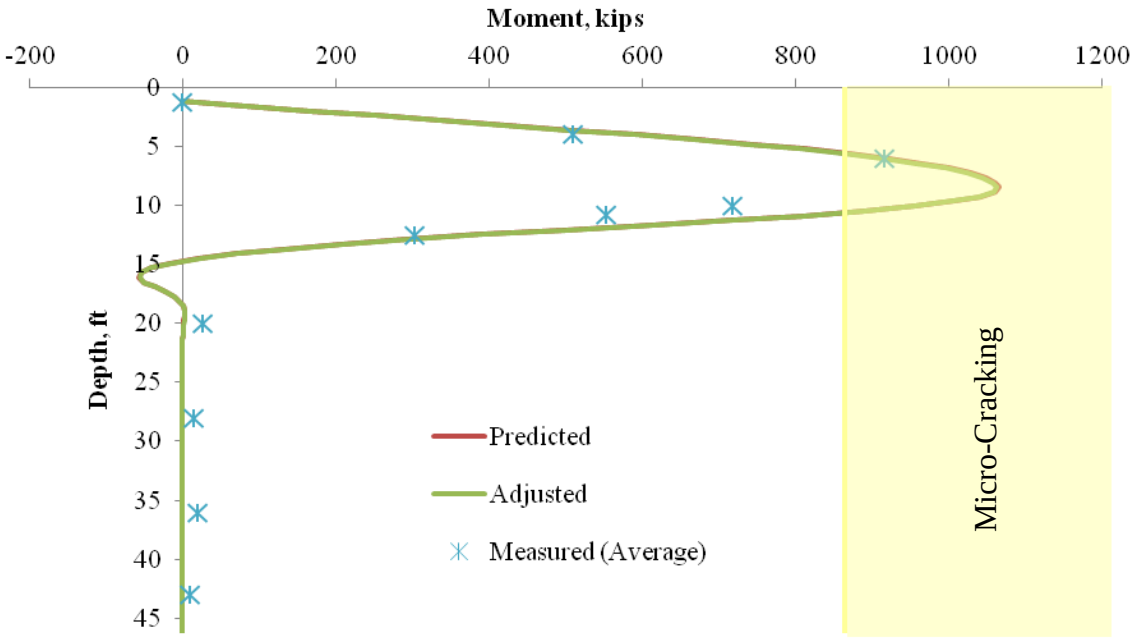

Figure E-7: Predicted, Adjusted and Average Measured Moments along the Length of P3 at the 17.0 kip Load Step during the Lateral Load Test

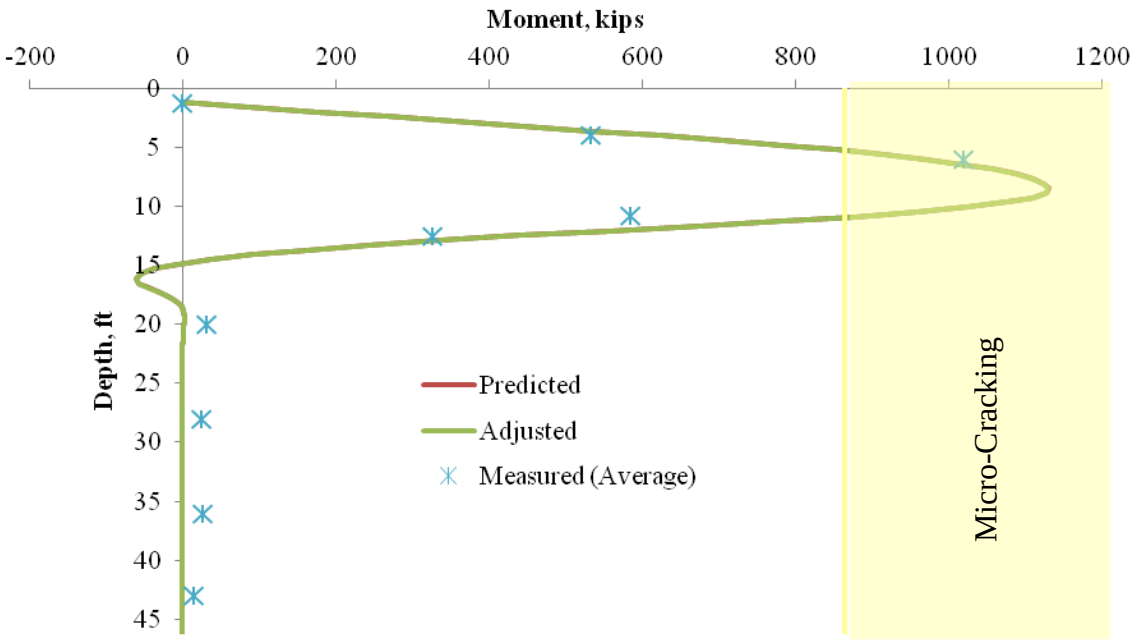

Figure E-8: Predicted, Adjusted and Average Measured Moments along the Length of P3 at the 18.0 kip Load Step during the Lateral Load Test

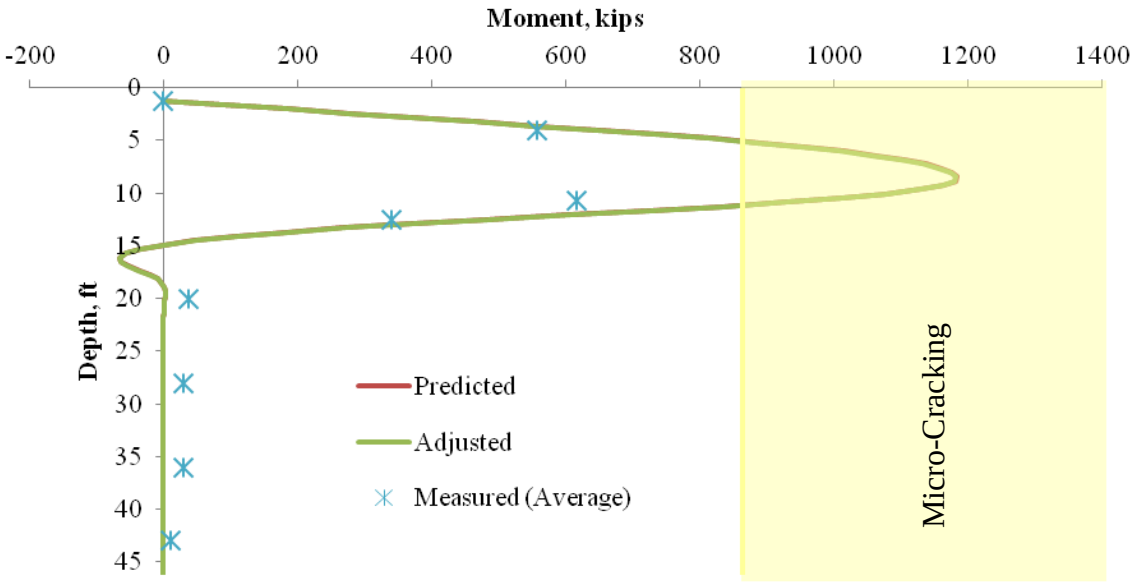

Figure E-9: Predicted, Adjusted and Average Measured Moments along the Length of P3 at the 19.0 kip Load Step during the Lateral Load Test

E.2 PREDICTED, ADJUSTED AND AVERAGE MEASURED MOMENTS ALONG THE LENGTH OF P4

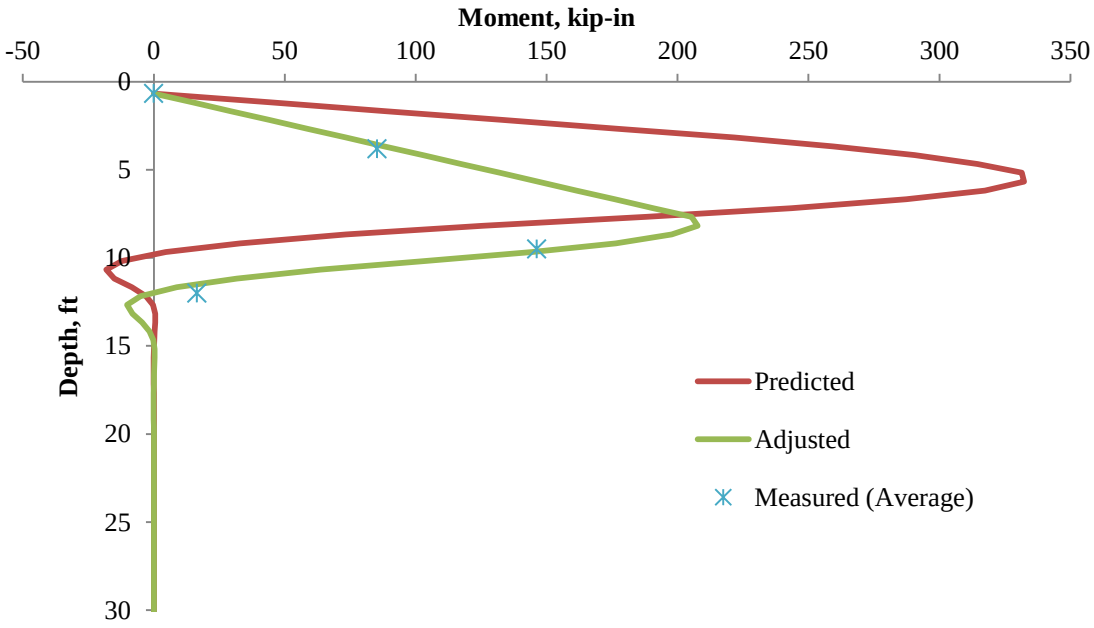

Figure E-10: Predicted, Adjusted and Average Measured Moments along the Length of P4 at the 2.5 kip Load Step during the Lateral Load Test

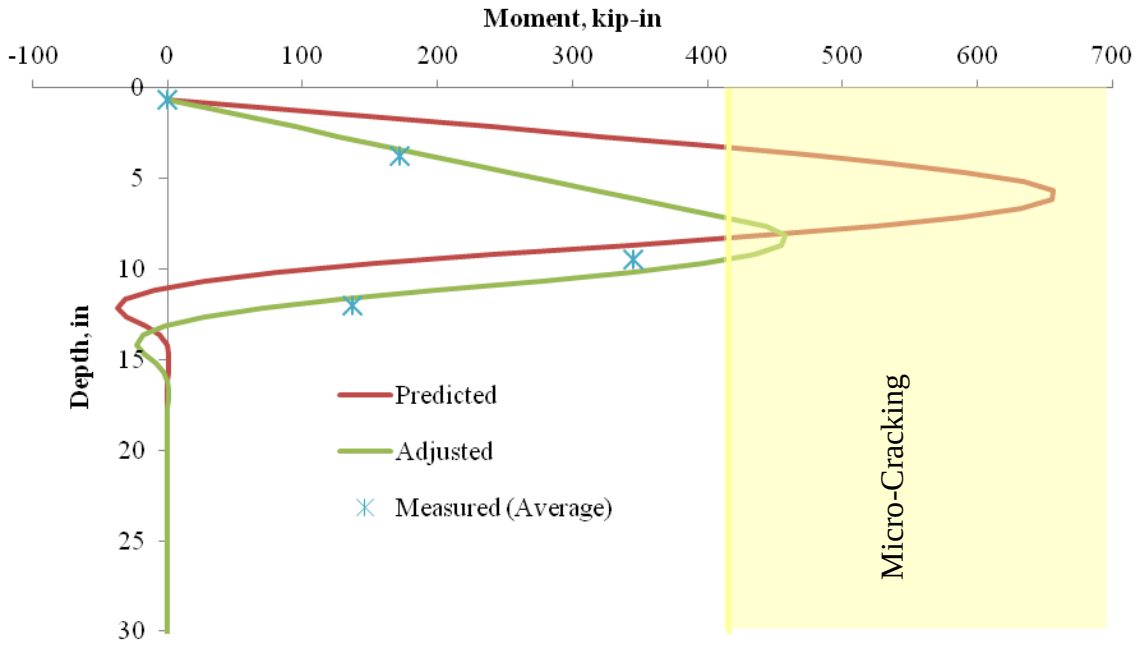

Figure E-11: Predicted, Adjusted and Average Measured Moments along the Length of P4 at the 5.0 kip Load Step during the Lateral Load Test

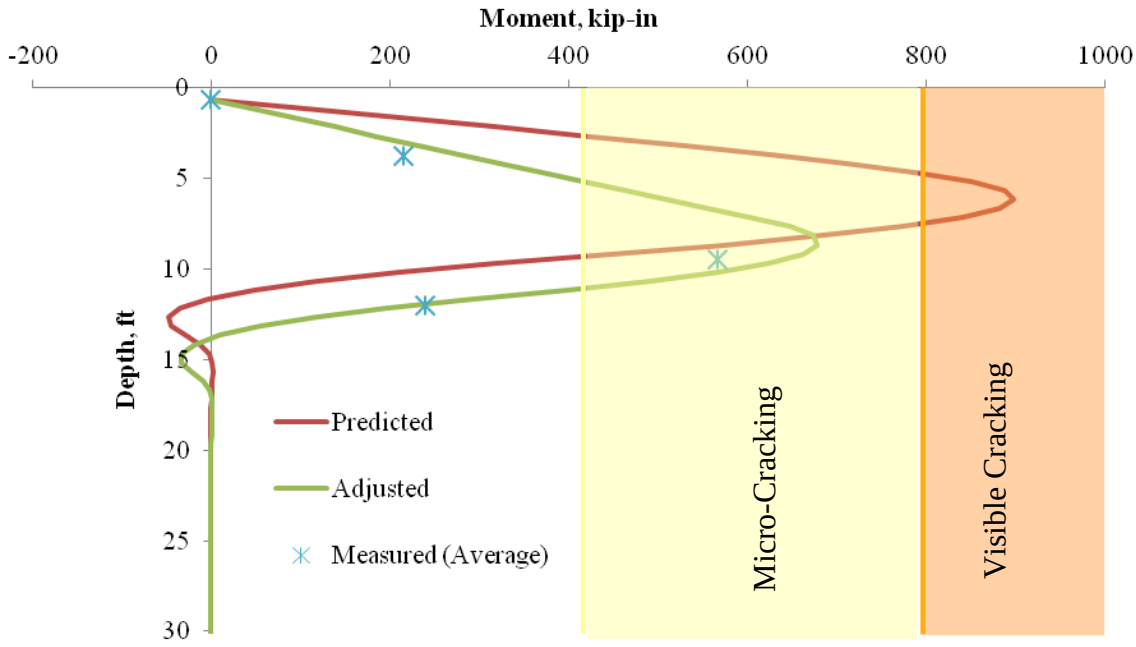

Figure E-12: Predicted, Adjusted and Average Measured Moments along the Length of P4 at the 7.5 kip Load Step during the Lateral Load Test

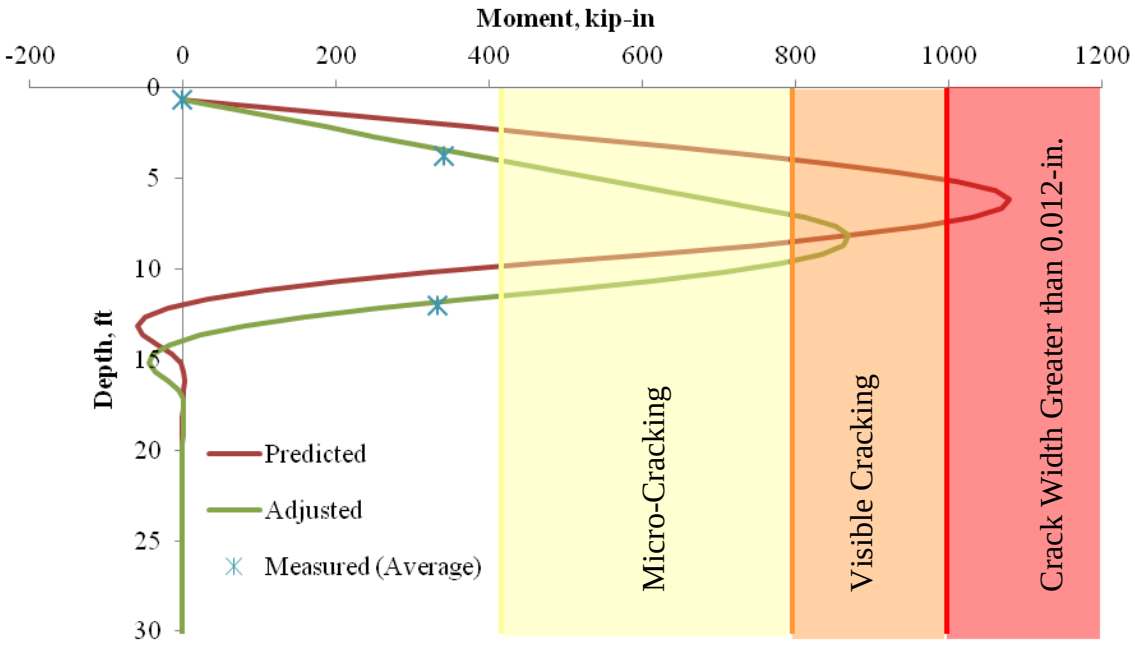

Figure E-13: Predicted, Adjusted and Average Measured Moments along the Length of P4 at the 10.0 kip Load Step during the Lateral Load Test

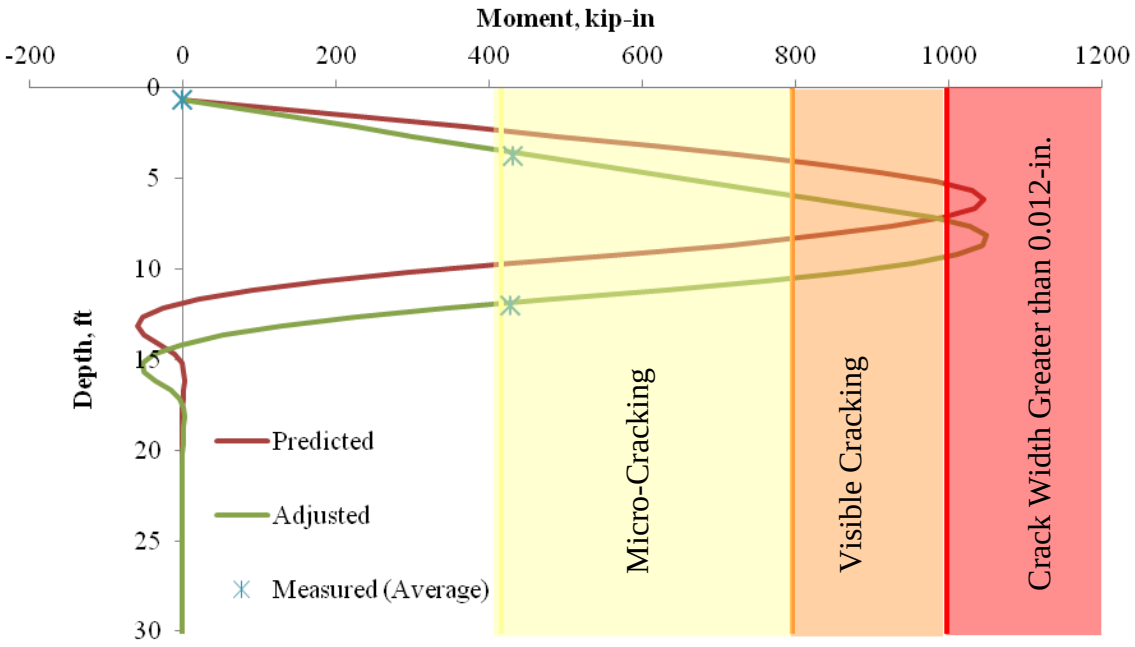

Figure E-14: Predicted, Adjusted and Average Measured Moments along the Length of P4 at the 12.5 kip Load Step during the Lateral Load Test

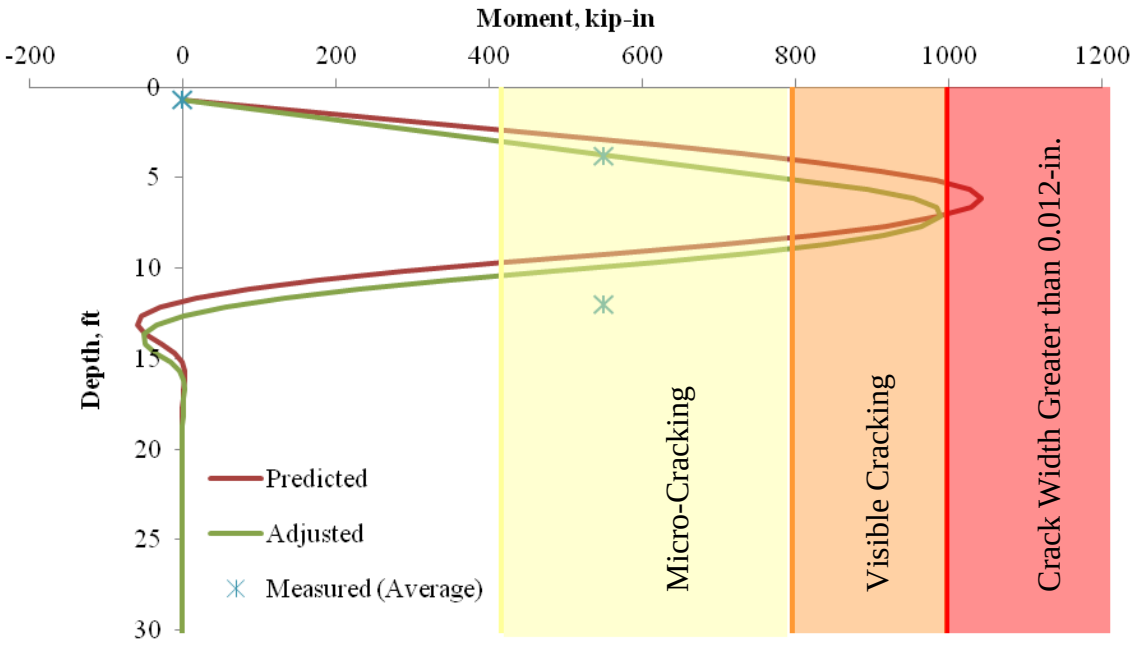

Figure E-15: Predicted, Adjusted and Average Measured Moments along the Length of P4 at the 15.0 kip Load Step during the Lateral Load Test

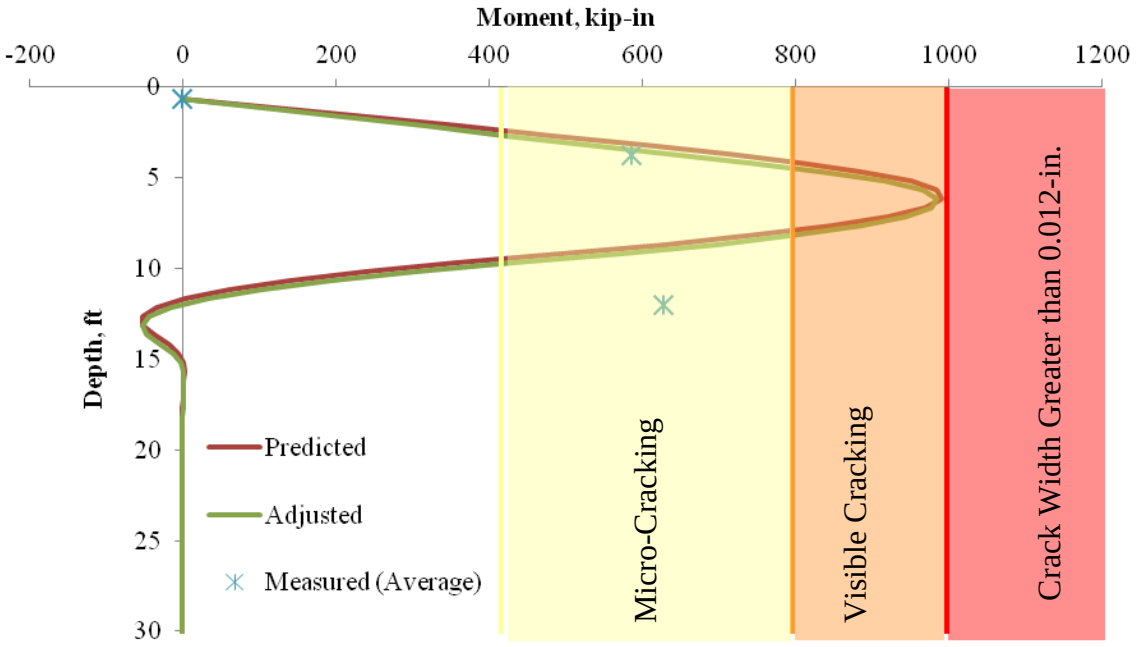

Figure E-16: Predicted, Adjusted and Average Measured Moments along the Length of P4 at the 17.0 kip Load Step during the Lateral Load Test

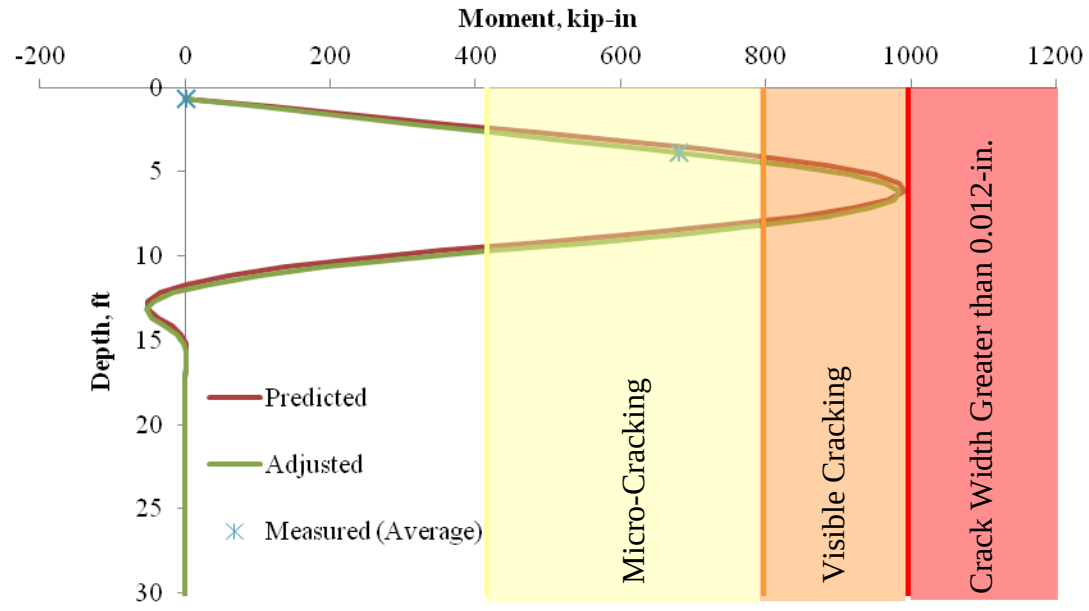

Figure E-17: Predicted, Adjusted and Average Measured Moments along the Length of P4 at the 18.0 kip Load Step during the Lateral Load Test

E.3 ADJUSTED AND MEASURED DISPLACEMENT ALONG THE LENGTH OF P4

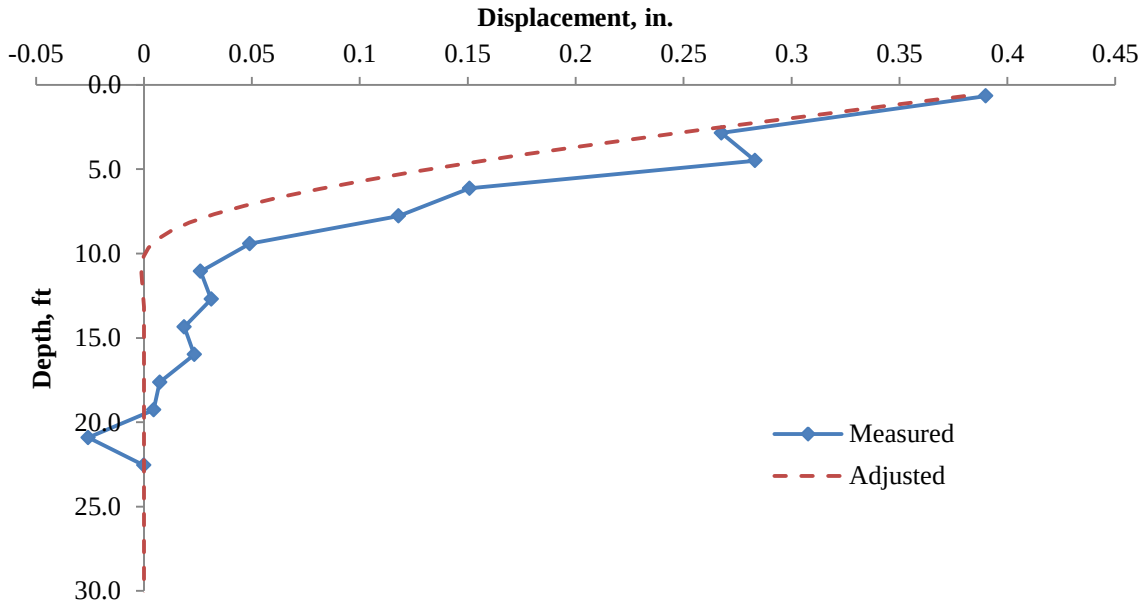

Figure E-18: Adjusted and Measured Displacements along the Length of P4 at the 2.5 kip Load Step during the Lateral Load Test

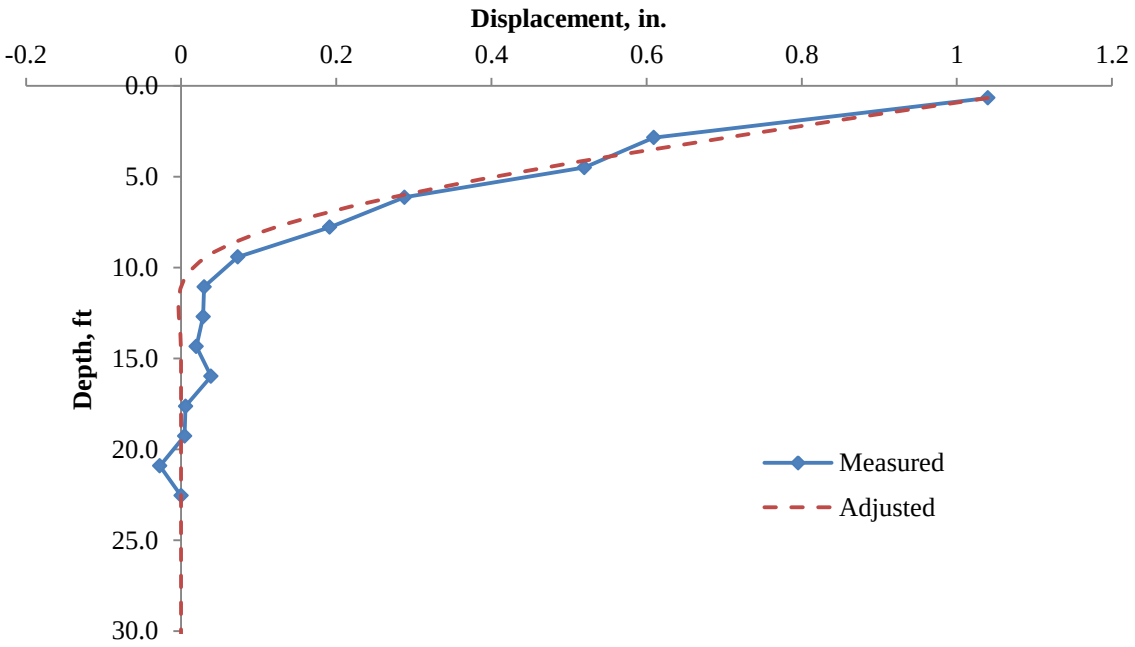

Figure E-19: Adjusted and Measured Displacements along the Length of P4 at the 5.0 kip Load Step during the Lateral Load Test

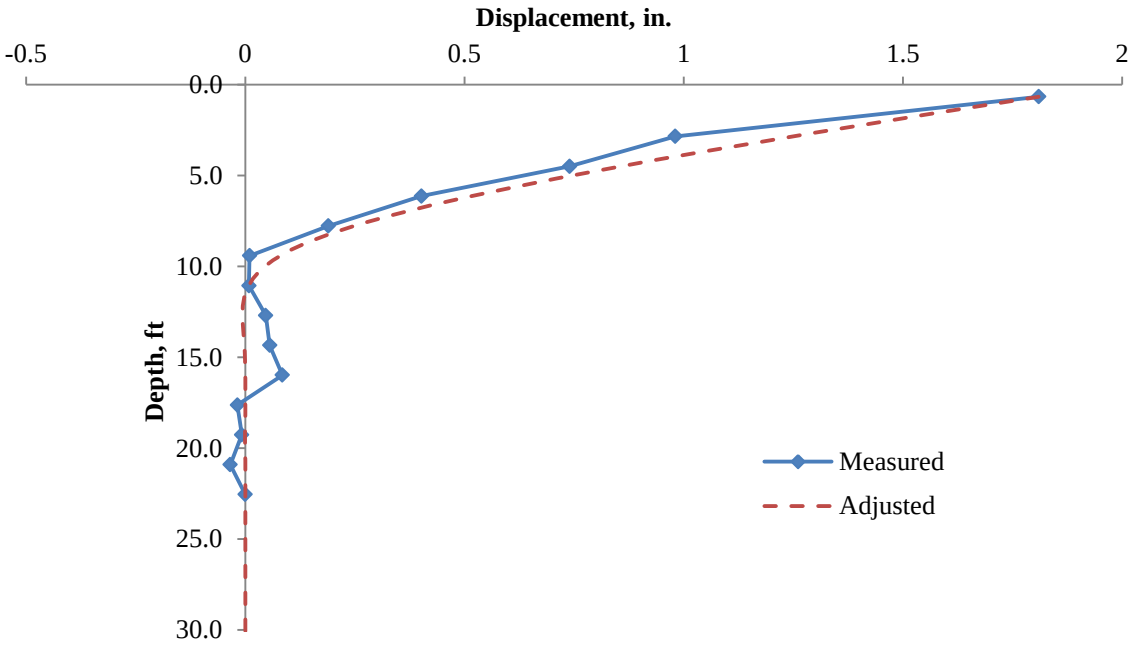

Figure E-20: Adjusted and Measured Displacements along the Length of P4 at the 7.5 kip Load Step during the Lateral Load Test

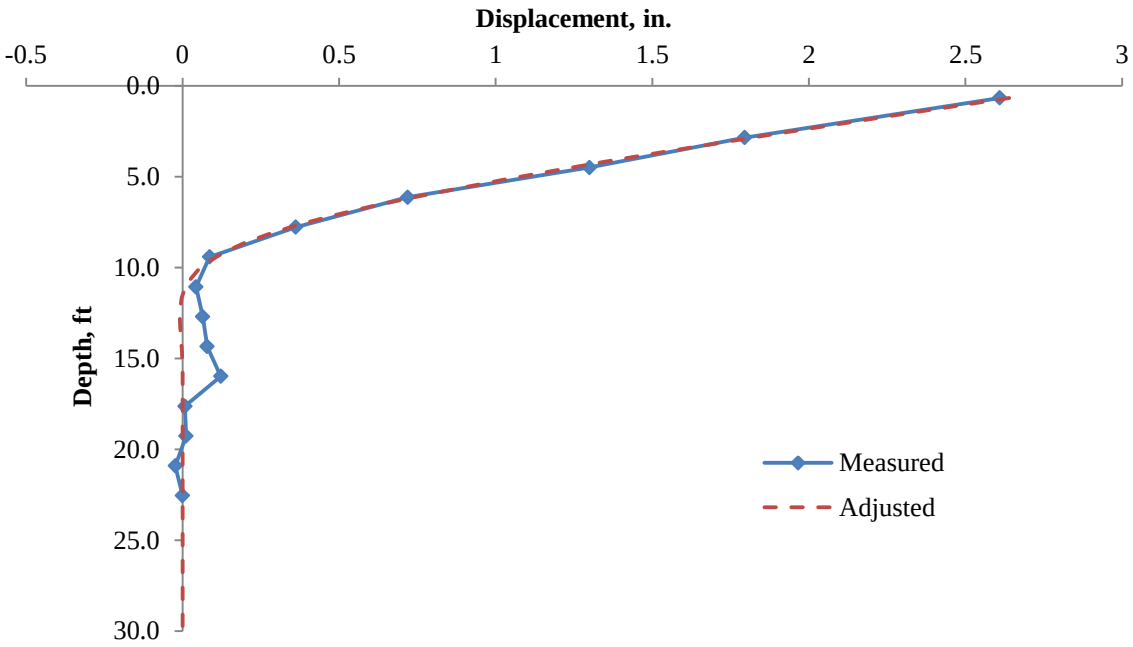

Figure E-21: Adjusted and Measured Displacements along the Length of P4 at the 10.0 kip Load Step during the Lateral Load Test

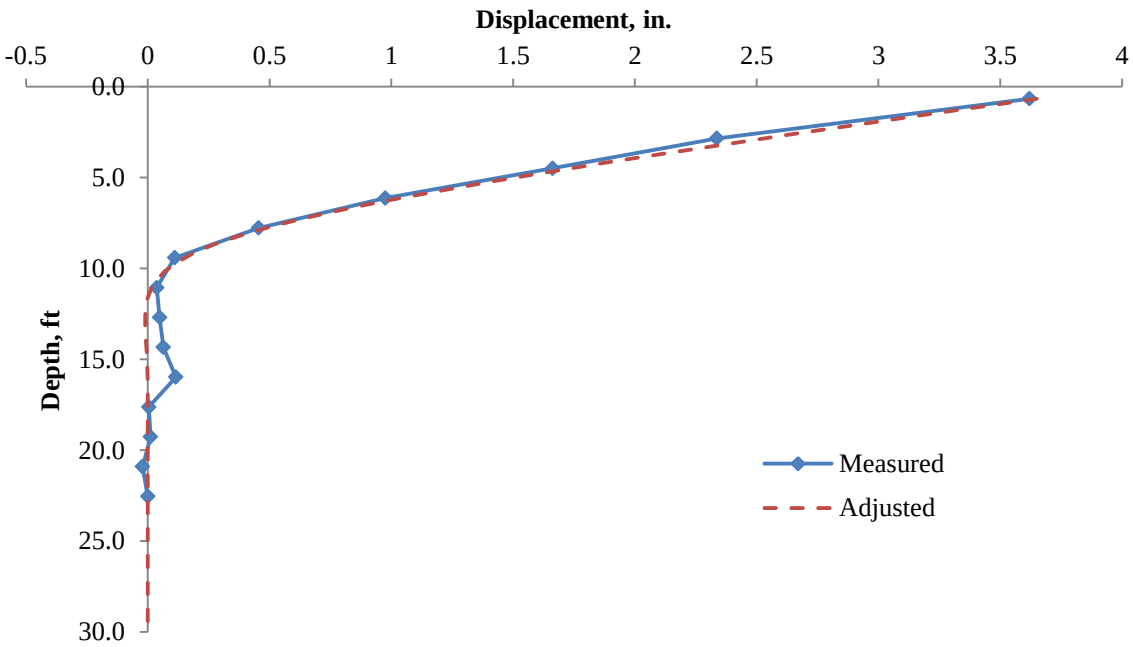

Figure E-22: Adjusted and Measured Displacements along the Length of P4 at the 12.5 kip Load Step during the Lateral Load Test

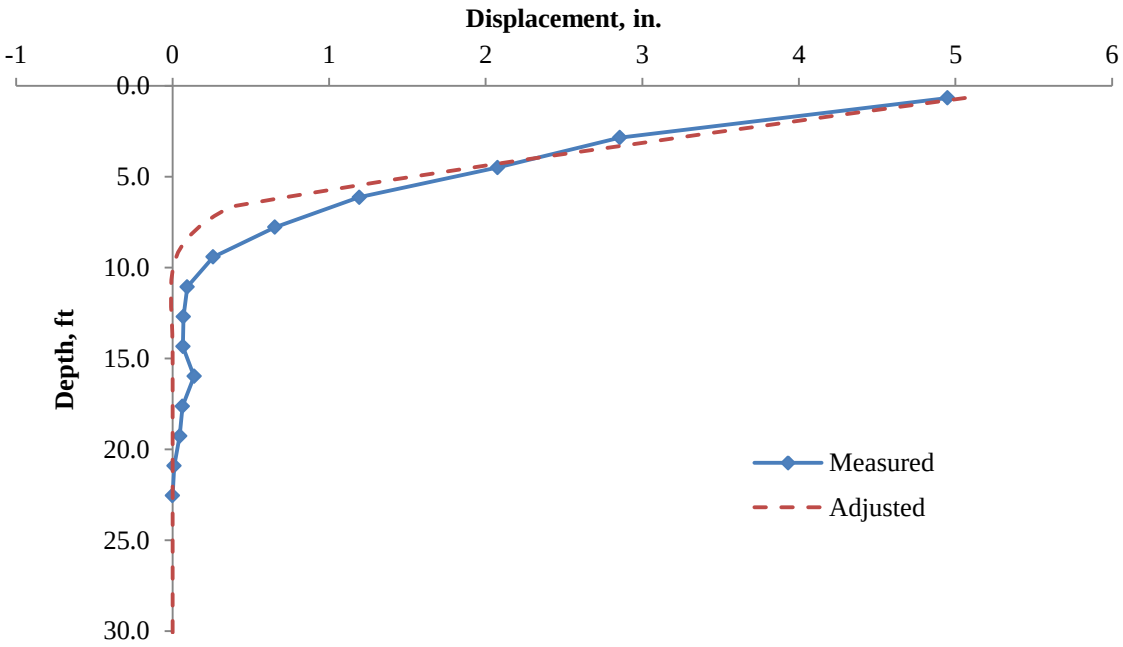

Figure E-23: Adjusted and Measured Displacements along the Length of P4 at the 15.0 kip Load Step during the Lateral Load Test

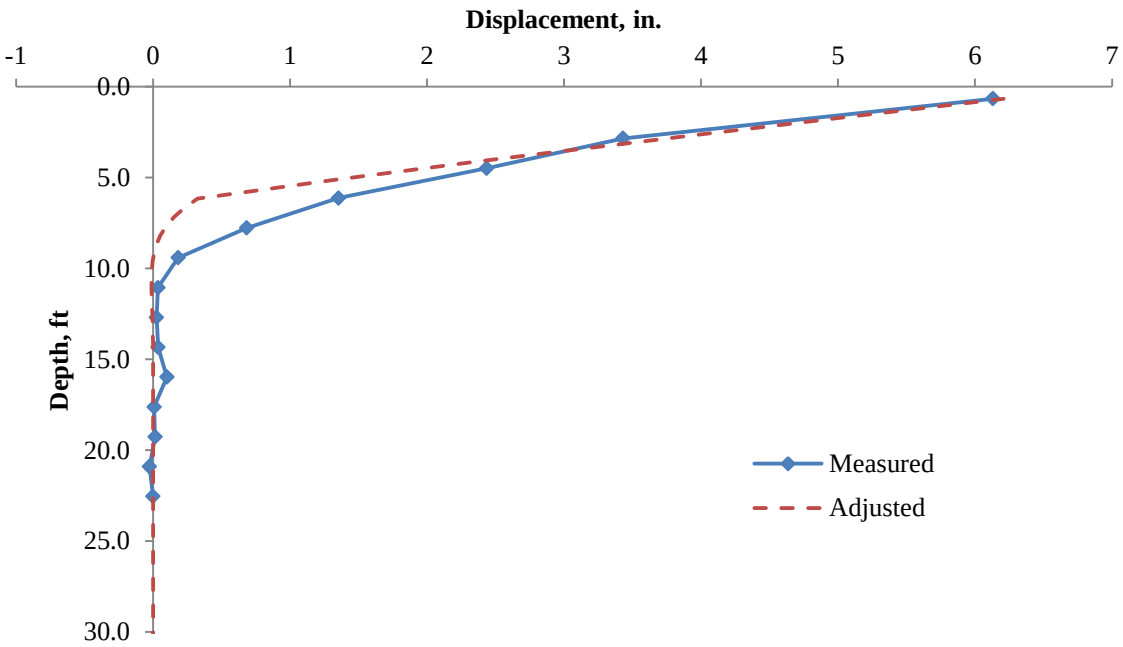

Figure E-24: Adjusted and Measured Displacements along the Length of P4 at the 17.0 kip Load Step during the Lateral Load Test

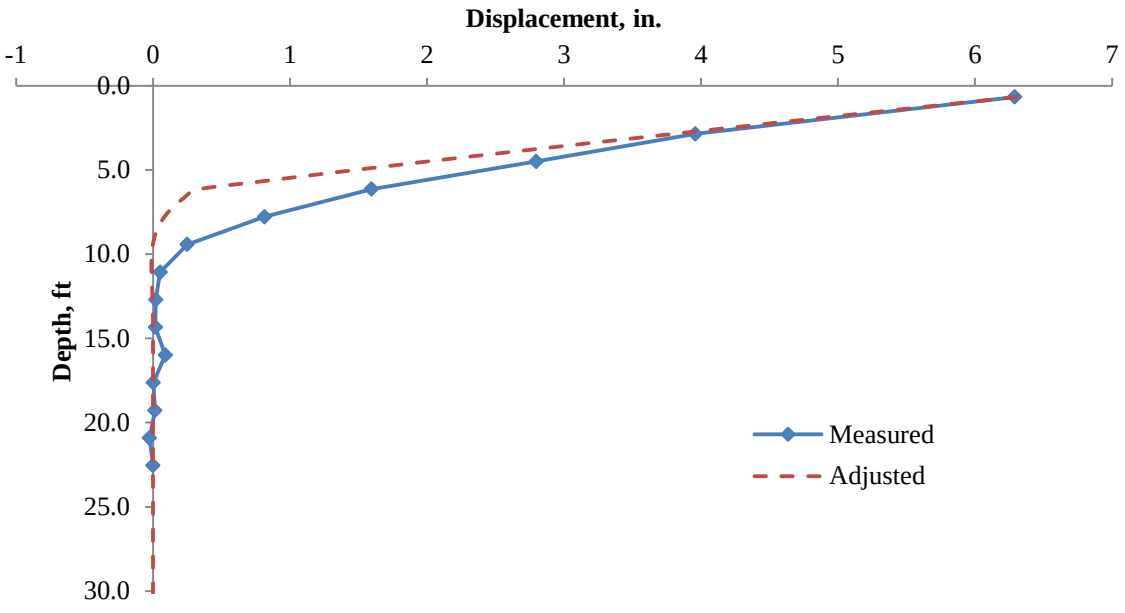

Figure E-25: Adjusted and Measured Displacements along the Length of P4 at the 18.0 kip Load Step during the Lateral Load Test

E.4 ADJUSTED SHEAR FORCE ALONG THE LENGTH OF P4

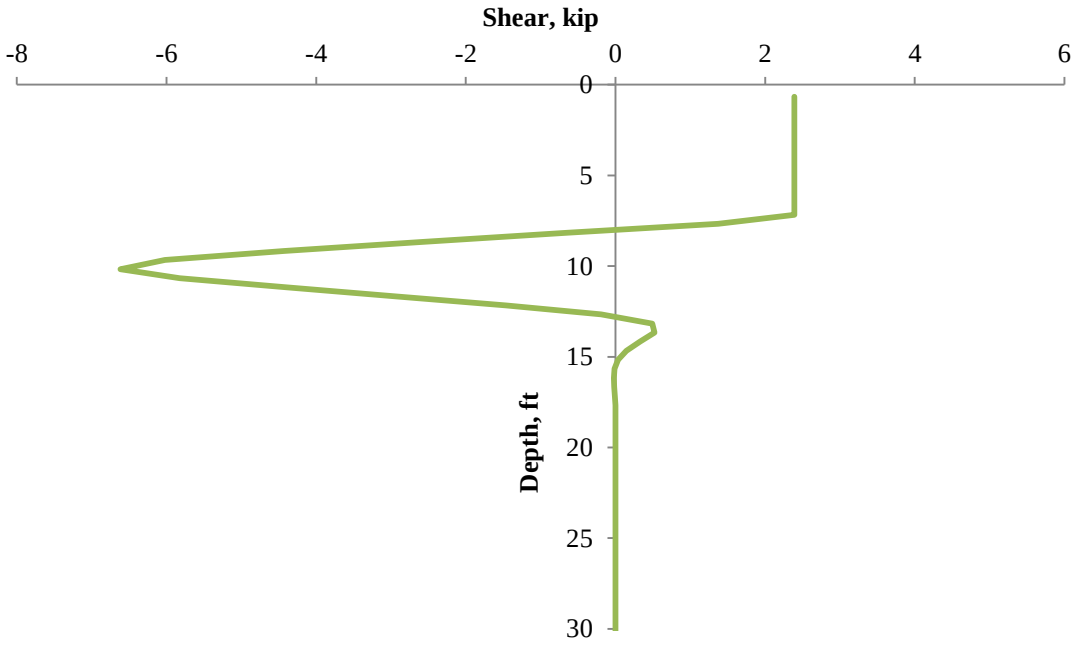

Figure E-26: Adjusted Shear Force along the Length of P4 at the 2.5 kip Load Step during the Lateral Load Test

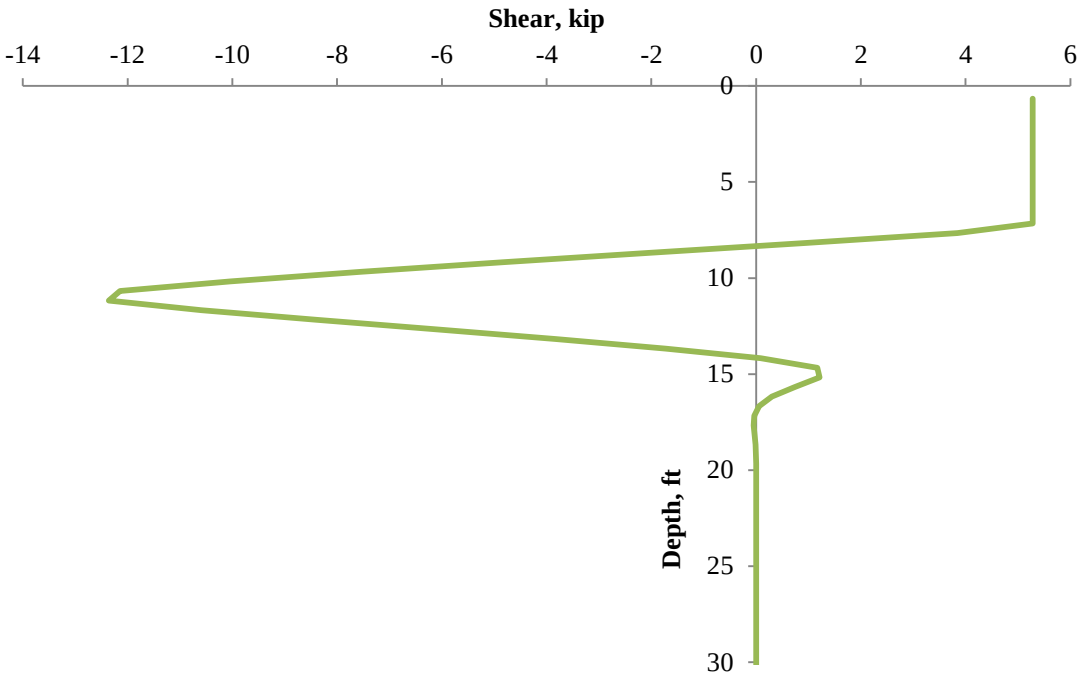

Figure E-27: Adjusted Shear Force along the Length of P4 at the 5.0 kip Load Step during the Lateral Load Test

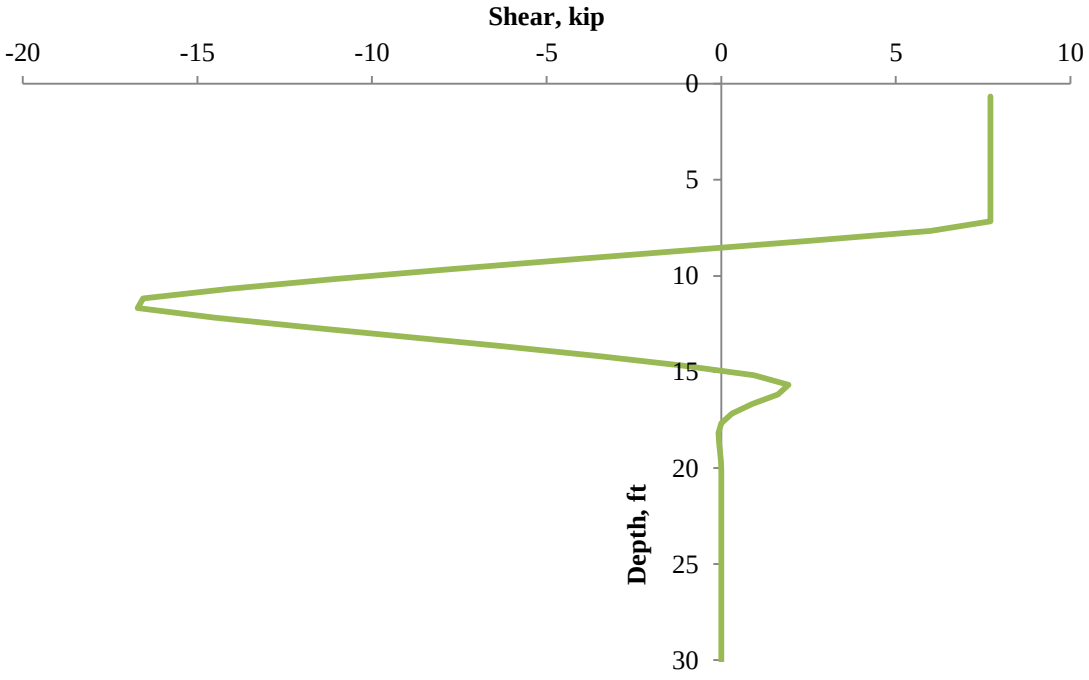

Figure E-28: Adjusted Shear Force along the Length of P4 at the 7.5 kip Load Step during the Lateral Load Test

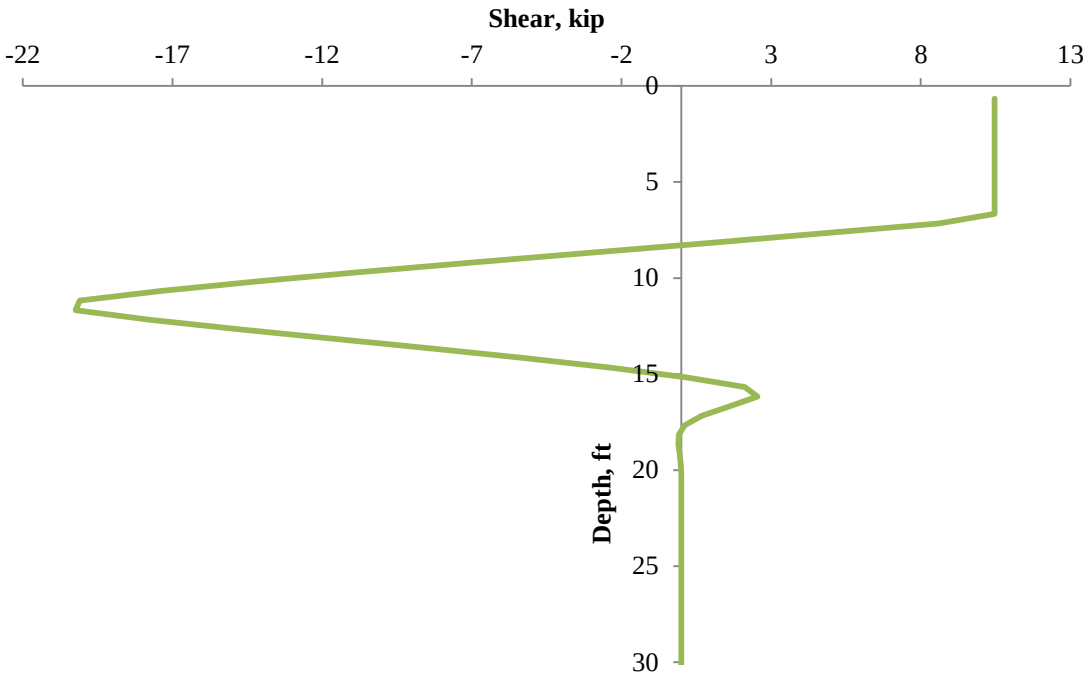

Figure E-29: Adjusted Shear Force along the Length of P4 at the 10.1 kip Load Step during the Lateral Load Test

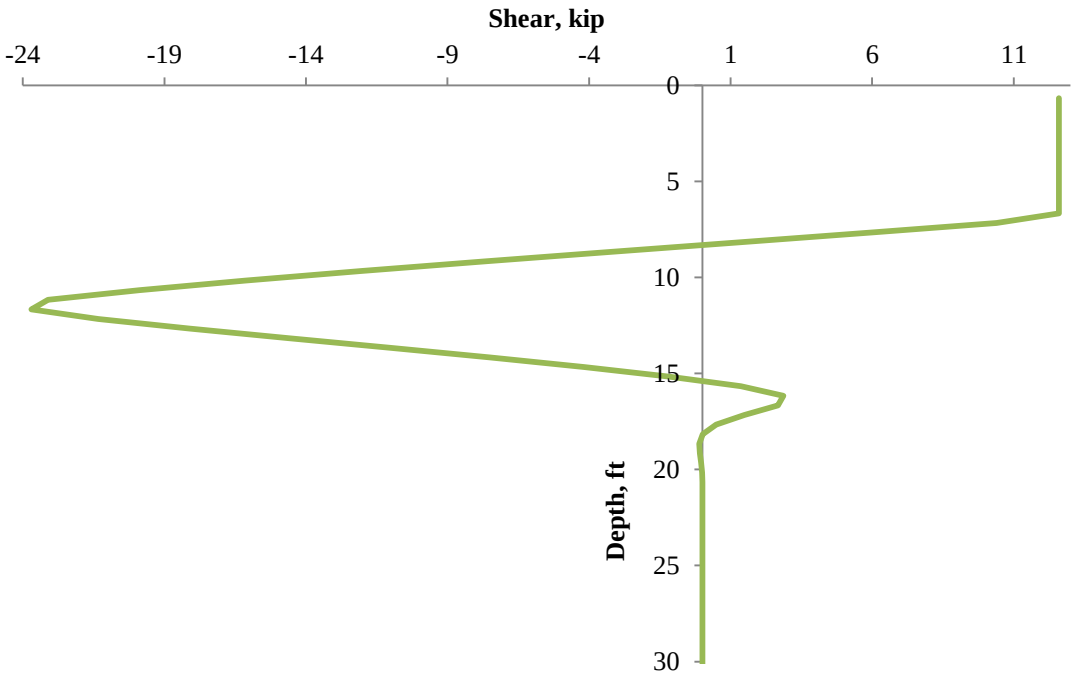

Figure E-30: Adjusted Shear Force along the Length of P4 at the 12.5 kip Load Step during the Lateral Load Test

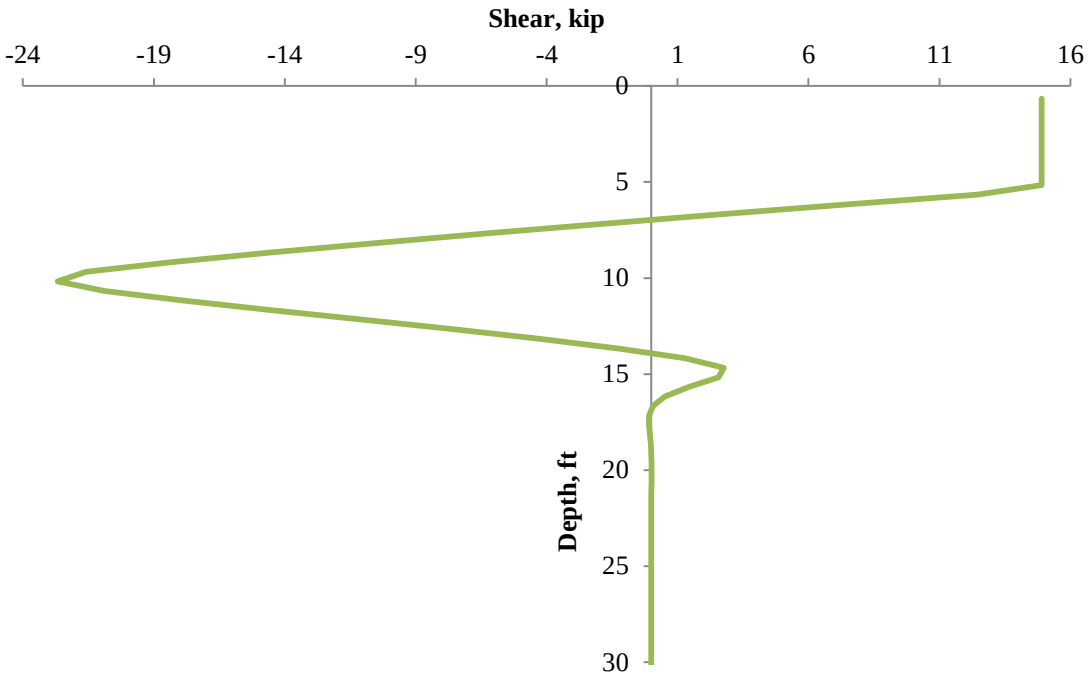

Figure E-31: Adjusted Shear Force along the Length of P4 at the 15.0 kip Load Step during the Lateral Load Test

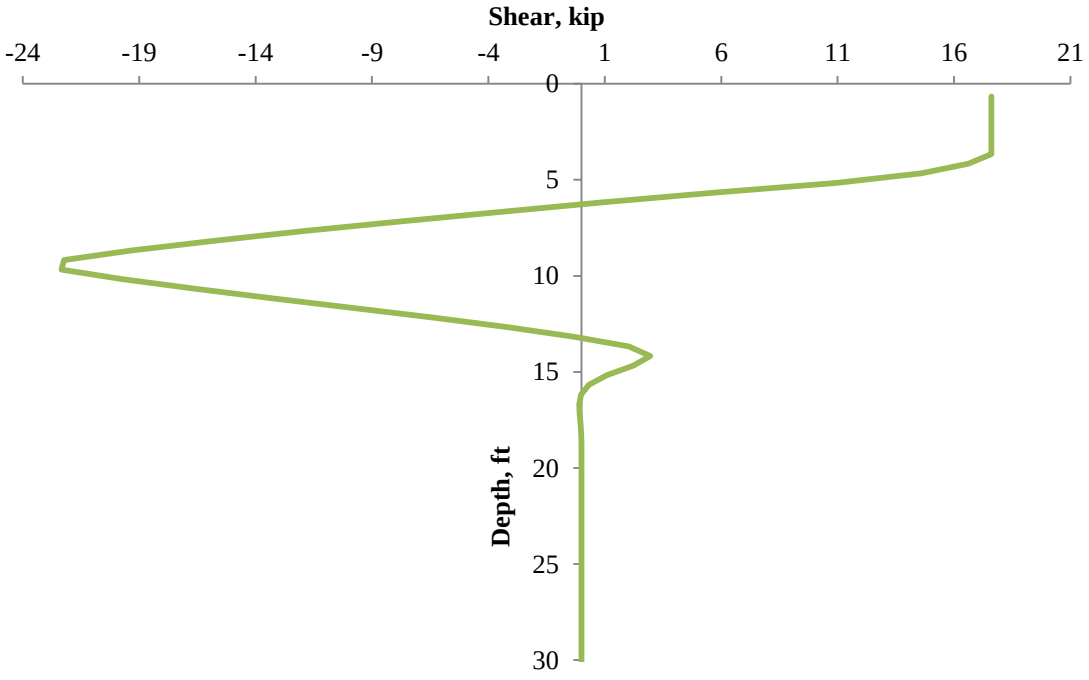

Figure E-32: Adjusted Shear Force along the Length of P4 at the 17.0 kip Load Step during the Lateral Load Test

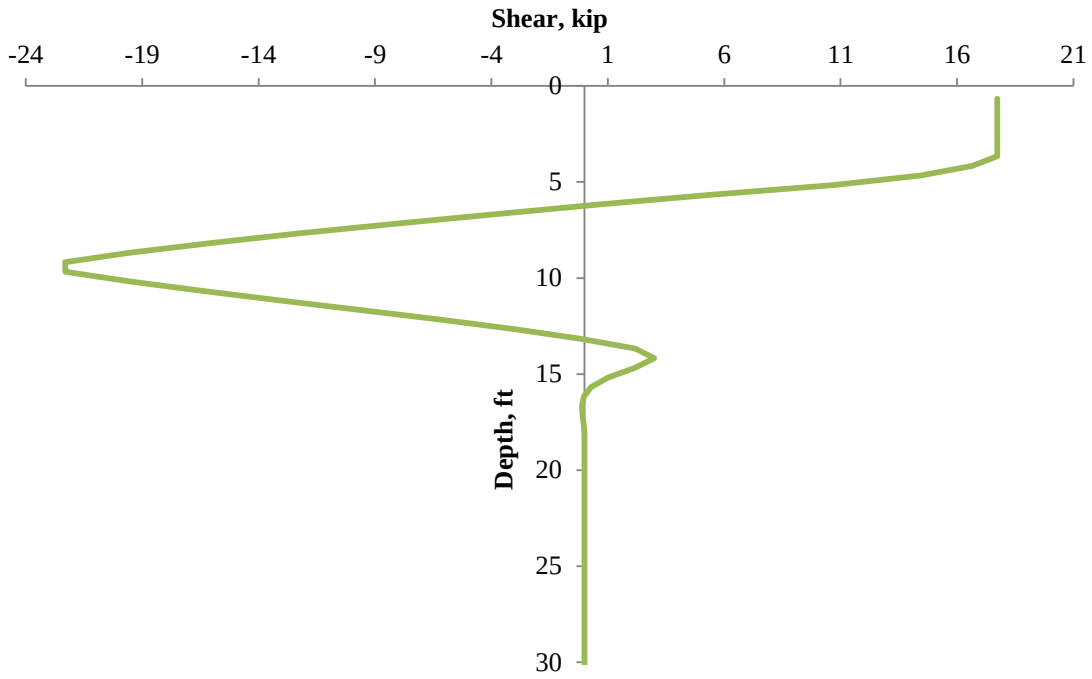

Figure E-33: Adjusted Shear Force along the Length of P4 at the 18.0 kip Load Step during the Lateral Load Test